# Multi-Scale Modeling of Organic Electro-Optic Materials

Lewis E. v.d.L. Johnson

A dissertation submitted in partial fulfillment of the requirements for the degree of

Doctor of Philosophy

University of Washington
2012

Reading Committee:
Bruce H. Robinson, Chair
Larry R. Dalton
Lutz G. Maibaum

Program Authorized to Offer Degree:
Department of Chemistry

University of Washington

**Abstract**

# Multi-Scale Modeling of Organic Electro-Optic Materials

Lewis E. v.d.L. Johnson

Chair of Supervisory Committee:
Professor Bruce H. Robinson
Department of Chemistry

Development of organic materials for photonics applications requires simultaneous optimization of molecular and bulk properties to obtain acceptable performance in device applications. In developing organic electro-optic materials based on the Pockels effect, these properties include the molecular hyperpolarizability ($\beta$) of organic non-linear optical (ONLO) chromophores, the extent to which chromophores can be acentrically ordered in a material, the number density of chromophores ($\rho_N$), and the dielectric constant ($\varepsilon$) of the environment surrounding the chromophores. Furthermore, constraint of orientational degrees of freedom (reduced dimensionality) due to engineered non-covalent interactions and/or high chromophore loading can strongly affect acentric ordering of chromophores. This parameter space can be efficiently searched through theory-aided design, but the vast differences in the spatial scales needed to simulate each property require a multi-scale approach to computational modeling. Coarse-grained, rigid-body Monte Carlo (RBMC) calculations can be used to simulate large ensembles of chromophores and analyze the effects of steric anisotropy and dipole moment on ordering. Fully

atomistic molecular dynamics (MD) calculations using classical force fields can be used to probe specific intermolecular interactions at the nanoscale, and electronic structure calculations at various levels (semi-empirical, DFT, and correlated, wavefunction-based methods such as MP2) can be used to calculate optical properties and provide parameters for lower-level (force field based) calculations. These techniques have been used to model the dielectric and phase behavior of strongly polar liquids such as acetonitrile, assist in the characterization of chomophore-containing complexes that exhibit a four-fold increase in poling efficiency compared to its parent chromophore, and in the molecular engineering of an OLNO dye for DNA-based biophotonics. Additionally, the importance of accounting for molecular shape, electrostatic boundary conditions, and choice of electronic structure methods are discussed and critically analyzed.

# TABLE OF CONTENTS

## LIST OF ABBREVIATIONS

| | |
|---|---|
| AMOEBA | Atomic Multipole Optimized Energetics for Biomolecular Applications, a polarizable force field |
| ATR | Attenuated Total Reflection |
| B3LYP | a hybrid DFT functional |
| BHandHLYP | a hybrid DFT functional |
| C1 (SBLD-1) | coumarin-functionalized chromophore with FTC-type bridge |
| CAM-B3LYP | a range-separated hybrid DFT functional |
| CLD-1 | a chromophore with a ring-protected polyene bridge |
| CL | conductor-like |
| CTAB | cetyltrimethylammonium bromide |
| CTMA | cetyltriethylammonium bromide |
| DAST | *trans*-4- [4-(Dimethylamino)styryl]-1-methylpyridinium toluenesulfonate |
| DFT | Density Functional Theory |
| DMSO | dimethyl sulfoxide |
| DNA | deoxyribonucleic acid |
| DR1 | Disperse Red 1, an azo dye |
| DSC | differential scanning calorimetry |
| EM1/EM2 | ellipsoidal model 1(2), coarse-grained model of acetonitrile |
| EO | Electro-optic |
| ESI | electrospray ionization |
| EZ-FTC | a chromophore with a thiophene-containg bridge |
| FAB | fast atom bombardment |
| FOM | Figure of Merit |
| GC | gas chromatography |
| GGA | generalized gradient approximation |
| HDFD | aryl/perfluoroaryl functionalized chromophore |
| HF | Hartree-Fock |
| HPLC | high-performance liquid chromatography |
| HRS | hyper-Rayleigh scattering |
| LC | liquid crystal |
| LC-BLYP | a range-separated hybrid DFT functional |
| LL-1 | internal name for a DAST-like dye for biophotonics applications |
| MC | Monte Carlo |
| MD | Molecular Dynamics |
| MI | minimum image |
| MMFF | Merck Molecular Force Field, a force field |
| M062X | a hybrid DFT functional |
| MP2 | second-order Møller-Plesset perturbation theory |
| MS | mass spectrometry |
| NMR | nuclear magnetic resonance |
| NPT | isothermal-isobaric ensemble |
| NVT | canonical ensemble |
| ONLO | organic nonlinear optical |

| | |
|---|---|
| OPLS | Optimized Potential for Liquid Simulations, a force field |
| PAMC | pseudo-atomistic Monte Carlo |
| PM3 and PM6 | Parameterized Model 3(6), semi-empirical QM methods |
| PMMA | poly(methyl methacrylate) |
| PBE0 | a hybrid DFT functional |
| PCM | polarizable continuum model |
| QM | quantum mechanics |
| RBMC | rigid-body Monte Carlo |
| RMS | root mean square |
| RF | reaction field |
| SC | spherical cutoff |
| SCRF | self-consistent reaction field |
| SM1 | Stockmayer Model 1 (coarse-grained, acetonitrile-like model) |
| SMFM | shear-modulation force microscopy |
| TCF | tricyanofuran, a class of strong electron acceptors |
| TE | a buffer containing tris(hydroxymethyl)aminomethane and ethylenediaminetetraacetic acid |
| $T_g$ | glass transition temperature |
| VAPRAS | variable-angle polarization-referenced absorption spectroscopy |
| VASE | variable angle spectroscopic ellipsometry |
| ωB97X | a range-separated hybrid DFT functional |
| YLD-124 | chromophore with CLD bridge and CF3-phenyl TCF acceptor |
| YLD-156 | chromophore with FTC bridge and CF3-phenyl TCF acceptor |
| ZINDO | Zerner's Intermediate Neglect of Differential Overlap, a semi-empirical QM method |

**Units:**

| | |
|---|---|
| Å | Angstrom |
| atm | atmospheres |
| cm | centimeters |
| D | Debye |
| esu | electrostatic units ($cm^5 statcoulomb^{-1}$ for hyperpolarizability) |
| J | Joule |
| K | Kelvin |
| mol | mole |
| M | Molar |
| μm | micron |
| nm | nanometers |
| pm | picometers |
| V | Volt |

**Constants:**

| | |
|---|---|
| $k_B$ | Boltzmann's constant |
| R | Gas constant |

# LIST OF FIGURES AND SCHEMES

**Synthetic Schemes:**

# LIST OF TABLES

# ACKNOWLEDGEMENTS

I am grateful for the support and advice from many excellent colleagues and friends throughout graduate school:

Firstly, I thank my advisor, Prof. Bruce Robinson, who has been an exemplary mentor. In addition to always being there when I needed advice, he gave me the support and freedom needed to pursue a wide range of projects, including combining theoretical and experimental work. I also thank Prof. Larry Dalton for his support, amazing knowledge of the field, and enthusiasm, and Prof. Rose Ann Cattolico for plenty of great discussions and providing a fresh perspective on research and whenever I encountered challenges. Furthermore, I thank Profs. Lutz Maibaum and Christine Luscombe for serving on my committee.

I thank Dr. Stephanie Benight for being a great friend, colleague, experimental collaborator, and for helping train me in organic synthesis; I enjoyed our many conversations throughout the last few years. Thanks to Nicholas Bigelow, with who I've been working on scientific endeavors since middle school, for also being a wonderful friend, collaborator, and for many engaging discussions, and to Andreas Tillack both for friendship throughout grad school, for taking the MC code development project in amazing new directions, and asking many great questions.

Thanks are also due to Dr. Robin Barnes, who helped train me and started the development of the C++ MC code, Dr. Bruce Eichinger for his amazing expertise in theoretical chemistry, Dr. Delwin Elder for being a great groupmate and synthetic collaborator, Dr. Josh Davies for collaboration on modeling work, and Dr. Phil Sullivan for many interesting discussions and ideas. I would also like to thank all of the undergraduate researchers who have worked with me, especially Luke Latimer and Zach Watanabe, for their impressive work and persistence on the biophotonics project. I would also like to thank other Dalton and Robinson group members, past and present for plenty of interesting discussions. I also thank Profs. Charles Campbell, David Masiello, J. Michael Schurr, Xiaosong Li, Philip Reid, and Thomas Engel for useful discussions and advice, as well as to the UW Chemistry department's administrative and technical staff for keeping things running smoothly and enabling our research.

Additionally, I would like to thank my teachers from all levels of education, and particularly Renee Fredrickson, Prof. Wayne Steinmetz, and Prof. Malkiat Johal for their encouragement in pursuing a career in chemistry, as well as Dr. James Farr and Prof. Renee LeBoeuf for their advice and many great conversations.

Most importantly, I would like to thank my family, particularly my parents, Larry and Lani Johnson, for all their love, support, and encouragement throughout my life. I also thank my friends, both from UW and elsewhere for many wonderful times together and for putting up with my erratic schedule and rambling about research. Grad school had its high and lows, but all of you have helped make the last five years enjoyable amidst all the hard work. Thanks!

# DEDICATION

To my mother, Lani Johnson, and my father, Larry Johnson

# 1. Introduction to Organic Electro-Optics and Multi-Scale Modeling

## 1.1. Introduction to Electro-Optics

### *1.1.1. Optical communications*

The rapid spread of information technology, from cable TV and personal computers several decades ago to the current explosive growth of mobile Internet, online video, and cloud computing has demanded ever-increasing amounts of bandwidth to transport data around the globe.[1] According to the 2010 Cisco Visual Networking Index, worldwide Internet traffic is expected to exponentially grow at a 32% compounded annual growth rate between 2010 and 2015. Predicted traffic, including three major sectors, is shown in Figure 1-1.

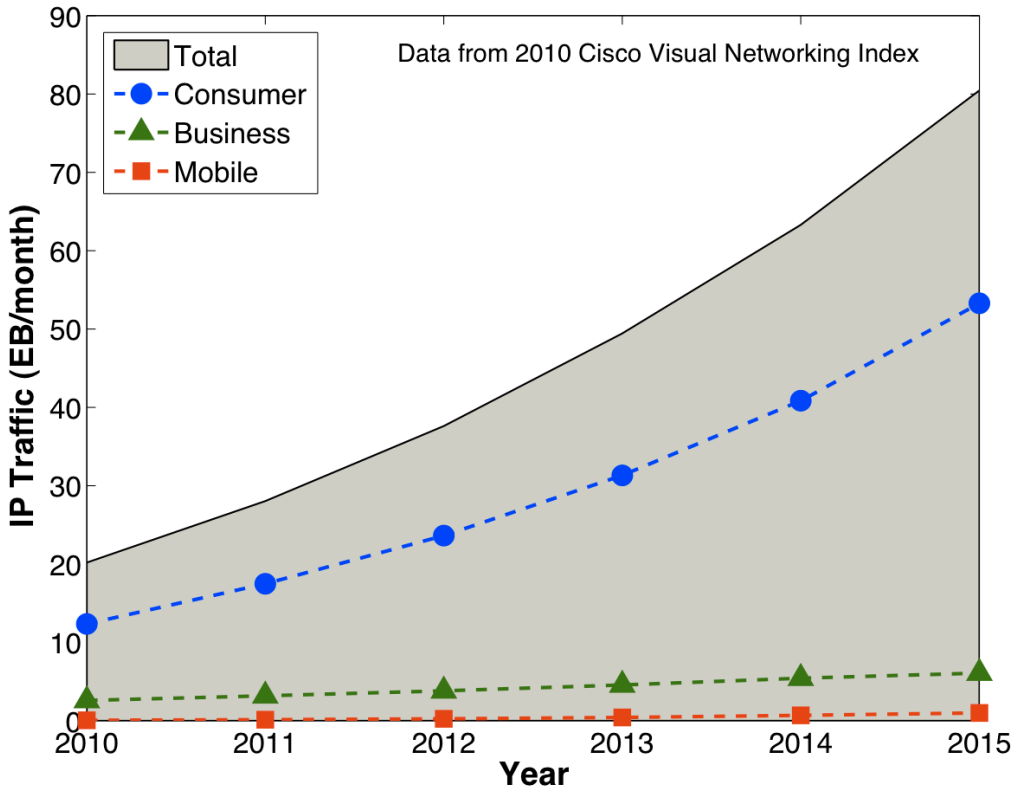


**Figure 1.1.** Projected global IP traffic 2010-2015 from the Cisco VNI

Moving such a large quantity of data efficiently requires high-bandwidth, low-latency, low-loss connections. Fiber optic networks provide one such solution due to high transparency of glass fibers at near-infrared wavelengths (especially 1310 and 1550nm) and far less crosstalk between signals than in electronic networks.[2]

Using light to process data falls within the field of photonics, the optical equivalent of electronics. In addition to long-distance communications, there has been substantial recent interest in photonics for short-range interconnects, including chip-scale integration with silicon-based electronics,[3] and all-optical communications[4] and computation, among other applications.[5] One particular component particularly crucial to systems involving both electrical and optical components, including fiber-optic communications, is electro-optic modulators, which transduce signals from electronic to photonic domains.[1b, 5-6]

### *1.1.2. Electro-optic modulators and the Pockels effect*

Electro-optic (EO) modulators encode electrical signals onto an optical carrier by varying the phase and/or intensity of the light in response to a change in electric field[5-6]. Some examples of electro-optic modulators are shown in Figure 1.2.

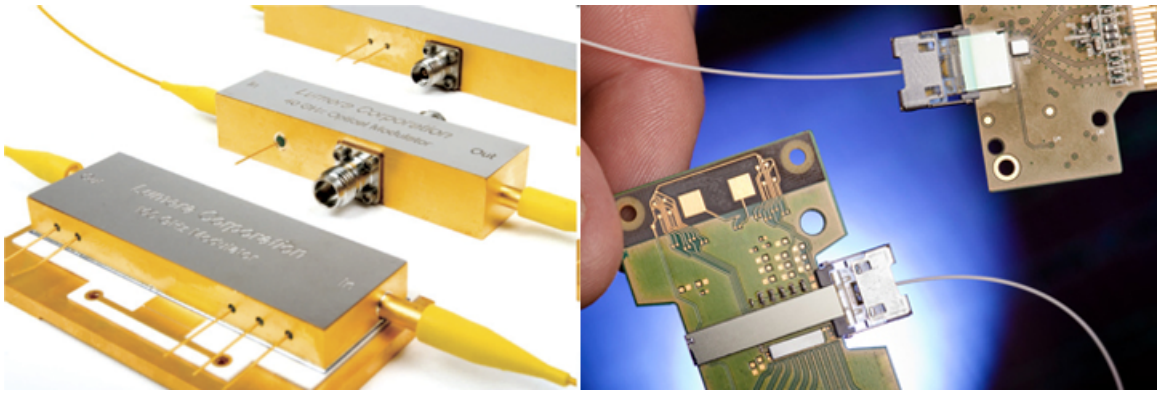

**Figure 1.2.** EO modulators (left, Photo: Lumera Corp.) and an optical interconnect containing integrated EO modulators (right, Photo: Intel Corp.)

Many commonly used types of EO modulators rely on the Pockels effect, in which the refractive index of a material (and therefore, speed of light in the material) varies linearly in response to an applied electric field[1b, 5]. This causes light passing through the EO-active material to undergo a shift in phase proportional to the distance travelled through the EO material. This effect can be harnessed in devices such as Mach-Zehnder modulators, micro-ring resonators, and directional couplers to switch or attenuate optical signals.

One of the simplest and most common modulator designs is the Mach-Zehnder modulator[1b, 5, 7], in which an incoming optical signal is split equally through two waveguides composed of an EO material. One of the signals is unperturbed and the other passes between a pair of electrodes; followed by merging the waveguides. A schematic Mach-Zehnder modulator is shown in Figure 3.

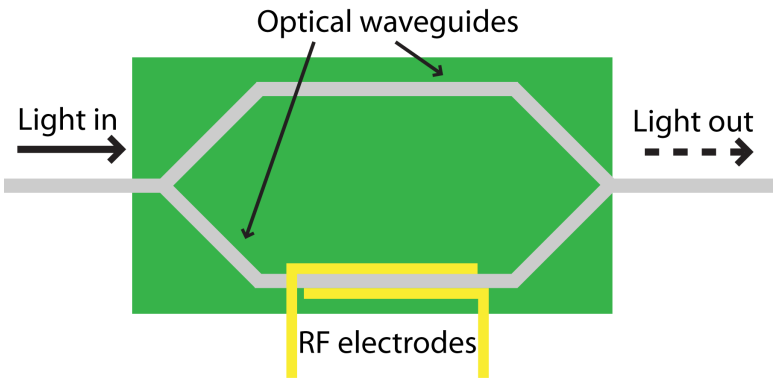


**Figure 1.3.** Schematic Mach-Zender EO modulator. Light passing through the device is split into active and passive waveguides, then recombined. Phase shifts introduced by applying an electric field across the active waveguide encode digital signals by constructive and destructive interference.

If a voltage is applied to the active arm, the shift in the refractive index introduces a phase delay in the light passing through the electrodes compared to the passive arm. If the voltage is sufficient to introduce a shift of one-half wavelength (π radians), destructive interference results in cancellation of the signals upon recombination, and no light emerging from the device. Consequently rapidly varying the voltage can allow a digital signal to be modulated on an optical carrier. The critical voltage for destructive interference[5] is that which will cause a phase shift of π radians over the length of the device. This voltage,

$$V_\pi = \frac{\lambda d}{2n^3 r_{33} L \Gamma} \qquad (1\text{-}1)$$

is determined by the wavelength of the light (λ), the refractive index of the material ($n$), the electro-optic coefficient ($r_{33}$), the device length ($L$), and the optical-electrical overlap integral (Γ). Consequently, device size and/or drive voltage can be reduced by increasing the EO coefficient of the material used in the device.

### *1.1.3. Origin of the EO coefficient $r_{33}$*

The Pockels effect is a non-linear optical effect, relying on non-linear polarization of the active material under an electric field of sufficient strength. The polarization of a bulk material can be represented as

$$\mathbf{P} = \mathbf{P}_0 + \chi_{ij}^{(1)}\mathbf{E}_j + \chi_{ijk}^{(2)}\mathbf{E}_j\mathbf{E}_k + \chi_{ijkl}^{(3)}\mathbf{E}_j\mathbf{E}_k\mathbf{E}_l + \ldots \quad (1\text{-}2)$$

where $\mathbf{P}_0$ is the intrinsic (ferroelectric) polarization of the material and $\chi^{(n)}$ is the nth-order susceptibility. The different **E** vectors represent electric fields, which may be of different frequencies.[8] In most materials, the expansion is truncated at first order. However, materials that are acentrically ordered (no center of inversion symmetry) can exhibit a second-order response. The electro-optic tensor[5]

$$r(\omega) = \frac{-2\chi^{(2)}(-\omega,0,\omega)}{n^4} \qquad (1\text{-}3)$$

is proportional to the second-order susceptibility $\chi^{(2)}$ of the material. One of the two interacting E-fields is light at frequency (ω), the other is the lower frequency (RF) applied electric field[8]. If the axis between the electrodes in the device is arbitrarily defined as the z-axis, the tensor element responsible for the EO effect for fields propagating along the waveguide is the *zzz* component, $r_{33}$. The shift in refractive index[8]

$$\Delta n = \frac{n^3 r E_j}{2} \quad (1\text{-}4)$$

is linearly proportional to the strength of the lower-frequency electric field $E_j$. While higher-order electro-optic effects exist, such as the Kerr effect, which is proportional to $\chi^{(3)}$, the Pockels effect is dominant in typical materials used to

build electro-optic modulators, such as lithium niobate and similar noncentrosymmetric inorganic crystals.[1b, 8-9]

## 1.2. Fundamentals of EO in Soft Matter

### *1.2.1. EO coefficient in organic materials*

While lithium niobate has been extensively used for electro-optic modulators for the past few decades due to its high stability and transparency at telecom wavelengths, it has several notable drawbacks.[10] These include a relatively low $r_{33}$ of 30 pm/V, limited bandwith due to its EO effect relying on ionic motion, difficulty in improving its electro-optic activity, and difficulty integrating with silicon-based components.[1b, 10] Use of soft matter materials containing organic dyes (chromophores) instead of ferroelectric crystals such as lithium niobate enables much higher electro-optic coefficients (> 500 pm/V) and much faster switching speeds, as well as lower noise and power usage due to lower drive voltages.[5, 10-11] In organic chromophores, the electro-optic effect originates from rapid movement of electron density instead of nuclear motion, as in a crystalline material.[12] Here, each molecule polarizes in response to the applied field, with the polarization given by

$$\mathbf{p} = \boldsymbol{\mu}_0 + \alpha_{ij}\mathbf{E}_j + \beta_{ijk}\mathbf{E}_j\mathbf{E}_k + \gamma_{ijkl}\mathbf{E}_j\mathbf{E}_k\mathbf{E}_l + \ldots \quad (1\text{-}5)$$

where $\mu_0$ is the permanent, ground state, dipole moment of the molecule, α is the linear polarizability, β is the first hyperpolarizability, and γ is the second hyperpolarizability of the molecule.[5] The bulk susceptibility of a given order is then the average response of the molecules throughout the system, depending on the (hyper)polarizability of individual EO-active chroomophores, the number

density of chromophores, and how those materials are aligned in the material. The second-order susceptibility along the electric field axis of the device can be written as[5, 13]

$$\chi_{zzz}^{(2)}(-\omega,0,\omega) = \rho_N g(\varepsilon,\omega)\beta_{zzz}(-\omega,0,\omega)\left\langle \cos^3\theta \right\rangle \qquad (1\text{-}6)$$

where $\rho_N$ is the number density of EO-active chromophores in the material and $\left\langle \cos^3\theta \right\rangle$ is the cubic average of the cosines of the angles between chromophores and the electric field axis. The Lorentz-Lorenz-Onsager local field factors[13]

$$g(\omega,\varepsilon) = \frac{\varepsilon\left(n_0^2+2\right)}{2\varepsilon+n_0^2}\left(\frac{n_\omega^2+2}{3}\right)^2 \qquad (1\text{-}7)$$

adjust for differences between the local and macroscopic electric fields due to the dielectric environment surrounding the chromophores. Here, $\varepsilon$ is the static dielectric constant, $n_0$ is the extrapolated zero-frequency refractive index, and $n_\omega$ is the refractive index at the frequency of light used to operate the device. Combining Equations (1-3) and (1-6) gives the electro-optic coefficient in a soft-matter material[14]

$$r_{33} = \frac{2\rho_N g(\varepsilon,\omega)\beta_{zzz}(-\omega,0,\omega)\left\langle \cos^3\theta \right\rangle}{n_\omega^4} \qquad (1\text{-}8)$$

This fundamental equation defines the parameters that must be optimized to produce a large electro-optic response, both at macroscopic and molecular levels. The origin and measurement of these parameters will be discussed in the next few sections.

### *1.2.2. Organic EO chromophores*

Typical chromophores used in organic electro-optic devices consist of a efficient electron-donating moiety connected to an efficient electron acceptor by a π-conjugated bridge. The donor and acceptor give the material a strong dipole moment and introduce asymmetry in the material's polarization response to an applied field, giving it a nonzero β. Chromophores of this type are known as 'push-pull' chromophores.[12] The structure of Disperse Red 1 (DR1), one of the earlier dyes used for electro-optic applications,[7b, 15] is shown in Figure 1.4.

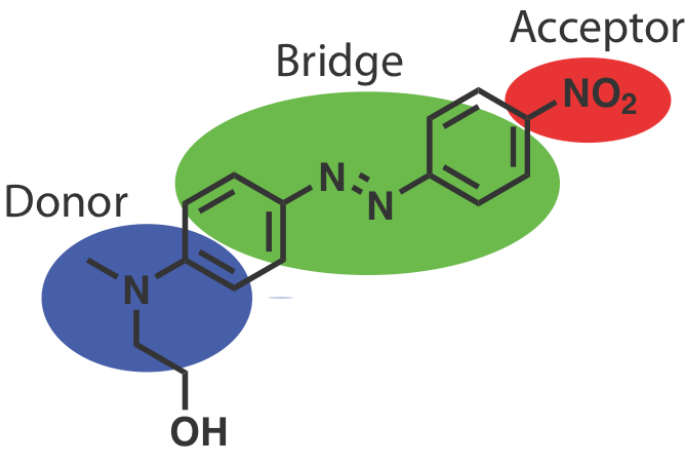


**Figure 1.4.** Disperse Red 1, an example of a push-pull NLO dye. The donor, π-conjugated bridge, and acceptor are highlighted.

While easy to synthesize, DR1 possesses a low first hyperpolarizability, with a $\beta_{zzz}(0)$ (static hyperpolarizability) of $(54 \pm 5)\times10^{-30}$ esu.[16] Much synthetic effort has been devoted to developing chromophores with higher hyperpolarizabilities.[5, 11a, 17] Four high-β chromophores[17c, 18] based on powerful tricyanofuran (TCF) acceptor[17c, 19] variants and long bridges (to further increase charge distribution asymmetry), but retaining the dialkylaniline donor of DR1 are shown in Figure 1.5.

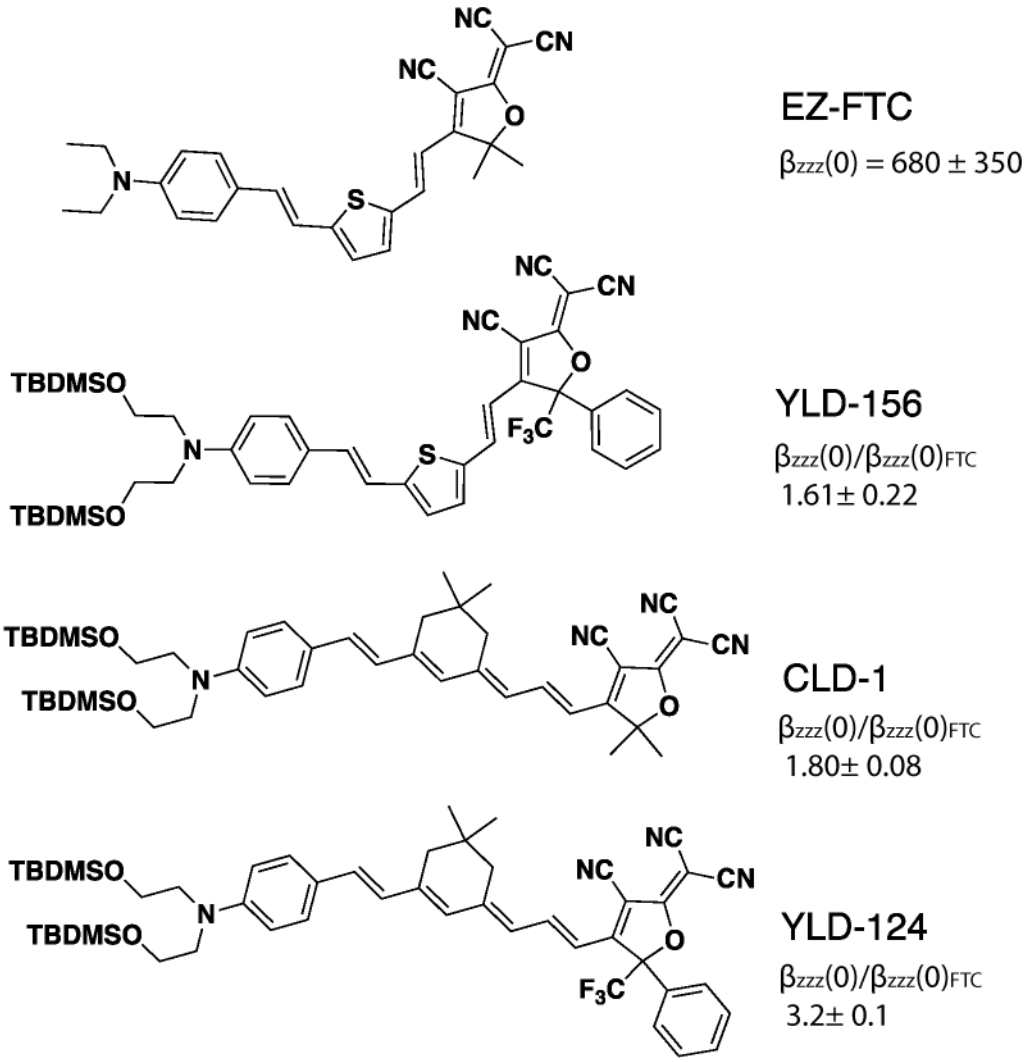


**Figure 1.5.** High-performance NLO dyes incorporating variants of the TCF (tricyanovinylfuran) acceptor, and their static hyperpolarizabilities as measured by Hyper-Rayleigh scattering[20] by Denise Bale and extrapolated to the static limit using methods described in Chapter 5.

Other, even higher-β chromophores have also been developed using more powerful electron donors such as triarylamines[21] and more powerful acceptors such as the TCP (tricyanovinylpyrroline) acceptor.[22]

In order to produce a processable material, EO chromophores are typically blended with or attached to an inert polymer[5, 18a, 23] such as amorphous polycarbonate (APC) or poly(methylmethacrylate) (PMMA). Alternately,

chromophores can be functionalized in a manner that prevents aggregation and improves solubility for processing, e.g. by placing them in dendretic structures[5, 17f]. In both cases, the organic glasses produced are typically disordered and require further preparation to have nonzero EO activity.[24]

### *1.2.3. Acentric order and electric field poling*

Only a few chromophores, such as DAST[25] and OH1,[26] spontaneously form noncentrosymmetric structures upon crystallization or can be used in sequentially synthesis in a manner that forms acentrically ordered materials.[23] Other chromophores order centrosymmetrically or form random, isotropic structures. Examples of isotropic, centrosymmetric and acentric order in case of simple dipolar spheroids are shown in Figure 1.6.

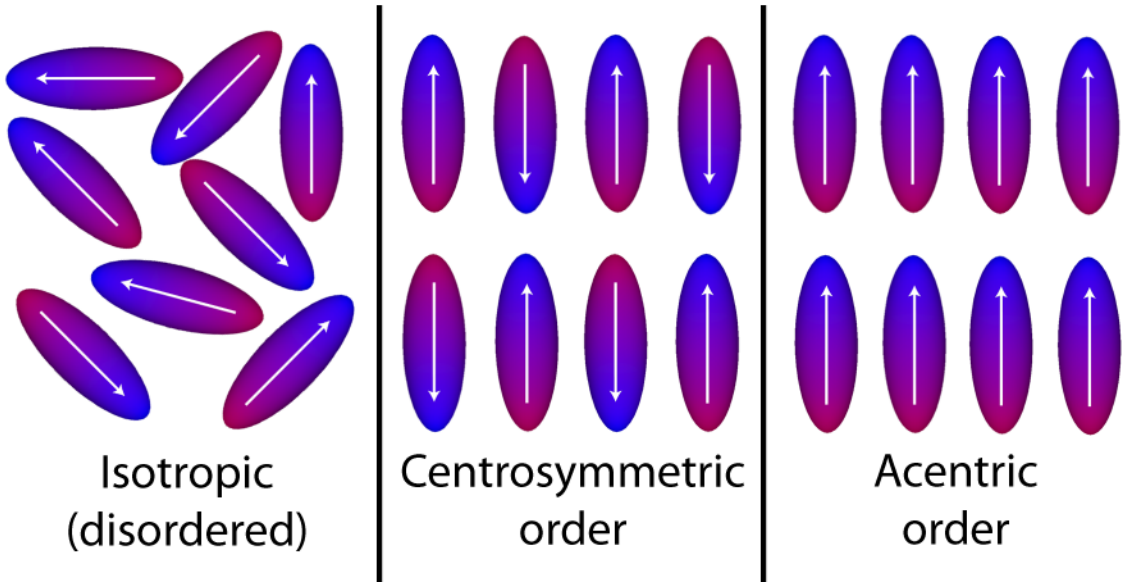


**Figure 1.6.** Cartoon illustrating the difference between isotropic, centrosymmetric and acentric order

While the acentric order parameter $\langle \cos^3 \theta \rangle$ cannot be directly quantified[27] by means of a single experiment in glassy materials, centrosymmetric order can be quantified by the order parameter[28]

$$\langle P_2 \theta \rangle = \frac{3\langle \cos^2 \theta \rangle - 1}{2} \quad (1\text{-}9)$$

by a variety of optical experiments. The change in centrosymmetric order is often used as a proxy for estimating acentric order in organic thin films.[29] The relationship between centrosymmetric and acentric order will be discussed more in Chapters 3 and 4.

Inducing acentric order in most chromophore systems requires an external potential to align the strongly polar chromophores, often provided by applying a strong DC field to the chromophore-containing film (electric-field poling).[5] The field may be applied across electrodes on the top and bottom of the film (contact poling) or via a single electrode on the bottom of the film and a needle suspended above the film (corona poling). The poling process may also be augmented with high intensity laser light at an appropriate wavelength to further induce ordering through photoisomerization of a photoactive polymer host material (laser-assisted poling).[30]

In the case of contact poling, the film containing the chromophores is heated to a temperature near its glass transition ($T_g$) to increase the mobility of the chromophores, subjected to a strong electric field, and then cooled while under the field, freezing in the induced order.[24, 31] A schematic of electric-field poling is shown in Figure 1.7.

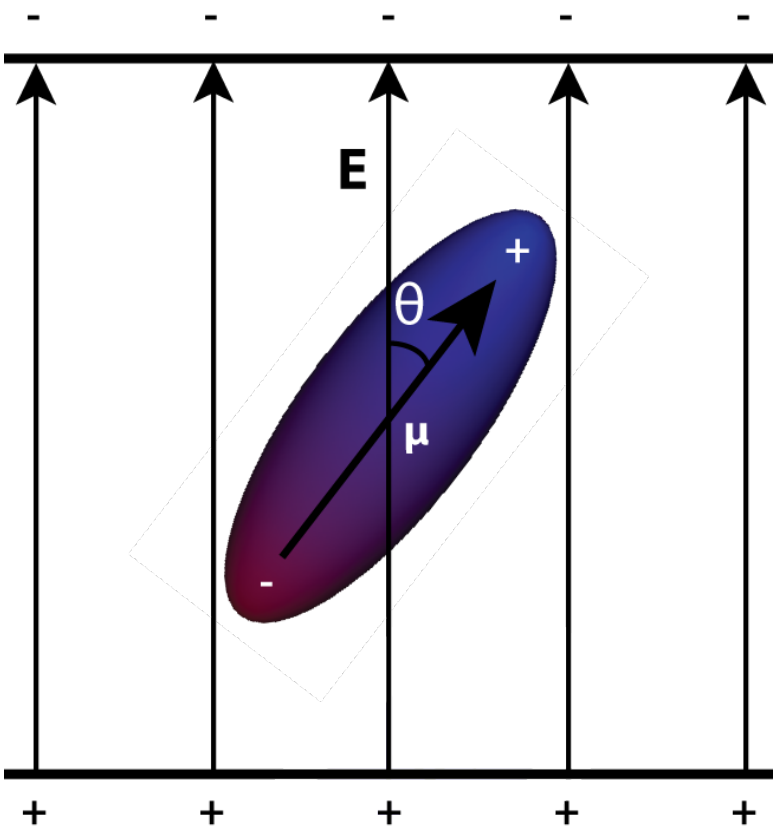


**Figure 1.7.** Simplified illustration of electric field poling; here, a dipolar chromophore rotates to align with an applied DC field.

In the first-order approximation that the chromophores are only interacting with the applied field (and not with each other) and assuming a relatively weak applied field, the acentric order parameter[18a]

$$\left\langle \cos^3\theta \right\rangle \approx g(\varepsilon)\frac{\mu_0 E_p}{5k_B T} \quad (1\text{-}10)$$

where T is the absolute temperature, $E_p$ is the applied poling field strength, and g(ε) is the zero-frequency local-field factor (first term of Eq. 1-7). However, as typical chromophores have dipole moments calculated to be between 20 and 30 Debye.[32] dipole-dipole interactions are often not negligible. Further, while the interaction between the poling field and chromophore dipole moment scales linearly as a function of the magnitude of the dipole moment, the potential

energy of interaction between dipoles scales quadratically[18a] as the magnitude of the dipole moment increases. In general, strong dipole-dipole interactions reduce acentric order. The reduction in acentric order is due to the chromophores aligning centrosymmetrically in order to minimize electrostatic potential energy. Improved estimates of ordering that account for intermolecular interactions can be obtained through mean-field models[23, 33] or computer simulations.[13, 27, 34] The tendency for the chromophores to align centrosymmetrically is minimized in chromophores with a more spherical shape as has been demonstrated by theoretical predictions.[35] The effect of molecular shape and electrostatics on ordering are further discussed in Chapters 2 and 3.

It is also important to note the parallel[13] between the static dielectric response of a material and the electro-optic coefficient

$$\begin{aligned} \varepsilon &\propto \rho_N \mu \langle \cos\theta \rangle \\ r_{33} &\propto \rho_N \beta_{zzz} \langle \cos^3\theta \rangle \end{aligned} \qquad (1\text{-}11)$$

Both are proportional to the number density of dipolar molecules in the system, a coefficient in the polarization expansion given by Equation (1-4), and an acentric order parameter. Given that the active portion of an EO modulator is essentially a parallel-plate capacitor filled with a dielectric material (see Figure 1.7), the acentric ordering of a material will be expressed by its dielectric response under a poling field, which allows for an indirect estimate[13] of $\langle \cos^3\theta \rangle$, which is itself proportional to $\langle \cos\theta \rangle$. Dielectric behavior of materials will be used as a proxy for examining acentric order in Chapters 2 and 3.

### *1.2.4. Matrix-assisted poling*

In order to maximize the order obtained through electric field poling, chromophore-containing EO materials have been engineered to minimize unfavorable dipole-dipole interactions between chromophores and introduce anisotropic, non-covalent interactions that encourage acentric alignment with the poling field.[5, 18a] Two of the most successful of such materials are HD-FD,[5, 36] developed in the Jen group, and C1,[12, 18a, 37] developed in the Dalton group. Both are derived from the YLD-156 chromopohore. HD-FD is functionalized with aryl and perfluoroaryl groups. C1 is functionalized with coumarin liquid-crystal mesogens[38] attached to alkyl side chains. The structures of both C1 and HD-FD are shown in Figure 1.8; moieties providing specific, spatially anisotropic interactions are highlighted in red.

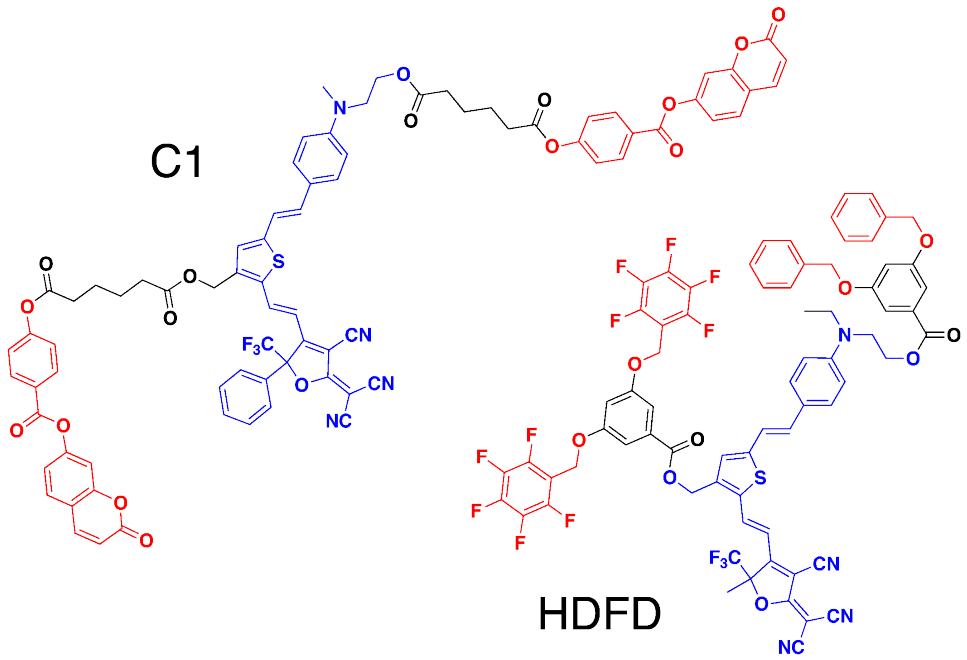


**Figure 1.8.** Representative chromophores for matrix assisted poling. These chromophores are agumented with side chains possessing specific, non-covalent interactions capable of improving acentric order and thermal stability

In HDFD, quadrupolar interactions between perfluorinated and non-fluorinated aryl groups preferentially drive alignment of chromophores, resulting in a poling efficiency ($r_{33}$/Ep) of 1.08 (nm/V)$^2$ and enhanced thermal stability compared to YLD-156/PMMA.[36a] Further EO activity was also obtained by doping the system with a higher-β analogue of YLD-124, giving a poling efficiency of 3.94 (nm/V).[2] at 1310nm. In the C1 chromophore, interactions between the coumarins restrict the orientational degrees of freedom available to the coumarins (reduced dimensionality), resulting in a poling efficiency of 1.92 ± 0.04 (nm/V).[2] at 1310nm compared to 0.45 ± 0.02 for 25% YLD-156 in PMMA.[37a] Both systems showed enhanced centrosymmetric order, with $\langle P_2\theta \rangle > 0.1$, about twice that observed in chromophore/polymer composites at similar poling voltages.[27, 37a] The effects of the coumarin side chains in C1 are discussed further in Chapter 4.

## 1.3. Characterization of Soft-Matter EO Materials

While most of this thesis will focus on modeling the properties leading to electro-optic activity in organic materials, assessing the performance and applicability of theoretical methods requires comparison with experiment. The following is a brief summary of three common methods used to assess properties relevant to the EO behavior of a material.

### *1.3.1. Measuring $r_{33}$ by attenuated total reflection*

The electro-optic coefficient of a material can be characterized by a number of methods, including interferometry[39], second-harmonic generation[8, 40], Teng-Man reflection ellipsometry,[41] among others. One accurate and rapid method is based on attenuated total reflection (ATR).[42] It can also be used to

measure the refractive index[43] of the unperturbed film at a given wavelength in which an EO-active film is tightly coupled to a high-index prism and subject to an alternating-current bias. A laser at the wavelength of interest (often 1310nm) is then reflected off the electrode on the EO-active film through the prism. The change in the material's refractive index with the applied modulating electric field affects the angles of total internal reflection in the film. The EO coefficient can then be determined as[42]

$$r_{33} = \frac{2d}{n_{TM}^3}\frac{\Delta R}{V}\frac{\partial n_{eff}}{\partial \theta}\left(\frac{\partial R}{\partial \theta}\frac{\partial n_{eff}}{\partial n_{TM}}\right)^{-1} \qquad (1\text{-}12)$$

where $n_{TM}$ is the refractive index of the TM (transverse magnetic) mode of light through the EO film, $d$ is the thickness of the EO film, $R$ is the intensity of reflected light, $V$ is the drive voltage, $n_{eff} = n_{prism}\sin\theta$, and $\theta$ is the angle of reflection. More information about the ATR technique can be found in dissertations by Stephanie Benight[44] and Benjamin Olbricht.[45]

### *1.3.2. Measuring hyperpolarizability by hyper-Rayleigh scattering*

As the electro-optic coefficient is a product of molecular hyperpolarizability and acentric order, hyperpolarizability cannot be uniquely determined by EO measurments such as ATR. A separate experiment is needed to determine the β of individual chromophores. This is primarily done using electric-field induced second-harmonic generation[46] (EFISHG) or hyper-Rayleigh scattering[16, 47] (HRS) techniques. The latter is more general as it does not require a priori knowledge of the molecule's dipole moment or second hyperpolarizability (γ) and can also be used for ionic chromophores.[16, 47b] In a HRS measurement, a dilute solution containing the EO chromophore to be characterized is exposed to

a high-intensity laser light at a frequency ω, and intensity of scattered light is measured at 2ω. The second harmonic intensity

$$I_{2\omega} = g\sum_i \rho_{N,i}\beta^2_{HRS,i}(-2\omega,\omega,\omega)I_0^2(\omega) \qquad (1\text{-}13)$$

depends on the rotationally-averaged hyperpolarizability $\beta_{HRS}$ of the solute and solvent, the number density (concentration) of each species, the intensity of the incident laser, and a variety of parameters ($g$) related to the experimental geometry and local field factors from the solvent.[47b] If the experiment is referenced against a solvent with known hyperpolarizability, these factors can be divided out, simplifying the experiment. The hyperpolarizability along the chromophore's dipole axis can then be estimated based on molecular symmetry.[47a, 48] The hyperpolarizability at other frequencies can be estimated using dispersion relations[13, 18b] based on the two-level model of Oudar and Chemla.[49] More information about the HRS technique can be found dissertations by Kimberly[50] Firestone and Denise Bale.[18b]

### *1.3.3. Characterization of ordering in EO films*

In glassy films, acentric order cannot be measured directly, although it can be inferred from the combination of ATR and HRS measurements using Equation (1-8), where $\langle\cos^3\theta\rangle$ can be calculated for a system with known number density, hyperpolarizability, and EO coefficient. The centrosymmetric order parameter, however, can be assessed using polarized absorbance spectroscopy. In the simplest case, the absorbance of linearly polarized light perpendicular to

the poling axis is measured at normal incidence before and after poling. The order parameter[28]

$$\langle P_2\theta \rangle = 1 - \frac{A_\perp}{A_0} \qquad (1\text{-}14)$$

reduces to a function of the initial absorbance ($A_0$) and the absorbance after poling ($A_\perp$). However, this simple method is imprecise.[37a] Precision can be improved by using methods such as variable-angle polarized absorption spectroscopy (VAPRAS)[27] or variable angle spectroscopic ellipsometry (VASE).[37a, 51] In the former method, absorbances are measured at multiple angles and referenced against the absorbance of light polarized parallel to the poling axis. Data can be analyzed using either a ratio method similar to Equation (1-14) or a more comprehensive analysis in terms of fields and optical constants,[52] evaluated using the Jones matrix formalism.[27, 53] VASE measurements are based on fitting ellipsometric data (phase shift and differential intensity between polarizations)[54] to obtain the optical constants,[51] *n* and *k*, which are, respectively, the real and imaginary components of the refractive index. Centrosymmetric order can then be calculated as[55]

$$\langle P_2\theta \rangle = \frac{k_e - k_o}{k_e - 2k_o} \qquad (1\text{-}15)$$

where $k_e$ and $k_o$ are the extraordinary (parallel) and ordinary (perpendicular) components of the imaginary portion of the refractive index.[12] The centrosymmetric order parameter provides a general sense of the change in ordering due to poling; the relationship between centrosymmetric and acentric

order will be discussed in more detail in Chapter 4. More information about the VAPRAS technique can be found in Olbricht et al., 2011.[27]

## 1.4. Multi-Scale Modeling

Just as multiple methods are needed to experimentally characterize soft matter electro-optic materials, a variety of computational methods are required to simulate such systems due to the range of length and time scales involved for estimating different properties.[13, 18a] Charge transfer within the chromophores occurs over distances of angstroms, while intermolecular correlations can extend for several nanometers and devices containing EO-active materials can range from hundreds of nanometers to centimeters in size.[10] Time scales can range from tens of femtoseconds[56] for electron displacement in response to an applied field to minutes for the poling process itself.[31] The large discrepancy between the amount of detail required for each calculation presents substantial challenges for efficient computational simulation of materials.

Using a computational method designed for smaller length scales on large systems is often not only inefficient, but computationally intractable due to steep scaling of the processor time and memory resources required. For example, if the number of particles (N) in a simulation is increased by a factor of ten, a simulation method with quadratic scaling in the number of mathematical operations required ($O(N^2)$ scaling) will require approximately 100 times as much processor time as before, but one with quartic scaling ($O(N^4)$) will now require approximately 10000 times as much processor time. Consequently, methods with steep computational scaling (e.g. *ab initio* electronic structure

methods) can become expensive or impractical even after relatively small increases in the size of a simulation. This problem is further compounded in condensed phases, where the number of particles increases as a function of volume, and therefore cubically with the length scale of the simulation.

Simulation of different aspects of soft-matter systems can be made more tractable through multi-scale modeling,[57] in which multiple methods are used in conjunction to cover different length and time scales. In addition to organic electro-optic materials,[13] multi-scale techniques have been used for other soft-matter systems such as proteins,[58] lipid bilayers,[59] and polymers.[57a, 60] One approach involves concurrently treating different portions of a system at different levels of detail, e.g. QM/MM calculations,[61] in which a portion of a system is treated using quantum mechanical methods, and other portions of the system are treated with less computationally expensive classical methods. Another example of concurrent multi-scale modeling is atomistic treatment of a molecule of interest in classical molecular dynamics, while treating its surrounding environment by a simplified representation of each molecule where atoms have been merged into a smaller number interacting sites (united atom model).[59] Alternately, systems can be modeled sequentially,[57b, 57d] with results from a higher-level calculation used to produce 'coarse-grained' parameters for less expensive calculation on a larger system. Sequential multiscale modeling can also start with lower-level calculations; a less-complex system can be mapped back to a higher level of detail to produce a more realistic description of the environment around molecules of interest.[57b, 60b] The sequential multi-scale modeling approach is outlined in Figure 1.9 with a chromophore and a highly simplified description of it as a dipolar spheroid.

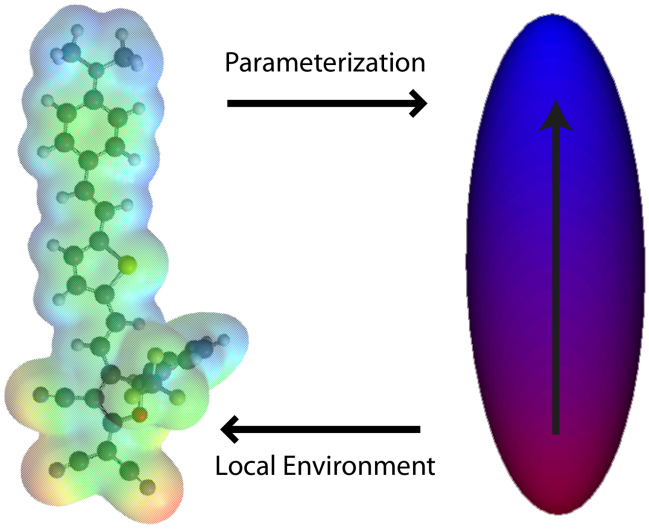


**Figure 1.9.** Cartoon showing the sequential multi-scale modeling process; higher-level methods are used to parameterize lower-level methods, which can in turn be used to generate representative configurations for high-level calculations

Our current approach for EO systems focuses on sequential multi-scale modeling, using higher-level calculations to obtain molecular properties and to generate parameters for lower-level calculations that can be used to study local structure and bulk properties in condensed phases. Each of these tiers of calculations is further broken down into specific methods depending on the property of interest. For example, poling-induced order can be efficiently calculated for thousands of dipolar spheroids, but details about specific interactions are lost,[37a] while a molecular dynamics calculation lasting nanoseconds might show the effects of those interactions on how molecules organize,[37b] but may not capture the (slow) poling process. The hierarchy of modeling methods used in this work are summarized in Table 1.1. They range

from least-expensive to most-expensive, along with that method's formal computational scaling with respect to the number of particles (atoms or electrons) being simulated. Note that the formal scaling represents an upper bound; effective scaling can be reduced for some methods by numerical approximations and more efficient algorithms[62] (fast multipole method,[63] particle-mesh Ewald,[64] sparse matrix Hartree-Fock,[65] etc).

**Table 1.1.** Methods used in multi-scale modeling of EO chromophores

| **Method** | **Formal Scaling[66]** | **Primary use in workflow** |
|---|---|---|
| Classical MC | $O(N^2)$ | Coarse-grained simulation of ordering |
| Classical MD | $O(N^2)$ | Atomistic simulation of specific interactions |
| Semi-empirical QM | $O(N^3)$ | Initial screening and geometry optimization |
| SCF (HF/DFT) | $O(N^3)$-$O(N^4)$ | Geometry, electrostatic, and optical properties |
| MP2 | $O(N^5)$ | High-level, *ab initio* geometry optimizations and hyperpolarizability calculations |
| CCSD | $O(N^6)$ | High-level *ab initio* calculations on small systems |

## 1.5. Computational Methods

The methods used in the multi-scale modeling workflow outlined above are briefly described below. Specific procedures and Hamiltonians used for simulations are further discussed in individual chapters. Additional general information about these methods can be found in several excellent books.[66b, 67]

### *1.5.1. Classical Simulation Methods*

Classical simulation methods (Monte Carlo and Molecular Dynamics) can be used to calculate statistical properties of materials such as the total potential energy $\langle U \rangle$, heat capacity ($C_v$), dielectric constant (ε), and order parameters

$\langle \cos^n \theta \rangle$. These properties are estimated by means of the classical configuration integral[67a, 68]

$$\langle A \rangle = \frac{\int A e^{\frac{-H(r^N, p^N)}{kT}} dr^N dp^N}{\int e^{\frac{-H(r^N, p^N)}{kT}} dr^N dp^N} \quad (1\text{-}16)$$

where $A$ is the observable of interest, $H$ is the Hamiltonian for the system (kinetic energy + interaction potentials), $r$ are generalized positional coordinates, and $p$ are generalized momenta. As these integrals are intractable for interacting many-body systems, and as only the resulting properties are usually of interest, the goal of many-body computer simulations is to sample a sufficiently large number of configurations to approximate Equation (1-16) to high precision.[67a] Configurations can be generated by propagating a system in time (molecular dynamics), or by randomly sampling from a statistical distribution (Monte Carlo).[66b] According to the ergodic principle, time averages and ensemble averages should yield equivalent properties if a sufficiently large number of configurations are sampled.[67a] The problem is further made tractable by the system being far more likely to be in low energy states, which compose a small subset of the possible states available to the system.[67b]

The energy of the system in a classical simulation is defined through pair potentials, which can range from simple monoatomic models such as the hard-sphere potential (no interaction if particles non-overlapped, infinite energy if particles are overlapped) to complex, all-atom molecular force fields such as AMBER,[69] OPLS,[70] and MMFF,[71] which include terms for electrostatic

interactions, bond stretching, bending, and rotation. One common example of a pair potential is the Lennard-Jones potential

$$u_{ij} = 4\varepsilon_{LJ}\left[\left(\frac{\sigma_{LJ}}{r_{ij}}\right)^{12} - \left(\frac{\sigma_{LJ}}{r_{ij}}\right)^{6}\right] \qquad (1\text{-}17)$$

where $r_{ij}$ is the inter-particle distance, $\varepsilon_{LJ}$ is the depth of the potential well (strength of the interaction), and $\sigma_{LJ}$ is the contact (zero-energy) distance for the interacting atoms. This potential is often used for modeling simple, monoatomic fluids,[68, 72] as well as for a dispersive and nuclear repulsive potential in more complex force fields.[66b] Interaction potentials used for sets of calculations discussed in this work are discussed in each chapter as needed.

The second main consideration common to many-body computer simulations is the size of the system. Simulations must be large enough that pair potentials between atoms that are farthest away from each other in the simulation cell decay to negligible levels.[67b] If a larger simulation cell is used, non-bonded short-range interactions are often truncated at some cutoff distance $R_{cut}$ to avoid calculating large numbers of negligible interactions.[66b] Furthermore, to avoid introducing bias from molecules at edges and to allow a finite simulation to represent a quasi-infinite (bulk) material, simulations are typically run using periodic boundary conditions, where interactions 'wrap around' the edge of a box, such that a particle near an edge will interact with particles on the opposite side of the simulation cell.[67b] Periodic boundary conditions are illustrated in Figure 1.10.

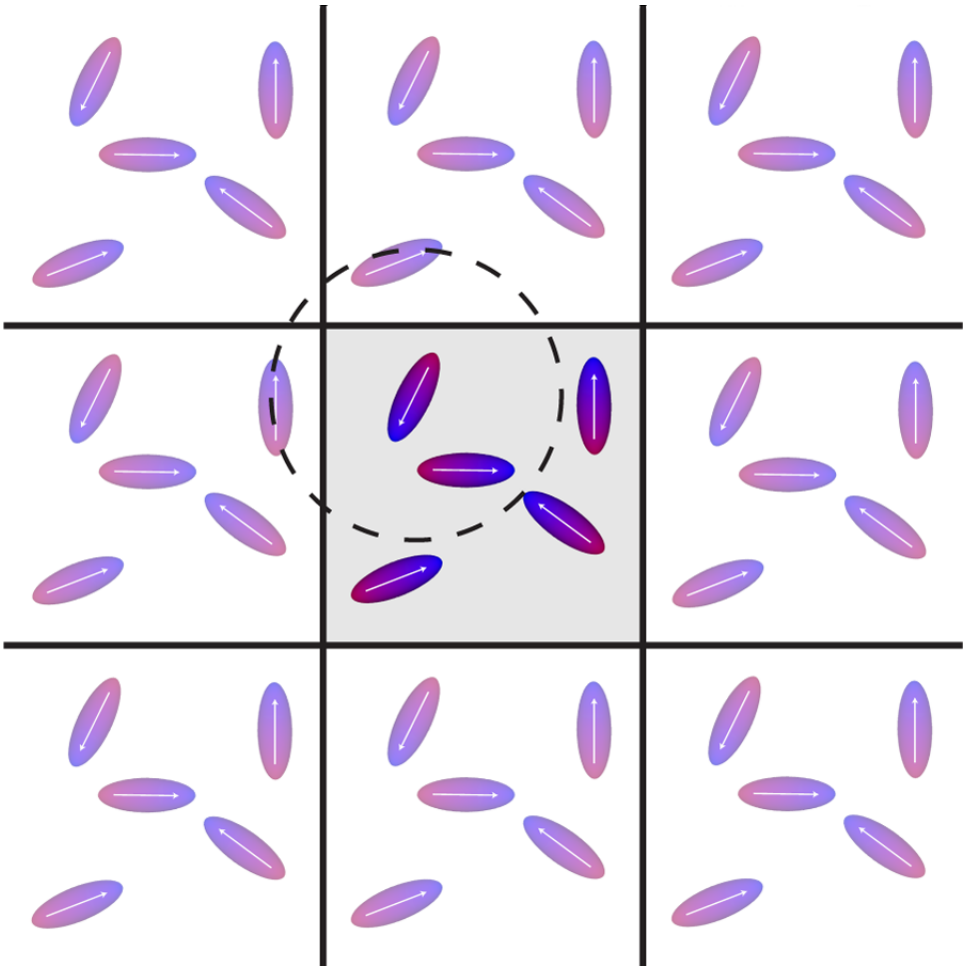

**Figure 1.10.** Periodic boundary conditions; the central cell is the real simulation cell; the others are images. The dashed circle represents a cutoff; the particles within it can interact with the particle at its center.

A further consideration in any simulation involving electrostatic interactions is the electrostatic boundary conditions, which can have large effects on intermolecular correlations. These are discussed in more detail in Chapter 2. Extensive information on classical methods of simulating molecular systems can also be found in *Understanding Molecular Simulation: From Algorithms to Applications* by Frenkel and Smit[67a] and *Computer Simulations of Liquids* by Allen and Tildesley.[67b]

### *1.5.2. Metropolis Monte Carlo*

The Metropolis[73] Monte Carlo algorithm generates configurations by randomly attempting to move (rotate or translate) particles, with the size and the direction of the move chosen from a uniform distribution within some maximum move size.[67a] The energy before and after the move are compared and weighted according to the Boltzmann distribution. The weighted energy is then compared with a uniformly distributed random number between zero and one. If the weighted energy change exceeds the random number,

$$e^{\frac{-\Delta U}{k_B T}} > rand(0,1) \qquad (18)$$

the move is accepted; otherwise the previous configuration is retained. As a result, moves that decrease the energy are always selected, and moves that increase energy substantially are unlikely to be selected. Properties are calculated from an average over many such configurations[66b]

$$\langle A \rangle = \frac{1}{M} \sum_{i=1}^{M} A_i \left( \mathbf{r}^N \right) \qquad (19)$$

where $A_i$ is the value of the observable in the *i*th configuration, $M$ is the number of configurations sampled over, and N is the number of degrees of freedom in the simulation. As particles move randomly instead of deterministically, they do not have momenta and only positional degrees of freedom are considered. Given that the simulation is sampling from the Boltzmann distribution at constant temperature, the 'natural' ensemble for such calculations is the Canonical (NVT) ensemble, although simulations can be adapted to sample from other ensembles also.[66b]

The Monte Carlo code used in this thesis was developed in-house in the C++ programming language by myself and Robin Barnes, based on earlier MATLAB code used in the group,[13, 35, 74] resulting in substantial performance increases (allowing for larger simulations) as well as calculation of more properties and improved ease of processing output data. All simulations were run in the rigid-body Monte Carlo (RBMC) approximation, where molecules were reduced to a coarse-grained representation consisting of a single isovolumetric spheroid and point dipole, with the molecular volume and dipole moment determined from electronic structure calculations. The ability to run simulations on flexible systems composed of atoms or coarse-grained representations of rigid groups (pseudo-atomistic Monte Carlo, or PAMC[13]) has since been ported to the new code by Andreas Tillack.

### *1.5.3. Molecular dynamics*

Unlike Monte Carlo simulations, which typically only consider positional degrees of freedom and only require calculation of potential energy, molecular dynamics[75] calculations involve propagating a system in time by calculating forces (F) for each potential function (U), with

$$F(\mathbf{r}) = -\nabla U(\mathbf{r}) \qquad (20)$$

and using them to update positions and velocities.[67a] For typical potential functions, these may be calculated analytically. The system follows a physical trajectory following Newton's equations of motion, which are numerically integrated using a stable but efficient method such as Velocity Verlet or Beeman algorithm and a small time step, often on the order of one femtosecond.[66b] The latter algorithm is shown below

$$\mathbf{r}(t+\Delta t) = \mathbf{r}(t) + \mathbf{v}(t)\Delta t + \frac{4\mathbf{f}(t) - \mathbf{f}(t-\Delta t)}{6m}\Delta t^2$$
$$\mathbf{v}(t+\Delta t) = \mathbf{v}(t) + \frac{2\mathbf{f}(t+\Delta t) + 5\mathbf{f}(t) - \mathbf{f}(t-\Delta t)}{6m}\Delta t \qquad (21)$$

where **v** is the velocity of a particle, **f** is the force on that particle, and m is the particle's mass.[67a] As the simulation conserves energy to within the error of the integrator, the natural ensemble for molecular dynamics calculations is the microcanonical (NVE) ensemble, though simulations can be run in the canonical or the isothermal-isobaric (NPT) ensembles through use of thermostat and barostat algorithms.[76]

Properties are calculated as an average over time steps, which may be broken up into an average over smaller blocks of steps

$$\langle A \rangle_b = \frac{1}{t_b} \sum_{i=1}^{t_b} A_i\left(r^N, p^N\right) \qquad (22)$$

where $t_b$ is the number of time steps in a block, for purposes of error analysis, since steps close to each other in time are likely to be highly correlated.

Molecular dynamics calculations used in this thesis were run using TINKER,[77] a software package developed by Jay Ponder at Washington University-St. Louis and used the Merck Molecular Force Field[71] (MMFF94) for interaction potentials. Data were analyzed using a mixture of built-in functions and in-house MATLAB code.

### *1.5.4. Electronic structure methods*

Electronic structure calculations were run with the commercial programs Gaussian 09,[78] developed by Gaussian, Inc., and Spartan 08,[79] developed by Wavefunction, Inc. All calculations were run in the LCAO (Linear Combination of Atomic Orbitals) approximation, representing molecular orbitals by basis sets of Gaussian-type orbitals, as well as the Born-Oppenheimer approximation (nuclear motion frozen during electronic energy calculations).[67c, 80] Routine ground-state calculations were run using *ab initio* Hartree-Fock theory,[67c] semi-empirical Hartree-Fock derivatives such as PM3[81] and PM6,[82] or density-functional[83] (DFT) methods. Most DFT calculations used hybrid functionals such as B3LYP[84] and M062X,[85] which mix in a fraction of Hartree-Fock exchange energy to correct for inexact calculation of electron exchange in current DFT functionals. Higher level methods such MP2 (second-order Møller-Plesset[86] perturbation theory) and CCSD (coupled cluster[87] with single and double excitations) were used for more rigorous validation calculations. These methods incorporate the majority of the effects of electron correlation (electron-electron interaction) without the empirical approximations[80] required in hybrid DFT. Excited state calculations were run using time-dependent DFT[88] (TDDFT) or Hartree-Fock[88b, 89] (TDHF). An abundance of information on wavefunction-based (non-DFT) electronic structure methods can be found in *Modern Quantum Chemistry: Introduction to Advanced Electronic Structure Theory* by Szabo and Ostlund.[67c]

## 1.6. Outline of Dissertation

Chapter 2 discusses the importance of shape effects, boundary conditions and system size in modeling the dielectric behavior of strongly polar systems. These systems are relevant to electro-optics due to similar dipole densities compared to chromophore-containing films at high loading. Tests are conducted using spherical and spheroidal models of an acetonitrile-like system. This chapter was published as Johnson, L. E.; Barnes, R.; Draxler, T. W.; Eichinger, B. E.; Robinson, B. H., *Journal of Physical Chemistry B* **2010,** *114* (25), 8431-8440.

Chapter 3 further explores shape effects in spheroidal systems, focusing on spheroids of similar size to those in Chapter 2, but with a range of dipole moments and aspect ratio on the dielectric behavior, spontaneous ordering, and phase behavior of these systems. Both simulations with and without applied electric fields are considered.

Chapter 4 explores a variety of methods used for predicting ordering behavior in organic electro-optic chromophores, including RBMC simulations similar to those in Chapters 2 and 3, as well as molecular dynamics calculations on C1 to study the effects of coumarin-coumarin interactions. This chapter combines new work as well as that from several co-authored papers.[27, 37]

Chapter 5 explores the difficulty in accurately calculating both the hyperpolarizability and absorption spectrum of high-b chromophores using hybrid DFT methods, and compares a variety of hybrid DFT calculations with higher-level MP2 calculations and results from HRS experiments.

Chapter 6 details the development, synthesis, and characterization of a novel chromophore developed for biophotonics applications using theory-aided

design and electronic structure calculations. Predicted hyperpolarizability is compared with HRS results, and binding affinity to DNA is benchmarked against common nucleic acid dye ethidium bromide.

## 1.7. References for Chapter 1


1. (a) *Cisco Visual Networking Index: Forecast and Methodology, 2010–2015*; Cisco Systems: San Jose, CA, 2011; (b) Dalton, L. R.; Steier, W. H.; Robinson, B. H.; Zhang, C.; Ren, A.; Garner, S.; Chen, A.; Londergan, T.; Irwin, L.; Carlson, B.; Fifield, L.; Phelan, G.; Kincaid, C.; Amend, J.; Jen, A., From molecules to opto-chips: organic electro-optic materials. *Journal of Materials Chemistry* **1999,** *9* (9), 1905-1920.
2. (a) Reed, G. T.; Mashanovich, G.; Gardes, F. Y.; Thomson, D. J., Silicon optical modulators. *Nature Photonics* **2010,** *4* (8), 518-526; (b) Maurer, R. D., Glass Fibers for Optical Communications. *Proceedings of the IEEE* **1973,** *61* (4), 452-462.
3. Baehr-Jones, T. W.; Hochberg, M. J., Polymer Silicon Hybrid Systems: A Platform for Practical Nonlinear Optics. *Journal of Physical Chemistry C* **2008,** *112* (21), 8085-8090.
4. (a) Clark, J.; Lanzani, G., Organic photonics for communications. *Nature Photonics* **2010,** *4*, 438-446; (b) Koos, C.; Vorreau, P.; Vallaitis, T.; Dumon, P.; Bogaerts, W.; Baets, R.; Esembeson, B.; Biaggio, I.; Michinobu, T.; Diederich, F.; Freude, W.; Leuthold, J., All-optical high-speed signal processing with silicon–organic hybrid slot waveguides. *Nature Photonics* **2009,** *3* (4), 216-219.
5. Dalton, L. R.; Sullivan, P. A.; Bale, D. H., Electric Field Poled Organic Electro-optic Materials: State of the Art and Future Prospects. *Chemical Reviews* **2010,** *110* (1), 25-55.
6. Paniccia, M.; Krutul, V.; Koehl, S. *Introducing Intel's Advances in Silicon Photonics*; Intel Corp.: Santa Clara, CA, 2004.
7. (a) Liu, A.; Jones, R.; Liao, L.; Samara-Rubio, D.; Rubin, D.; Cohen, O.; Nicolaescu, R.; Paniccia, M., A high-speed silicon optical modulator based on a metal–oxide–semiconductor capacitor. *Nature* **2004,** *427*, 615-618; (b) Lee, M.; Katz, H. E.; Erben, C.; Gill, D. M.; Gopalan, P.; Heber, J. D.; McGee, D. J., Broadband Modulation of Light by Using an Electro-Optic Polymer. *Science* **2002,** *298*, 1401-1403.
8. Zernike, F.; Midwinter, J. E., *Applied Nonlinear Optics*. Dover Publications, Inc.: Mineola, NY, 1973.
9. Melnichuk, M.; Wood, L., Direct Kerr electro-optic effect in noncentrosymmetric materials. *Physical Review A* **2010,** *82* (1), 013821.
10. Benight, S. J.; Bale, D. H.; Olbricht, B. C.; Dalton, L. R., Organic electro-optics: Understanding material structure/function relationships and device fabrication issues. *Journal of Materials Chemistry* **2009,** *19* (40), 7466.
11. (a) Shi, Y.; Zhang, C.; Zhang, H.; Bechtel, J. H.; Dalton, L. R.; Robinson, B. H.; Steier, W. H., Low (Sub-1-Volt) Halfwave Voltage Polymeric Electro-optic Modulators Achieved by Controlling Chromophore Shape. *Science* **2000,** *288* (5463), 119-122; (b) Luo, J.; Huang, S.; Shi, Z.; Polishak, B. M.; Zhou, X.-H.; Jen, A.

K. Y., Tailored Organic Electro-optic Materials and Their Hybrid Systems for Device Applications. *Chemistry of Materials* **2011,** *23* (3), 544-553.
12. Benight, S. J.; Robinson, B. H.; Dalton, L. R., Nano-Engineering of Molecular Interactions in Organic Electro-Optic Materials. In *Molecular Interactions*, Meghea, A., Ed. Intech: Rijeka, Croatia, 2011.
13. Sullivan, P. A.; Rommel, H. L.; Takimoto, Y.; Hammond, S. R.; Bale, D. H.; Olbricht, B. C.; Liao, Y.; Rehr, J.; Eichinger, B. E.; Jen, A. K.-Y.; Reid, P. J.; Dalton, L. R.; Robinson, B. H., Modeling the Optical Behavior of Complex Organic Media: From Molecules to Materials. *Journal of Physical Chemistry B* **2009,** *113* (47), 15581-15588.
14. Sullivan, P. A.; Dalton, L. R., Theory-Inspired Development of Organic Electro-optic Materials. *Accounts of Chemical Research* **2009,** *43* (1), 10-18.
15. Kaino, T.; Tomaru, S., Organic Materials for Nonlinear Optics. *Advanced Materials* **1993,** *5* (3), 172-178.
16. Olbrechts, G.; Wostyn, K.; Clays, K.; Persoons, A., High-frequency demodulation of multiphoton fluorescence in long-wavelength hyper-Rayleigh scattering. *Optics Letters* **1999,** *24* (6), 403-405.
17. (a) Szablewski, M.; Thomas, P. R.; Thornton, A.; Bloor, D.; Cross, G. H.; Cole, J. M.; Howard, J. A. K.; Malagoli, M.; Meyers, F.; Brédas, J.-L.; Wenseleers, W.; Goovaerts, E., Highly Dipolar, Optically Nonlinear Adducts of Tetracyano-p-quinodimethane: Synthesis, Physical Characterization, and Theoretical Aspects. *Journal of the American Chemical Society* **1997,** *119* (13), 3144-3154; (b) Ma, H.; Chen, B.; Sassa, T.; Dalton, L. R.; Jen, A. K.-Y., Highly Efficient and Thermally Stable Nonlinear Optical Dendrimer for Electrooptics. *Journal of the American Chemical Society* **2001,** *123* (5), 986-987; (c) Zhang, C.; Dalton, L. R., Low Vπ Electrooptic Modulators from CLD-1: Chromophore Design and Synthesis, Material Processing, and Characterization. *Chemistry of Materials* **2001,** *13* (9), 3043-3050; (d) Liao, Y.; Bhattacharjee, S.; Firestone, K. A.; Eichinger, B. E.; Paranji, R.; Anderson, C. A.; Robinson, B. H.; Reid, P. J.; Dalton, L. R., Antiparallel-Aligned Neutral-Ground-State and Zwitterionic Chromophores as a Nonlinear Optical Material. *Journal of the American Chemical Society* **2005,** *128* (21), 6847-6853; (e) Liao, Y.; Anderson, C. A.; Sullivan, P. A.; Akelaitis, A. J. P.; Robinson, B. H.; Dalton, L. R., Electro-Optical Properties of Polymers Containing Alternating Nonlinear Optical Chromophores and Bulky Spacers. *Chemistry of Materials* **2006,** *18* (4), 1062-1067; (f) Sullivan, P. A.; Rommel, H.; Liao, Y.; Olbricht, B. C.; Akelaitis, A. J. P.; Firestone, K. A.; Kang, J.-W.; Luo, J.; Davies, J. A.; Choi, D. H.; Eichinger, B. E.; Reid, P. J.; Chen, A.; Jen, A. K. Y.; Robinson, B. H.; Dalton, L. R., Theory-Guided Design and Synthesis of Multichromophore Dendrimers: An Analysis of the Electro-optic Effect. *Journal of the American Chemical Society* **2007,** *129* (24), 7523-7530; (g) Hammond, S. R.; Clot, O.; Firestone, K. A.; Bale, D. H.; Lao, D.; Haller, M.; Phelan, G. D.; Carlson, B.; Jen, A. K.-Y.; Reid, P. J.; Dalton, L. R., Site-Isolated Electro-optic Chromophores Based on Substituted 2,2′-Bis(3,4-propylenedioxythiophene) π-Conjugated Bridges. *Chemistry of Materials* **2008,** *20* (10), 3425-3434.
18. (a) Dalton, L. R.; Benight, S. J.; Johnson, L. E.; Knorr, D. B.; Kosilkin, I.; Eichinger, B. E.; Robinson, B. H.; Jen, A. K. Y.; Overney, R. M., Systematic Nanoengineering of Soft Matter Organic Electro-optic Materials. *Chemistry of Materials* **2011,** *23* (3), 430-445; (b) Bale, D. H.; Eichinger, B. E.; Liang, W.; Li, X.;

Dalton, L. R.; Robinson, B. H.; Reid, P. J., Dielectric dependence of the first molecular hyperpolarizability for electro-optic chromophores. *J Phys Chem B* **2011,** *115* (13), 3505-13.
19. Melikian, G.; Rouessac, F. P.; Alexandre, C., Synthesis of Substituted Dicyanomethylendihydrofurans. *Synthetic Communications* **1995,** *25*, 3045-3051.
20. Bale, D. H. Nonlinear optical materials characterization studies employing photostability, hyper-Rayleigh scattering, and electric field induced second harmonic generation techniques. University of Washington, Seattle, WA, 2008.
21. Davies, J. A.; Elangovan, A.; Sullivan, P. A.; Olbricht, B. C.; Bale, D. H.; Ewy, T. R.; Isborn, C. M.; Eichinger, B. E.; Robinson, B. H.; Reid, P. J.; Li, X.; Dalton, L. R., Rational Enhancement of Second-Order Nonlinearity: Bis-(4-methoxyphenyl)hetero-aryl-amino Donor-Based Chromophores: Design, Synthesis, and Electrooptic Activity. *Journal of the American Chemical Society* **2008,** *130* (32), 10565-10575.
22. Jang, S.-H.; Luo, J.; Tucker, N. M.; Leclercq, A.; Zojer, E.; Haller, M. A.; Kim, T.-D.; Kang, J.-W.; Firestone, K.; Bale, D.; Lao, D.; Benedict, J. B.; Cohen, D.; Kaminsky, W.; Kahr, B.; Brédas, J.-L.; Reid, P.; Dalton, L. R.; Jen, A. K.-Y., Pyrroline Chromophores for Electro-Optics. *Chemistry of Materials* **2006,** *18* (13), 2982-2988.
23. Dalton, L. R.; Harper, A. W.; Ghosn, R.; Steier, W. H.; Ziari, M.; Fetterman, H.; Shi, Y.; Mustachich, R. V.; Jen, A. K.-Y.; Shea, K. J., Synthesis and Processing of Improved Organic Second-Order Nonlinear Optical Materials for Applications in Photonics. *Chemistry of Materials* **1995,** *7* (6), 1060-1081.
24. Singer, K. D.; Sohn, J. E.; Lalama, S. J., Second harmonic generation in poled polymer films. *Applied Physics Letters* **1986,** *49* (5), 248.
25. Pan, F.; Wong, M. S.; Bosshard, C.; Günter, P., Crystal Growth and Characterization of the Organic Salt 4-N,N-Dimethylamino-4'-N'- methyl-stilbazolium Tosylate (DAST). *Advanced Materials* **1996,** *8* (7), 592-595.
26. Kwon, O. P.; Kwon, S.-J.; Jazbinsek, M.; Brunner, F. D. J.; Seo, J.-I.; Hunziker, C.; Schneider, A.; Yun, H.; Lee, Y.-S.; Günter, P., Organic Phenolic Configurationally Locked Polyene Single Crystals for Electro-optic and Terahertz Wave Applications. *Advanced Functional Materials* **2008,** *18* (20), 3242-3250.
27. Olbricht, B. C.; Sullivan, P. A.; Dennis, P. C.; Hurst, J. T.; Johnson, L. E.; Benight, S. J.; Davies, J. A.; Chen, A.; Eichinger, B. E.; Reid, P. J.; Dalton, L. R.; Robinson, B. H., Measuring Order in Contact-Poled Organic Electrooptic Materials with Variable-Angle Polarization-Referenced Absorption Spectroscopy (VAPRAS). *Journal of Physical Chemistry B* **2011,** *115* (2), 231-241.
28. Kuzyk, M. G.; Singer, K. D.; Zahn, H. E.; King, L. A., Second-order nonlinear-optical tensor properties of poled films under stress. *Journal of the Optical Society of America B* **1989,** *6* (4), 742-752.
29. Mortazavi, M. A.; Knoesen, A.; Kowel, S. T.; Higgins, B. G.; Dienes, A., Second-harmonic generation and absorption studies of polymer-dye films oriented by corona-onset poling at elevated temperatures. *Journal of the Optical Society of America B* **1989,** *6* (4), 733-741.
30. Olbricht, B. C.; Sullivan, P. A.; Wen, G.-A.; Mistry, A. A.; Davies, J. A.; Ewy, T. R.; Eichinger, B. E.; Robinson, B. H.; Reid, P. J.; Dalton, L. R., Laser-Assisted Poling of Binary Chromophore Materials. *Journal of Physical Chemistry C* **2008,** *112* (21), 7983-7988.

31. Firestone, M. A.; Ratner, M. A.; Marks, T. J., Electric Field Poling in Polymeric Nonlinear Optical Materials.
Relaxation Dynamics, Model, and Experiment. *Macromolecules* **1995,** *28* (18), 6296-6310.
32. Liang, W.; Li, X.; Dalton, L. R.; Robinson, B. H.; Eichinger, B. E., Solvents level dipole moments. *J Phys Chem B* **2011,** *115* (43), 12566-70.
33. Nielsen, R. D.; Rommel, H. L.; Robinson, B. H., Simulation of the Loading Parameter in Organic Nonlinear Optical Materials. *Journal of Physical Chemistry B* **2004,** *108* (25), 8659-8667.
34. Leahy-Hoppa, M. R.; Cunningham, P. D.; French, J. A.; Hayden, L. M., Atomistic Molecular Modeling of the Effect of Chromophore Concentration on the Electro-optic Coefficient in Nonlinear Optical Polymers. *The Journal of Physical Chemistry A* **2006,** *110* (17), 5792-5797.
35. Rommel, H. L.; Robinson, B. H., Orientation of Electro-optic Chromophores under Poling Conditions: A Spheroidal Model. *Journal of Physical Chemistry C* **2007,** *111* (50), 18765-18777.
36. (a) Kim, T.-D.; Kang, J.-W.; Luo, J.; Jang, S.-H.; Ka, J.-W.; Tucker, N.; Benedict, J. B.; Dalton, L. R.; Gray, T.; Overney, R. M.; Park, D. H.; Herman, W. N.; Jen, A. K.-Y., Ultralarge and Thermally Stable Electro-Optic Activities from Supramolecular Self-Assembled Molecular Glasses. *Journal of the American Chemical Society* **2007,** *129* (3), 488-489; (b) Knorr, D. B., Jr.; Zhou, X. H.; Shi, Z.; Luo, J.; Jang, S. H.; Jen, A. K.; Overney, R. M., Molecular mobility in self-assembled dendritic chromophore glasses. *J Phys Chem B* **2009,** *113* (43), 14180-8.
37. (a) Benight, S. J.; Johnson, L. E.; Barnes, R.; Olbricht, B. C.; Bale, D. H.; Reid, P. J.; Eichinger, B. E.; Dalton, L. R.; Sullivan, P. A.; Robinson, B. H., Reduced Dimensionality in Organic Electro-Optic Materials: Theory and Defined Order. *Journal of Physical Chemistry B* **2010,** *114* (37), 11949-11956; (b) Benight, S. J.; Daniel B. Knorr, J.; Johnson, L. E.; Sullivan, P. A.; Lao, D.; Sun, J.; Kocherlakota, L. S.; Elangovan, A.; Robinson, B. H.; Overney, R. M.; Dalton, L. R., Nano-Engineering Soft Matter Lattice Dimensionality for an Organic Electro-Optic Material. *Advanced Materials* **2012,** *IN PRESS*.
38. Jackson, P. O.; Karapinar, R.; O'Neill, M.; Hindmarsh, P.; J.Owen, G.; Kelly, S. M., Alignment models for coumarin-containing polymers for liquid crystal. *Proceedings of SPIE* **1999,** *3635*, 38-47.
39. Greenlee, C.; Guilmo, A.; Opadeyi, A.; Himmelhuber, R.; Norwood, R. A.; Fallahi, M.; Luo, J.; Huang, S.; Zhou, X.-H.; Jen, A. K. Y.; Peyghambarian, N., Mach-Zehnder interferometry method for decoupling electro-optic and piezoelectric tensor components in poled polymer films. **2010**, 77740D-77740D-10.
40. Hayden, L. M.; Sauter, G. F.; Ore, F. R.; Pasillas, P. L.; Hoover, J. M.; Lindsay, G. A.; Henry, R. A., Second-order nonlinear optical measurements in guest-host and side-chain polymers. *Journal of Applied Physics* **1990,** *68* (2), 456.
41. Teng, C. C.; Man, H. T., Simple reflection technique for measuring the electro-optic coefficient of poled polymers. *Applied Physics Letters* **1990,** *56* (18), 1734.
42. Chen, A.; Chuyanov, V.; Garner, S.; Steier, W. H.; Dalton, L. R. In *Modified attenuated total reflection for the fast and routine electro-optic measurement of nonlinear optical polymer thin films*, Organic Thin Films for Photonics Applications, Long Beach, CA, Long Beach, CA, 1997; pp 158-160.

43. Onodera, H.; Awal, I.; Ikenoue, J.-i., Refractive-index measurement of bulk materials: prism coupling method. *Applied Optics* **1983,** *22* (8), 1194-1197.
44. Benight, S. J. Nanoengineering of soft matter interactions in organic electro-optic materials. University of Washington, Seattle, WA, 2011.
45. Olbricht, B. C. Characterization and processing of organic nonlinear optical materials using ellipsometric, waveguiding, and absorption spectroscopy techniques. University of Washington, Seattle, WA, 2010.
46. (a) Finn, R. S., Measurements of hyperpolarizabilities for some halogenated methanes. *The Journal of Chemical Physics* **1974,** *60* (2), 454; (b) Levine, B. F., Absolute signs of hyperpolarizabilities in the liquid state. *The Journal of Chemical Physics* **1974,** *60* (10), 3856; (c) Singer, K. D.; Kuzyk, M. G.; Sohn, J. E., Second-order nonlinear-optical processes in orientationally ordered materials: relationship between molecular and macroscopic properties. *Journal of the Optical Society of America B* **1987,** *4* (6), 968-976.
47. (a) Clays, K.; Persoons, A., Hyper-Rayleigh Scattering in Solution. *Physical Review Letters* **1991,** *66* (23), 2980-2983; (b) Clays, K.; Persoons, A., Hyper-Rayleigh scattering in solution. *Review of Scientific Instruments* **1992,** *63* (6), 3285; (c) Firestone, K. A.; Reid, P.; Lawson, R.; Jang, S.-H.; Dalton, L. R., Advances in organic electro-optic materials and processing. *Inorganica Chimica Acta* **2004,** *357* (13), 3957-3966.
48. Cyvin, S. J.; Rauch, J. E.; Decius, J. C., Theory of Hyper-Raman Effects (Nonlinear Inelastic Light Scattering): Selection Rules and Depolarization Ratios for the Second-Order Polarizability. *The Journal of Chemical Physics* **1965,** *43* (11), 4083.
49. Oudar, J. L.; Chemla, D. S., Hyperpolarizabilities of the nitroanilines and their relations to the excited state dipole moment. *The Journal of Chemical Physics* **1977,** *66* (6), 2664-2668.
50. Firestone, K. A. Frequency-agile hyper-Rayleigh scattering studies of nonlinear optical chromophores. University of Washington, Seattle, 2005.
51. Bortchagovsky, E. G., Ellipsometric method for investigation of the optical anisotropy of thin films: theory and calculations. *Thin Solid Films* **1997,** *307*, 192-199.
52. Mansuripur, M., Analysis of multilayer thin-film structures containing magneto-optic and anisotropic media at oblique incidence using 2×2 matrices. *Journal of Applied Physics* **1990,** *67* (10), 6466.
53. Jones, R. C., A New Calculus for the Treatment of Optical Systems. *Journal of the Optical Society of America* **1941,** *31*, 488-493.
54. Johal, M. S., *Understanding Nanomaterials*. CRC Press: Boca Raton, FL, 2011.
55. Sturm, J.; Tasch, S.; Niko, A.; Leising, G.; Toussaere, E.; Zyss, J.; Kowalczyk, T. C.; Singer, K. D.; Scherf, U.; Huber, J., Optical anisotropy in thin films of a blue electroluminescent conjugated polymer. *Thin Solid Films* **1997,** *298*, 138-142.
56. Drenser, K. A.; Larsen, R. J.; Strohkendl, F. P.; Dalton, L. R., Femtosecond, Frequency-Agile, Phase-Sensitive-Detected, Multi-Wave-Mixing Nonlinear Optical Spectroscopy Applied to π-Electron Photonic Materials. *Journal of physical Chemistry A* **1999,** *103* (14), 2290-2301.
57. (a) Praprotnik, M.; Site, L. D.; Kremer, K., Multiscale simulation of soft matter: from scale bridging to adaptive resolution. *Annu Rev Phys Chem* **2008,** *59*, 545-71; (b) Peter, C.; Kremer, K., Multiscale simulation of soft matter systems –

from the atomistic to the coarse-grained level and back. *Soft Matter* **2009,** *5* (22), 4357; (c) Peter, C.; Kremer, K., Multiscale simulation of soft matter systems. *Faraday Discussions* **2010,** *144*, 9; (d) Izvekov, S.; Voth, G. A., Multiscale coarse graining of liquid-state systems. *The Journal of Chemical Physics* **2005,** *123* (13), 134105.
58. Zhou, J.; Thorpe, I. F.; Izvekov, S.; Voth, G. A., Coarse-grained peptide modeling using a systematic multiscale approach. *Biophys J* **2007,** *92* (12), 4289-303.
59. Shi, Q.; Izvekov, S.; Voth, G. A., Mixed Atomistic and Coarse-Grained Molecular Dynamics: Simulation of a Membrane-Bound Ion Channel. *Journal of Physical Chemistry B* **2006,** *110* (31), 15045-15048.
60. (a) Zeng, Q. H.; Yu, A. B.; Lu, G. Q., Multiscale modeling and simulation of polymer nanocomposites. *Progress in Polymer Science* **2008,** *33* (2), 191-269; (b) Handgraaf, J.-W.; Serral Gracia, R.; Nath, S. K.; Chen, Z.; Chou, S.-H.; Ross, R. B.; Schultz, N. E.; Fraaije, J. G. E. M., A Multiscale Modeling Protocol To Generate Realistic Polymer Surfaces. *Macromolecules* **2011,** *44* (4), 1053-1061.
61. (a) Vreven, T.; Byun, K. S.; Komáromi, I.; Dapprich, S.; John A. Montgomery, J.; Morokuma, K.; Frisch, M. J., Combining Quantum Mechanics Methods with Molecular Mechanics Methods in ONIOM. *Journal of Chemical Theory and Computation* **2006,** *2* (3), 815-826; (b) Woodcock, H. L.; Miller, B. T.; Hodoscek, M.; Okur, A.; Larkin, J. D.; Ponder, J. W.; Brooks, B. R., MSCALE: A General Utility for Multiscale Modeling. *Journal of Chemical Theory and Computation* **2011,** *7* (4), 1208-1219.
62. Shao, Y.; Molnar, L. F.; Jung, Y.; Kussmann, J.; Ochsenfeld, C.; Brown, S. T.; Gilbert, A. T.; Slipchenko, L. V.; Levchenko, S. V.; O'Neill, D. P.; DiStasio, R. A., Jr.; Lochan, R. C.; Wang, T.; Beran, G. J.; Besley, N. A.; Herbert, J. M.; Lin, C. Y.; Van Voorhis, T.; Chien, S. H.; Sodt, A.; Steele, R. P.; Rassolov, V. A.; Maslen, P. E.; Korambath, P. P.; Adamson, R. D.; Austin, B.; Baker, J.; Byrd, E. F.; Dachsel, H.; Doerksen, R. J.; Dreuw, A.; Dunietz, B. D.; Dutoi, A. D.; Furlani, T. R.; Gwaltney, S. R.; Heyden, A.; Hirata, S.; Hsu, C. P.; Kedziora, G.; Khalliulin, R. Z.; Klunzinger, P.; Lee, A. M.; Lee, M. S.; Liang, W.; Lotan, I.; Nair, N.; Peters, B.; Proynov, E. I.; Pieniazek, P. A.; Rhee, Y. M.; Ritchie, J.; Rosta, E.; Sherrill, C. D.; Simmonett, A. C.; Subotnik, J. E.; Woodcock, H. L., 3rd; Zhang, W.; Bell, A. T.; Chakraborty, A. K.; Chipman, D. M.; Keil, F. J.; Warshel, A.; Hehre, W. J.; Schaefer, H. F., 3rd; Kong, J.; Krylov, A. I.; Gill, P. M.; Head-Gordon, M., Advances in methods and algorithms in a modern quantum chemistry program package. *Phys Chem Chem Phys* **2006,** *8* (27), 3172-91.
63. Greengard, L., Fast Algorithms for Classical Physics. *Science* **1994,** *265* (5174), 909-914.
64. Darden, T.; York, D.; Pedersen, L., Particle mesh Ewald: An N•log(N) method for Ewald sums in large systems. *The Journal of Chemical Physics* **1993,** *98* (12), 10089-10092.
65. Schwegler, E.; Challacombe, M., Linear scaling computation of the Hartree–Fock exchange matrix. *Journal of Chemical Physics* **1996,** *105* (7), 2726-2734.
66. (a) Cramer, C. J., *Essentials of Computational Chemistry: Theories and Models*. John Wiley & Sons Ltd.: Chinchester, UK, 2004; (b) Leach, A. R., *Molecular Modeling: Principles and Applications*. 2nd ed.; Pearson Education: Harlow (UK), 2001.

67. (a) Frenkel, D., Smidt, B., *Understanding Molecular Simulation: From Algorithms to Applications*. Elsevier: Amsterdam (ND), 2002; (b) Allen, M. P., Tildesley, D.J., *Computer Simulations of Liquids*. Clarendon: Oxford (UK), 1987; (c) Szabo, A.; Ostlund, N. S., *Modern Quantum Chemistry: Introduction to Advanced Electronic Structure Theory*. 1st (revised) ed.; Dover Publications, Inc.: New York, NY, 1989.
68. McQuarrie, D. A., *Statistical Mechanics*. University Science Books: Sausalito, CA, 2000.
69. Cornell, W. D.; Cieplak, P.; Bayly, C. I.; Gould, I. R.; Kenneth M. Merz, J.; Ferguson, D. M.; Spellmeyer, D. C.; Fox, T.; Caldwell, J. W.; Kollman, P. A., A Second Generation Force Field for the Simulation of Proteins, Nucleic Acids, and Organic Molecules. *Journal of the American Chemical Society* **1995,** *117* (19), 5179-5197.
70. Jorgensen, W. L.; Tirado-Rives, J., The OPLS Potential Functions for Proteins. Energy Minimizations for Crystals of Cyclic Peptides and Crambin. *Journal of the American Chemical Society* **1988,** *110* (6), 1657-1666.
71. Halgren, T. A., Merck Molecular Force Field. I. Basis, Form, Scope, Parameterization, and Performance of MMFF94. *Journal of Computational Chemistry* **1996,** *17* (5), 490-519.
72. Hansen, J.-P., McDonald, I.R., *Theory of Simple Liquids*. 3rd ed.; Elsevier: Amsterdam, Netherlands, 2006.
73. Metropolis, N., Rosenbluth, A. W., Rosenbluth, M. N., Teller, A H., Teller, E., Equation of State Calculations by Fast Computing Machines. *Journal of Chemical Physics* **1953,** *21* (6), 1087-1092.
74. Robinson, B. H.; Dalton, L. R., Monte Carlo statistical mechanical simulations of the competition of intermolecular electrostatic and poling-field interactions in defining macroscopic electro-optic activity for organic chromophore/polymer materials. *Journal of Physical Chemistry A* **2000,** *104* (20), 4785-4795.
75. Alder, B. J., Wainright, T.E., Phase Transition for a Hard Sphere System. *Journal of Chemical Physics* **1957,** *27*, 1208-1209.
76. Berendsen, H. J. C.; Postma, J. P. M.; van Gunsteren, W. F.; DiNola, A.; Haak, J. R., Molecular dynamics with coupling to an external bath. *The Journal of Chemical Physics* **1984,** *81* (8), 3684.
77. Ponder, J. *TINKER*, 5.1; Washington University: St. Louis MO, 2010.
78. Frisch, M. J.; Trucks, G. W.; Schlegel, H. B.; Scuseria, G. E.; Robb, M. A.; Cheeseman, J. R.; G. Scalmani, V. B.; Mennucci, B.; Petersson, G. A.; Nakatsuji, H.; Caricato, M.; Li, X.; Hratchian, H. P.; Izmaylov, A. F.; Bloino, J.; Zheng, G.; Sonnenberg, J. L.; Hada, M.; Ehara, M.; Toyota, K.; Fukuda, R.; Hasegawa, J.; Ishida, M.; Nakajima, T.; Honda, Y.; Kitao, O.; Nakai, H.; Vreven, T.; J. A. Montgomery, J.; Peralta, J. E.; Ogliaro, F.; Bearpark, M.; Heyd, J. J.; Brothers, E.; Kudin, K. N.; Staroverov, V. N.; Kobayashi, R.; Normand, J.; Raghavachari, K.; Rendell, A.; Burant, J. C.; Iyengar, S. S.; Tomasi, J.; Cossi, M.; Rega, N.; Millam, J. M.; Klene, M.; Knox, J. E.; Cross, J. B.; Bakken, V.; Adamo, C.; Jaramillo, J.; Gomperts, R.; Stratmann, R. E.; Yazyev, O.; Austin, A. J.; Cammi, R.; Pomelli, C.; Ochterski, J. W.; Martin, R. L.; Morokuma, K.; Zakrzewski, V. G.; Voth, G. A.; Salvador, P.; Dannenberg, J. J.; Dapprich, S.; Daniels, A. D.; Farkas, Ö.; Foresman, J. B.; Ortiz, J. V.; Cioslowski, J.; Fox, D. J. *Gaussian 09*, Revision C.01; Gaussian, Inc.: Wallingford, CT, 2009.

79. *Spartan '08*, 1.2.0; Wavefunction, Inc.: Irvine, CA, 2008.
80. Levine, I. N., *Quantum Chemistry*. Prentice-Hall, Inc.: Upper Saddle River, NJ, 2000.
81. Stewart, J. J. P., Optimization of parameters for semiempirical methods I. Method. *Journal of Computational Chemistry* **1989,** *10* (2), 209-220.
82. Stewart, J. J., Optimization of parameters for semiempirical methods V: modification of NDDO approximations and application to 70 elements. *J Mol Model* **2007,** *13* (12), 1173-213.
83. Hohenberg, P.; Kohn, W., Inhomogeneous Electron Gas. *Physical Review* **1964,** *136* (3B), B864-B871.
84. (a) Stephens, P. J.; Devlin, F. J.; Chabalowski, C. F.; Frisch, M. J., Ab Initio Calculation of Vibrational Absorption and Circular Dichroism Spectra Using Density Functional Force Fields. *Journal of Physical Chemistry* **1994,** *98* (45), 11623-11627; (b) Becke, A. D., A new mixing of Hartree-Fock and local density-functional theories. *The Journal of Chemical Physics* **1993,** *98* (2), 1372-1377.
85. Zhao, Y.; Truhlar, D. G., The M06 suite of density functionals for main group thermochemistry, thermochemical kinetics, noncovalent interactions, excited states, and transition elements: two new functionals and systematic testing of four M06-class functionals and 12 other functionals. *Theoretical Chemistry Accounts* **2007,** *120* (1-3), 215-241.
86. Møller, C.; Plesset, M. S., Note on an Approximation Treatment for Many-Electron Systems. *Physical Review* **1934,** *46* (7), 618-622.
87. Čížek, J. i., On the Correlation Problem in Atomic and Molecular Systems. Calculation of Wavefunction Components in Ursell-Type Expansion Using Quantum-Field Theoretical Methods. *The Journal of Chemical Physics* **1966,** *45* (11), 4256.
88. (a) Runge, E.; Gross, E. K. U., Density-Functional Theory for Time-Dependent Systems. *Physical Review Letters* **1984,** *52* (12), 997-1000; (b) Dreuw, A.; Head-Gordon, M., Single-Reference ab Initio Methods for the Calculation of Excited States of Large Molecules. *Chemical Reviews* **2005,** *105* (11), 4009-4037.
89. McLachlan, A.; Ball, M., Time-Dependent Hartree—Fock Theory for Molecules. *Reviews of Modern Physics* **1964,** *36* (3), 844-855.

# 2. Dielectric Constants of Simple Liquids: Stockmayer and Ellipsoidal Fluids

This chapter is adapted with permission from Johnson, L. E.; Barnes, R.; Draxler, T. W.; Eichinger, B. E.; Robinson, B. H., Dielectric Constants of Simple Liquids: Stockmayer and Ellipsoidal Fluids. *Journal of Physical Chemistry B* **2010,** *114* (25), 8431-8440. 

## 2.1. Introduction

Accurately modeling the dielectric behavior of liquids, whether using continuum models or explicit representations of molecules, has remained one of the major challenges of molecular modeling[1] since the landmark papers by Onsager[2] and Kirkwood[3] in the 1930s. Their models combined statistical mechanics and continuum electrostatics to approximate real liquids. As computer simulation methods began to be applied to polar and polarizable materials, a need emerged for accurately and efficiently representing the electrostatic behavior in many-body systems. Extensive work in the 1980s[4] focused on testing different electrostatic boundary conditions on simple models of liquids, *e.g.*, the dipolar hard-sphere[1b, 5] and Stockmayer[4e] (Lennard-Jones spheres containing a single point dipole in the center) fluids, and settled on a variant of the Ewald summation method[6] as the dominant boundary condition.[1c, 7] This early work also included development and validation of integral equation models for these fluids.[4c, 4e, 8] While simple liquid models can be examined both analytically and numerically, their dielectric properties often exhibit significant disagreement with real liquids. These include the prediction from Stockmayer-type systems that strongly polar aprotic liquids such as acetonitrile would have dielectric constants an order of magnitude larger than experiment and exhibit ferroelectric behavior.[1c, 9]

Many attempts have been made to examine simple Stockmayer-like liquids that go beyond the model of a non-polarizable point dipole. Several recent papers[10] have examined a linearly polarizable variant of the Stockmayer fluid; Valisko and Boda[11] compared simulations for polarizable Stockmayer models with experimental data. A recent paper by Szalai, et al.[12] discusses nonlinear dielectric behavior in the dipolar Yukawa fluid, accounting for saturation effects under high field strengths. Earlier work by Groh and Dietrich[13] also examined the orientational ordering of spherocylinders and ellipsoids containing magnetic dipoles using classical density-functional theory, as well as the structure of ferromagnetic domains in a magnetic Stockmayer fluid. Finally, our group has previously examined acentric ordering of dipolar ellipsoids under minimum image boundary conditions[14].

The exponential growth in available computing power in the past three decades has allowed systems that were previously intractable on supercomputers[5] to now be easily simulated on inexpensive hardware.[1c] More complex simulations of tens of thousands of multi-center molecules[9a] have also become commonplace. Simulations using united-atom or fully atomistic methods have been able to obtain reasonable dielectric constants for strongly dipolar liquids such as acetonitrile[9a, 15] or dimethyl sulfoxide[16], or hydrogen-bonding liquids such as ethanol[17]. While more complex models can be used to obtain reasonable estimates of dielectric behavior, the present work was undertaken to explore the boundary condition problem for relatively simple systems so as to separate electrostatic and steric influences on dielectric behavior. We re-examine the effects of electrostatic boundary conditions on systems involving thousands of non-polarizable Stockmayer particles, going well beyond the dozens[18] or

hundreds[4b] of particles in previous studies in order to evaluate both dipolar correlation in more distant neighbor shells and the effects of system size on dielectric behavior. We also examine steric effects by means of an anisotropic modified Stockmayer-like fluid consisting of prolate spheroids (ellipsoidal fluid) and compare the behavior of both models with strongly dipolar liquids such as acetonitrile.

## 2.2. Theory

Studies of the static dielectric constant must start with the relationship between the electric field in a material and the polarization of that material in response to the field. In linear isotropic materials the polarization is given by

$$\left(\varepsilon - 1\right)\mathbf{E} = 4\pi\mathbf{P} \qquad (2\text{-}1)$$

where $\varepsilon$ is the relative dielectric constant, **E** is the electric field within the (bulk) material, and **P** is the total dipole moment of the material per unit volume.[19] If the electronic polarizability $\alpha$ and higher-order terms are neglected, leaving only permanent dipoles, the equation reduces to

$$\begin{aligned}\left(\varepsilon - 1\right)\mathbf{E} &= \frac{4\pi\mathbf{M}}{V} = 4\pi\rho_N\left\langle\boldsymbol{\mu}\right\rangle \\ \left(\varepsilon - 1\right)\left|E\right| &= 4\pi\rho_N\left|\mu\right|\left\langle\cos\theta\right\rangle_E\end{aligned} \qquad (2\text{-}2)$$

where $V$ is the volume of the system, $\mathbf{M} = \sum_{i=1}^{N}\boldsymbol{\mu}_i$ is the total dipole moment of the system, $\rho_N$ is the number density, $\left\langle\boldsymbol{\mu}\right\rangle$ is the ensemble average molecular dipole moment, $\left|\mu\right|$ is the magnitude of the dipole moment, and $\left\langle\cos\theta\right\rangle_E$ is the angle between the thermally averaged dipole moment of the system and **E**.

Determining the relationship between $\langle \boldsymbol{\mu} \rangle$ and **E** also requires making assumptions about the local electric field **F** acting on individual molecules. All three of the major mean-field dielectric models for liquids (Debye, Onsager, and Kirkwood-Fröhlich) invoke continuum electrostatics and consider the molecules to be within a spherical cavity embedded within a large volume of dielectric material.[2-3, 20] These theories further decompose the field into external, cavity, and molecular dipole components. Debye's treatment of the induced polarization of the dielectric continuum around the spherical cavity assumes complete correlation of the dipoles and incorrectly predicts ferroelectric behavior at a low dipole density[2], while the Onsager model assumes no correlation between dipoles[10d].

Kirkwood improved upon the Onsager model by adding a parameter to represent short-range dipolar correlation. Kirkwood's model considers an ensemble of dipoles within a spherical cavity surrounded by a large spherical shell of continuous dielectric, where the average polarization is calculated in terms of fluctuations in the total dipole moment **M** within the inner sphere at $\mathbf{E}_0 = 0$. The model accounts for short-range correlations between dipoles by means of a scalar correlation factor[3, 4d, 21]

$$g_K = 1 + z\langle \cos\gamma \rangle \qquad (2\text{-}3)$$

where γ is the internal angle between a pair of dipoles and $z$ is the number of neighboring dipoles examined. His result, known as the Kirkwood, or Kirkwood-Fröhlich equation, has the same fundamental form as Onsager's equation despite being derived using different boundary conditions. The relationship between $\varepsilon$ and dipole density in the Kirkwood result is

$$\frac{(\varepsilon-1)(2\varepsilon+1)}{3\varepsilon}=\frac{4\pi\rho_N\mu^2}{3kT}g_K \quad (2\text{-}4)$$

and differs from the Onsager[2] result by the inclusion of the correlation function $g_K$. A rigorous derivations of the Kirkwood-Fröhlich equation can be found in Kirkwood's 1939 paper, as well as several newer sources.[21-22]

While the inclusion of short-range correlation makes the Kirkwood-Fröhlich equation a more realistic option for calculating dielectric constants, it requires an accurate estimate of the local correlation, which can come from integral equation approximations, experiments, or computer simulations. Our work focuses on computer simulations of the dielectric constant.

Unlike the continuum models described above, computer simulations consider systems containing a large but finite number of particles, and are typically implemented with periodic boundary conditions using the Minimum Image (MI) convention[6a] for short-range electrostatic and van der Waals (i.e. Lennard-Jones) interactions. Either type of interaction may also be truncated to a region (typically spherical) smaller than the minimum image.[1a, 6a] Long-range interaction models are typically used to represent electrostatic interactions with the region beyond the minimum image

Long-range electrostatic models can be divided into two main categories, (1) Ewald Sums, and (2) Reaction Field. The Ewald summation method augments the minimum image convention by means of repeating images of the central box.[6b, 23] While Ewald sums are known to impose artificial periodicity and overestimate the magnitude of fluctuations in simulations,[1a] they converge rapidly with simulation size[7] and have been widely accepted in the modeling community.

An alternate method of simulating long-range electrostatic interactions is to implement the Onsager reaction field (RF) method.[10d, 18] Interactions are evaluated explicitly out to some cutoff distance $R_{cut}$, with anything outside the cutoff treated as a continuous medium with dielectric constant $\varepsilon_s$. Polarization of the continuous medium in response to the total polarization from the net dipole moment within the cutoff radius ($\mathbf{M}_{\mathbf{sphere}}$) produces an electric field $\mathbf{R}_i$ that acts back on the *i*th dipole, located at the center of the cavity. The reaction field is expressed as

$$\mathbf{R}_i = \frac{2(\varepsilon_s - 1)}{(2\varepsilon_s + 1) R_{cut}^3} \sum_{r_{ij} < R_{cut}} \boldsymbol{\mu}_j \qquad (2\text{-}5)$$

Since the orientation of each dipole is not necessarily parallel to $\mathbf{M}_{\text{sphere}}$, the reaction field is able to exert torque on the *i*th dipole. While the continuum can be defined as having any arbitrary dielectric constant, simulation stability is greatest when $\varepsilon_s > \varepsilon$.[6a] Three special cases for the reaction field have been employed: $\varepsilon_s = 1$ (spherical cutoff/SC), $\varepsilon_s = \varepsilon$ (self-consistent reaction field/SCRF), and $\varepsilon_s = \infty$ (conductive boundary/CB). Under the SC boundary condition, $\mathbf{R}_i$ is always zero, so only short-range pair-wise interactions are considered. Simulations using the method of Ewald sums and the method of (non-SC) RF boundary conditions have given equivalent dielectric behavior.[7]

Solutions to the electrostatic boundary-value problems for computer simulations are similar to mean-field models. Neumann[4a, b] and others[4e, 23] proved that a minimum-image cube or Ewald lattice of a dielectric material surrounded by a continuous medium with a dielectric constant $\varepsilon_s$ is equivalent to a dielectric sphere surrounded by the same continuous medium (as used in the RF method).

The general form of the relationship between the external contribution to the local field $\mathbf{E}_0$ acting on the dipole, and the bulk external field, $\mathbf{E}$, is given by[4b]

$$\mathbf{E}_0 = \frac{2\varepsilon_S + \varepsilon}{2\varepsilon_S + 1}\mathbf{E} \qquad (2\text{-}6)$$

If $\varepsilon_s$ in Equation 2-6 is set to unity (MI/SC), long-range correlations are neglected, and $\mathbf{E}_0$ reduces to the Lorentz field[19] used in the Debye model. Applying the self-consistency condition $\varepsilon_s = \varepsilon$ causes $\mathbf{E}_0$ to equal the Onsager cavity field.[2] Implementing the latter condition in a simulation requires iteratively recalculating the dielectric constant during a simulation.[20b] The special case of $\varepsilon_s = \infty$ (CB) results in $\mathbf{E}_0$ limiting to $\mathbf{E}$.

The total dipole moment along the (arbitrary) field axis can be calculated from a fluctuation expansion of $\mathbf{M}$ in the absence of an external field (Kirkwood-like approach), or directly using $\mathbf{E}_0$ (Onsager-like approach). The fluctuation expansion [6a, 22a] is

$$\left\langle M_E \right\rangle_{E_0} \approx \left\langle M_E \right\rangle_{E_0=0} + \frac{E_0}{3kT}\left(\left\langle \mathbf{M}^2 \right\rangle_0 - \left\langle \mathbf{M} \right\rangle_0^2\right) \quad (2\text{-}7)$$

The $\left\langle M_E \right\rangle_0$ and $\left\langle \mathbf{M} \right\rangle_0^2$ terms in the expansion are typically assumed to vanish,[1b, 4e] leaving only the $\left\langle \mathbf{M}^2 \right\rangle_0$ term. This approximation is valid for isotropic systems. For systems with any spontaneous polarization, the $\left\langle \mathbf{M} \right\rangle_0^2$ term will be nonzero, as will the linear term, though the effects from the $\left\langle M_E \right\rangle_0$ term should be small when averaged over many simulations since the director axis in a spontaneously polarizing system will be random with respect to an arbitrarily defined field axis

in the absence of external influence. Our calculations do not include the effects of the $\langle M_E \rangle_{E_0=0}$ term, as it is negligible for simulations in isotropic phases and fluctuates around zero with large uncertainty in ferroelectric phases.

A number of parameters can be combined to define a reduced dipole density [1b, 6a]

$$y = \frac{4\pi\rho_N \mu^2}{9kT} \quad (2\text{-}8)$$

and the Kirkwood correlation factor can be found as

$$g_K = \frac{\langle \mathbf{M}^2 \rangle_0 - \langle \mathbf{M} \rangle_0^2}{N\mu^2} \approx \frac{\langle \mathbf{M}^2 \rangle_0}{N\mu^2} \qquad (2\text{-}9)$$

which can be calculated from the fluctuation expansion of **M,** [4d, 6a] scaled by $N$, the number of particles in the simulation. Combining Equations 2-2, 2-7, 2-8, and 2-9 and rearranging to separate terms containing ε from those containing $\varepsilon_s$ gives a relation for calculating the dielectric constant in the absence of an external field,[6a]

$$\frac{1}{\varepsilon - 1} = \frac{1}{3yg_K} - \frac{1}{2\varepsilon_S + 1} \qquad (2\text{-}10)$$

Equation 2-10 is analogous to Equation 2-4 but is applicable to simulations using arbitrary reaction field boundary conditions.

## 2.3. Computational Methods

Most prior work[4b, 4e, 8, 18, 23-24] on dielectric constants of simple liquids focused on dipole densities of $y < 3$; the present work will examine the behavior

of the Stockmayer fluid with dipole densities ranging up to $y = 8.1$ at number densities and dipole moments similar to those of common polar liquids. The Stockmayer model will also be compared to an ellipsoidal model for an acetonitrile-like system ($y = 6.64$), using SC, RF, SCRF, and conductor-like (CL) boundary conditions in periodic simulations. We will also explore the effects of simulation size on the dielectric constant using simulations containing 512 to 4096 particles.

All simulations for the Stockmayer model were run using the Metropolis[25] Monte Carlo technique with Hamiltonian

$$U = \sum_i \left\{ \sum_{j>i} \left[ 4\varepsilon_{LJ} \left( \left( \frac{\sigma_{LJ}}{r_{ij}} \right)^{12} - \left( \frac{\sigma_{LJ}}{r_{ij}} \right)^{6} \right) + \frac{1}{r_{ij}^3} \left( \boldsymbol{\mu}_i \cdot \boldsymbol{\mu}_j - 3 \left( \boldsymbol{\mu}_i \cdot \hat{\mathbf{r}}_{ij} \right) \left( \hat{\mathbf{r}}_{ij} \cdot \boldsymbol{\mu}_j \right) \right) - \frac{1}{R_{cut}^3} \frac{2(\varepsilon_S - 1)}{2\varepsilon_S + 1} \boldsymbol{\mu}_i \cdot \boldsymbol{\mu}_j \right] \right\} \quad (2\text{-}11)$$

which includes Lennard-Jones, dipole-dipole, and reaction field terms. This Hamiltonian is based on that used by Bartke and Hentschke,[10d] but excludes electronic polarizability. Since no self-consistent field calculation for electronic polarizability is used here, $U$ is computed directly instead of computing the local electric field at the location of each particle as an intermediate step. The electrostatic cutoff radius $R_{cut}$ is defined as half of the box length. An $\varepsilon_s$ value of 16000 was assumed for the CL boundary condition, and the $\varepsilon_s$ for SCRF calculations was recalculated at the beginning of each simulation cycle (every $N$ trial moves).[20b]

Calculations involving non-spherical ellipsoids used Perram and Wertheim's method[26] for computing the contact function between two ellipsoids to generate an effective Lennard-Jones zero-energy distance $\sigma_{eff}(i,j)$, which replaces $\sigma_{LJ}$ in Equation 11. The parameter $\sigma_{eff}(i,j)$ is the distance between the

centers of the two ellipsoids if moved into contact along $\mathbf{r}_{ij}$. The first three neighbor shells around each particle were treated as ellipsoids for calculation of Lennard-Jones interactions, and the fourth shell was calculated as if those neighbors were spheres. For the moderate eccentricities used in these simulations, this approximation introduces negligible error. The explicit neighbor sum was truncated just beyond the fourth neighbor distance. The Hamiltonian for ellipsoidal simulations was otherwise the same as Equation 11.

One particle was moved per Monte Carlo step, with each trial move consisting of simultaneous independent translations along all three Cartesian axes, followed by a rotation around a single randomly chosen axis using the method of Barker and Watts.[27] While the acceptance rate that results in the fastest convergence is still a subject of debate,[22a] move sizes were optimized to yield steady-state acceptance rates of 40-60%, consistent with common practice.[1a, 22a] For systems with a dipole density similar to that of acetonitrile, the most efficient step sizes were ±0.2 Å for the translational degrees of freedom, and $\pm\pi/6$ radians for rotational degrees of freedom. Move sizes for ellipsoidal systems were ±0.18 Å and ±0.13 π radians, respectively.

All simulations were run in the canonical (NVT) ensemble, with $N$ = 512, 1728, or 4096. The particles were started on a simple cubic lattice, which was allowed to melt subject only to Lennard-Jones interactions for the first 1000 sampling cycles (2000 cycles for the EM1 fluid with $N$ = 4096) of the simulation, where each cycle involved $N$ trial moves. Unless specified otherwise, simulations of the Stockmayer fluid were run for 30000 total cycles ($5.2\times10^7$ configurations for $N$ = 1728), averaging over the last 10000 cycles. Simulations of the ellipsoidal

fluid were run for a greater number of MC cycles (45000 cycles for $N = 512$ ( $2.3\times10^7$ configurations), or $N = 1728$ ( $7.8\times10^7$ configurations), and 120000 cycles ( $4.9\times10^8$ configurations) for $N = 4096$). Ensemble averages for ellipsoidal simulations were obtained from the last 15000 cycles for the $N = 1728$ runs, or the last 60000 cycles for the $N = 4096$ runs. Five replicas of each simulation were run with different random number seeds, and the replicas were averaged to obtain means and standard errors.

The orientational correlation function function[18]

$$g_\mu(r) = \frac{\sum_{i=1}^{N}\sum_{j>i}^{N}\cos\gamma_{ij}(r, r+dr)}{2\pi N\rho_N r^2 dr} \qquad (2\text{-}12)$$

was calculated every hundred cycles during the averaging period, where the inner sum is over neighbors in $r$ to $r+dr$, and $\cos\gamma_{ij} = \hat{\boldsymbol{\mu}}_i \cdot \hat{\boldsymbol{\mu}}_j$, the internal angle between the $i$th and $j$th dipoles. The average is calculated for all particles with inter-dipolar distances of between $r$ and $r+dr$. Our simulations evaluated $g_\mu(r)$ from $r = 0$ out to half the box length, divided into 200 radial shells of width $dr$. Note that the value of the function can exceed unity since the denominator contains the uniform density function instead of the actual number of particles in the sum. While similar in form to the radial distribution function[1b, 20b] $g(r)$, Equation 2-12 is used to quantify angular correlations, with $g_\mu(r)$ positive where dipoles are more likely to be parallel to the $i$th dipole and negative where dipoles are more likely to be anti-parallel to the $i$th dipole. While several similar functions for quantifying such behavior exist,[4b, 9a, 28] we chose the form used by

Barker and Watts,[18] with an additional $N$ in the denominator to make the function independent of simulation size.

A histogram of $\left\langle \cos\gamma_{ij} \right\rangle$ as a function of $\cos(\alpha) = \hat{\mathbf{r}}_{ij} \cdot \hat{\boldsymbol{\mu}}_i$ was also calculated for the nearest neighbor shell of every particle, consisting of all particles within 1.25 times the $\sigma_{LJ}$ value of the longest axis of the particles. The histogram was recorded at the same point in the simulations as $g_\mu(r)$. These two histograms each provide one-dimensional slices of information similar to the two-dimensional orientational correlation function used by Pounds and Madden.[9a]

Simulation convergence was checked by examining the potential energy of the system as a function of sampling cycle to see whether any clear trend could be distinguished within the averaging period.[20b] Fluctuation-based simulations used the full variance-based definition[4e, 6a, 22a] of $g_K$ in Equation 2-9, including the $\left\langle \mathbf{M} \right\rangle_0^2$ term. This term was typically very small compared to $\left\langle \mathbf{M}^2 \right\rangle_0$ for low dipole densities, but became very large if a system developed ferroelectric order.

The acetonitrile-like model was parameterized based on the van der Waals volume, $V_{vdW}$, from a gas-phase B3LYP/6-311+G** geometry calculation for acetonitrile using Spartan '08.[29] The dipole moment of 4.09D differs from the gas-phase dipole moment[30] (3.92 D) in order to approximately represent the effects of electronic polarization. The Lennard-Jones energy parameter $\varepsilon_{LJ}$ was 217K, similar those used for other small organic molecules[31]. As the model was not systematically parameterized to model thermodynamic properties, it should not be considered to be a quantitative parameterization of acetonitrile, but as a

semi-quantitative acetonitrile-like model. A similar model using an ellipsoidal van der Waals surface was also parameterized. Parameters for the spheres (SM1) and ellipsoids (EM1) are given in Table 2.1, and the temperature and density used in the calculations are the same as those listed for acetonitrile in Table 2.2.

**Table 2.1.** Parameters for highly polar Stockmayer and ellipsoidal fluids

| Model | μ(D) | $\sigma_{LJ}$ (Å) | $\varepsilon_{LJ}$ (K) | $V_{vdW}$ (Å$^3$) | $\rho_N$ (Å$^{-3}$) | $y$ |
|---|---|---|---|---|---|---|
| Stockmayer (SM1) | 4.09 | 4.66 | 217.4 | 53.0 | 0.0115 | 6.64 |
| Ellipsoidal (EM1) | 4.09 | 4.08 (x,y), 6.08 (z) | 217.4 | 53.0 | 0.0115 | 6.64 |

These parameters yield a reduced density $\rho^* = \rho_N \sigma_{LJ}^3 = 1.16$, and a reduced dipole density $\mu^{*2} = \mu^2 / \sigma_{LJ}^3 \, kT = 4.09$ in dimensionless, Lennard-Jones units for the SM1 model.[1b] The packing fraction $f = \rho_N V_{vdW} = 0.61$ for both models.

Other polar liquids (Table 2.2) were parameterized as Stockmayer fluids with the van der Waals radius calculated from B3LYP/6-31G* geometry calculations in Spartan. Gas-phase dipole moments, densities, and the temperatures at which the dipole moment and density measurements were taken were obtained from the CRC Handbook of Chemistry and Physics, [30] and $\varepsilon_{LJ}$ values were the same as the models in Table 2.1 based on an examination of united-atom models for other small organic liquids.[32]

**Table 2.2.** Parameters for Stockmayer models of polar aprotic liquids

| Species | $T$ (K) | $\mu$ (D) | $\sigma_{LJ}$ (Å) | $\rho_N$ (Å$^{-3}$) | $y$ |
|---|---|---|---|---|---|
| Toluene | 298 | 0.38 | 6.08 | 0.00682 | 0.034 |
| Ether | 293 | 1.1 | 5.72 | 0.0058 | 0.242 |
| Dichloromethane | 293 | 1.6 | 4.90 | 0.00935 | 0.827 |
| Acetone | 293 | 2.88 | 5.18 | 0.00813 | 2.33 |
| Dimethylformamide | 298 | 3.82 | 5.48 | 0.00778 | 3.85 |
| Nitromethane | 298 | 3.46 | 4.72 | 0.0112 | 4.55 |
| Acetonitrile | 293 | 3.92 | 4.66 | 0.0115 | 6.10 |

All simulations were implemented using a custom simulation engine written in C++.[33] The present code replaced an earlier Matlab-based simulation engine.[14, 34] Data were processed using Matlab,[35] and simulations were visualized using a custom X3D-based visualizer.[36]

## 2.4. Results and Discussion

### *2.4.1. Size and boundary condition effects for Stockmayer fluid*

We have examined the effects of system size and outer boundary conditions on the SM1 system, using SC, CL, and SCRF boundary conditions, with $R_{cut}$ equal to half the box length. Results are shown in Figure 1. The SC boundary condition showed almost no variation in the dielectric constant with simulation size, and remained stable even at $N = 512$ despite the steep slope of $\varepsilon(yg_K)$ as the discontinuity in eq. (10) when $yg_K = 1$ is approached. The relative stability of ε is likely due to using substantially more configurations than in earlier simulations.[4b] The simulations using the SCRF boundary condition indicated a higher dielectric constant at $N = 1728$, but seemed to level off at large $N$ and exhibited both a much larger dielectric constant and larger variance than the SC boundary condition. The CL boundary condition behaved similarly to the SCRF boundary condition, though it did not show an increase at $N = 1728$. The behavior of each boundary condition as a function of box size can be seen in Figure 2.1.

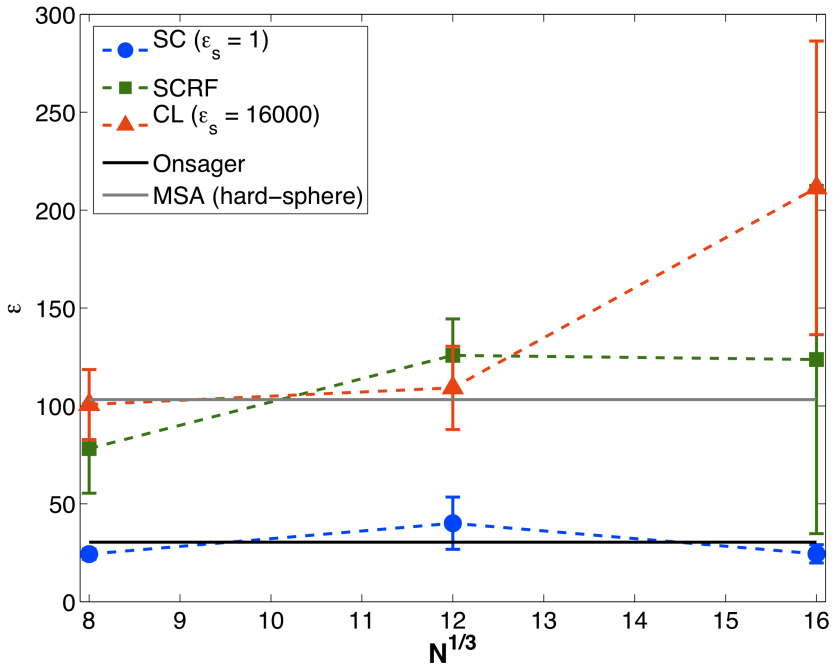


**Figure 2.1.** Dielectric constant of the SM1 fluid calculated from dipole fluctuations at three different box sizes (512, 1728, and 4096 particles). All simulations were run at 293K, and results were averaged from the last 10000 cycles of five 30000-cycle MC runs. The Onsager and hard-sphere mean spherical approximation[1b] (MSA) solutions for the SM1 model are included for comparison. Lennard-Jones interactions were truncated after 17.72Å (four neighbor shells) for all box sizes.

Varying the size of the electrostatic cutoff radius had minimal effect on the dielectric constant under the SC boundary condition so long as at least the first two shells of neighbors around each particle were included. Simulations using the CL and SCRF boundary conditions yielded more erratic behavior with cutoff size, likely due to increased domain size with the strong reaction field. As a result of this, we used the largest possible (1/2 of the box length) electrostatic cutoff for all simulations.

Energy convergence of our SM1 simulations was satisfactory, with a relative standard error of the mean energy of less than 0.25% for all boundary

conditions, with CL being the most stable, followed by SCRF, and SC being substantially less stable than the other two. Total energy values were also similar for CB and SCRF, and slightly lower for SC since dipole-dipole interactions were not mediated by a reaction field. Energy values and errors are shown in Table 2.3.

**Table 2.3.** Average energies of SM1 simulations

| Boundary Condition | $\langle U/Nk_BT \rangle$ (1728) | Rel. Std. Error (%) | $\langle U/Nk_BT \rangle$ (4096) | Rel. Std. Error (%) |
|---|---|---|---|---|
| SC | -15.636 ± 0.040 | 0.25 | -15.822 ± 0.031 | 0.20 |
| SCRF | -14.992 ± 0.011 | 0.075 | -15.012 ± 0.019 | 0.13 |
| CL | -14.986 ± 0.007 | 0.046 | -15.000 ± 0.014 | 0.092 |

For comparison, the standard enthalpy of vaporization of acetonitrile at 298K is 13.7 $k_BT$ per molecule,[37] giving an energy of vaporization of approximately 12.7 $k_BT$. Therefore, the SM1 fluid exhibits stronger cohesive intermolecular interactions than acetonitrile.

While the SCRF and CL simulations indicated a dielectric constant consistent with the expected behavior[1b, 8] of a Stockmayer fluid at high dipole density, the SC boundary condition yielded a value of $\varepsilon = 24.48 \pm 4.68$ for $N$ = 4096.The SC number compared well with the value of $\varepsilon = 27$ obtained by Pounds and Madden in a large-scale molecular dynamics simulation using a united-atom model of acetonitrile with Ewald sums for long-range interactions and a conductive outer boundary.[9a] The latter simulation in turn compared well with a smaller ($N$ = 500) simulation by Edwards and Madden,[38] which used the same potential, showing the fast convergence of the Ewald summation technique. Both of Madden's simulations also neglected polarizability. The wide discrepancy between the SC boundary condition and other two boundary conditions led us to

investigate trends in the calculated dielectric constant as a function of dipole density for these boundary conditions.

### *2.4.2. Effects of dipole density on dielectric constant of Stockmayer fluid*

Given that the Stockmayer fluid has been shown to produce much higher dielectric constants than that of acetonitrile at lower dipole densities,[1b, 4b, 4e, 8] we varied the dipole moment of the SM1 model to generate a range of $y$ values from 0.81 to 8.12, as shown in Figure 2. Note that the ρ* of the SM1 model is substantially larger than the values of 0.80 or 0.82 used in the literature cited above, though it is consistent with the density and molecular volume of acetonitrile. The dielectric constant, when calculated using the full variance-based fluctuation method (Equation 2-9), exhibited non-monotonic behavior as a function of $y$ for all three boundary conditions. The dielectric constant leveled off at a $y$ of between 3 and 4 for all boundary conditions, although the SCRF boundary condition fluctuated wildly when $y$ was between 4 and 5. Previously reported simulations of the dielectric constant of the Stockmayer fluid have generally focused on the isotropic phase, though spontaneous ordering has been observed in dipolar hard spheres[39] and soft spheres[40] at high dipole density. Bartke and Hentschke[10d] also studied the phase transition as a function of temperature. The results in Figure 2.2 show the dielectric constant in both the isotropic and ferroelectric phases as a function of dipole density.

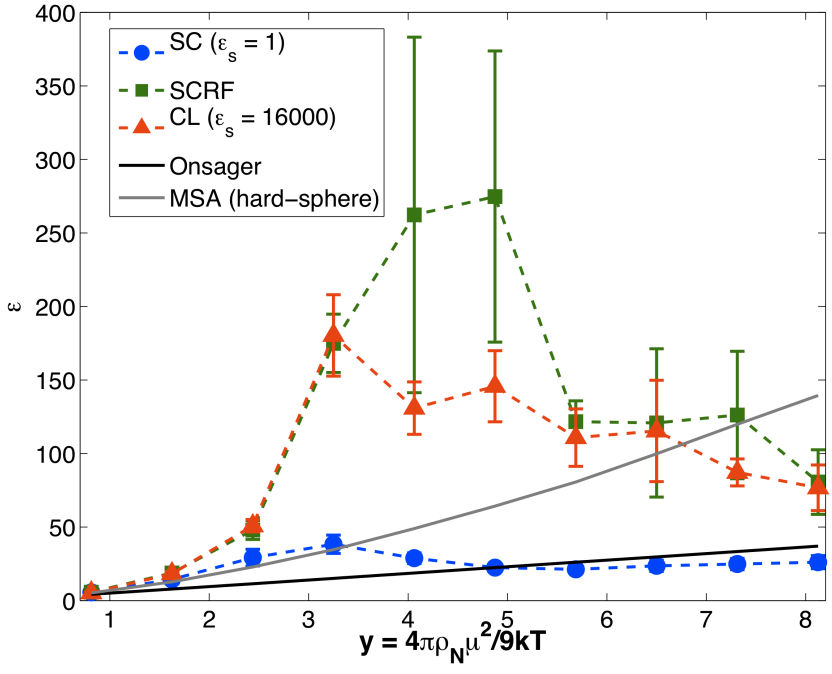


**Figure 2.2.** Dielectric constants of Stockmayer fluids at different dipole densities. All other parameters are the same as given in Table 1. Details are listed in Table 4. All simulations were run at 293K with $N = 1728$ particles, averaging the last 10000 cycles from five 30000-cycle runs. Lennard-Jones interactions were truncated after 17.72 Å (four neighbor shells).

The decrease in the dielectric constant as $\mu$ or $y$ increases comes from a reduction in $g_K$ of sufficient size to counterbalance the increase in dipole density, resulting in the product $yg_K$ staying stable or even decreasing. If the SC boundary condition is used, the decrease in $yg_K$ is insensitive to the use of Var(**M**) or $\langle \mathbf{M}^2 \rangle_0$ for calculation of $g_K$; the system does not develop any net polarization. For the SCRF and CB boundary conditions, the decline only appears when the Var(**M**) definition is used, as both $\langle \mathbf{M}^2 \rangle_0$ and $\langle \mathbf{M} \rangle_0^2$ become very large. Such behavior would indicate that the system has spontaneously

developed net polarization and become ferroelectric, as is expected for highly polar Stockmayer fluids.[9a, 10d] Because the system develops net order at high dipole density, the assumption that. $\langle \mathbf{M} \rangle_0^2 = 0$ .becomes invalid. By $y = 4.06$, $\langle \mathbf{M}^2 \rangle_0$ is nearly twenty times the magnitude of Var(**M**) as the ferroelectric contribution to **M** is combined with the fluctuating contribution. The Var(**M**) and $\langle \mathbf{M}^2 \rangle_0$ for the dipole densities shown in Figure 2 are compared in Table 2.4.

**Table 2.4.** Kirkwood g-factor from SCRF simulations

| $y$ | $\mu$ (D) | $g_K$ (Var(M)) | $g_K$ ($\langle \mathbf{M}^2 \rangle_0$) | Var(M)/ $\langle \mathbf{M}^2 \rangle_0$ |
|---|---|---|---|---|
| 0.81 | 1.43 | 1.44 ± 0.06 | 1.47 ± 0.06 | 0.97 |
| 1.62 | 2.02 | 2.54 ± 0.14 | 2.66 ± 0.15 | 0.96 |
| 2.44 | 2.48 | 4.53 ± 0.54 | 5.05 ± 0.54 | 0.90 |
| 3.25 | 2.86 | 13.72 ± 1.31 | 19.76 ± 2.02 | 0.69 |
| 4.06 | 3.20 | 21.07 ± 6.61 | 414.5 ± 19.2 | 0.051 |
| 4.87 | 3.50 | 18.57 ± 4.51 | 761.9 ± 9.4 | 0.024 |
| 5.69 | 3.78 | 7.06 ± 0.55 | 935.0 ± 4.4 | 0.0075 |
| 6.50 | 4.04 | 6.13 ± 1.72 | 1065 ± 9 | 0.0058 |
| 7.31 | 4.29 | 5.70 ± 1.31 | 1099 ± 41 | 0.0052 |
| 8.12 | 4.52 | 3.26 ± 1.19 | 1189 ± 11 | 0.0027 |

### *2.4.3. Comparison with highly polar organic liquids*

Because the SC values for the dielectric constant remained low at high dipole density, we examined Stockmayer models of other solvents to see whether simulations using the SC boundary condition would yield a trend similar to experiment. We selected seven common polar aprotic liquids with $y$ values in the range from 0.03 to 6.1 and parameterized them as Stockmayer fluids (see Table 2.2). Protic liquids were omitted to avoid the complication that hydrogen bonding introduces into the relationship between dipole moment and dielectric constant.[2] We also calculated $y$-values for 33 aprotic liquids (including the seven

mentioned above) based on data in the CRC Handbook of Chemistry and Physics[30] to determine the experimental trend in the dielectric constant as a function of $y$ in a manner similar to that used by Wyman.[41] Results appear in Figure 2.3.

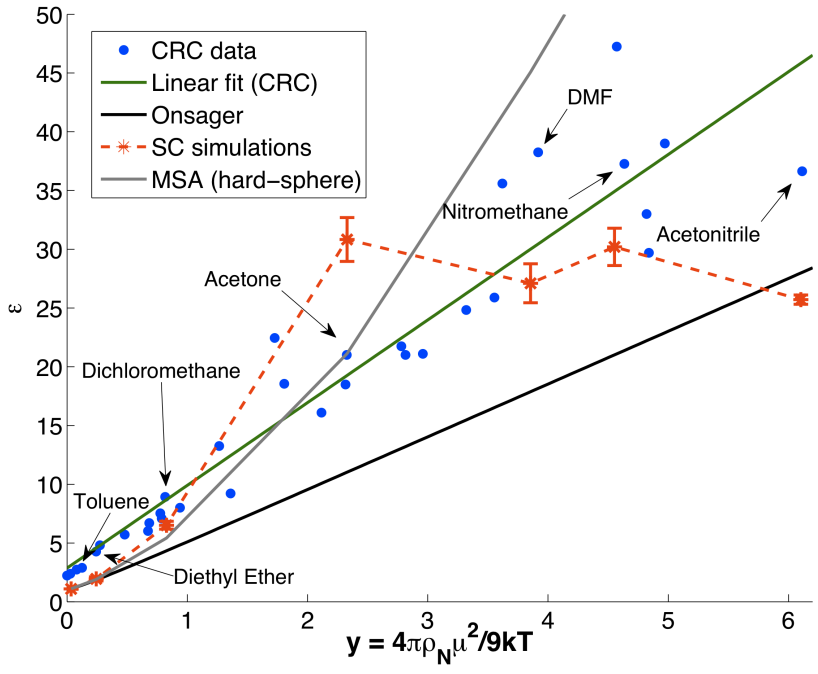


**Figure 2.3.** Comparison of dielectric constants of selected aprotic liquids. Experimental data are from the CRC Handbook of Chemistry and Physics, and are compared with predictions from the non-polarizable Onsager model. The liquids shown in Table 2 were also compared with Stockmayer simulations using the SC boundary condition and with the predictions of the hard-sphere MSA. Simulations were run with $N = 1728$ at the temperatures given in Table 2, averaging over the last 8000 cycles of five 24000-cycle runs. Lennard-Jones interactions were truncated after 26.58 Å (six neighbor shells).

The CRC values for the dielectric constant exhibited a linear trend in $y$, albeit one showing a large spread at higher values of $y$, consistent with Wyman's analysis.[41] The regression line indicates a dielectric constant for the solvents greater than unity at $y = 0$, because the experimental values include contributions

from both permanent dipoles and electronic polarizability. Use of the polarizable Onsager[2] equation instead of the non-polarizable variant yielded a trend very similar to the regression line, indicating that $g_K$ values are close to unity for the liquids that we examined.[20b]

Simulated values using the SC boundary condition leveled off near $y = 2$, consistently underestimating the dielectric constant of highly polar liquids such as DMF, nitromethane, and acetonitrile, and indicating that the Stockmayer fluid resists polarization at large values of $y$ under the SC boundary condition. While the Stockmayer fluid under the SC boundary condition may generate values that seem more plausible when compared with real liquids than with other boundary conditions, it shows an insensitivity to changes in $y$ beyond the ferroelectric transition that occurs in the range $2 < y < 4$.

### *2.4.4. Orientational correlation and ferroelectric domains in Stockmayer fluid*

In order to examine why simulations using the SCRF or CL boundary condition developed net ferroelectric polarization while those using the SC boundary never developed a large dielectric constant and became resistant to further polarization, we examined the orientational correlation function[18] $g_\mu(r)$ as a function of reaction field strength for the SM1 Stockmayer fluid. Results are shown in Figure 2.4.

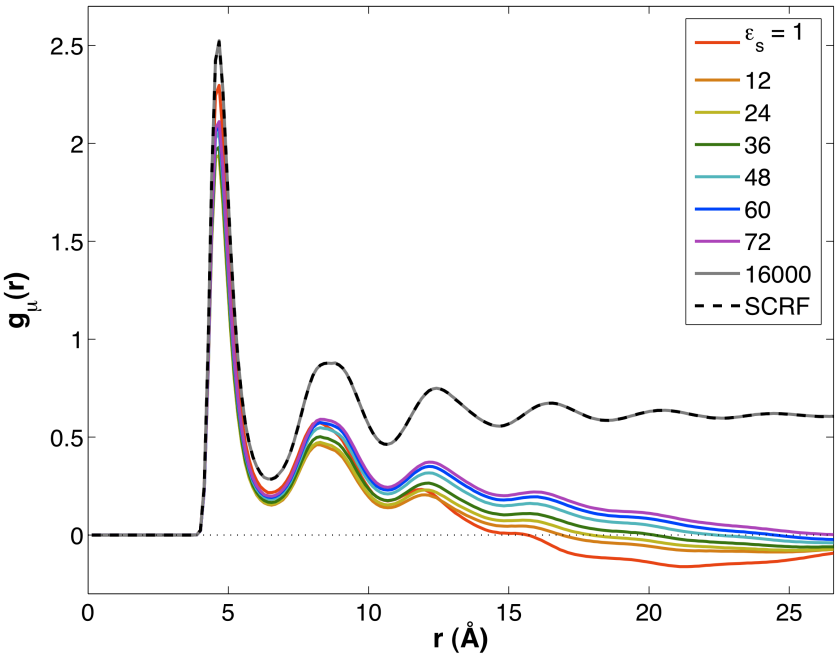


**Figure 2.4.** Orientation correlation function $g_\mu(r)$, (Equation 2-12), for SM1 with $N = 1728$ and $T = 293$K. Correlation functions were sampled every hundred cycles during the last 10000 steps (equilibrium phase) of five 30000-step simulations. The correlation between dipoles is always positive except in a nearly featureless anti-correlated region at long distance that occurs for $\varepsilon_s \leq 60$. The CB and SCRF boundary conditions led to pervasive, positive correlation of the entire box. Lennard-Jones interactions were truncated after 17.72 Å (four neighbor shells).

Examination of the orientational correlation function $g_\mu(r)$ showed that neighbors in the first shell around each particle are strongly aligned with the central particle regardless of reaction field strength, with second and third-nearest neighbors showing a lesser degree of alignment with the central dipole. At low reaction field strengths, the function crosses below zero, entering a nearly featureless anti-correlated region that persists until the edge of the box. As the reaction field strength increased further, more and more shells of neighbors became positively correlated, until no negative correlation is observed for $\varepsilon_s > 60$. The anti-correlated behavior with weak reaction fields is consistent with earlier

small-scale simulations by Barker and Watts[18] and Neumann.[4b] Patey, *et al.*[4c] assert that the anti- correlation should disappear as $R_{cut}$ is increased, while work by Neumann has shown that a second correlation peak emerges after the cutoff if a small $R_{cut}$ is used.[22b] Our simulations used far larger $R_{cut}$ values than earlier work, but extending explicit electrostatic interactions to half the box length of a 4096-particle box (35.44 Å) was still insufficient to eliminate the anti-correlated region. The CL and SCRF boundary conditions led to strong, pervasive correlation of the entire box, as previously observed by Neumann.[4b] As the SCRF and CL dielectric values are substantially larger than 60, the net correlation for these boundary conditions is much larger than for the other reaction field strengths used. The lack of any short-range anti-correlation, combined with shrinking long-range anti-correlation as the reaction field grows stronger, indicates that the system develops ferroelectric domains that grow as the reaction field strength increases, until the domain size reaches the size of the box and the entire system spontaneously develops net polarization.

The smaller domains seen with the SC boundary condition oppose each other in direction and do not result in any net order, but constrain the ability of dipoles within a domain to fluctuate, reducing the system's ability to undergo dielectric polarization. Observing this effect under the SCRF or CL boundary conditions requires that one subtract the net polarization at zero external field in the fluctuation expansion, using the two-term definition of $g_K$ in Equation 2-9. Visualizations of an SC simulation and an SCRF simulation can be seen in Figure 2.5.

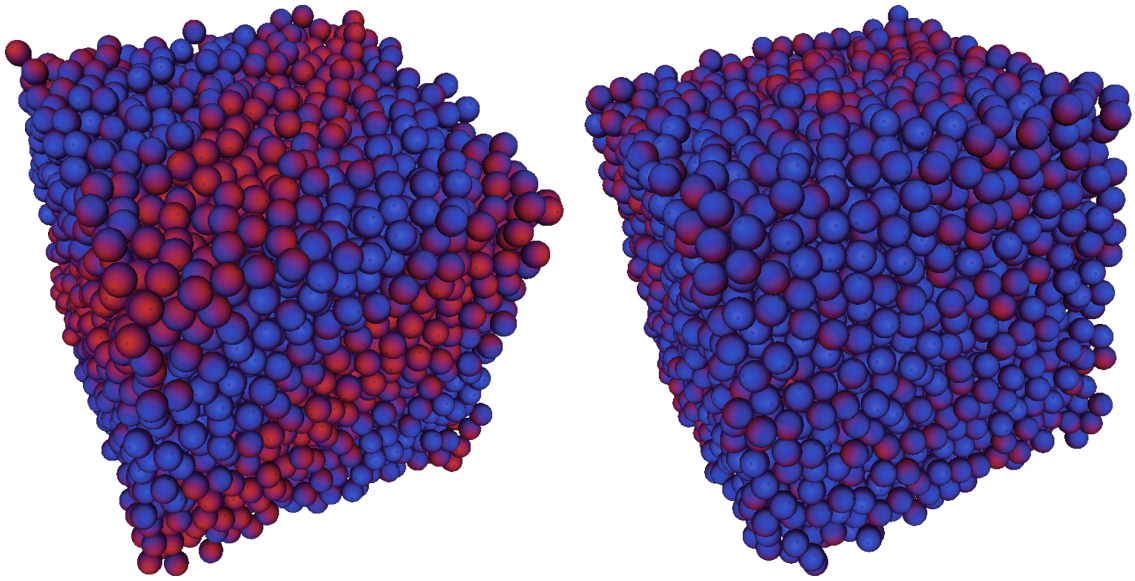

**Figure 2.5.** Snapshots of ferroelectric domains in simulations of SM1 with $N$ = 4096 and $T$ = 293K. The image on the left is from a simulation using the SC boundary condition ($\varepsilon = 24.48 \pm 4.68$); the one on the right is from a simulation using the SCRF boundary condition ($\varepsilon = 123.7 \pm 89.0$). Lennard-Jones interactions were truncated after 17.72 Å (four neighbor shells).

Visual examination of the alignment of the dipoles in the simulation indicates the presence of striated domains under the SC boundary condition and pervasive polarization under the SCRF boundary condition, consistent with the expansion of domains with reaction field strength indicated by the orientational correlation function. While the domains are easiest to see in large simulations, they are present at smaller box sizes as well. Furthermore, while pervasive ferroelectric behavior only occurs under a strong reaction field, locally ferroelectric domains form at large $y$ values regardless of reaction field strength.

The presence of aligned (ferroelectric) domains is consistent with other Stockmayer simulations conducted to evaluate Shelton's[9b] controversial Hyper-Rayleigh scattering data on acetonitrile and other fluids.[1c, 9a, 9c] These simulations showed that domain formation occurred only with Stockmayer,[1c] or quasi-Stockmayer[9a] (multiple point charges in a sphere) models, and did not occur in

aspherical models,[9a, 9c] indicating that the domains are probably a property of the Stockmayer fluid itself instead of fluids with high dipole densities.

### *2.4.5. Dielectric behavior of ellipsoidal model*

To test this assertion, we parameterized an anisotropic Stockmayer-like model (EM1) consisting of a 3:2 prolate ellipsoid surface surrounding a single point dipole (see Table 2.1) in the center of the ellipsoid and aligned with the unique axis of the ellipsoid, and examined the behavior of this model as a function of simulation size and reaction field strength. Results appear in Figure 2.6.

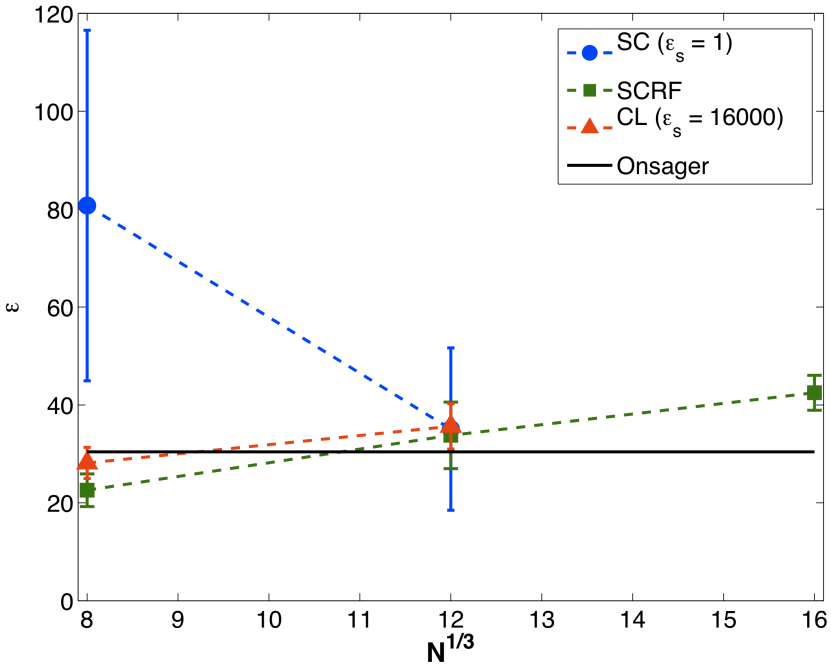


**Figure 2.6.** Dielectric constant of the EM1 fluid calculated from dipole fluctuations at three different box sizes (512, 1728, and 4096 particles). All simulations were run at 293K. Results were averaged from the last 15000 cycles of five 45000-cycle MC runs for $N$ = 512 or 1728 and from the last 60000 cycles of five 120000-cycle runs for $N$ = 4096. The Onsager model is included for comparison. Lennard-Jones interactions were truncated after 17.72Å (four neighbor shells) for all box sizes.

The dielectric constant of the EM1 fluid was far lower than the SM1 fluid with the same dipole density, with $\varepsilon = 33.79 \pm 6.79$ for 1728 EM1 particles under the SCRF boundary condition, as opposed to $\varepsilon = 125.8 \pm 18.6$ for the SM1 fluid under the same boundary condition. Results for the EM1 fluid using the CL boundary condition were comparable to SCRF results for $N = 1728$, but slightly higher than the SCRF results for $N = 4096$, and results using the SC boundary condition were far less stable between simulations than those from the other two boundary conditions. Simulations with $N = 4096$ yielded $\varepsilon = 42.48 \pm 3.57$ under the SCRF boundary conditions, slightly larger than the value obtained using $N = 1728$. Results using the SCRF and CL boundary conditions and $N = 512$ were also produced somewhat lower dielectric constants than the $N = 1728$ simulations, indicating that longer-ranged dipolar correlations ( > 4-6 neighbor shells) may have a nontrivial effect on the dielectric constant of the EM1 fluid. While the EM1 results at the largest simulation size slightly overshoot the dielectric constant of acetonitrile[30] (36.64 at 293K) despite the absence of polarizability, they exhibit remarkable agreement with experimental dielectric constants compared to the Stockmayer fluid.

While simulations of EM1 took longer to reach equilibrium than those of SM1, energy convergence of the EM1 simulations was satisfactory, with relative standard errors for 1728 particles on the order of 0.1% or less regardless of boundary conditions. Energies for the $N = 4096$ had even smaller uncertainties and were consistent with the N = 1728 results, except for the SC boundary condition, where the average energy of the larger simulation was slightly lower.

Average energy values and uncertainties were calculated from sets of five simulations and are given in Table 2.5.

**Table 2.5.** Average energies for EM1 simulations

| Boundary Condition | $\langle U/NkT \rangle$ (1728) | Rel. Std. Error (%) | $\langle U/NkT \rangle$ (4096) | Rel. Std. Error (%) |
|---|---|---|---|---|
| SC | -11.554 ± 0.012 | 0.13 | -11.658 ± 0.009 | 0.078 |
| SCRF | -11.277 ± 0.005 | 0.042 | -11.273 ± 0.001 | 0.009 |
| CL | -11.274 ± 0.005 | 0.046 | -11.275 ± 0.002 | 0.014 |

These energies are both higher and less dependent on boundary conditions than those of the SM1 fluid, indicating that the EM1 fluid exhibits weaker cohesive intermolecular interaction strength than acetonitrile; the average energy is close to the energy of vaporization for acetonitrile. The reduction of cohesive interaction strength compared to the SM1 fluid is due entirely to changing the shape of the van der Waals surface.

### *2.4.6. Orientational correlation in ellipsoidal fluid*

We also calculated orientational correlation functions for the EM1 fluid using the same set of reaction field strengths used for the SM1 fluid; these results are shown in Figure 2.7.

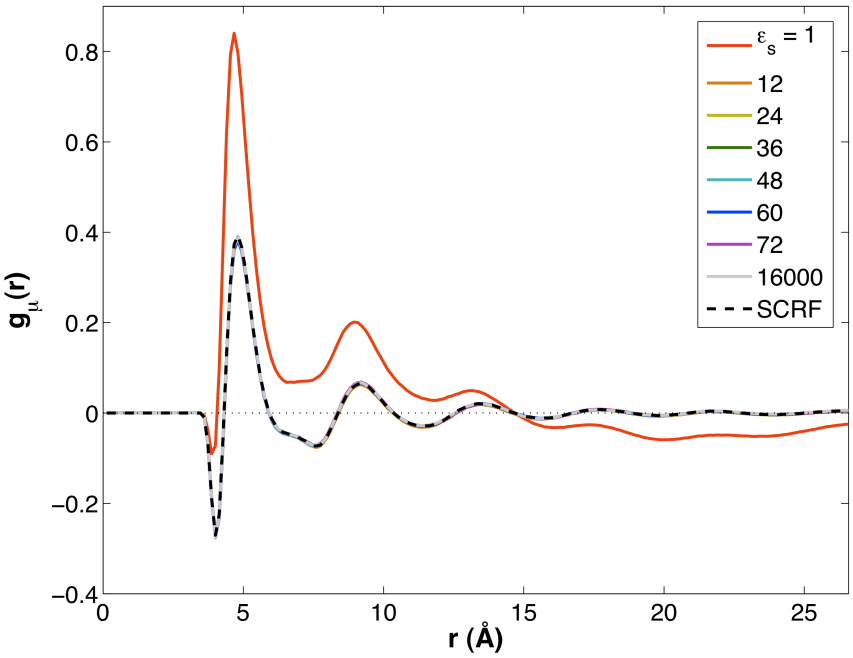


**Figure 2.7.** Orientational correlation function $g_\mu(r)$, eq. (12), for EM1 with $N$ = 1728 and $T$ = 293K. Correlation functions were sampled every 100 cycles during the last 15000 steps (equilibrium phase) of five 45000-step simulations. No pervasive correlation was observed, and the fluid was isotropic under nontrivial RF boundary conditions. Lennard-Jones interactions were truncated after 17.72 Å (four neighbor shells).

The SC results for $g_\mu(r)$ for EM1 did not differ greatly from those for SM1, except for the presence of a small anti-correlated peak at short distance. Shape effects were much stronger for the other boundary conditions. Any behavior indicative of ferroelectric domains disappeared once a reaction field was applied, and the angular correlation functions at different reaction field strengths, including CL and SCRF, were almost indistinguishable from one another. All exhibited initial anti-correlation from side–side (closest possible approach) ordering of molecules, where dipole moments are anti-parallel, followed by initial correlation from head–tail ordering of molecules (parallel dipole moments), with further neighbor shells alternating between anti-parallel and parallel until the correlation faded to zero, indicating an isotropic liquid instead

of a ferroelectric liquid. A visualization of such a simulation can be seen in Figure 2.8.

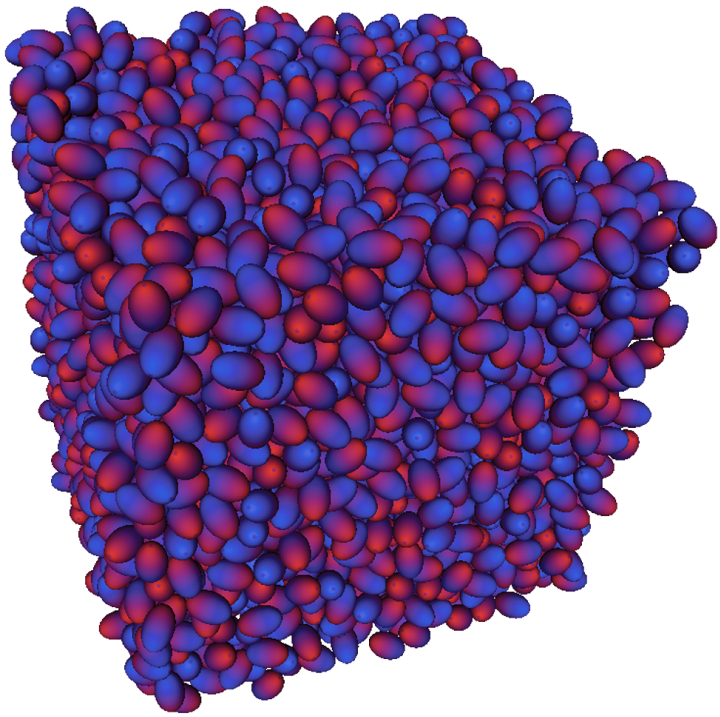

**Figure 2.8.** Snapshot of a simulation of EM1 with $N = 4096$, $T = 293$K, and a SCRF boundary condition ($\varepsilon = 42.48 \pm 3.57$). Lennard-Jones interactions were truncated after 17.72 Å (four neighbor shells).

To quantify the degree of parallel versus anti-parallel ordering of neighbors as a function of position around a central molecule, we examined the distribution of average internal angles $\langle \cos\gamma_{ij} \rangle$ as a function of $\cos(\alpha) = \hat{\mathbf{r}}_{ij} \cdot \hat{\boldsymbol{\mu}}_i$, where $\hat{\mathbf{r}}_{ij}$ is a unit vector in the direction from the *i*th particle to the *j*th particle within the nearest neighbor shell of the *i*th particle. Results are shown in Figure 2.9.

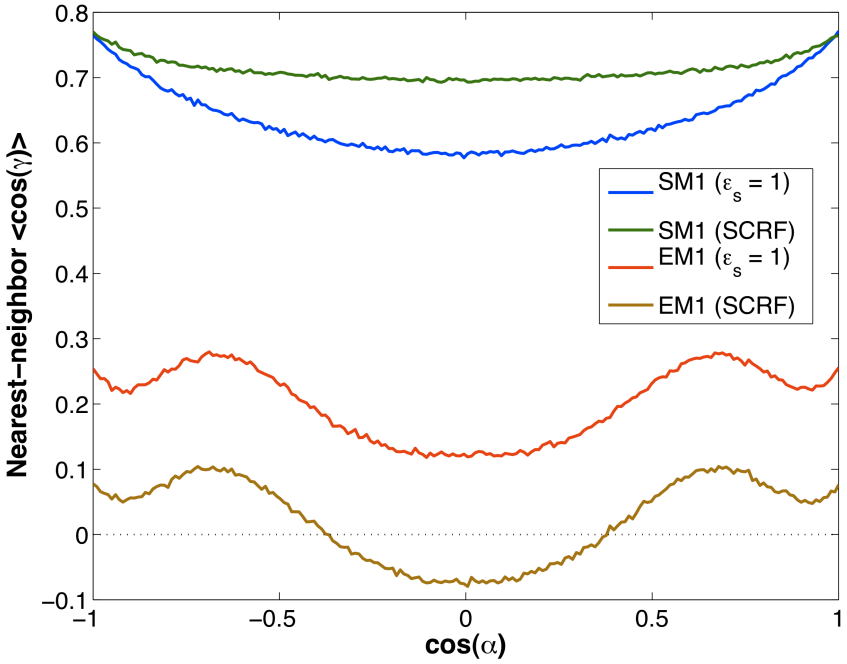


**Figure 2.9.** Plot of $\langle \cos\gamma_{ij} \rangle$ as a function of $\cos(\alpha)$ for both SM1 and EM1, each under two different boundary conditions, with $N = 1728$ and $T = 293$K. The expectation value was calculated over the nearest neighbor shell ($\mathbf{r}_{ij} < 5.83$ for SM1 and $\mathbf{r}_{ij} < 7.6$ for EM1) around each particle. Histograms were sampled every hundred cycles during the last 15000 cycles of five 45000-cycles simulations. Lennard-Jones interactions were truncated after 17.72 Å (four neighbor shells).

For the Stockmayer fluid, SM1, this function is positive for all $\cos(\alpha)$, showing that on average, all neighbors are correlated and ferroelectric domains are present, consistent with the large positive initial peak in $g_\mu(r)$. The function reaches a minimum for $\cos(\alpha) = 0$; where the *j*th particle is located alongside $\mu_i$, and a maximum for $\cos(\alpha) = \pm 1$, where the *j*th particle is located above or below dipole $\mu_i$. The difference between the extreme values of $\cos(\alpha)$ is small for the pervasively correlated SCRF SM1 model. The function also exhibits a parabolic shape for the SM1 model, showing the absence of a rotational barrier for the Stockmayer fluid.

Compared to the SM1 model, the EM1 model shows a much lower degree of correlation between nearest neighbors; the function is not parabolic for all $\cos(\alpha)$, but instead reaches a maximum at $\cos(\alpha) \approx \pm 0.7$, then decreases and rises again near $\cos(\alpha) \approx \pm 1$. This behavior is due to competition between electrostatics and sterics in the EM1 model. Head-to-tail alignment of dipoles is electrostatically favorable, but a $\cos(\alpha)$ value near ±1 would mean that the particles are sitting with the longest axes of their van der Waals surfaces in close proximity, which is an energetically unfavorable configuration for dispersive interactions. This steric barrier to parallel dipole orientation mitigates the tendency of the dipoles to form ferroelectric domains and is similar to what has been observed from simulations using united-atom models.[9a] Under SCRF boundary conditions, the EM1 model shows anti-correlation at small values of $\cos(\alpha)$ and correlation at $\cos(\alpha)$ near ±1, indicative of the absence of ferroelectric domains and showing that first anti-correlated peak in $g_\mu(r)$ is due to side–side aligned particles, and the first positively correlated peak is due to head–tail aligned particles.

### *2.4.7. Spontaneous polarization in Stockmayer and ellipsoidal fluids*

To further explore the isotropic behavior of the EM1 fluid, we also compared its degree of spontaneous polarization with that of the SM1 fluid. Spontaneous polarization was quantified by means of an inter-simulation average of the expectation value of the net dipole moments from the several simulations, using the parameter

$$\frac{RMS\left(\langle \mathbf{M} \rangle\right)}{N\mu} = \frac{\sqrt{\frac{1}{n}\sum_{k=1}^{n}\langle \mathbf{M} \rangle_{o,k}^{2}}}{N\mu} \quad (2\text{-}13)$$

where $k$ is the index of the simulation and $n = 5$ simulations per set. As the parameter defined by Equation 2-13 depends only on the magnitude of the spontaneous polarization and not the direction of the polarization, it does not require specifying a director axis. This parameter is a useful measure of the degree of local ordering because there is no preferred director axis in the absence of an external field. The three simulation sizes for the SM1 are compared with each other and with the EM1 fluid in Figure 2.10. Equation 2-13 will approach unity if material in the simulation cell develops net ferroelectric order, and will be near zero for isotropic material or small ferroelectric domains. We conjectured that as domain size grows with reaction field strength, small simulation cells would be expected to pervasively polarize, with the entire cell filled by a single domain, at a weaker reaction field strength than would be require to pervasively polarize a larger simulation cell. This is confirmed by the results are shown in Figure 2.10.

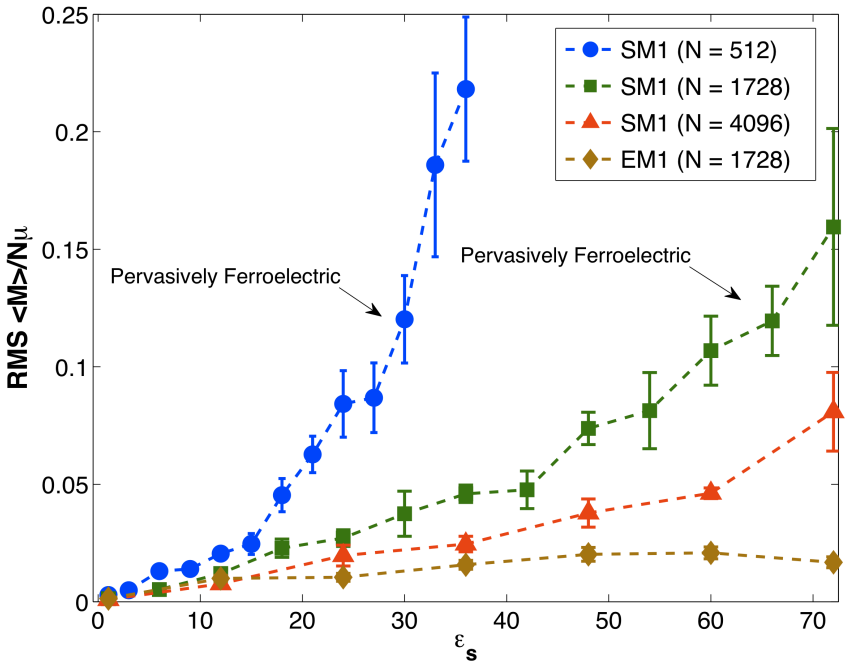


**Figure 2.10.** Normalized RMS magnitude of **M**, (Equation 2-13), as a function of the reaction field dielectric strength for the SM1 and EM1 fluids at different box sizes. Expectation values were obtained from averaging sets of five simulations ($n = 5$). All simulations were run at 293K. Points at which the size of the ferroelectric domains approaches the size of the box and the system becomes pervasively ferroelectric are labeled.

All SM1 Stockmayer fluid simulations show increased net spontaneous polarization as the dielectric strength determining the reaction field increases, with the rate of increase being faster for smaller box sizes. The $N = 512$ simulations became pervasively polarized, as indicated by $g_\mu(r)$, at an $\varepsilon_s$ near 33, while the $N = 1728$ simulations became pervasively polarized near $\varepsilon_s \approx 66$. The $N = 4096$ particle SM1 simulations had not yet become pervasively polarized over the range of reaction fields shown, though they were for the SCRF ( $\varepsilon = 123.7 \pm 88.9$ ) and CL boundary conditions (see Figure 5). Under the CL

boundary condition, all of the SM1 simulations showed strong pervasive polarization, with values of $RMS(\mathbf{M})/N\mu$ in excess of 0.7.

The EM1 fluid; however, leveled off at a small residual polarization at an $\varepsilon_s$ near 60, and did not develop pervasive spontaneous polarization for any box size or reaction field strength, including the CL and SCRF boundary conditions. Even under the CL boundary condition, the value $RMS(\mathbf{M})/N\mu$ for the EM1 fluid was 0.022 ± 0.003, not substantially higher than the value of 0.021 ± 0.002 at $\varepsilon_s = 60$. This indicates that even slight shape anisotropy in a Stockmayer-like fluid is sufficient to frustrate molecular correlation, thereby preventing the phase transition from an isotropic fluid to a ferroelectric fluid under the conditions examined.

Furthermore, the reduced correlations that are found in the EM1 simulations resulted in a far smaller dielectric constant at the same dipole density, as discussed earlier. Instead of a dielectric constant in the hundreds, as predicted by the Stockmayer model, the EM1 model deviates by only 16% from acetonitrile, the liquid that it most resembles. The coarse-grained parameterization of EM1 as a highly polar "acetonitrile-like" fluid does not exhibit the ferroelectric behavior of the SM1 Stockmayer fluid that causes the model to deviate greatly from the dielectric behavior of real polar liquids at high dipole density.

## 2.5. Conclusion

In this comprehensive Monte Carlo simulation study of simple models of dipolar fluids, we have shown that the while the Stockmayer fluid, consisting of spherical particles containing embedded dipoles, exhibits ferroelectric ordering at high dipole densities, a modified model using ellipsoidal particles to break the spherical symmetry does not. We have also observed that the selection of boundary conditions representing the effects of long-range electrostatic interactions has a profound effect on the Stockmayer fluid, sometimes eclipsing effects due to changes in molecular properties. The ellipsoidal model exhibits substantially less dependence on electrostatic boundary conditions, remains isotropic under very strong reaction fields, and only develops ferroelectric domains in the absence of a reaction field. The isotropic behavior at high dipole density, low sensitivity to reaction field strength, and physically realistic dielectric constant indicate that ellipsoidal fluids may be useful as coarse-grained solvent models for large-scale simulations.

## 2.6. Acknowledgements for Chapter 2

Thanks to Robin Barnes for initial development work on the C++ MC simulation code, Thomas W. Draxler for compiling experimental data and for useful discussion, Benjamin H. Sibelman for developing a visualizer for our simulations, Bruce E. Eichinger, J. Michael Schurr, Philip A. Sullivan, and Stephanie J. Benight for useful discussion, Larry Dalton for encouragement, as well as the National Science Foundation (STC-MDITR DMR-0120967 and DMR-

0905686), the Air Force Office of Scientific Research (FA9550-09-1-0589), and the University of Washington Student Technology Fund for financial support.

## 2.7. Supplemental information for Chapter 2

Computational details, simulation convergence information, and additional data are included in Appendix A. Additional simulation results on acetonitrile are included in Appendix B.

## 2.8. References for Chapter 2

1. (a) Leach, A. R., *Molecular Modeling: Principles and Applications*. 2nd ed.; Pearson Education: Harlow (UK), 2001; (b) Hansen, J.-P., McDonald, I.R., *Theory of Simple Liquids*. 3rd ed.; Elsevier: Amsterdam, Netherlands, 2006; (c) Karlstrom, G., Formation of ferroelectric domains observed in simulation of droplets of dipolar particles. *The journal of physical chemistry B* **2007,** *111* (36), 10745-58.
2. Onsager, L., Electric moments of molecules in liquids. *Journal of the American Chemical Society* **1936,** *58*, 1486-93.
3. Kirkwood, J. G., The dielectric polarization of polar liquids. *Journal of Chemical Physics* **1939,** *7*, 911-19.
4. (a) Neumann, M.; Steinhauser, O., The influence of boundary conditions used in machine simulations on the structure of polar systems. *Molecular Physics* **1980,** *39* (2), 437-54; (b) Neumann, M., Dipole moment fluctuation formulas in computer simulations of polar systems. *Molecular Physics* **1983,** *50* (4), 841-58; (c) Patey, G. N.; Levesque, D.; Weis, J. J., On the theory and computer simulation of dipolar fluids. *Molecular Physics* **1982,** *45* (3), 733-46; (d) Schurr, J. M., Dielectric relaxation and depolarized dynamic light scattering of a generalized Debye model fluid. *Molecular Physics* **1980,** *40* (5), 1025-51; (e) De Leeuw, S. W.; Perram, J. W.; Smith, E. R., Computer Simulation of the Static Dielectric Constant of Systems with Permanent Electric Dipoles. *Annual Review of Physical Chemistry* **1986,** *37*, 245-270.
5. Adams, D. J., Computer simulation of highly polar liquids. The hard sphere plus point dipole potential. *Molecular Physics* **1980,** *40* (5), 1261-71.
6. (a) Allen, M. P., Tildesley, D.J., *Computer Simulations of Liquids*. Clarendon: Oxford (UK), 1987; (b) Perram, J. W.; Petersen, H. G.; De Leeuw, S. W., An algorithm for the simulation of condensed matter which grows as the 3/2 power of the number of particles. *Molecular Physics* **1988,** *65* (4), 875-93.
7. Gray, C. G.; Sainger, Y. S.; Joslin, C. G.; Cummings, P. T.; Goldman, S., Computer simulation of dipolar fluids. Dependence of the dielectric constant on system size: a comparative study of Ewald sum and reaction field approaches. *Journal of Chemical Physics* **1986,** *85* (3), 1502-4.

8. Tani, A.; Henderson, D.; Barker, J. A.; Hecht, C. E., Application of perturbation theory to the calculation of the dielectric constant of a dipolar hard sphere fluid. *Molecular Physics* **1983,** *48* (4), 863-9.
9. (a) Pounds, M. A.; Madden, P. A., Are dipolar liquids ferroelectric? Simulation studies. *Journal of Chemical Physics* **2007,** *126* (10), 104506/1-104506/7; (b) Shelton, D. P., Are dipolar liquids ferroelectric? *Journal of Chemical Physics* **2005,** *123* (8), 084502/1-084502/8; (c) Kumar, P.; Franzese, G.; Buldyrev, S. V.; Stanley, H. E., Molecular dynamics study of orientational cooperativity in water. *Physical Review E: Statistical, Nonlinear, and Soft Matter Physics* **2006,** *73* (4-1), 041505/1-041505/8.
10. (a) Valisko, M.; Boda, D.; Liszi, J.; Szalai, I., A systematic Monte Carlo simulation and renormalized perturbation theoretical study of the dielectric constant of the polarizable Stockmayer fluid. *Mol. Phys.* **2003,** *101* (14), 2309-2313; (b) Jia, R.; Hentschke, R., Dipolar particles in an external field: Molecular dynamics simulation and mean field theory. *Physical Review E: Statistical, Nonlinear, and Soft Matter Physics* **2009,** *80* (5-1), 051502/1-051502/9; (c) Bartke, J.; Hentschke, R., Phase behavior of the Stockmayer fluid via molecular dynamics simulation. *Physical Review E: Statistical, Nonlinear, and Soft Matter Physics* **2007,** *75* (6-1), 061503/1-061503/11; (d) Bartke, J.; Hentschke, R., Dielectric properties and the ferroelectric transition of the Stockmayer-fluid via computer simulation. *Molecular Physics* **2006,** *104* (19), 3057-3068.
11. Valisko, M.; Boda, D., Relative Permittivity of Polar Liquids. Comparison of Theory, Experiment, and Simulation. *Journal of Physical Chemistry B* **2005,** *109* (13), 6355-6365.
12. Szalai, I.; Nagy, S.; Dietrich, S., Nonlinear dielectric effect of dipolar fluids. *The Journal of Chemical Physics* **2009,** *131* (15), 154905-9.
13. (a) Groh, B.; Dietrich, S., Orientational order in dipolar fluids consisting of nonspherical hard particles. *Physical Review E: Statistical Physics, Plasmas, Fluids, and Related Interdisciplinary Topics* **1997,** *55* (3-A), 2892-2901; (b) Groh, B.; Dietrich, S., Spatial structures of dipolar ferromagnetic liquids. *Physical Review Letters* **1997,** *79* (4), 749-752.
14. Rommel, H. L.; Robinson, B. H., Orientation of Electro-optic Chromophores under Poling Conditions: A Spheroidal Model. *Journal of Physical Chemistry C* **2007,** *111* (50), 18765-18777.
15. Fries, P. H.; Richardi, J.; Krienke, H., Dielectric and structural results for liquid acetonitrile, acetone and chloroform from the hypernetted chain molecular integral equation. *Molecular Physics* **1997,** *90* (5), 841-853.
16. Skaf, M. S., Static dielectric properties of a model for liquid DMSO. *Molecular Physics* **1997,** *90* (1), 25-34.
17. Saiz, L.; Guardia, E.; Padro, J.-A., Dielectric properties of liquid ethanol. A computer simulation study. *Journal of Chemical Physics* **2000,** *113* (7), 2814-2822.
18. Barker, J. A.; Watts, R. O., Monte-Carlo studies of the dielectric properties of water-like models. *Molecular Physics* **1973,** *26* (3), 789-92.
19. Böttcher, C. J. F., *Theory of Electric Polarization*. Elsevier: Amsterdam, Netherlands, 1952.
20. (a) Debye, P., *Polar Molecules*. Dover Publications: New York, 1929; (b) See supporting information.
21. Fröhlich, H., *Theory of Dielectrics*. 2nd ed.; Clarendon Press: Oxford, 1958.

22. (a) Frenkel, D., Smidt, B., *Understanding Molecular Simulation: From Algorithms to Applications*. Elsevier: Amsterdam (ND), 2002; (b) Neumann, M.; Steinhauser, O.; Pawley, G. S., Consistent calculation of the static and frequency-dependent dielectric constant in computer simulations. *Molecular Physics* **1984,** *52* (1), 97-113.
23. De Leeuw, S. W.; Perram, J. W.; Smith, E. R., Simulation of electrostatic systems in periodic boundary conditions. I. Lattice sums and dielectric constants. *Proceedings of the Royal Society of London, Series A: Mathematical, Physical and Engineering Sciences* **1980,** *373* (1752), 27-56.
24. Goldman, S., Determination of the static dielectric constant-temperature-density surfaces of a Stockmayer fluid by perturbation theory. *Molecular Physics* **1990,** *71* (3), 491-507.
25. Metropolis, N., Rosenbluth, A. W., Rosenbluth, M. N., Teller, A H., Teller, E., Equation of State Calculations by Fast Computing Machines. *Journal of Chemical Physics* **1953,** *21* (6), 1087-1092.
26. Perram, J. W.; Wertheim, M. S., Statistical mechanics of hard ellipsoids. I. Overlap algorithm and the contact function. *Journal of Computational Physics* **1985,** *58* (3), 409-16.
27. Barker, J. A.; Watts, R. O., Structure of water; A Monte Carlo calculation. *Chemical Physics Letters* **1969,** *3* (3), 144-145.
28. Alder, B. J.; Pollock, E. L., Simulation of Polar and Polarizable Fluids. *Annual Review of Physical Chemistry* **1981,** *32*, 311-329.
29. *Spartan '08*, 1.2.0; Wavefunction, Inc.: Irvine, CA, 2008.
30. Lide, D. R., *CRC Handbook of Chemistry and Physics*. 90th ed.; CRC Press: Baton Rouge, LA, 2009.
31. McQuarrie, D. A., *Statistical Mechanics*. University Science Books: Sausalito, CA, 2000.
32. Jorgensen, W. L.; Briggs, J. M.; Contreras, M. L., Relative partition coefficients for organic solutes from fluid simulations. *Journal of Physical Chemistry* **1990,** *94* (4), 1683-6.
33. *Intel C++ Compiler*, 11.1; Intel, Inc.: 2009.
34. Robinson, B. H.; Dalton, L. R., Monte Carlo statistical mechanical simulations of the competition of intermolecular electrostatic and poling-field interactions in defining macroscopic electro-optic activity for organic chromophore/polymer materials. *Journal of Physical Chemistry A* **2000,** *104* (20), 4785-4795.
35. *Matlab*, r2009b; The Mathworks: Natick, MA, 2009.
36. Sibelman, B. H. *Dipole X3D Translator*, 2.0; 2009.
37. NIST Chemistry WebBook. http://webbook.nist.gov (accessed 12/23/2009).
38. (a) Edwards, D. M. F.; Madden, P. A., A computer simulation study of the dielectric properties of a model of methyl cyanide. II. The interference of permanent and induced dipoles. *Molecular Physics* **1984,** *51* (5), 1163-79; (b) Edwards, D. M. F.; Madden, P. A.; McDonald, I. R., A computer simulation study of the dielectric properties of a model of methyl cyanide. I. The rigid dipole case. *Molecular Physics* **1984,** *51* (5), 1141-61.
39. (a) Weis, J. J.; Levesque, D., Orientational order in high density dipolar hard sphere fluids. *The Journal of Chemical Physics* **2006,** *125* (3), 034504-5; (b)

Weis, J. J.; Levesque, D., Ferroelectric phases of dipolar hard spheres. *Physical Review E* **1993,** *48* (5), 3728.
40. Klapp, S. H. L.; Schoen, M., Spontaneous orientational order in confined dipolar fluid films. *Journal of Chemical Physics* **2002,** *117* (17), 8050-8062.
41. Wyman, J., Jr., Polarization and dielectric constant of liquids. *Journal of the American Chemical Society* **1936,** *58*, 1482-6.

# 3. Dielectric and Phase Behavior of Dipolar Spheroids

## 3.1. Introduction

Coarse-grained spheroidal models of molecules allow for approximation of the steric behavior of a wide variety of molecules, including small organic liquids[1], organic electro-optic chromophores[2], and liquid crystals[3] at low computational cost. Such models, typically implemented using the Gay-Berne potential[4], variants thereof[5], or the method of Perram and Wertheim[6], introduce anisotropy into the van der Waals surface of the molecule, breaking the spherical symmetry of the ubiquitous Lennard-Jones potential. The steric anisotropy can result in dramatically different behavior from purely spherical models such as the Stockmayer fluid[7] (sphere containing a point dipole).

Molecular aspect ratio (length/width) is particularly crucial for liquid crystals. In his pioneering 1949 paper[8] on liquid crystal phases of colloidal materials, Onsager demonstrated that smectic or nematic phases could be induced in rigid spherocylinders (cylinders with hemispherical ends) by increasing their aspect ratio. It was later shown that LC phases could also be formed by prolate spheroids[9] and that steric anisotropy was a necessary, but not sufficient condition for forming LC phases.[10] Sufficiently oblate (discotic) spheroids with axial dipoles were demonstrated to form LC phases by Frenkel,[11] Patey,[12] Zannoni,[13] and others. Oblate spheroids with transverse dipoles[14] have also been demonstrated. Further work by Baus[15] and others[1c, 12a] demonstrated that dipolar spheroids could form ferroelectric LC phases. In addition, work by Berne[1b, 3] and co-workers explored the effects of electronic polarizability on

simple models of LC systems. All of this previously reported work is crucial to the development of the research project described in this chapter herein: simulating chromophore molecules for investigation of molecular ordering in electro-optic materials.

In addition to changes in centrosymmetric (LC) and acentric (ferroelectric) ordering at equilibrium, changes in the aspect ratio of a molecule can have dramatic effects for induced acentric ordering of dipole moments with respect to an applied electric field. Both analytic models and Monte Carlo simulations have demonstrated that dipolar spheres tend to align more strongly with an electric field than prolate spheroids[2a, 16]. The dramatic difference in ordering behavior has had significant implications for design of chromophores for electro-optic applications, which are typically highly prolate due to their long π-systems.[17] In electro-optics, the ordering is typically quantified by the acentric order parameter $\langle \cos^3 \theta \rangle$, where θ is the angle between the molecular dipole moment and the poling field used to align the chromophores. This cubic average cannot be measured directly and is generally estimated through simulation or measured indirectly based on electro-optic response[18].

However, a related quantity that can be directly quantified through capacitance measurements[19] is the dielectric constant ε, where

$$(\varepsilon - 1)\mathbf{E} = 4\pi\mathbf{P} \qquad (3\text{-}1)$$

**E** is the macroscopic electric field applied to the material and **P** is the total polarization of the material. If the following conditions are met: (1) ε is isotropic (scalar), (2) the material is composed of identical molecules with permanent dipole moment μ, (3) all polarization of the system is due to reorientation of

permanent dipoles (α = 0), and (4) the system is oriented such that the electric field is aligned along the z-axis, then

$$\varepsilon - 1 = \frac{4\pi M_z}{VE_z} = \frac{4\pi\rho_N \mu \langle \cos\theta \rangle}{E_z} \qquad (3\text{-}2)$$

in the static (DC) limit. Here, $V$ is the volume of the system, $\rho_N$ is the number density of the dipoles and $\theta$ is the angle between any individual dipole and the applied field, such that $\langle \cos\theta \rangle$ is the cosine of the angle between the total dipole moment $M$ and the applied field. Within the assumptions of Equation 3-2, this is simply the normalized projection of the dipole moment along the $z$-axis.

Furthermore, if the system is composed of spherical molecules, its thermodynamic state can be uniquely represented as a function of reduced dipole moment and reduced density,[7]

$$\mu^{*2} = \frac{\mu^2}{\sigma_{LJ}^3 k_B T} \quad (3\text{-}3)$$
$$\rho^* = \rho_N \sigma_{LJ}^3$$

Here, $T$ is the absolute temperature and $\sigma_{LJ}$ is the Lennard-Jones diameter of the molecule. These reduced parameters can be generalized[12a] to non-spherical molecules by replacing the single $\sigma_{LJ}$ with the molecular semi-axes ($a$, $b$, and $c$). Additionally, the dipole density of any polar material can be reduced to a single dimensionless parameter[20]

$$y = \frac{4\pi\rho_N \mu^2}{9 k_B T} \quad (3\text{-}4)$$

which removes dependence on molecular size, but is not unique.[7]

While the linear relationship in Equation 2-2 holds for most dielectric materials, it does not hold for ferroelectric materials. The Stockmayer fluid can

form ferroelectric[21] phases at sufficiently large dipole densities, but the transition occurs at a dipole density greater than the value of $y = 1$ as predicted by the Debye model of dielectric liquids[22]. This value is still far below that of many real polar liquids[1a, 23]. Such transitions can also be introduced in other polar spheroids at appropriate temperatures and pressures[1c].

The presence of the ferroelectric transition in spherical systems at comparatively low dipole densities (between $\mu^{*2} = 2$ and 2.5 at $\rho^* = 1.16$, or y between 3.25 and 4.06)[1a] compared to common highly polar solvents[24] such as acetonitrile ($y$=6.11), DMSO ($y$=4.57), and DMF ($y$=3.85) not only underscores the need for anisotropic steric representations, but also raises an interesting conundrum. Originally, the Onsager model of dielectric liquids[23a]

$$\frac{\left(\varepsilon - n^2\right)\left(2\varepsilon + n^2\right)}{\varepsilon\left(n^2 + 2\right)} = y \quad \text{(3-5)}$$

where $n$ is the refractive index of the liquid, was developed to correct for the Debye[22] model's incorrect prediction of a ferroelectric transition at $y$=1. However, while capable of reasonably approximating experimental data from macroscopic parameters, it is qualitatively incorrect in modeling the behavior of the system it is based on (the dipolar sphere) in many-body simulations[7, 25]. As a result, the Onsager model does not predict a ferroelectric phase transition under any conditions. By neglecting intermolecular interactions, it "right for the wrong reasons" as actual highly-polar liquids tend exhibit little net long-range intermolecular correlation[21c].

The present work will examine the ordering behavior and degree of intermolecular correlation (as quantified by deviation from the Onsager model)

for a range of dipolar spheroids. While previous work has often focused on wide ranges of aspect ratios (up to several orders of magnitude)[10a] and/or temperatures[13] and densities[11], this work will focus on the effects of dipole moment and aspect ratio alone at constant temperature, density, and molecular volume. The range of aspect ratios considered is small and centered around unity, to allow determination of how quickly the ordering behavior of dipolar spheroids fluid departs from that of the Stockmayer fluid.

## 3.2. Computational Methods

Simulations of dipolar spheroids were run at nine different spheroid eccentricities and five different dipole moments, holding all other input parameters except maximum translational and rotational move sizes constant. Methods were substantially identical to those used in Chapter 2. All simulations used self-consistent reaction field (SCRF) electrostatic boundary conditions, and run lengths were extended compared to Johnson *et al*. to account for slower convergence of simulations involving more eccentric spheroids and improve convergence of fluctuations in the dipole moment and energy[26]. Simulation size was set at $N = 1728$ particles for a length of 120,000 cycles, with $N$ trial moves per cycle for a total of $2.07 \times 10^8$ configurations per simulation. The last half (60,000 cycles) of each simulation was used for calculating properties, and five independent simulations were run for each set of conditions and averaged to produce reported results. Temperature was held constant at 293 K for all simulations, which were run using the canonical (NVT) ensemble and the following Hamiltonian:

$$U = \sum_i \left\{ \sum_{j>i} \left[ 4\varepsilon_{LJ} \left( \left( \frac{\sigma_{eff}(i,j)}{r_{ij}} \right)^{12} - \left( \frac{\sigma_{eff}(i,j)}{r_{ij}} \right)^{6} \right) + \frac{1}{r_{ij}^3} \left( \boldsymbol{\mu}_i \cdot \boldsymbol{\mu}_j - \left( \boldsymbol{\mu}_i \cdot \hat{\mathbf{r}}_{ij} \right) \left( \hat{\mathbf{r}}_{ij} \cdot \boldsymbol{\mu}_j \right) \right) - \frac{1}{R_{cut}^3} \frac{2(\varepsilon_S - 1)}{2\varepsilon_S + 1} \boldsymbol{\mu}_i \cdot \boldsymbol{\mu}_j \right] - \frac{2\varepsilon_S + \varepsilon}{2\varepsilon_S + 1} \boldsymbol{\mu}_i \cdot \mathbf{E} \right\} \quad (3\text{-}6)$$

Here, $\varepsilon_{LJ}$ is the Lennard-Jones energy (set to 217 K), $\sigma_{eff}$ is the effective Lennard-Jones contact distance calculated using the method of Perram and Wertheim[6], $R_{cut}$ is the cutoff distance for calculating electrostatic interactions (27.96 A), $\varepsilon_S$ is the reaction field dielectric constant, which is self-consistently updated every cycle,[1a] and **E** is a homogeneous external field (if used). Lennard-Jones interactions were truncated at 18.64 A.

Each spheroid of the nine spheroid geometries were run at all five dipole densities. The electrostatic parameters for each Table 3.1, and the spheroid geometries for the different aspect ratios are listed in Table 3.2.

**Table 3.1.** Simulation parameters – dipole strength

| $y$ | $\boldsymbol{\mu}$ (D) | **T** (K) | $\boldsymbol{\mu}^{*2}$ | $\boldsymbol{\rho}^*$ |
|---|---|---|---|---|
| 2 | 2.42 | 293 | 1.43 | 1.0 |
| 3 | 2.96 | 293 | 2.14 | 1.0 |
| 4 | 3.42 | 293 | 2.86 | 1.0 |
| 5 | 3.82 | 293 | 3.57 | 1.0 |
| 6 | 4.19 | 293 | 4.29 | 1.0 |

**Table 3.2.** Simulation parameters – spheroid geometries

| **Eccentricity** | $\boldsymbol{\sigma}$(b) (Å) | $\boldsymbol{\sigma}$(a) (Å) | **Aspect ratio** | **V** (Å$^3$) |
|---|---|---|---|---|
| 1:2 | 5.88 | 2.94 | 0.50 | 52.98 |
| 4:7 | 5.62 | 3.20 | 0.57 | 52.98 |
| 2:3 | 5.34 | 3.56 | 0.67 | 52.98 |
| 4:5 | 5.02 | 4.02 | 0.80 | 52.98 |
| 1:1 | 4.66 | 4.66 | 1.00 | 52.98 |
| 5:4 | 4.32 | 5.40 | 1.20 | 52.99 |
| 3:2 | 4.08 | 6.10 | 1.50 | 52.98 |
| 7:4 | 3.86 | 6.76 | 1.75 | 52.98 |
| 2:1 | 3.70 | 7.40 | 2.00 | 52.98 |

All simulations were run under both zero applied field and under an applied field of $\mathbf{E} = 50\ \mathrm{V/\mu m}$, with the local field

$$\mathbf{E}_0 = \frac{2\varepsilon_S + \varepsilon}{2\varepsilon_S + 1}\mathbf{E} \qquad (3\text{-}7)$$

calculated self-consistently based on the reaction field. The latter calculations were used to determine for which calculations the assumption of linear response to the field was valid, with close agreement between the calculated dielectric constants from the two methods indicating linearity. The dielectric constant was calculated directly from the ordering in the direction of the applied field (Equation 3-2) in the calculations with an external field, and using a Kirkwood fluctuation expansion[20, 27]

$$\langle M_z \rangle_{E_{0,z}} = \frac{E_{0,z}}{3k_B T}\left(\langle \mathbf{M}^2 \rangle_0 - \langle \mathbf{M} \rangle_0^2\right) \qquad (3\text{-}8)$$

of the total dipole moment **M** of the system at zero applied field to estimate the linear response of **M** to $\mathbf{E}_0$.

The Onsager model (Equation 3-5) was used as a control with values calculated at each dipole density, neglecting electronic polarizability as per the assumptions of Equation 3-2 such that $n = 1$. Additionally, the Onsager model can be generalized to spheroids (as suggested by Onsager[23a]) by means of a Dirichlet correction[28] on the local field factor such that

$$\frac{(\varepsilon - 1)(\varepsilon + A(a,b)(1-\varepsilon))}{3\varepsilon} = y \qquad (3\text{-}9)$$

where *a* is the major (dipole) semiaxis of the molecule, and *b* is the minor semiaxis, such that the aspect ratio is a/b, and

$$A(a,b) = \frac{1}{2}\int_0^x \frac{dx}{(x+1)\left(xa^2/b^2+1\right)} \qquad (3\text{-}10)$$

which allowed for treatment of purely electrostatic effects of molecular anisotropy in the absence of intermolecular correlations.

In addition to degree of ordering induced by an external field, spontaneous order was calculated from simulations at zero field. As these simulations do not have an external director axis that is known *a priori*, ordering is quantified by means of the de Gennes[29] Q-tensor

$$\mathbf{Q} = \frac{3\left\langle \mu_i \otimes \mu_j \right\rangle - \mathbf{I}}{2} \qquad (3\text{-}11)$$

averaged over all $\mu_i \neq \mu_j$. The dominant eigenvalue of **Q** is the nematic order parameter $P_2$ with respect to the internal director axis **d** of the system (the dominant eigenvector of **Q**).[21a] The acentric order parameter $P_1 = \hat{\mathbf{M}} \cdot \mathbf{d}$ can be obtained by projection of the total dipole moment of the system on the director, and is analogous to $\langle \cos\theta \rangle$.

Finally, the radial distribution function[20, 30]

$$g(r) = \frac{V\sum_i^N \sum_{j>i}^N n_{ij}(r, r+\Delta r)}{2\pi N\left(N-1\right) r^2 \Delta r} \qquad (3\text{-}12)$$

and first-order dipole correlation function[1a, 31]

$$g_\mu(r) = \frac{\sum_{i=1}^N \sum_{j>i}^N \cos\gamma_{ij}(r, r+\Delta r)}{2\pi N\left(N-1\right) r^2 \Delta r} \qquad (3\text{-}13)$$

were calculated, where $n_{ij}(r,r+\Delta r)$ is the number of particles where the center-center distance $r_{ij}$ is between $r$ and $r+\Delta r$ and $\cos\gamma = \hat{\boldsymbol{\mu}}_i \cdot \hat{\boldsymbol{\mu}}_j$. The former indicates the degree of correlation between the positions of atoms, with the function decaying to unity in a disordered structure such as an isotropic liquid or a glass and exhibiting repeating peaks in a system with strong positional order such as a smectic liquid crystal. The latter indicates the degree of correlation between dipoles, with negative values indicating net anti-correlation at a given distance, and positive values indicating net correlation. In an isotropic material, the correlation will decay to zero (no correlation), but in a ferroelectric material, it will limit to a positive value[12b, 32].

## 3.3. Results and Discussion

### *3.3.1. Static dielectric constant*

The static dielectric constant was calculated using both the applied-field and fluctuation method at six dipole densities, from $y$=2 (lowest) to $y$=6 (highest); results are shown in Figure 3.1.

**3.1a** ($y$=2)

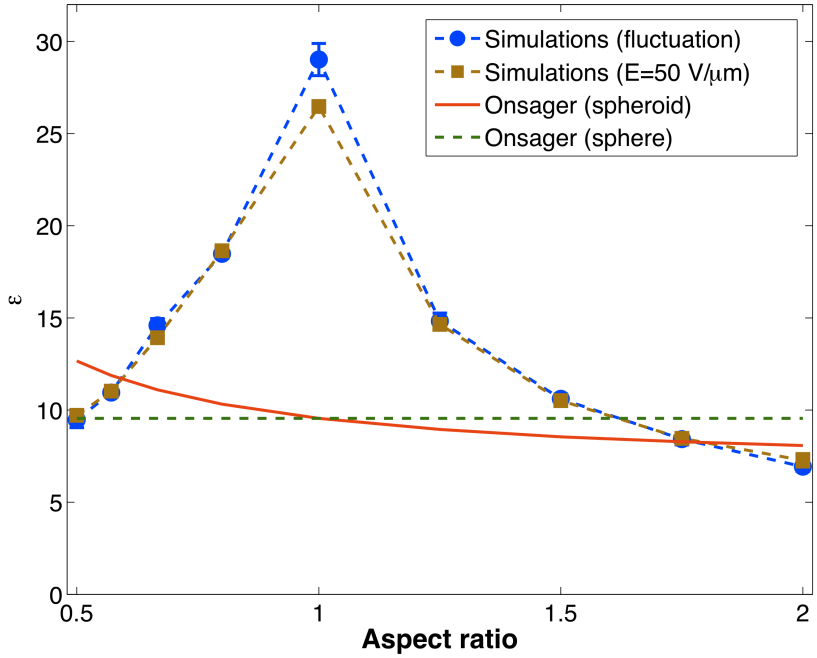
Simulations (fluctuation)
Simulations (E=50 V/μm)
Onsager (spheroid)
Onsager (sphere)
ε
Aspect ratio
0
5
10
15
20
25
30
0.5
1
1.5
2

**3.1b** ($y$=3)

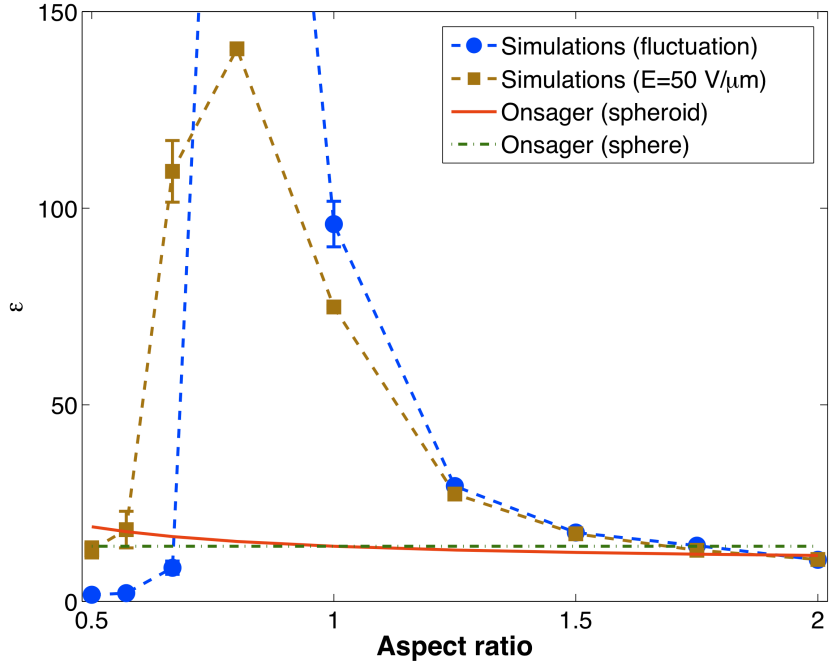
Simulations (fluctuation)
Simulations (E=50 V/μm)
Onsager (spheroid)
Onsager (sphere)
ε
Aspect ratio
0
50
100
150
0.5
1
1.5
2

**3.1c** ($y$=4)

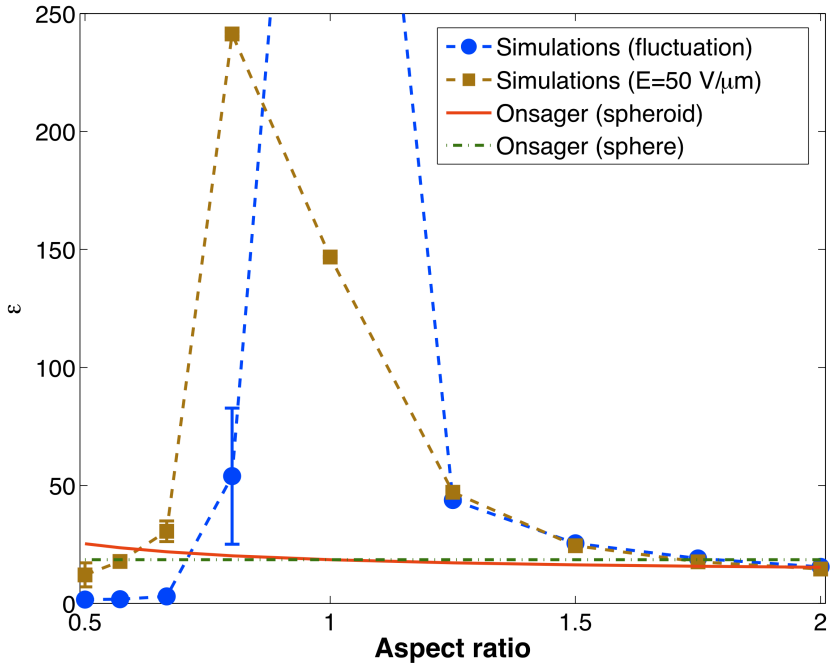
Simulations (fluctuation)
Simulations (E=50 V/μm)
Onsager (spheroid)
Onsager (sphere)
ε
Aspect ratio
0
50
100
150
200
250
0.5
1
1.5
2

**3.1d** ($y$=5)

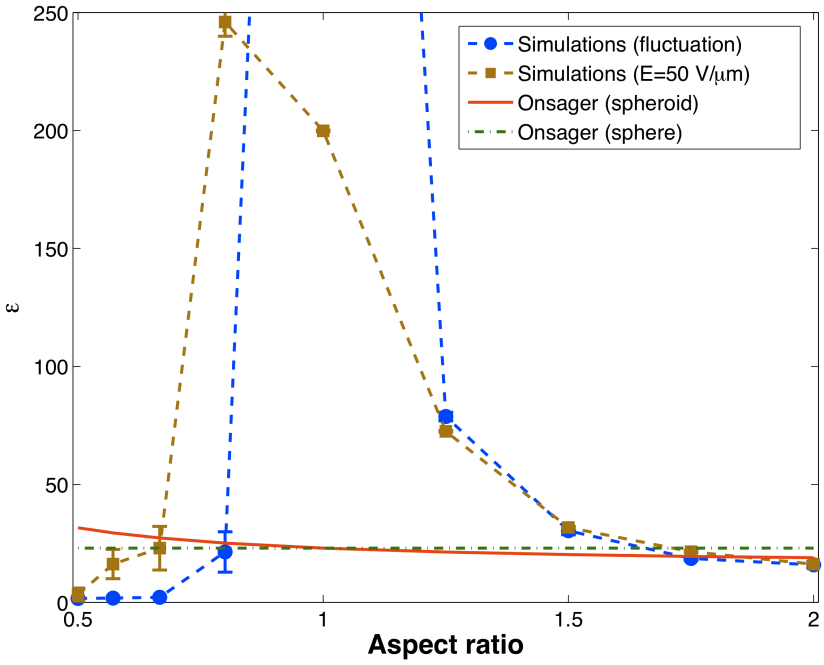
Simulations (fluctuation)
Simulations (E=50 V/μm)
Onsager (spheroid)
Onsager (sphere)
ε
Aspect ratio
0
50
100
150
200
250
0.5
1
1.5
2

**3.1e** ($y$=6)

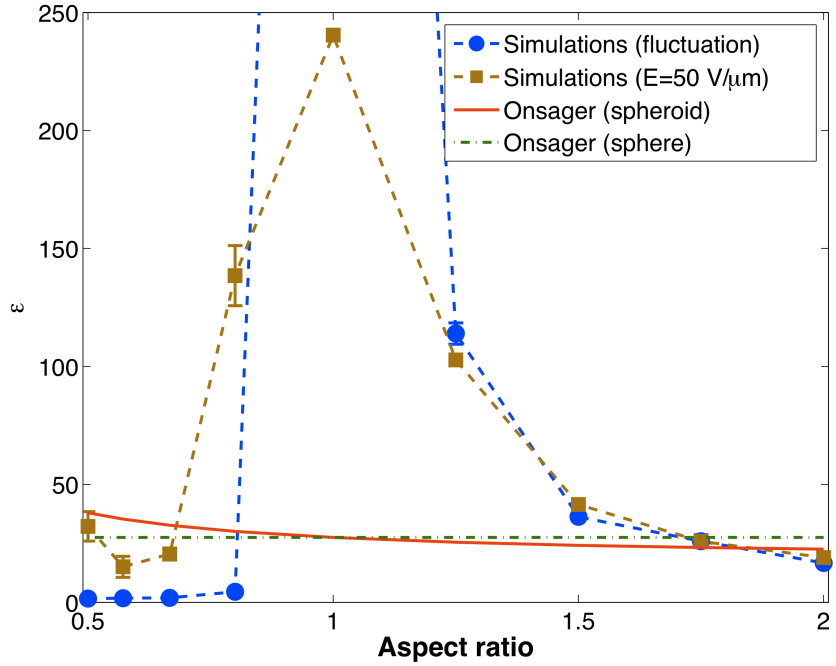


**Figure 3.1.** Static dielectric constant of spheroids of different aspect ratios, calculated using both dipole fluctuations and in response to an applied external field of 50 V / μm. Calculations were run at 293K, ρ* = 1, using SCRF boundary conditions, at dipole densities in the range $y$=2-6.

Results at the lowest dipole density ($y$=2) were well-behaved, with strong correlation between the applied-field and fluctuation results at all aspect ratios. The dielectric constant depended strongly on aspect ratio, forming a Lorentzian-like distribution around the Stockmayer (spherical) result, which was almost four times larger than the lowest (2:1 prolate) result, and the Stockmayer result was consistent with literature values for similar systems[25]. Spheres and nearly-spherical systems were poorly described by the Onsager model (with or without the Equation 3-9). However, the more prolate spheroids were reasonably well described by Equation 3-9, indicating a very low degree of net intermolecular correlation.

While results for prolate spheroids at $y$=3 followed similar trends to $y$=2, the behavior of oblates differed dramatically. Mildly oblate (4:5) spheroids exhibited dielectric behavior approximately twice as strong as the Stockmayer fluid. Furthermore, the oblate spheroids began to exhibit substantially different behaviors between results calculated from fluctuations and those in response to an applied field, with the fluctuation method yielding much lower dielectric constants. While this could be due to slow oscillation of $\langle \mathbf{M}^2 \rangle$ and/or difficulty in averaging out any net dipole moment[26, 33], the results exhibited little difference between simulations. Prolate spheroids with an aspect ratio of 3:2 or higher were still reasonably approximated by the Onsager model.

Behavior at $y$=4 was qualitatively similar to $y$=3 at all aspect ratios, however the dielectric constant for 4:5 oblates became very large (241 ± 1) for the applied field simulations, as did the Stockmayer results for the fluctuation calculations (>500). Prolates exhibited much lower dielectric constants and strong agreements between the fluctuation and applied-field methods, although the range of aspect ratios for which the Onsager model was approximately valid decreased.

By $y$=5, the Stockmayer fluid exhibited a very high dielectric constant, consistent with our prior results. Trends were otherwise similar to $y$=4. However, by $y$=6, the 4:5 oblates were no longer exhibiting an unusually large degree of dielectric polarization. However, the 1:2 oblates at the highest dipole density began to show an increase in their dielectric response to an applied field, although this was not reflected in the fluctuation calculations. Interestingly, even at the highest dipole densities, the applied-field and fluctuation-based responses

for prolates closely mirrored each other. The spheroidal Onsager model (Equation 3-9) a reasonable approximation for the 7:4 and 2:1 prolates.

The close match between the Onsager model and results for prolates at the wide range of dipole densities examined raises the possibility that the Onsager model's ability to closely fit experimental data for polar liquids is due to their shape. Two of the most polar small organic liquids (acetonitrile and nitromethane) are highly prolate, and others such as acetone and DMF are oblate but with an in-plane dipole instead of an axial one. As such, the reduction of ordering due to frusturation of intermolecular correlation[1a, 34] due to the sterics of real molecules. The relatively small difference between results calculated with Equations 3-5 and 3-9 may explain why the Onsager model, although constructed using spheres, works much better in explaining experimental results than as a stand-alone theory.

### *2.3.2. Spontaneous order*

The spontaneous order parameters $\langle P_1 \rangle$ and $\langle P_2 \rangle$ were calculated for all of the simulations at zero field. Results appear in Figure 3.2.

**3.2a.** Acentric order

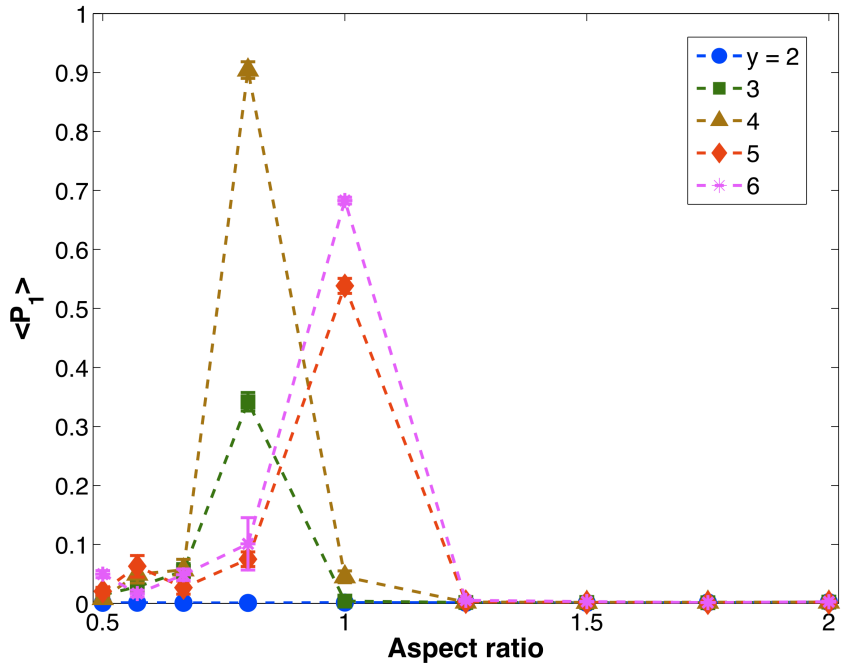


**3.2b.** Centrosymmetric order

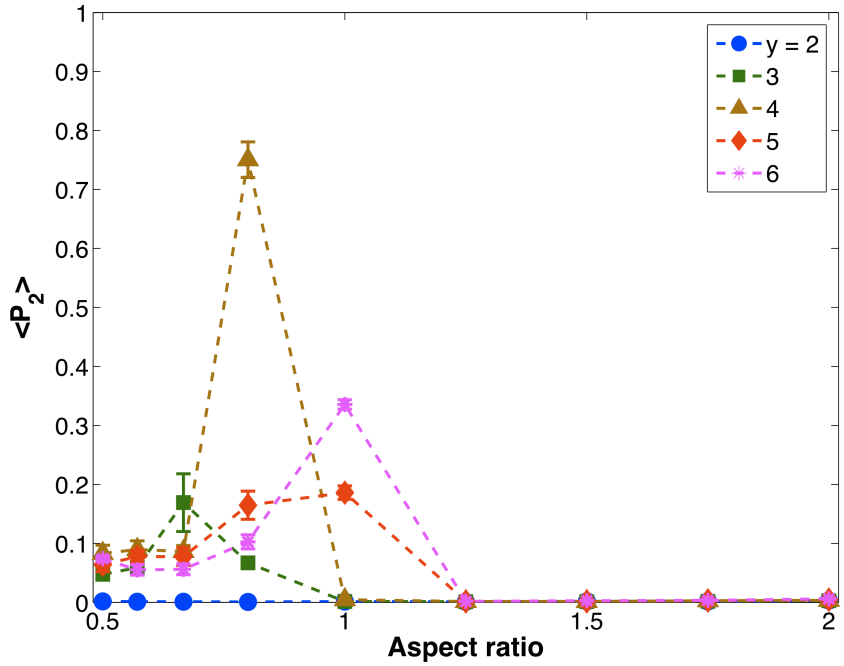


**Figure 3.2.** Spontaneous acentric (2.2a) and centrosymmetric (2.2b) ordering in dipolar spheroids of different dipole densities at 293K and $\rho^* = 1$ under SCRF boundary conditions in the absence of an applied field, as obtained from the ordering matrix **Q** (Equation 2-11).

No spontaneous ordering was observed in prolate ellipsoids at any dipole density under the conditions studied; prolates that form nematic phases at ρ* = 1 often have substantially aspect ratios then considered here.[1c, 11, 32, 35] Furthermore, no spontaneous ordering was observed for any aspect ratio at *y*=2. At the other dipole densities, the more oblate systems, with aspect ratios between 2:3 and 1:2 exhibited little spontaneous ordering, with $\langle P_2 \rangle$ typically larger than $\langle P_1 \rangle$. This could be potentially indicative of very weak anti-ferroelectric ordering. Strong ( $\langle P_1 \rangle > 0.3$) acentric ordering was observed for 4:5 oblates at *y*=3 and *y*=4, and for the Stockmayer fluid at *y*=5 and *y*=6, consistent with the singularities in the dielectric constant seen in Figure 1. This strong ordering in the absence of a field is indicative of formation of a ferroelectric[12a, 36] phase, and is most pronounced for 4:5 oblates at *y*=4, where $\langle P_1 \rangle$ approaches unity. For all of these strongly ordered systems, $\langle P_2 \rangle$ was smaller than $\langle P_1 \rangle$. Furthermore, the only system with a degree of centrosymmetric ordering similar to its amount of acentric ordering was the 4:5 oblates at *y*=4 (medium dipole density). Strong centrosymmetric order in the absence of acentric order was not observed over the range of aspect ratios and dipole densities studied.

### *3.3.3. Thermodynamics*

In addition to ordering behavior, the total energy and constant-volume heat capacity ($C_v$) were examined for signs of phase transitions; results appear in Figure 3.3.

**3.3a.** Total potential energy

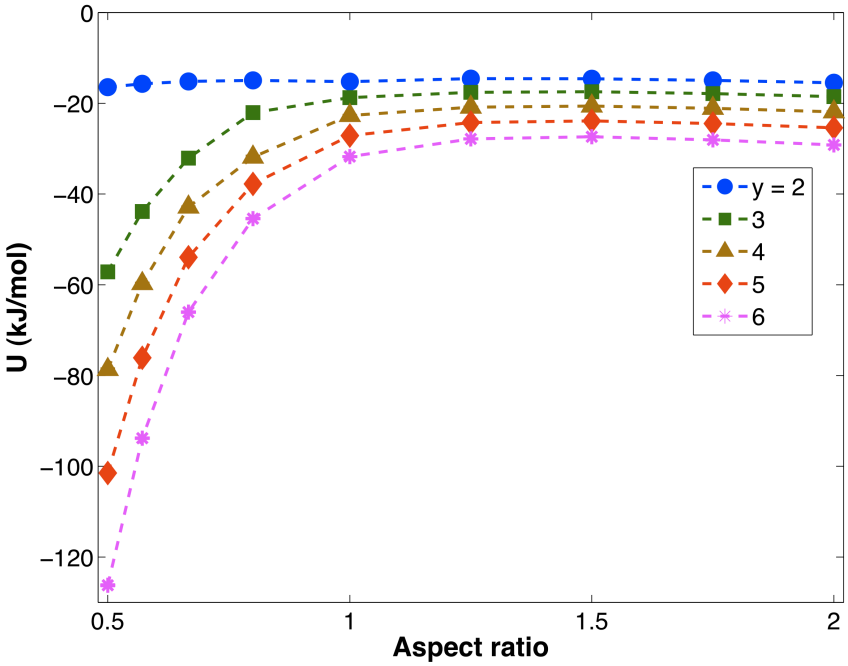


**3.3b.** Heat capacity

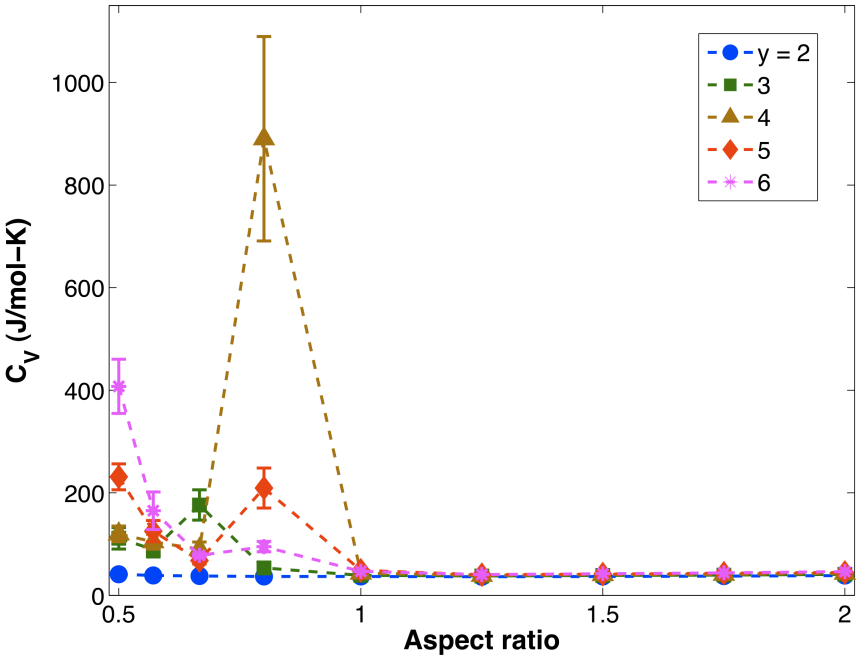


**Figure 3.3.** Total potential energy (3.3a) and constant-volume heat capacity (3.3b) of ensembles of dipolar spheroids at 293K and ρ* = 1 under SCRF boundary conditions in the absence of an applied field. The heat capacity was calculated from fluctuations in the total energy[30b].

Both the energy and heat capacity further illustrate the large difference in behavior between oblates and both prolates and spheres at dipole densities of $y > 2$. At each dipole density, energy remains nearly constant for aspect ratios between 1 and 2, with 5:4 prolates having the highest energy. For oblates, the total energy decreases dramatically with aspect ratio, consistent with previously observed trends in electrostatic energy with aspect ratio[12a]. As the reduction in aspect ratio allows for close, energetically favorable stacking of dipoles, and as $\varepsilon_{LJ}$ is held constant, the electrostatic term dominates this decrease in energy. The total energy also decreases with increasing dipole density, again due to stronger electrostatic interactions.

An even larger shift as the aspect ratio is decreased below 1 is seen in $C_v$. The heat capacity remains nearly constant at all dipole densities for prolates and spheres, even for dipole densities in which the Stockmayer fluid exhibits ferroelectric order, but increases rapidly for oblates with $y > 2$. The highest heat capacity is observed for the highly-ordered 4:5 oblates at $y$=4, and for 1:2 oblates at the highest dipole densities. The large shift in heat capacities is strongly indicative that the oblates at $y > 2$ inhabit a different phase than the other spheroids considered.

### *3.3.4. Radial distribution function*

Positional ordering was examined by means of the radial distribution function (equation 12) for five aspect ratios at $y$=2 and $y$=4; results appear in Figure 3.4.

**3.4a.** ($y$=2)

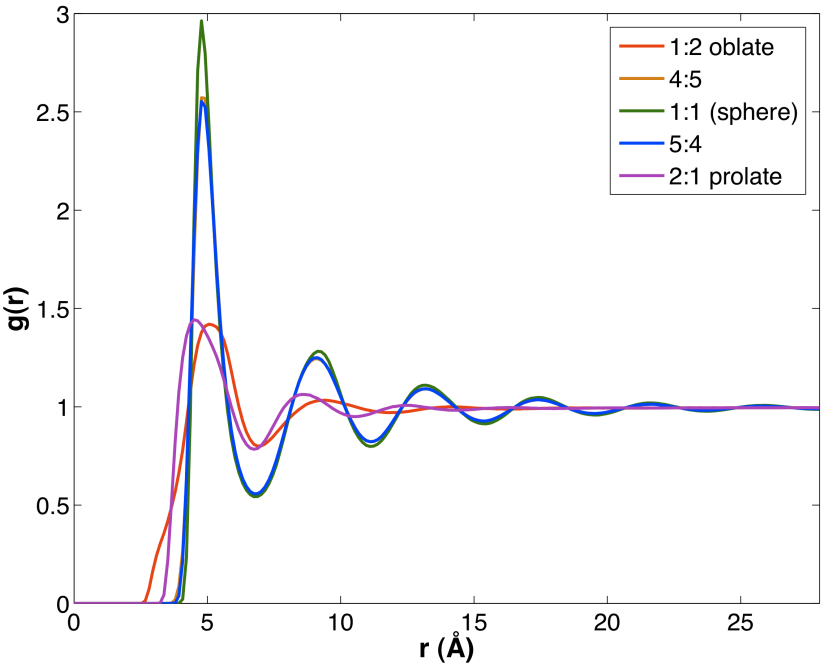


**3.4b.** ($y$=4)

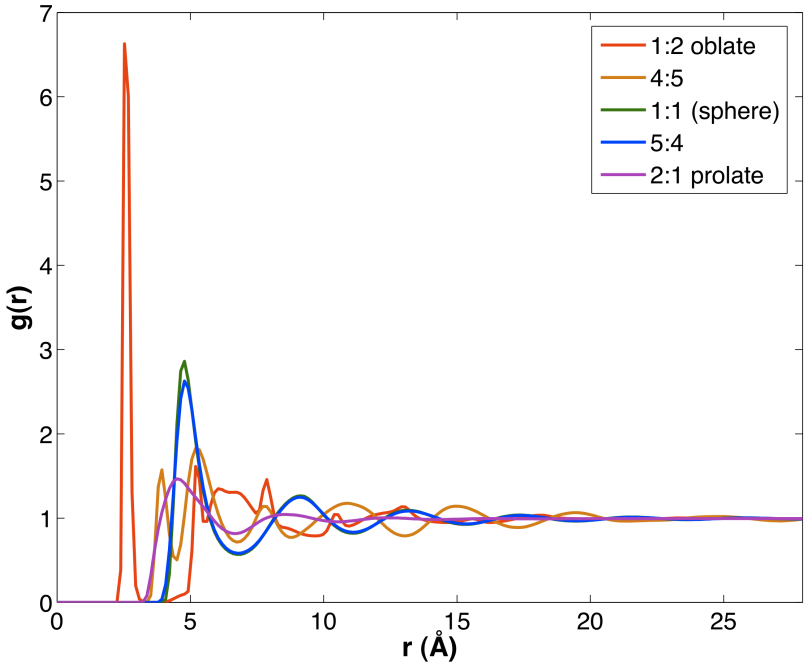


**Figure 3.4.** Radial distribution functions (g(r)) at two dipole densities at 293K and ρ* = 1 under SCRF boundary conditions in the absence of an applied field.

At $y$=2, the most oblate (1:2) and prolate (2:1) spheroids show only weak positional correlation, decaying rapidly after two neighbor shells. Spheroids with intermediate aspect ratios show stronger positional correlation with uniform peak spacing and a longer persistence distance, but do not have any long-range positional order, as evinced by g(r) decaying to unity before the edge of the simulation cell is reached. The rapid decay of the radial distribution function may be indicative of a system in the liquid phase. At $y$=4, spheres and mild-prolates showed similar behavior to y =2. The 4:5 oblates showed weaker initial correlation, but it persisted slightly longer than for spheres or prolates. The 1:2 oblates, however, showed a distinct structure, with narrow peaks and very strong correlation of the first neighbor shell and erratic correlation thereafter. The order did not persist any longer than with spheres or prolates, and may be indicative of a disordered (glassy) solid.

### *3.3.5. Dipole correlation function*

The persistence distance for dipole alignment was examined by means of the first-order dipole correlation function (Equation 3-13) for the same conditions as the radial distribution function. Results appear in Figure 3.5.

**3.5a.** ($y$=2)

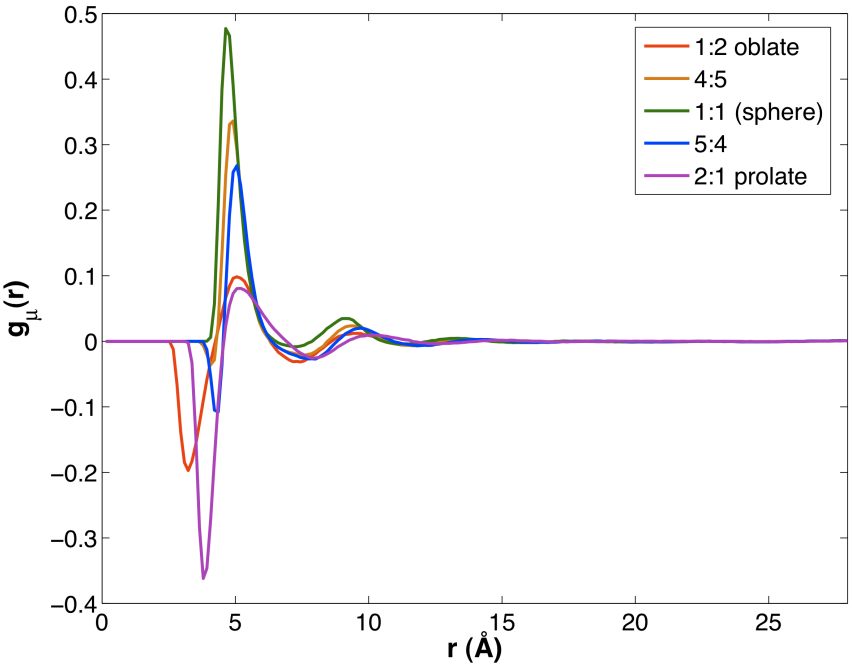


**3.5b.** ($y$=4)

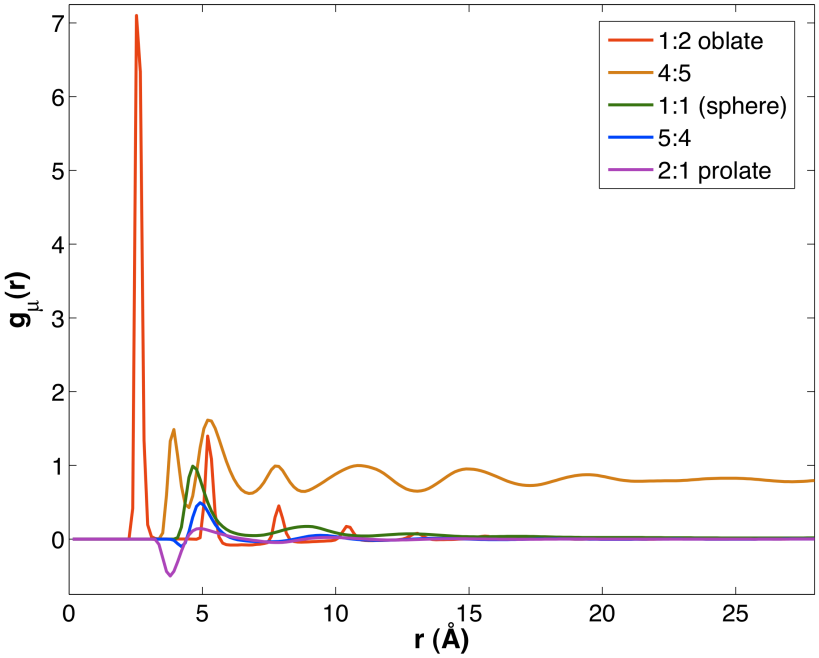


**Figure 3.5.** Dipole correlation functions ($g_\mu(r)$) at two dipole densities at 293K and $\rho^* = 1$ under SCRF boundary conditions in the absence of an applied field.

Prolate spheroids and 1:2 oblates exhibited similar dipole correlation functions at $y$=2, with an initial anti-correlated peak followed by a shell of aligned dipoles, with rapid decay of correlation beyond that such that it is negligible at 15 Å. Neither spheres nor 4:5 oblates show any initial anti-correlation; both also show stronger short-range correlation than the prolates, albeit persisting for about the same distance. The negative correlation is strongest for the highest aspect ratio (2:1) as the spheroids can approach each other more closely in a direction orthogonal to the dipole moment, favoring anti-parallel stacking of dipoles.[1a] The positive correlation is strongest for the Stockmayer fluid.

At $y$=4, the behavior of the prolate spheroids is relatively unchanged compared to $y$=2, but the behavior of spheres and oblates is greatly altered. Instead of oscillating around zero, the curve for the Stockmayer fluid remains positive until it decays to zero, indicating net short-range correlation (formation of ferroelectric domains), but not pervasive ferroelectric behavior[1a]. Similar local correlation of dipoles is seen for the 1:2 oblates, albeit to a greater extent and in the form of sharp peaks instead of a smooth, polarized region. The 4:5 oblates, however, are strongly ferroelectric, with dipole correlation remaining positive over the entire system.

### *3.3.6. Phase behavior*

Based on dielectric, thermodynamic, and structural data, simulations at each aspect ratio and dipole density were assigned to one of the following four phases:[12b, 15]

1. Isotropic liquid — little/no spontaneous order, smooth correlation functions, rapid decay of both dipole-dipole and positional correlation
2. Ferroelectric liquid — substantial spontaneous acentric order, smooth correlation functions, rapid decay of positional correlation but nonzero dipolar correlation at long range.
3. Ferroelectric-nematic — large spontaneous acentric and centrosymmetric order, smooth correlation functions with net long-range dipolar correlation, but without long-range positional correlation, and larger heat capacity than isotropic
4. Glassy solid – little/no spontaneous order, sharply peaked but decaying dipolar and positional correlation functions, larger heat capacity than isotropic, fluctuation method yields much substantially smaller dielectric response than applied-field method.

Some results were also transitional, for example, exhibiting ferroelectric domains, but not net ferroelectric behavior over the entire system. Representative visualizations of the four phases listed above are shown in Figure 3.6.

**3.6a** (isotropic liquid – $y$=2, 3:2 prolates)

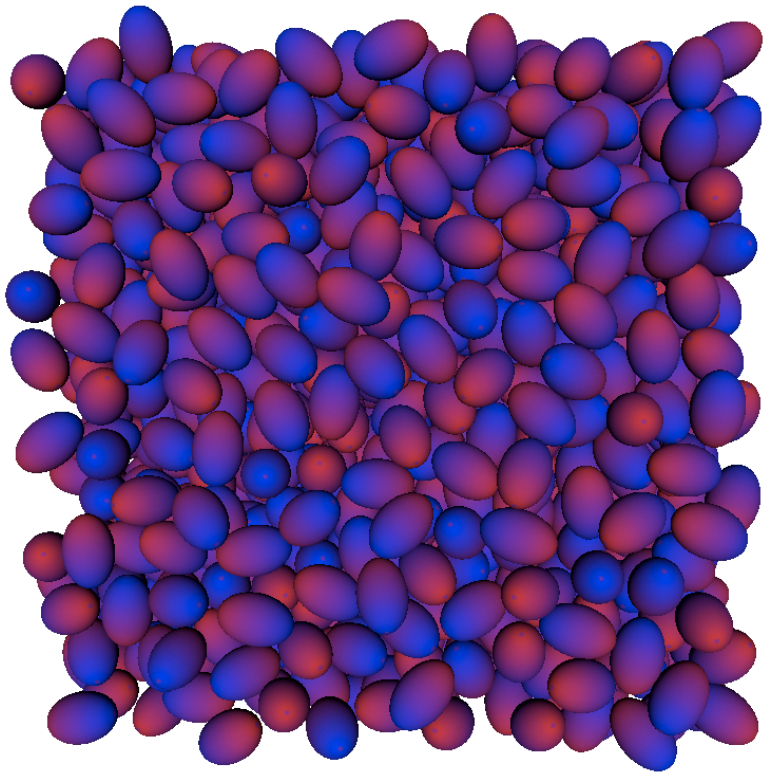

**3.6b** (ferroelectric liquid – $y$=6, 1:1 spheres)

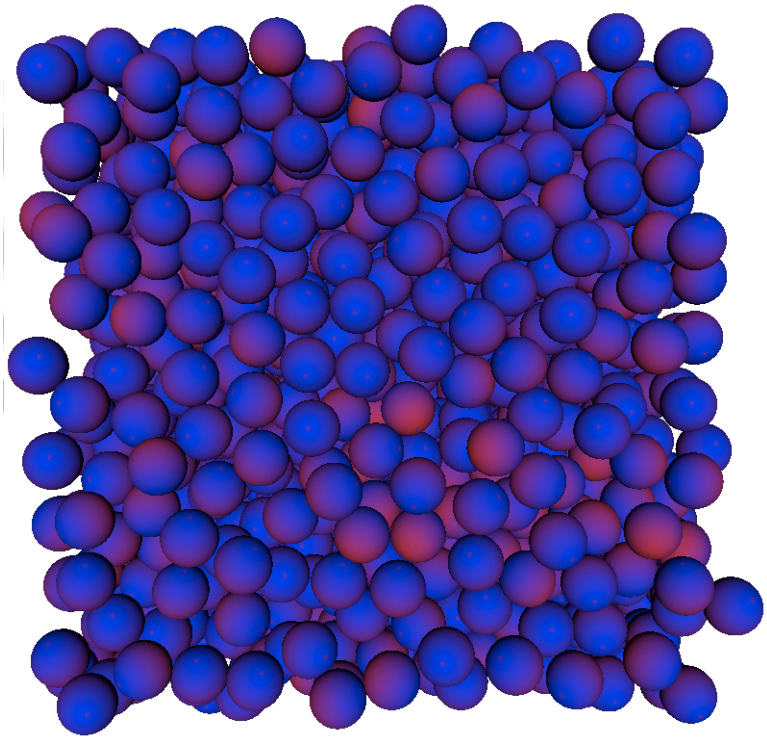

**3.6c** (ferroelectric-nematic – $y$=4, 4:5 oblate

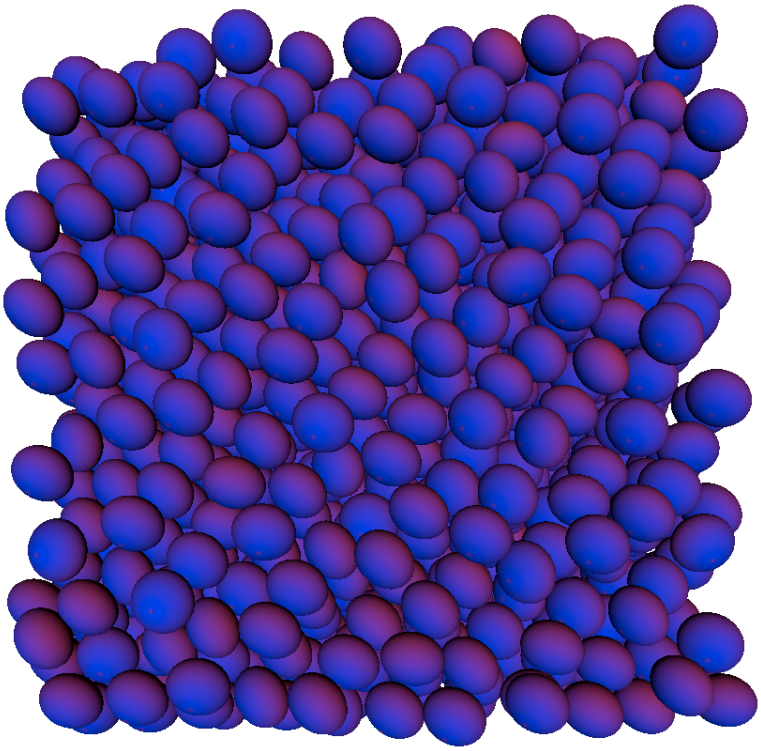

**3.6d** (glassy solid – $y$=4, 2:1 oblates)

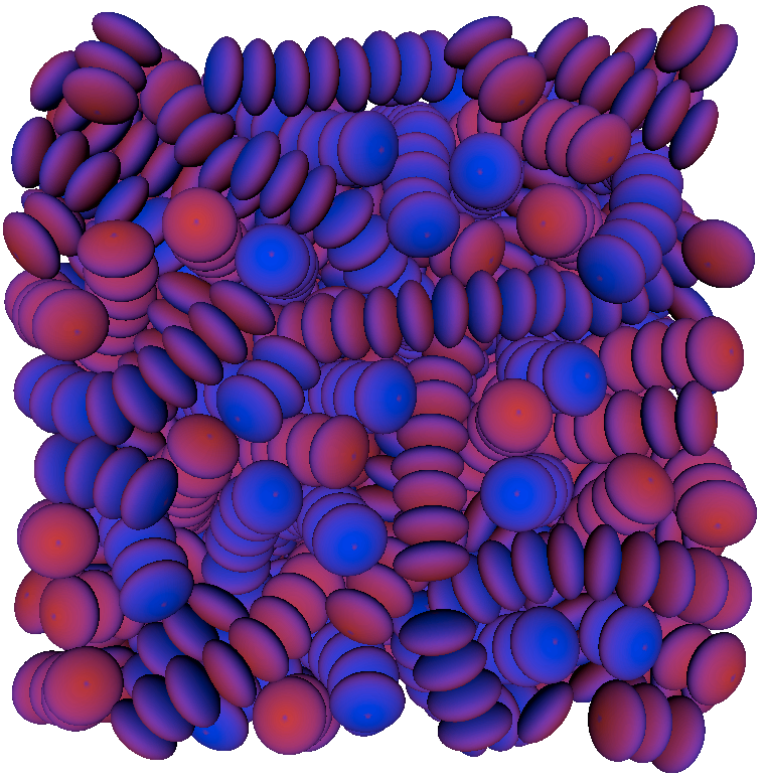

**Figure 3.6.** Representative simulation visualizations at 293K and ρ* = 1 under SCRF boundary conditions and in the absence of an applied field.

In comparing Figure 6b and 6c, it can be seen that the ferroelectric-nematic phase, which only appeared for a single set of conditions (4:5 oblates at $y$=4) is distinct from the ferroelectric liquid phase in that it exhibits 1-dimensional order with particles consistently aligned along a single axis, whereas the ordinary ferroelectric phase exhibits net polarization without strong centrosymmetric alignment. None of the strongly aligned phases exhibited the periodic, positional correlation (formation of layers) observed in smectic phases.

Simulations in the glassy phase exhibited peculiar polymer-like structures with the molecular dipoles aligned along each chain, but the chains randomly ordered such that the system had little or no net order. Both the polymerization and reduced ordering/dielectric constant in oblate systems that formed these

sorts of chains was consistent with prior simulation work by Rommel and Robinson[2a], and such chains have also been observed in the Stockmayer fluid under a variety of temperatures and densities[37].

Results from all 45 sets of simulations were combined into a phase diagram defined by their dipole density and aspect ratio, which appears in Figure 3.7.

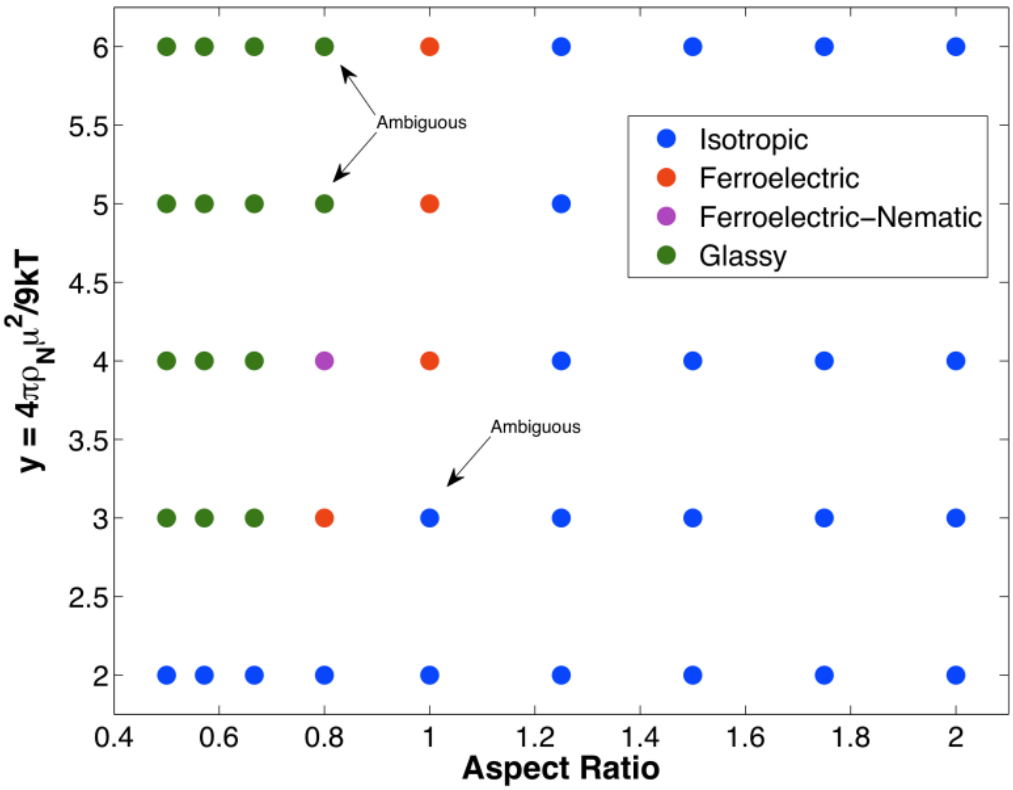


**Figure 3.7.** Dipole density / Aspect ratio phase diagram for dipolar spheroids at 293K and ρ* = 1 under SCRF boundary conditions and in the absence of an applied field.

At the temperature and density examined, the ferroelectric phase was found to exist within a narrow band of aspect ratios, with clear or ambiguous ordering occurring only for spheres and 4:5 oblates, and only for $y \geq 3$. Spheroids

more oblate than those in the narrow ferroelectric band formed glassy polymer-like materials, and all of the prolate spheroids examined remained in the isotropic phase even at a 5:4 aspect ratio and $y$=6. The highly-ordered, ferroelectric-nematic phase was confined to a single dipole density/aspect ratio combination. However, as previously mentioned, these results represent only a single temperature and density and small range of aspect ratios, albeit one relevant for studying small, polar organic liquids.

## 3.4. Conclusion

Subtle changes in the aspect ratio of dipolar spheroids can have dramatic effects on their ordering behavior at r*=1 and 293K. While only an isotropic phase was observed at $y$=2, ferroelectric behavior was observed in a very narrow range of aspect ratios (either spheres or slight oblates) at higher dipole densities. None of the prolate spheroids studied, even those with a 5:4 aspect ratio, exhibited ferroelectric behavior, indicating that slight anisotropy is enough to disrupt dipole correlation. However, a wide variation in dielectric constants was observed for prolates at each dipole density, with the dielectric constant decreasing as the aspect ratio was increased. The much-lower dielectric constant of spheroids with aspect ratios above 3:2 (compared to the Stockmayer fluid) is close to that predicted by the Onsager model, and may provide a partial explanation for the success of the Onsager model in predicting the dielectric behavior of small organic liquids in spite of its poor predictions for the dielectric constant of the Stockmayer fluid.

## 3.5. Acknowledgements for Chapter 3

Thanks to Stephanie J. Benight for collaborating on this project, Andreas F. Tillack and Bruce E. Eichinger for useful discussion, Robin Barnes for her initial work on this project, Benjamin H. Sibelman for developing the software used to visualize these simulations, as well as the National Science Foundation (STC-MDITR DMR-0120967 and DMR-0905686), the Air Force Office of Scientific Research (FA9550-09-1-0589), and the University of Washington Student Technology Fund for financial support.

## 3.6. References for Chapter 3

1. (a) Johnson, L. E.; Barnes, R.; Draxler, T. W.; Eichinger, B. E.; Robinson, B. H., Dielectric Constants of Simple Liquids: Stockmayer and Ellipsoidal Fluids. *Journal of Physical Chemistry B* **2010,** *114* (25), 8431-8440; (b) Cao, J.; Berne, B. J., Theory and simulation of polar and nonpolar polarizable fluids. *Journal of Chemical Physics* **1993,** *99* (9), 6998-7011; (c) Groh, B.; Dietrich, S., Orientational order in dipolar fluids consisting of nonspherical hard particles. *Physical Review E: Statistical Physics, Plasmas, Fluids, and Related Interdisciplinary Topics* **1997,** *55* (3-A), 2892-2901.
2. (a) Rommel, H. L.; Robinson, B. H., Orientation of Electro-optic Chromophores under Poling Conditions: A Spheroidal Model. *Journal of Physical Chemistry C* **2007,** *111* (50), 18765-18777; (b) Benight, S. J.; Johnson, L. E.; Barnes, R.; Olbricht, B. C.; Bale, D. H.; Reid, P. J.; Eichinger, B. E.; Dalton, L. R.; Sullivan, P. A.; Robinson, B. H., Reduced Dimensionality in Organic Electro-Optic Materials: Theory and Defined Order. *Journal of Physical Chemistry B* **2010,** *114* (37), 11949-11956; (c) Olbricht, B. C.; Sullivan, P. A.; Dennis, P. C.; Hurst, J. T.; Johnson, L. E.; Benight, S. J.; Davies, J. A.; Chen, A.; Eichinger, B. E.; Reid, P. J.; Dalton, L. R.; Robinson, B. H., Measuring Order in Contact-Poled Organic Electrooptic Materials with Variable-Angle Polarization-Referenced Absorption Spectroscopy (VAPRAS). *Journal of Physical Chemistry B* **2011,** *115* (2), 231-241.
3. Cao, J.; Berne, B. J., Theory of polarizable liquid crystals: Optical birefringence. *Journal of Chemical Physics* **1993,** *99* (3), 2213-2220.
4. Gay, J. G., Modification of the overlap potential to mimic a linear site–site potential. *The Journal of Chemical Physics* **1981,** *74* (6), 3316.
5. Everaers, R.; Ejtehadi, M., Interaction potentials for soft and hard ellipsoids. *Physical Review E* **2003,** *67* (4).
6. Perram, J. W.; Wertheim, M. S., Statistical mechanics of hard ellipsoids. I. Overlap algorithm and the contact function. *Journal of Computational Physics* **1985,** *58* (3), 409-16.

7. Hansen, J.-P., McDonald, I.R., *Theory of Simple Liquids*. 3rd ed.; Elsevier: Amsterdam, Netherlands, 2006.
8. Onsager, L., The Effects of Shape on the Interaction of Colloidal Particles. *Annals of the New York Academy of Sciences* **1949,** *51*, 627-659.
9. Frenkel, D.; Mulder, B. M., The hard ellipsoid-of-revolution fluid I. Monte Carlo simulations. *Molecular Physics* **1985,** *55* (5), 1171-1192.
10. (a) Frenkel, D., Computer simulations of hard-core models for liquid crystals. *Molecular Physics* **1987,** *60* (1), 1-20; (b) Frenkel, D., Onsager's Spherocylinders Revisited. *Journal of Physical Chemistry* **1987,** *91* (9), 4912-4916.
11. Frenkel, D.; Mulder, B.; McTague, J., Phase Diagram of a System of Hard Ellipsoids. *Physical Review Letters* **1984,** *52* (4), 287-290.
12. (a) Ayton, G.; Patey, G. N., Ferroelectric Order in Model Discotic Nematic Liquid Crystals. *Physical Review Letters* **1996,** *76* (2), 239-242; (b) Ayton, G.; Wei, D. Q.; Patey, G. N., Liquid crystal phases of dipolar discotic particles. *Physical Review E* **1997,** *55* (1), 447-454.
13. Berardi, R.; Orlandi, S.; Zannoni, C., Monte Carlo simulation of discotic Gay–Berne mesogens with axial dipole. *Journal of the Chemical Society, Faraday Transactions* **1997,** *93* (8), 1493-1496.
14. Berardi, R.; Orlandi, S.; Zannoni, C., Columnar phases and field induced biaxiality of a Gay–Berne discotic liquid crystal. *Physical Chemistry Chemical Physics* **2000,** *2* (13), 2933-2942.
15. Baus, M.; Colot, J.-L., Ferroelectric nematic liquid-crystal phases of dipolar hard ellipsoids. *Physical Review A* **1989,** *40* (9), 5444-5446.
16. Nielsen, R. D.; Rommel, H. L.; Robinson, B. H., Simulation of the Loading Parameter in Organic Nonlinear Optical Materials. *Journal of Physical Chemistry B* **2004,** *108* (25), 8659-8667.
17. Dalton, L. R.; Harper, A. W.; Robinson, B. H., The role of London forces in defining noncentrosymmetric order of high dipole moment–high hyperpolarizability chromophores in electrically poled polymeric thin films. *Proceedings of the National Academy of Sciences* **1997,** *94*, 4842-4847.
18. Dalton, L. R.; Benight, S. J.; Johnson, L. E.; Knorr, D. B.; Kosilkin, I.; Eichinger, B. E.; Robinson, B. H.; Jen, A. K. Y.; Overney, R. M., Systematic Nanoengineering of Soft Matter Organic Electro-optic Materials. *Chemistry of Materials* **2011,** *23* (3), 430-445.
19. Sullivan, P. A.; Rommel, H. L.; Takimoto, Y.; Hammond, S. R.; Bale, D. H.; Olbricht, B. C.; Liao, Y.; Rehr, J.; Eichinger, B. E.; Jen, A. K.-Y.; Reid, P. J.; Dalton, L. R.; Robinson, B. H., Modeling the Optical Behavior of Complex Organic Media: From Molecules to Materials. *Journal of Physical Chemistry B* **2009,** *113* (47), 15581-15588.
20. Allen, M. P., Tildesley, D.J., *Computer Simulations of Liquids*. Clarendon: Oxford (UK), 1987.
21. (a) Weis, J. J.; Levesque, D., Ferroelectric phases of dipolar hard spheres. *Physical Review E* **1993,** *48* (5), 3728; (b) Bartke, J.; Hentschke, R., Dielectric properties and the ferroelectric transition of the Stockmayer-fluid via computer simulation. *Molecular Physics* **2006,** *104* (19), 3057-3068; (c) Pounds, M. A.; Madden, P. A., Are dipolar liquids ferroelectric? Simulation studies. *Journal of Chemical Physics* **2007,** *126* (10), 104506/1-104506/7.
22. Debye, P., *Polar Molecules*. Dover Publications: New York, 1929.

23. (a) Onsager, L., Electric moments of molecules in liquids. *Journal of the American Chemical Society* **1936,** *58*, 1486-93; (b) Edwards, D. M. F.; Madden, P. A.; McDonald, I. R., A computer simulation study of the dielectric properties of a model of methyl cyanide. I. The rigid dipole case. *Molecular Physics* **1984,** *51* (5), 1141-61.
24. Lide, D. R., *CRC Handbook of Chemistry and Physics*. 90th ed.; CRC Press: Baton Rouge, LA, 2009.
25. Tani, A.; Henderson, D.; Barker, J. A.; Hecht, C. E., Application of perturbation theory to the calculation of the dielectric constant of a dipolar hard sphere fluid. *Molecular Physics* **1983,** *48* (4), 863-9.
26. Zarragoicoecha, G. J.; Levesque, D.; Weis, J. J., Monte Carlo study of dipolar ellipsoids. I. The isotropic phase. *Molecular Physics* **1991,** *74* (3), 629-637.
27. Kirkwood, J. G., The dielectric polarization of polar liquids. *Journal of Chemical Physics* **1939,** *7*, 911-19.
28. Böttcher, C. J. F., *Theory of Electric Polarization*. Elsevier: Amsterdam, Netherlands, 1952.
29. de Gennes, P. G.; Prost, J., *The Physics of Liquid Crystals*. Oxford University Press: Oxford, UK, 1993.
30. (a) Frenkel, D., Smidt, B., *Understanding Molecular Simulation: From Algorithms to Applications*. Elsevier: Amsterdam (ND), 2002; (b) Leach, A. R., *Molecular Modeling: Principles and Applications*. 2nd ed.; Pearson Education: Harlow (UK), 2001.
31. Barker, J. A.; Watts, R. O., Monte-Carlo studies of the dielectric properties of water-like models. *Molecular Physics* **1973,** *26* (3), 789-92.
32. Houssa, M.; Rull, L. F.; McGrother, S. C., Effect of dipolar interactions on the phase behavior of the Gay–Berne liquid crystal model. *The Journal of Chemical Physics* **1998,** *109* (21), 9529.
33. (a) Levesque, D.; Weis, J. J., On the Calculation of Dielectric Properties from Computer Simulations. *Physica A* **1984,** *125*, 270-274; (b) Kusalik, P. G., Computer simulation results for the dielectric properties of a highly polar fluid. *The Journal of Chemical Physics* **1990,** *93* (5), 3520.
34. Edwards, D. M. F.; Madden, P. A., A computer simulation study of the dielectric properties of a model of methyl cyanide. II. The interference of permanent and induced dipoles. *Molecular Physics* **1984,** *51* (5), 1163-79.
35. McGrother, S. C.; Gil-Villegas, A.; Jackson, G., The effect of dipolar interactions on the liquid crystalline phase transitions of hard spherocylinders with central longitudinal dipoles. *Molecular Physics* **1998,** *95* (3), 657-673.
36. Klapp, S. H. L.; Schoen, M., Spontaneous orientational order in confined dipolar fluid films. *Journal of Chemical Physics* **2002,** *117* (17), 8050-8062.
37. (a) Ouyang, W.-Z.; Hentschke, R., From gas-liquid to liquid crystalline phase behavior via anisotropic attraction: A computer simulation study. *Journal of Chemical Physics* **2007,** *127* (16), 164501/1-164501/7; (b) Van Workum, K.; Douglas, J. F., Equilibrium polymerization in the Stockmayer fluid as a model of supermolecular self-organization. *Physical Review E: Statistical, Nonlinear, and Soft Matter Physics* **2005,** *71* (3-1), 031502/1-031502/15.

# 4. Monte Carlo and Molecular Dynamics Simulations of Organic EO Materials

## 4.1. Introduction

One of the most crucial aspects of developing new materials for electro-optic applications is prediction and optimization of bulk acentric order[1]. The electro-optic coefficient

$$r_{33} = \frac{2\rho_N \beta_{zzz}(\varepsilon,\omega) g(\omega) \langle \cos^3\theta \rangle}{n_\omega^4} \quad (4\text{-}1)$$

is linearly proportional to the acentric order parameter $\langle \cos^3\theta \rangle$, as well as the chromophore number density $\rho_N$, such that an ideal material would contain a high density of perfectly-aligned, high-β chromophores. While a few organic chromophores such as DAST[2] have intrinsically acentric crystal structures, and others can be sequentially assembled into highly ordered structures,[3] most organic NLO materials must be ordered by electric-field poling.[4] The degree of acentric ordering obtained from poling is often small in conventional guest-host poled polymer materials, with $\langle \cos^3\theta \rangle < 0.1$ in many cases.[1c] Furthermore, $\langle \cos^3\theta \rangle$ cannot be directly measured in amorphous materials,[5] requiring indirect estimation from electro-optic or dielectric behavior,[6] simulations,[1b, 1d, e] or mean-field models.[1a, 1e]

The simplest method of estimating molecular ordering involves treating the system as a non-interacting gas of rigid, freely rotating, dipolar particles[7] (independent-particle model). Here, the only relevant interactions are those

between the dipoles and the external poling field, and the order parameters can be calculated using basic statistical mechanics as[8]

$$\left\langle \cos^n \theta \right\rangle = \frac{\int_0^{2\pi}\int_0^{\pi} \cos^n \theta e^f \sin\theta \, d\theta}{\int_0^{2\pi}\int_0^{\pi} e^f \sin\theta \, d\theta} \qquad (4\text{-}2)$$

where $f = \mu E_0 / k_B T$ . Here, μ is the chromophore dipole moment, T is the absolute temperature, and $E_0 = 3\varepsilon/(2\varepsilon + \varepsilon_\infty) \cdot E_P$ is the local electric field.[7b, 9] Here, ε is the low-frequency dielectric constant, $\varepsilon_\infty$ is the high-frequency dielectric constant, and $E_P$ is the applied poling field. If a gas-phase dipole moment is used, it is often scaled by the Lorentz local field factor[7b] $(\varepsilon_\infty + 2)/3$ to account for polarization from the dielectric environment. When solved, Equation 4-2 yields the *n*th-order Langevin functions ($L_n$), of which the first three are shown in Equation 4-3.

$$\begin{aligned} \left\langle \cos\theta \right\rangle &= \coth(f) - f^{-1} \approx \frac{f}{3} \\ \left\langle \cos^2 \theta \right\rangle &= 1 + 2f^{-2} - 2f^{-1}\coth(f) \approx \frac{1}{3} + \frac{2}{45} f^2 \\ \left\langle \cos^3 \theta \right\rangle &= \coth(f) - 3f^{-1} + 6f^{-2}\coth(f) - 6f^{-3} \approx \frac{f}{5} \end{aligned} \qquad (4\text{-}3)$$

The linear approximation is obtained as by truncating a Taylor expansion around *f*=0 at the lowest non-constant order in *f*.

While facile to calculate, the non-interacting rigid gas model fails to predict ordering in dense or highly polar materials, which exhibit a 'roll-off' behavior where order decreases as dipoles are brought closer together.[1a, 1e]

Therefore, ordering is often estimated computationally or inferred from the centrosymmetric order parameter[10]

$$\langle P_2\theta \rangle = \frac{3\langle \cos^2\theta \rangle - 1}{2} \quad (4)$$

which can be measured experimentally.[5, 11] Note that as $\langle P_2\theta \rangle$ is defined with respect to the poling axis, it is not identical to the nematic order parameter $\langle P_2 \rangle$ discussed in Chapter 3.

While experimental measurements of $\langle P_2\theta \rangle$ can be used to gain some insight on the ordering of a material, caution is warranted in attempting to quantitatively infer acentric ordering from them. In comparing measured centrosymmetric order with acentric order as calculated from electro-optic activity, materials can exhibit substantial deviations from the relation expected from Equation 4-3b and 4-3c, particularly in materials that use engineered anisotropic interactions to increase order[8]. In these materials, and in conventional materials with high chromophore loading, molecular motion is restricted and Equation 4-2 is no longer accurate. The restriction of molecular rotation can be expressed through the concept of lattice dimensionality[1c, 8, 11]; materials described by Equation 4-2 are 3D since they can rotate over all space. If rotation is constrained to a plane, the material is 2D. Finally, if it is constrained to two discrete states (up and down), the material is 1D, and always exhibits perfect centrosymmetric order. Idealized examples of one-dimensional and three-dimensonal regular lattices of non-interacting spheroids are shown in Figure 4.1. The two-dimensional lattice appears qualitatively similar to the three-dimensional case.

**4.1a.** 1D lattice

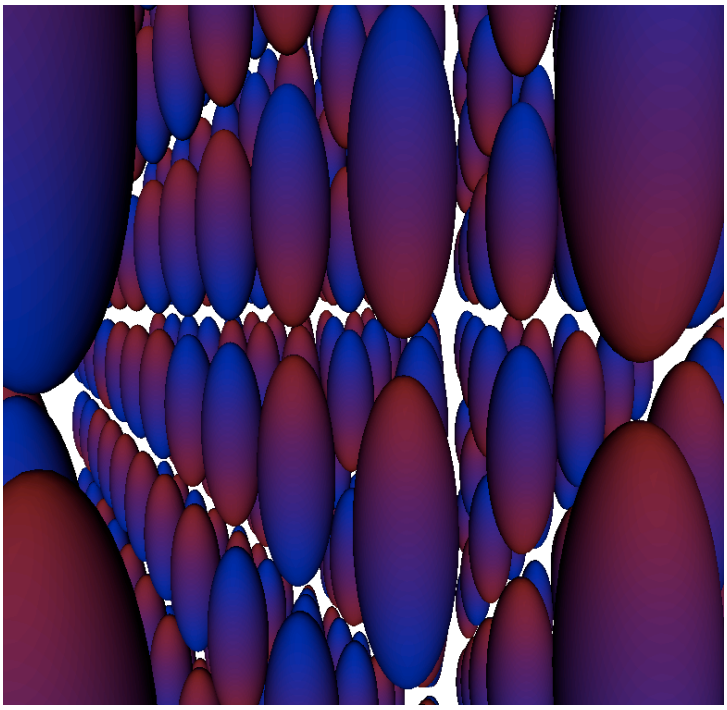

**4.1b.** 3D lattice

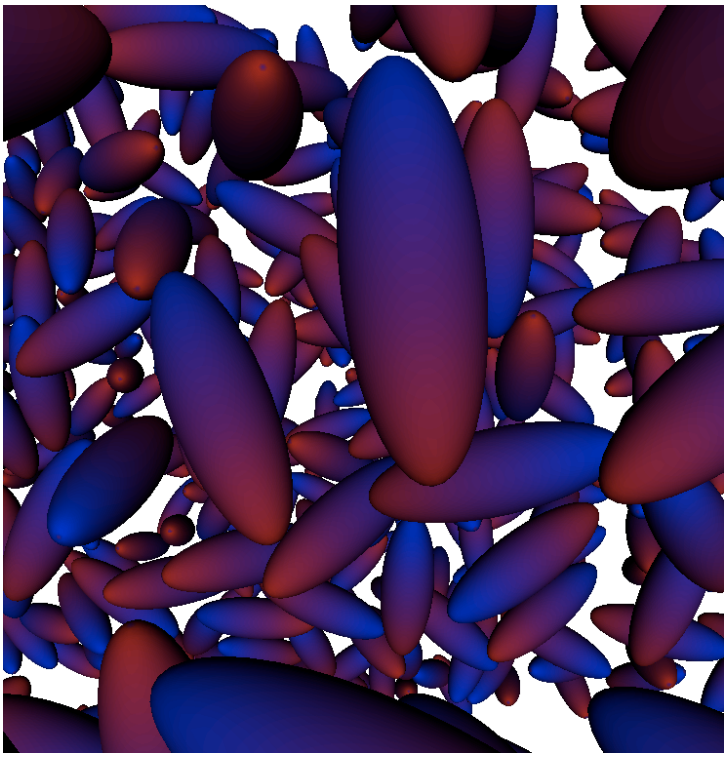

**Figure 4.1.** Examples of a 1D lattice (perfect centrosymmetric order) and a 3D lattice where molecular rotation is unrestricted.

In the case of a 2D material, Equation 4-2 becomes

$$\left\langle \cos^n \theta \right\rangle_{2D} = \frac{\int_0^{2\pi} \cos^n \theta \, \mathrm{e}^{f \cos\theta} \, d\theta}{\int_0^{2\pi} \mathrm{e}^{f \cos\theta} \, d\theta} \qquad (4\text{-}7)$$

with the following solutions[8] for $n$=1-3

$$\begin{aligned} \left\langle \cos\theta \right\rangle_{2D} &= \frac{i \cdot J_1(-if)}{J_0(-if)} \approx \frac{f}{2} \\ \left\langle \cos^2 \theta \right\rangle_{2D} &= \frac{1}{2} - \frac{J_2(-if)}{2 \cdot J_0(-if)} \approx \frac{1}{2} + \frac{f^2}{16} \\ \left\langle \cos^3 \theta \right\rangle_{2D} &= \frac{i}{4}\left( \frac{3 \cdot J_1(-if)}{J_0(-if)} - \frac{J_3(-if)}{J_0(-if)} \right) \approx \frac{3}{8} f \end{aligned} \qquad (4\text{-}8)$$

where $J_n$ are Bessel functions of the first kind. The relationship between $\left\langle P_2\theta \right\rangle$ and $\left\langle \cos^3 \theta \right\rangle$ for the 2D and 3D non-interacting rigid gas models are shown in Figure 4.2.

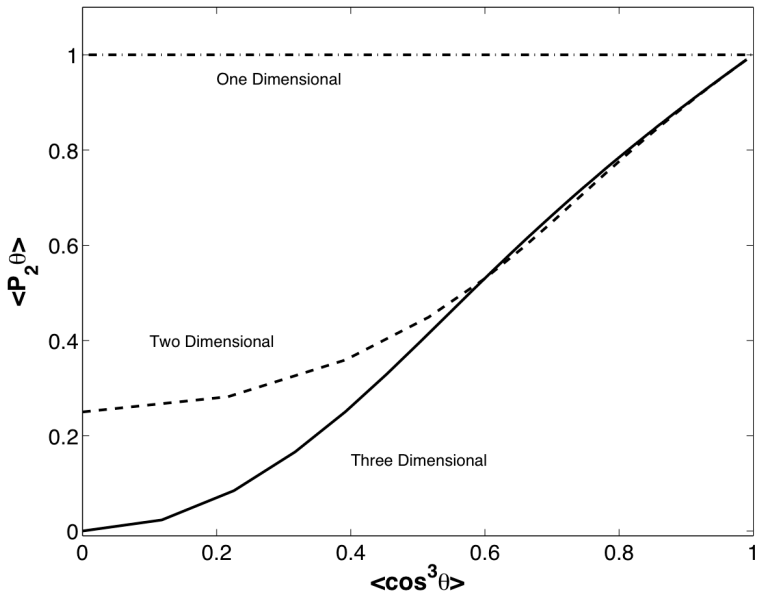


**Figure 4.2.** Relation between centrosymmetric and acentric order for the rigid, non-interacting gas model. (figure reproduced from Benight, S. J.; Johnson, L. E.; Barnes, R.; Olbricht, B. C.; Bale, D. H.; Reid, P. J.; Eichinger, B. E.; Dalton, L. R.; Sullivan, P. A.; Robinson, B. H., Reduced Dimensionality in Organic Electro-Optic Materials: Theory and Defined Order. *Journal of Physical Chemistry B* **2010,** *114* (37), 11949-11956. ©2010 American Chemical Society)

Here, it can be seen that for a lower-dimensional material, lower values of $\langle \cos^3\theta \rangle$ will have higher $\langle P_2\theta \rangle$ values for $\langle \cos^3\theta \rangle < 0.6$, and that in the case of an one-dimensional material, measurements of centrosymmetric order provide no information on acentric order. However, for materials with dimensionalities between 2D and 3D, a fractional dimensionality *M* can be calculated from the following approximate relation[8]

$$\langle \cos^3\theta \rangle_{MD} \approx \sqrt{\left(\frac{9-2M}{2+M}\right)\left(\langle P_2\theta \rangle_{MD} - \frac{3-M}{2M}\right)} \qquad (4\text{-}9)$$

based on interpolation between the 2D and 3D rigid, non-interacting gas solutions. Equation 4-9 can either be used for characterizing the dimensionality of a material where estimates of both order parameters are available, or for estimating one order parameter from the other based on similar materials or simulation results.

One of the primary motivations for development of the reduced dimensionality theory was developing materials with enhanced acentric order[1c]. In comparing Equations 4-3 and 4-8, 2D materials also order more strongly than 3D materials as the poling parameter *f* increases in the absence of other intermolecular interactions. While not *necessarily* more ordered, a 2D material had the *potential* to exhibit stronger poling-induced order at a given field strength. This theoretical development lead to a family of chromophores functionalized with side-chains intended to restrict chromophore motion. One of the early chromophores designed for this purpose was C1 (SBLD-1), developed by Stephanie Benight; it contains coumarin liquid-crystal mesogens in order to form a more ordered environment for the core YLD-156-like chromophore.[1c, 8, 11-12] The 3D structure of C1 is shown in Figure 4.3.

**4.3a.** 3D structure of C1

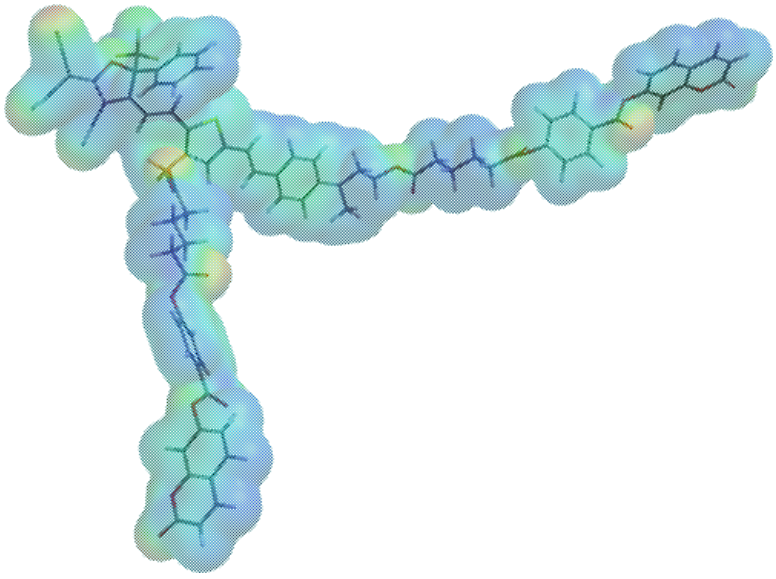

**4.3b.** Detail of 7-hydroxycoumarin

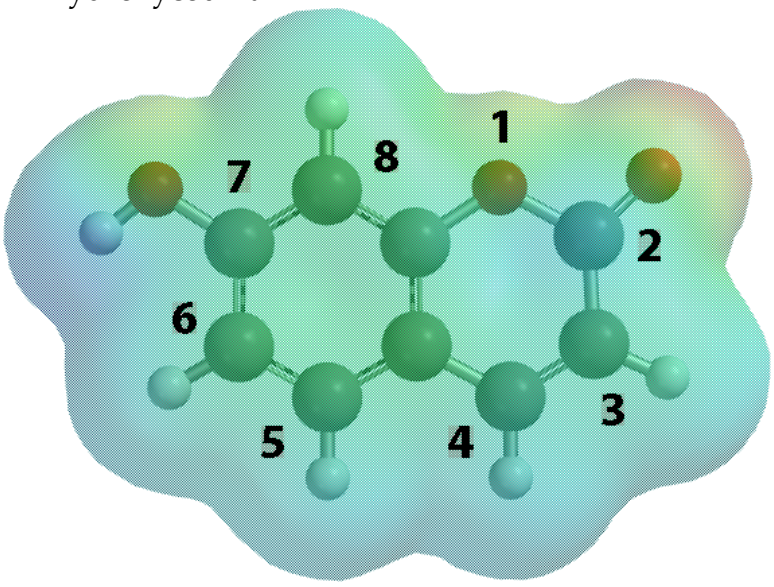


**Figure 4.3.** 3D structure of the C1 (SBLD) coumarin-functionalized chromophore (4a) for matrix-assisted poling. The geometry and the electrostatic potential surface were calculated at the PM3 semi-empirical level. The atom numbering scheme of the coumarins (4b) is also detailed.

The C1 chromophore exhibits much higher order[8] than its both parent chromophore, F2 (also known as YLD-156) and a multi-chromophore dendrimer[13] (P3, also known as PSLD-33) without coumarin-containing side

chains. The increase in order and in the number density of the material led to a large increase in the electro-optic coefficient, with a poling efficiency ($r_{33}/E_p$) of 1.92 ± 0.04 compared to 0.45 ± 0.02 for F2 in PMMA (25% chromophore by weight) and 1.42 ± 0.04 for P3[8]. The experimental order parameters appear in Figure 4. The centrosymmetric order parameter $\langle P_2\theta \rangle$ was determined by VAPRAS and analyzed using the rigorous Jones Matrix method[5]; $\langle \cos^3\theta \rangle$ was calculated from[8] electro-optic coefficients and refractive indices measured by ATR and hyperpolarizabilities measured by HRS unless otherwise stated, and dielectric constants measured from capacitance. Comprehensive data is tabulated in Table 4.1.

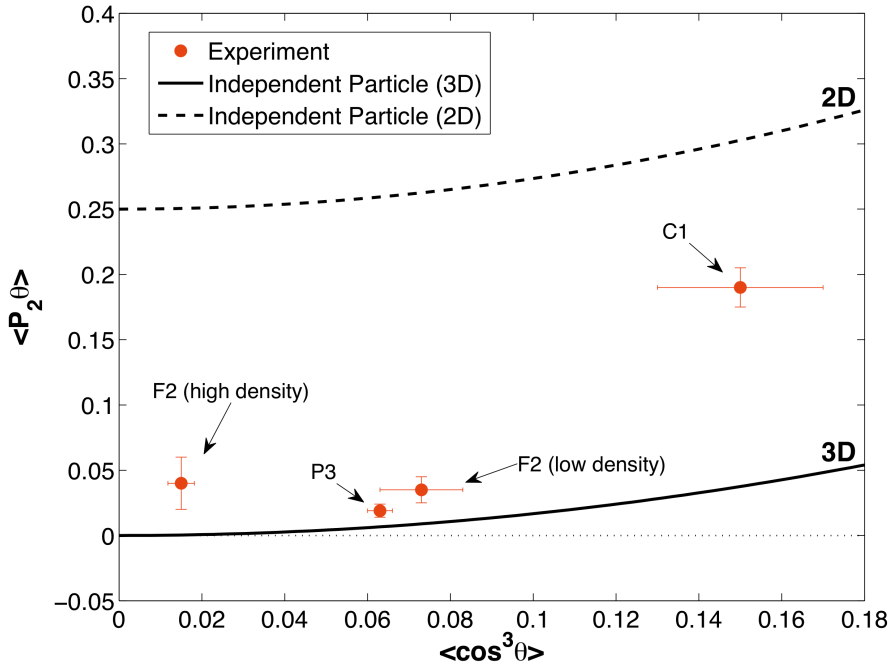


**Figure 4.4.** Relationship between experimental centrosymmetric and acentric order in two conventional organic EO materials (F2 and P3) and MAP material C1. (Figure reproduced from Benight, S. J.; Johnson, L. E.; Barnes, R.; Olbricht, B. C.; Bale, D. H.; Reid, P. J.; Eichinger, B. E.; Dalton, L. R.; Sullivan, P. A.; Robinson, B. H., Reduced Dimensionality in Organic Electro-Optic Materials: Theory and Defined Order. *Journal of Physical Chemistry B* **2010,** *114* (37), 11949-11956. ©2010, American Chemical Society)

**Table 4.1.** Experimental ordering and EO performance data for C1, F2, and P3

| Material | $r_{33}/E_p$ [a] | $N$ [b] | $\langle P_2 \rangle$ [c] | $\beta_{zzz}(-\omega;0,\omega)$ [d] | $g(\omega)/n^4$ | $\langle \cos^3\theta \rangle$ [e] | $M$ |
|---|---|---|---|---|---|---|---|
| C1 (TiO2) | 1.92 ± 0.04 | 4.4 | 0.19±0.015 | 3000 ± 300 | 0.57 | 0.15 ± 0.02 | 2.2 |
| F2/PMMA | 0.45 ± 0.02 | 1.7 | 0.035±0.01 | 3500 ± 600 | 0.62 | 0.073 ± 0.01 | 2.8 |
| F2/PMMA[f] | 0.15 ± 0.02 | 3.6 | 0.04±0.02 | 3500 ± 600 | 0.57 | 0.015 ± 0.003 | 2.8 |
| P3[g] | 1.42 ± 0.04 | 6.4 | 0.019±0.005 | 4033[h] ± 126 | 0.52 | 0.063 ± 0.003 | 2.9 |

[a] $(nm/V)^2$ [b] $N \times 10^{20}$ molecules/cc [c] $\langle P_2 \rangle$ at $E_p = 50V/\mu m$ for C1, low density F2/PMMA, and P3; $E_p = 60V/\mu m$ for high density F2/PMMA [d] $\beta_{zzz}(-\omega;0,\omega) \times 10^{30}$ esu [e] estimated from equation (1) using $r_{33}/E_p$ ($E_p = 50V/\mu m$), except for F2 at high density where $E_p = 60V/\mu m$ [f] $E_p = 60V/\mu m$ for F2 at high density [g] P3 data from Sullivan et al. 2009[6a]. [h] theoretical value calculated using TD-DFT[6b]. (Table adapted from Benight, S. J.; Johnson, L. E.; Barnes, R.; Olbricht, B. C.; Bale, D. H.; Reid, P. J.; Eichinger, B. E.; Dalton, L. R.; Sullivan, P. A.; Robinson, B. H., Reduced Dimensionality in Organic Electro-Optic Materials: Theory and Defined Order. *Journal of Physical Chemistry B* **2010,** *114* (37), 11949-11956. ©2010, American Chemical Society)

In addition to the dramatic increase in poling efficiency, the dimensionality of C1 dropped to nearly two-dimensional. Further VASE experiments[1c] established that the coumarin molecules were themselves ordered in a plane perpendicular to the chromophores, and experiments using scanned-probe techniques including intrinsic friction analysis and shear-modulation force microscopy determined that C1 exhibited an additional thermal transition[1c, 12] at a temperature lower than its glass transition temperature. This transition was attributed to disruption of inter-coumarin interactions, and combined with the optical data, led to a predicted structure where coumarins stack together to form a lattice that constrains chromophore motion, shown in an idealized form in Figure 4.5.

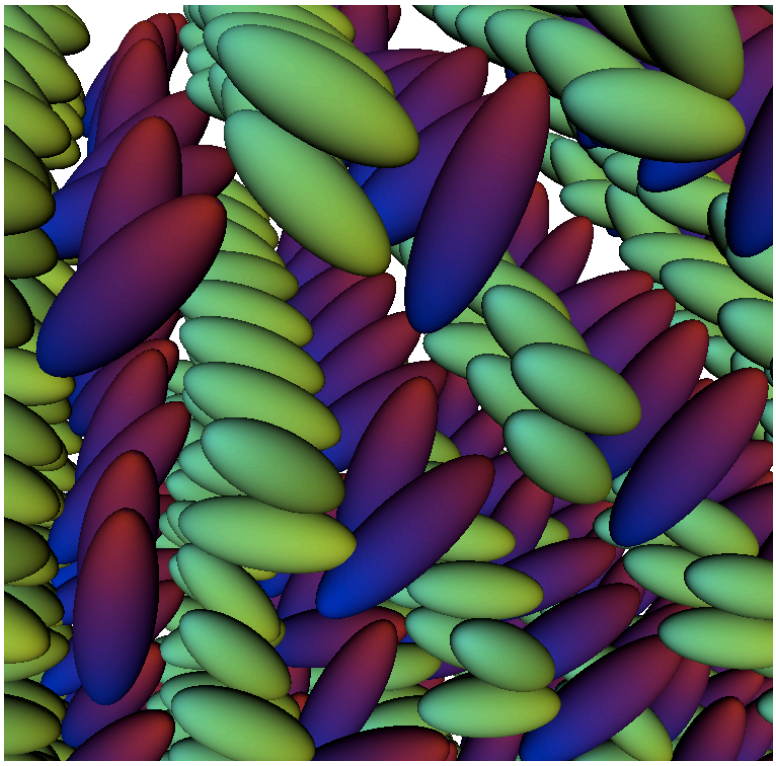

**Figure 4.5.** Cartoon showing dimensional restriction due to coumarin-coumarin interactions. Chromophores are represented by red/blue spheroids, and coumarins by yellow/green spheroids. This model is highly idealized for clarity and is not representative of actual simulation results.

Further characterization of the specific interactions leading to improved ordering in C1, as well as characterization of the dimensionality model itself in systems with strong intermolecular interactions, were conducted using computer simulations. These calculations complemented both analytic theory and experiment by enabling direct determination of both $\langle P_2\theta \rangle$ and $\langle \cos^3\theta \rangle$, as well as examining inter-atomic and inter-molecular correlations for specific interactions.

## 4.2. Computational Methods

Two complementary techniques were used for simulations of ordering of electro-optic chromophores. Rigid-body Monte Carlo (RBMC) simulations[1c, 14]

were used to characterize ordering of systems containing in excess of a thousand chromphores in response to an applied electric field. The large simulations size was enabled through use of coarse-grained representation of the dyes as single spheroids. Specific interactions were probed by fully atomistic molecular dynamics (MD) simulations of small numbers of chromophores in explicitly represented (solvent or polymer) media. These simulations were run in the absence of an external poling field.

### *4.2.1. RBMC methods*

Rigid-Body Monte Carlo simulations used a protocol nearly identical to that from Chapter 3. The potential energy function was, however, modified to account for the much lower packing fraction compared to the simulations in Chapter 3 and the presence of an inert polymer medium in comparable experimental systems. Firstly, the high-frequency dielectric constant $\varepsilon_\infty = n^2$ of the material was used to attenuate electrostatic interactions[6a, 15]. This parameter represented effects from polarization of both the molecules and the otherwise-neglected medium. Secondly, the dispersion term was removed such that the Lennard-Jones potential was entirely repulsive (soft spheroid model). Removal of this term implicitly modeled steric hindrance from the medium with similar effects to, but much lower computational overhead, than a potential including dispersion and a solvent parameter, as used in prior work[1d, 6a]. The modified potential energy function

$$U = \sum_i \left\{ \sum_{j>i} \left[ 4\varepsilon_{LJ} \left( \frac{\sigma_{eff}(i,j)}{r_{ij}} \right)^{12} + \frac{1}{\varepsilon_\infty r_{ij}^3} \left( \boldsymbol{\mu}_i \cdot \boldsymbol{\mu}_j - 3(\boldsymbol{\mu}_i \cdot \hat{\mathbf{r}})(\hat{\mathbf{r}} \cdot \boldsymbol{\mu}_j) \right) - \frac{1}{\varepsilon_\infty R_C^3} \frac{2(\varepsilon - \varepsilon_\infty)}{(2\varepsilon + \varepsilon_\infty)} \boldsymbol{\mu}_i \cdot \boldsymbol{\mu}_j \right] - \left( \frac{3\varepsilon}{2\varepsilon + \varepsilon_\infty} \right) \boldsymbol{\mu}_i \cdot \mathbf{E}_p \right\} \quad (4\text{-}10)$$

was used for all simulations, where $\sigma_{eff}$ is the effective Lennard-Jones radius calculated using the method of Perram and Wertheim,[16] $\varepsilon_{LJ}$ is the strength of repulsive potential, μ is the chromophore dipole moment, and $r_{ij}$ is the center-center distance between chromophores. Calculations were run under self-consistent reaction field (SCRF) boundary conditions,[14, 17] where $\mathbf{E}_p$ is the applied poling field (along the z-axis) and $R_C$ is the radius of the reaction field sphere, defined as half the length of the simulation cell for all simulations.

While several chromophores were parameterized for RBMC simulations, this chapter focuses on calculations on F2 (also known as YLD-156), YLD-124, and DR1. Parameters are shown in Table 4.2. Molecular volumes and dipole moments were calculated at the B3LYP/6-31g(d) level using Spartan '08[18] based on geometries optimized at the same level using Gaussian '09.[19] The strength of the nuclear repulsive potential was held constant for all of the dyes.

**Table 4.2.** Rigid-body parameters for F2, YLD-124, and DR1

| Chromophore | σ(a) (Å) | σ(b) (Å) | AR | $\varepsilon_{LJ}$ (K) | μ (D) | V (Å$^3$) |
|---|---|---|---|---|---|---|
| F2 (YLD-156) | 21.00 | 7.00 | 3.0 | 217.4 | 23.50 | 538.8 |
| YLD-124 | 20.38 | 7.56 | 2.7 | 217.4 | 25.00 | 608.7 |
| DR1 | 14.48 | 6.30 | 2.3 | 217.4 | 11.66 | 299.7 |

All RBMC simulations were run in the canonical (NVT) ensemble; all simulations discussed in this chapter contained N=1728 chromophores. Energies and order parameters were recorded every MC cycle. The number of Monte Carlo cycles (N trial moves) varied between 40000 and 300000; denser systems typically took more moves to converge. The sizes of the Monte Carlo moves were hand-optimized for each simulation condition to maximize RMS rotational and translational displacement of molecules. All simulations were started from a

simple cubic lattice, and interactions other than the nuclear repulsive potential were disabled for the first 1000 to 8000 cycles to assist in breaking up the lattice. Simulated annealing[20] was also used during these initial iterations in some runs, with the annealing schedule and maximum temperature set such that the equilibrium temperature would be reached halfway through the initial iterations.

Average properties were calculated from the last 20000 to 80000 cycles, depending on simulation length, but never for more than the last half of the simulation. Unless otherwise specified, five replicates of each simulation were run with different RNG seeds, with the averages from those runs used to calculate final averages and uncertainties.

### *4.2.2. Molecular dynamics methods*

Procedures for Molecular dynamics simulations were loosely based on those of Hayden and co-workers, who previously simulated fully atomistic models of ONLO chromophores in polymer matrices[21]. Simulations were run using Tinker 5.1[22] and the Merck Molecular Force Field (MMFF94),[23] which was chosen due to its extensive coverage of small organic molecules. Force field parameters, including charges, were used without modification. All simulations were run using the particle-mesh Ewald[24] method for long-range electrostatics, with conductive/'tin foil' outer boundary conditions. Short-range interaction cutoffs were set t 9 Å, except for the dilute solutions in chloroform, which used a larger cutoff of 13.2 Å. Default settings were used for the MD integrator (Beeman), energy minimizer (the LBFGS implementation in the Tinker MINIMIZE utility), thermostat (Berendsen[25]) and barostat (Berendsen[25]). Simulation lengths ranged from 1.5 ns to 44.0 ns, and all simulations used an

integration time step of 1.0 fs. The time between saving coordinates to the trajectory file depended on the simulation length, ranging from 0.1 ps to 10.0 ps.

Simulation cells were created using TINKER's XYZEDIT utility; if multiple components were included, cells were created for each component and merged. All trajectories consisted of a series of annealing steps to break up the starting lattice followed by a production phase in which data were recorded. Annealing phases began with energy minimization to ensure integrator stability, followed by a high-temperature randomization phase with charge-charge interactions disabled, and one or more additional randomization phases and/or minimizations with all interactions enabled. Unless otherwise specified, velocities were re-randomized between phases. Constant-pressure simulations were started at reduced density to improve chromophore mobility during the randomization phase. Randomization was followed by a production phase under the same conditions as the final randomization phase. One trajectory was run per condition. Individual protocols were as follows:

*Simulations of F2 and C1 in chloroform at constant volume*

1. Generate a simulation cell 37.42 Å per side, fill with 5% chromophore by mass and sufficient chloroform to reach a density of 1.48 g/cc (density of liquid chloroform at 298K). Under these conditions, each simulation cell contained four chromophores. The C1 side chains were counted towards solvent mass, not chromophore mass.
2. Minimize to RMS gradient of 1.0 Kcal/mol-Å
3. NVT MD at 500K for 50 ps with charge-charge interactions disabled
4. Minimize to RMS gradient of 0.1 Kcal/mol-Å
5. NVT MD at 298K for 200ps
6. NVT MD at 500K for 50ps
7. Minimize to RMS gradient of 0.1 Kcal/mol-Å
8. NVT MD at 298K for 200ps
9. NVT MD at 298K for 1.0ns, sampling every 0.1 ps, using the entire 1.0 ns run for calculating correlation functions *(Production phase)*

*Isothermal-isobaric simulations of F2 in PMMA and of neat C1*

1. Generate a simulation cell 36 Å per side, fill with chromophore and octamers of poly(methyl methacrylate) (PMMA) to a density of ~0.8 g/cc. The contents of the simulation boxes were as follows:
    a. 19% F2: 5 F2, 22 PMMA
    b. 38% F2: 10 F2, 17 PMMA
    c. C1: 16 C1 (neat)
2. Minimize to a RMS gradient of 1.0 Kcal/mol-Å
3. NVT MD at 700K for 100ps with charge-charge interactions disabled
4. Minimize to a RMS gradient of 0.1 Kcal/mol-Å
5. NVT MD at 700K for 100ps.
6. Minimize to a RMS gradient of 0.1 Kcal/mol-Å
7. NVT MD at 353K for 300ps
8. NPT MD at 353K and 1 atm for 500 ps
9. NPT MD at 353K and 1 atm for 5.0 ns. The final 3.0 ns of this run were used to calculate average values and correlation functions, and data was sampled every 0.5 ps. *(Production phase)*

*Simulations of density-temperature behavior of C1 at constant pressure*

1. Start with simulation cell from phase 2 of isothermal-isobaric simulation of C1; expand size to 40 Å per side.
2. Minimize to RMS gradient of 1.0 Kcal/mol-Å
3. NVT MD at 700K for 5.0 ns with charge-charge interactions disabled
4. Minimize to RMS gradient of 0.1 Kcal/mol-Å
5. NVT MD at 700K for 1.0 ns
6. Minimize to a RMS gradient of 0.1 Kcal/mol-Å
7. NPT MD at 550K and 1 atm external pressure for 4.0 ns
8. NPT MD with 1 atm external pressure, starting at 500K and ramping the temperature down by 25K every 2.0 ns, and sampling every 1.0 ps. The last 1.0 ns of each segment was used for calculating densities and correlation functions. Velocities were not re-randomized between segments. (*Production phase*).
9. Additional high-temperature segments: The temperature was ramped up from 550K to 600K in the same manner. (*Production phase)*

### *4.2.3. Analysis of MD data*

Densities were extracted directly from the simulation log file generated by TINKER; where each datum was recorded as a 0.1 ps block average. Radial distribution functions were also calculated in a similar manner to those in Chapter 3, but between individual atoms instead of between molecular centers. The thiophene sulfur found in both C1 and F2 was chosen to represent the center

of the chromophore bridge, and the carbon between C8 and O1 on each coumarin in C1 (see Figure 4.3b) was chosen to represent the center of each coumarin π-system. Homogeneous radial distribution functions[26] were calculated as

$$g(r) = \frac{V \sum_{i}^{N} \sum_{j>i}^{N} n_{ij}(r, r+\Delta r)}{2\pi N \left(N-1\right) r^2 \Delta r} \qquad (4\text{-}11)$$

where $V$ is the volume of the simulation cell, $n_{ij}(r,r+\Delta r)$ is the number of particles $j$ between a distance of $r$ and $r+\Delta r$ of particle $i$. Heterogeneous (Sulfur-Coumarin) radial functions were calculated as

$$g_{AB}(r) = \frac{V \sum_{i}^{N_A} \sum_{j}^{N_B} n_{ij}(r, r+\Delta r)}{4\pi N_A N_B r^2 \Delta r} \qquad (4\text{-}12)$$

where $N_A$ and $N_B$ are the total number of each type of particle being correlated.

Additionally, orientational correlation functions[14, 27]

$$g_{\mu}^{n}(r) = \frac{\sum_{i=1}^{N} \sum_{j>i}^{N} \cos^{n} \gamma_{ij}(r, r+\Delta r)}{2\pi N \left(N-1\right) r^2 \Delta r} \qquad (4\text{-}13)$$

were calculated for coumarin in the isothermal-isobaric simulation of C1, where $\cos\gamma = \hat{\boldsymbol{\mu}}_i \cdot \hat{\boldsymbol{\mu}}_j$. The vector $\boldsymbol{\mu}$ was defined to approximate the dipole moment of each coumarin, extending between C2 and C6. The first-order orientational correlation function ($n$=1) measures correlation between dipoles, where positive values indicate net alignment between dipoles at that distance and negative values indicating net anti-alignment. The second-order correlation function ($n$=2) is a metric of centrosymmetric alignment at that distance (analogous to the bulk

nematic order parameter $\langle P_2 \rangle$)[28], with larger positive values indicating that dipoles are either parallel or anti-parallel. In the absence of intermolecular correlation, $g_\mu^2(r)$ approaches 1/3.

## 4.3. Results and Discussion

### *4.3.1. RBMC simulations of chromophore ordering*

During the development of the VAPRAS technique, RBMC calculations on YLD-124 were performed as a benchmark to test the level of agreement between experimental data and theory. These calculations were run at low densities to reduce the effects of intermolecular interactions. Results are shown in Figure 4.6; blue circles are simulation results and red stars are VAPRAS results analyzed with the Jones Matrix method. Dotted black lines represent a fit of experimental data to Equation (4-3b) to calculate an effective poling parameter *f* and dipole moment $\mu_{eff}$.

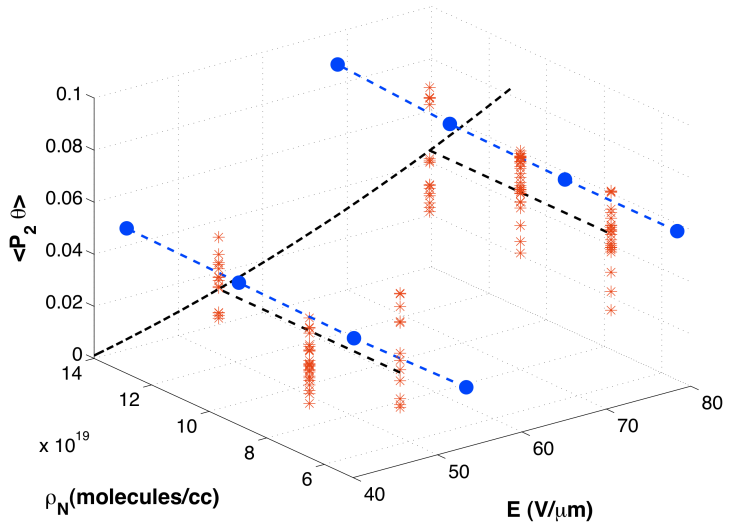


**Figure 4.6.** Comparison of VAPRAS data[5] (red) for YLD-124 at two poling field strengths and 382K with RBMC simulations of a spheroidal model of YLD-124 under the same conditions, assuming a refractive index of $n$=1.6. Simulations were 80000 cycles long, calculating properties from the last 30000 cycles.

Simulation results and experimental values were within error of each other, and both exhibited an increase in $\langle P_2\theta \rangle$ of approximately 2.25-fold as the poling field strength was increased from 50 Vμm to 75 Vμm, as predicted by Equation 4-3b.[5] Order was nearly constant as a function of density for the low-density systems studied (5-15% w/w chromophore) for both the RBMC simulations and VAPRAS data. The overall ordering was, however, lower than would be expected from the 3D non-interacting rigid gas; fitting to Equation 4-3b and allowing the dipole moment to float while constraining all other parameters to the values obtained from the simulations gave a $\mu_{eff}$ of approximately 15 D; substantially lower than the 25 D used in the simulations[5]. The discrepancy may be due to an overestimate of the dipole moment by the DFT calculations (despite using the gas-phase value) and/or by inter-chromophore anti-correlation in the experimentally measured systems.

To explore the effects of chromophore correlation with increased density and dipole moment, simulations were run on spheroidal representations of DR1 and F2 at a wide variety of densities; results appear in Figures 4.7 and 4.8, respectively. As noted in Table 3, the molecular volume of F2 is nearly twice that of DR1. The highest density F2 system ($6.3\times10^{20}$ molecules/cc) evaluated has a volume packing fraction of 0.35; a similar packing fraction is reached at a density of $12\times10^{20}$ molecules/cc for DR1. The 3D independent–particle (Langevin) solutions are shown for comparison; local electric field strengths ($E_0$) used for the Langevin model were obtained from the simulations. Changes in the Langevin solution are due entirely to changes in the local field; i.e. a higher dielectric

results in a stronger local field, and consequently, a larger value of the poling parameter *f*.

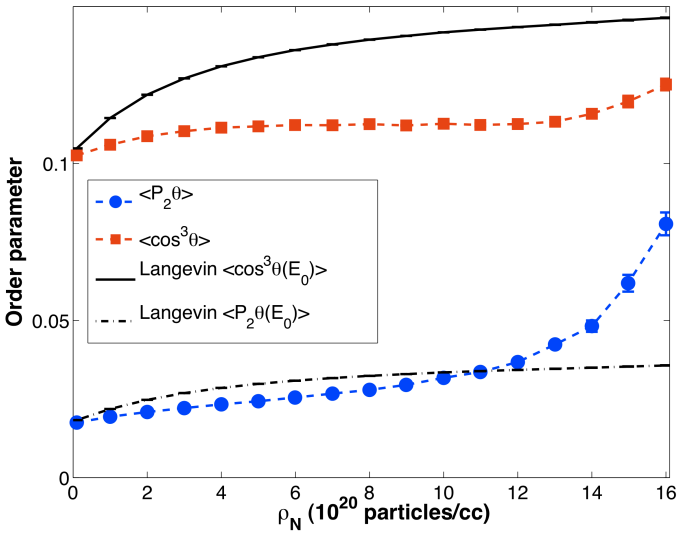


**Figure 4.7.** Centrosymmetric and acentric ordering as a function of density for a spheroidal model of DR1 poled at 50 V/μm and 408K, assuming $n$=1.6. All simulations were 200000 cycles long, averaging over the last 80000 cycles.

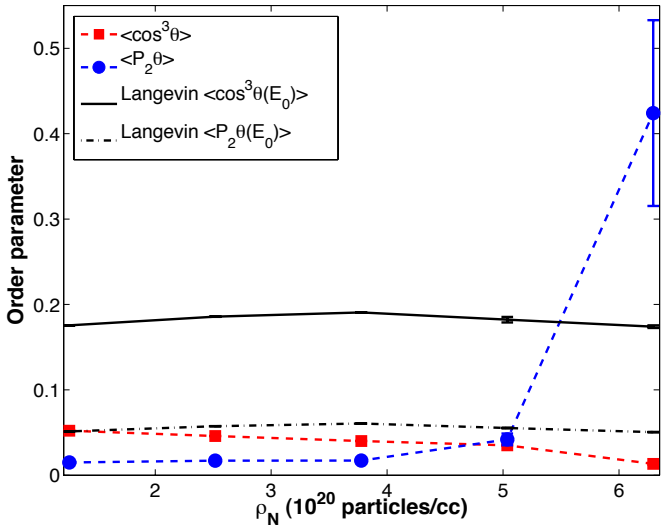


**Figure 4.8.** Centrosymmetric and acentric ordering as a function of density for a spheroidal model of F2 poled at 50 V/μm and 382K, assuming $n$=1.5. Simulations at the lowest two densities were were 40000 cycles long, averaging over the last 20000 cycles; simulations at $5.04\times10^{20}$ molecules/cc were 80000 cycles long, averaging over the last 20000, and simulations at $6.3\times10^{20}$ molecules/cc were 300000 cycles long, averaging over the last 50000.

Changing the dipole moment by a factor of two caused a dramatic difference in observed ordering, in which acentric order was strongly depressed at high number densities for the more polar and prolate F2, but did not show roll-off behavior for DR1. These results were consistent with prior simulations that showed lessened roll-off for less polar chromophores[1c]. At the lowest density calculated for DR1 ($1.0\times10^{19}$ molecules/cc) ordering was nearly identical to that predicted from Equation 4-3, and maximum deviation from the independent-particle limit for $\langle\cos^3\theta\rangle$ was on the order of 25%. The centrosymmetric order parameter $\langle P_2\theta\rangle$ remained at near the independent-particle limit until the density reached $12\times10^{20}$ molecules/cc, after which $\langle P_2\theta\rangle$ increased by a factor of nearly three. This rapid shift in P2 likely signaled a reduction of lattice dimensionality. Acentric order did not decrease, indicating that the system may have been trending towards an inherently acentric phase. However, assuming a mass density of 0.92 g/cc (as measured[5] for YLD-124/PMMA) for a hypothetical film and a molecular weight of 300 g/mol for DR1, a material with a chromophore number density of $16\times10^{20}$ molecules/cc would be composed of 87% chromophore and unlikely to be processable.

In comparison, acentric ordering of F2 exhibits strong roll-off behavior, with a $\langle\cos^3\theta\rangle$ of nearly zero at a density of $6.3\times10^{20}$ molecules/cc. Acentric ordering was consistently well below the independent-particle limit. Centrosummetric order was also low at low densities, but increased sharply at $5.04\times10^{20}$ g/cc, with $\langle P_2\theta\rangle$ rapidly increasing by an order of magnitude after

that point. Analysis of the nematic order parameter $\langle P_2 \rangle$ (see Chapter 3) and visual inspection of the simulations indicated formation of a smectic-A[29] liquid crystal phase with $\langle P_2 \rangle = 0.852 \pm 0.026$. The difference between $\langle P_2\theta \rangle$ and $\langle P_2 \rangle$ indicates that while the external field improved the likelihood of the director axis being close to the poling axis, chromophore-chromophore interactions dominated over chromophore-field interactions. However, the corresponding acentric order parameter was very small ($\langle P_1 \rangle = 0.0131 \pm 0.0016$), indicating that the material would likely be anti-ferroelectric in the absence of a field. Furthermore, dimensionality decreased to less than 2D. Visualizations at low and high density are shown in Figure 4.9.

**4.9a.** Low density ($2.54 \times 10^{20}$ molecules/cc)

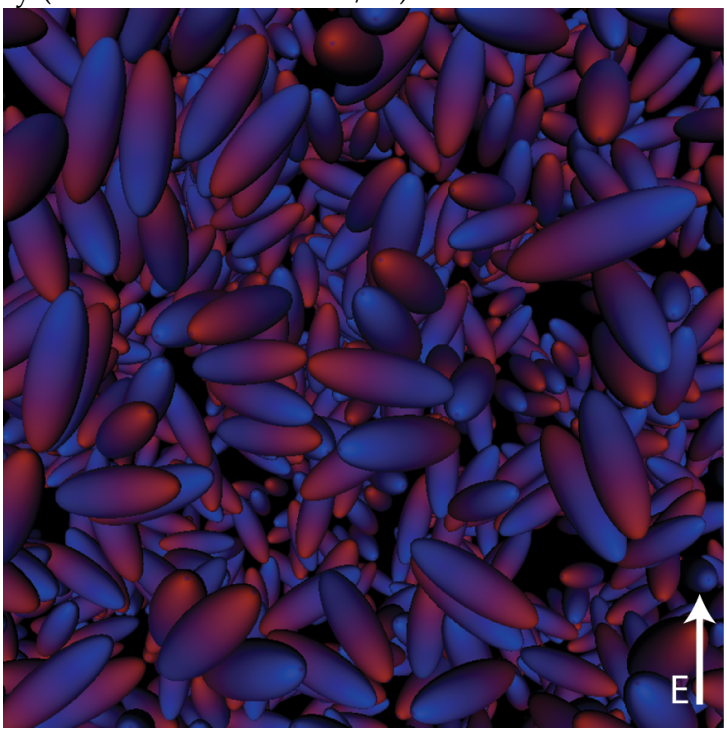


**4.9b.** High density ($6.3 \times 10^{20}$ molecules/cc)

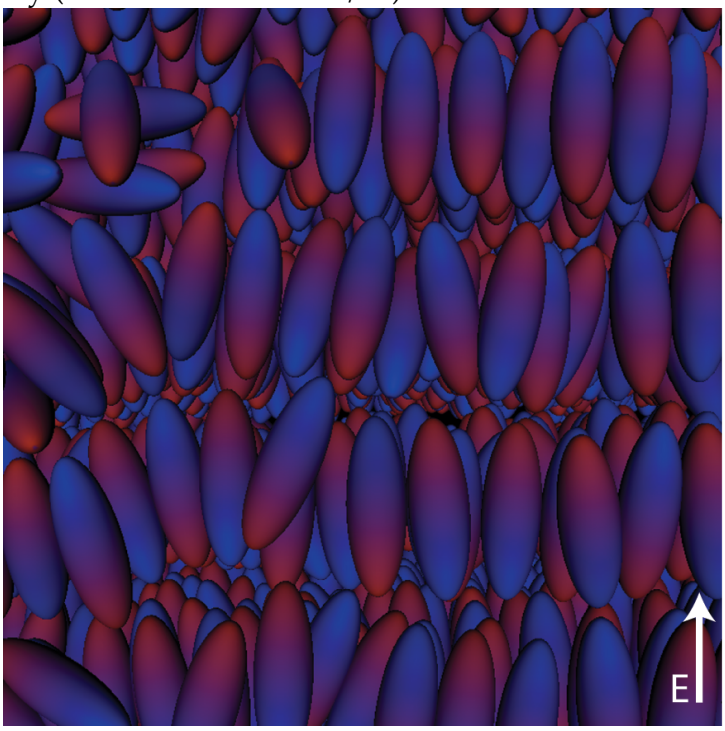


**Figure 4.9.** Visualizations of low and high-density spheroidal models of F2 at 382K and 50 V/μm. The layered, smectic-A phase can clearly be seen in Figure 8b.

In order to further explore the dimensionality of the spheroidal F2 system, calculations were run at three of the same densities at three additional field strengths (25, 75, and 100 V/μm). Results are plotted in Figure 4.10.

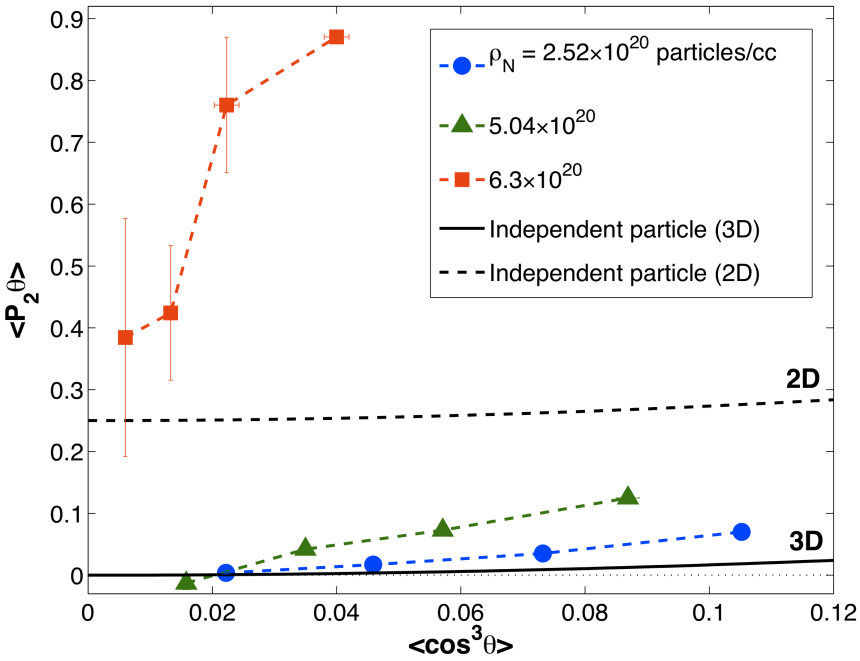


**Figure 4.10.** Dimensionality plot for a spheroidal model of F2 at four field strengths (25, 50, 75, and 100 V/μm). Calculation protocols were identical to those used for the simulations shown in Figure 4.8.

Here, the decrease in acentric ordering with respect to density can be seen clearly; the $\langle \cos^3 \theta \rangle$ achieved at any field strength is much lower for the two high-density cases. Additionally, the dimensionality of the system shows a much larger dependence on density than on field strength; the lowest-density system remains nearly 3D at all field strengths; the intermediate-density system undergoes reduction of dimensionality in the presence of an applied field, and the highest-density system remains consistently sub-2D. Furthermore, it illustrates that even though the independent-particle model does not produce quantitative estimates of order for F2 at the densities shown without adjustment

of parameters, it does predict the relationship between acentric and centrosymmetric order at low densities. Furthermore, these results show the utility of the concept of reduced dimensionality in interpreting simulations of ordering of dipolar materials by reducing complex many-body interactions to a single parameter.

However, none of the RBMC simulations shown above incorporate specific interactions for controlling lattice dimensionality, with any changes in the relationship between order parameters due entirely to steric and electrostatic effects. Exploring the presence of these interactions requires higher levels of detail, such as all-atom molecular dynamics[30] or pseudo-atomistic Monte Carlo[13]. New Monte Carlo methods allowing ordering calculations of molecules represented with multiple levels of coarse-graining are currently under development in the Robinson group.

### *4.3.2. Molecular dynamics of chromophores in solution*

All-atom molecular dynamics were used to further analyze intermolecular interactions in C1 and in its parent chromophore, F2. While rare, molecular dynamics simulations of chromophore ordering have been conducted on chromophores such as FTC[21], DR1[31], and p-nitroaniline derivatives[32], as well as for investigating the effects of aryl-perfluoroaryl interactions on the glass transition of functionalized CLD-like chromophores[30]. Here, molecular dynamics simulations are used in a similar manner to characterize thermal transitions, coumarin-coumarin interactions, and chromophore-chromophore interactions under several simulation conditions.

Initially, obtaining adequate chromophore motion at experimental densities proved difficult, so preliminary simulations were run in dilute chloroform solution (5%) chromophore by mass, with only four chromophores (C1 or F2) per simulation cell. While limited in terms of statistical robustness, they provided a useful proof of concept. A visualization of a simulation of C1 appears in Figure 4.11.

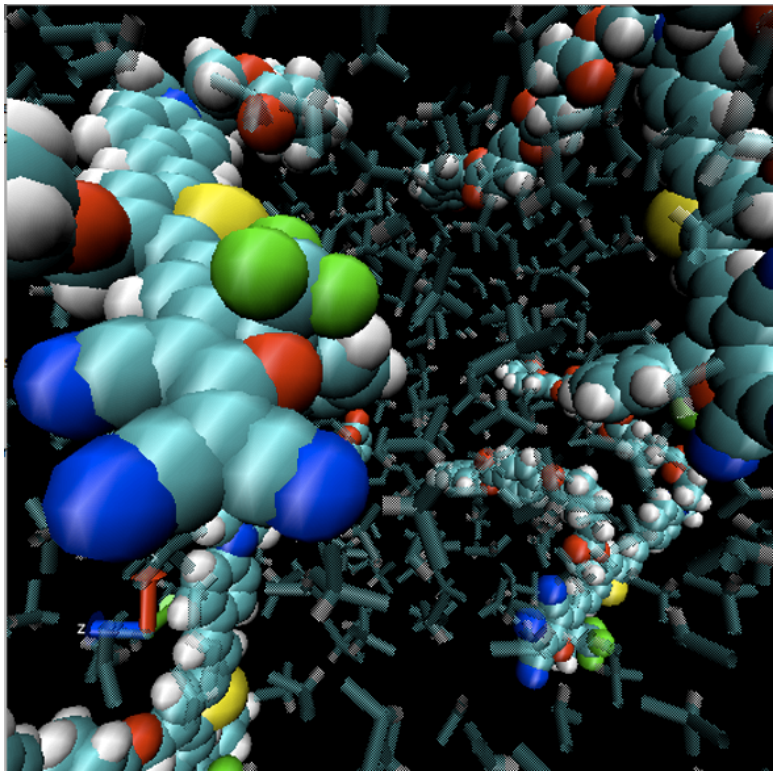

**Figure 4.11.** Visualization of MD simulation of C1 in chloroform (5% chromophore by mass) at 298K and 1.48 g/cc. C1 molecules are shown as space-filling representations.

Intermolecular interactions were analyzed by means of the radial distribution function (Equation 4-11) between thiophene sulfurs on the chromophore centers and between coumarins. Values of g(r) above unity represent a greater probability of atoms/molecules being located a distance r from each other than expected in an isotropic and uniformly distributed material[26a, b], values less than

unity indicate a decreased probability molecules interacting at that distance; distances for which g(r) is zero are excluded due to intermolecular interactions. Radial distributions for F2 and C1 in chloroform are shown in Figure 4.12.

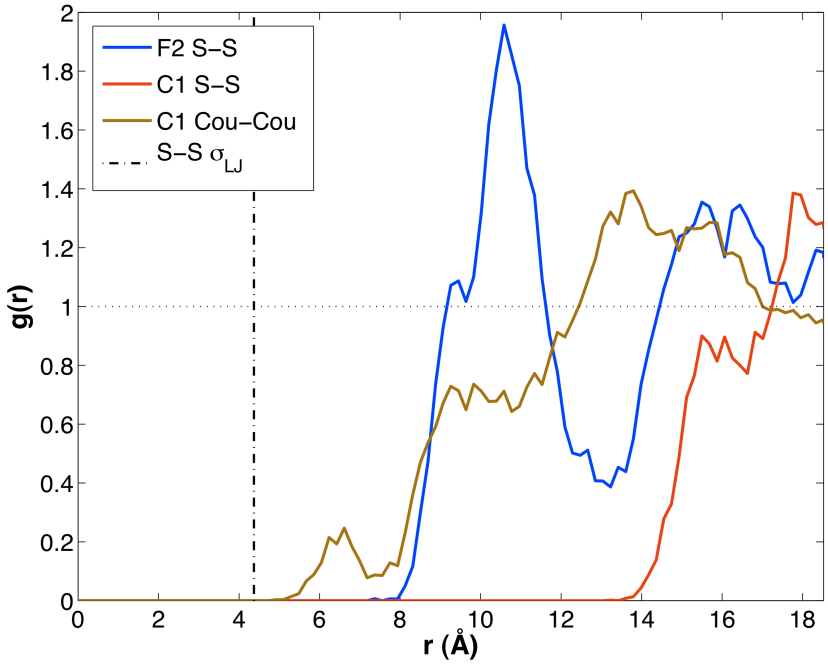


**Figure 4.12.** Radial distribution function for C1 and F2 in chloroform (5% chromophore by mass) at 298K and 1.48 g/cc, averaging over 1.0 ns (10000 frames). (Pending publication in Benight, S. J.; Daniel B. Knorr, J.; Johnson, L. E.; Sullivan, P. A.; Lao, D.; Sun, J.; Kocherlakota, L. S.; Elangovan, A.; Robinson, B. H.; Overney, R. M.; Dalton, L. R., Nano-Engineering Soft Matter Lattice Dimensionality for an Organic Electro-Optic Material. *Advanced Materials* **2012**. ©2012 Wiley-VCH, used with permission)

No strong correlation occurred between chromophores or coumarins in dilute chloroform solution; the strongest interaction was chromophore pairing in F2 at a distance of approximately 10 Å. This peak was suppressed in C1, where the shortest distance non-negligible interaction between sulfurs in the chromophores was near 16 Å, corresponding to the second peak (second-nearest neighbors) observed for F2. Coumarin-coumarin interaction was minimal and observed at longer distances. Finally, none of the major peaks were near closest contact; the

Lennard-Jones σ (zero-energy distance)[26b] for the MMFF representation of sulfur in thiophene is shown for comparison.

### *4.3.3. Molecular dynamics of chromophores in polymer matrix*

Improved annealing protocols (as implemented in the Methods section) combined with a switch from the canonical (NVT) ensemble to the isothermal-isobaric (NPT) ensemble, as used in some newer poling simulations[31], greatly improved the rate of convergence and allowed for simulations of F2/PMMA (19% and 38% chromophore by mass) and C1 at experimental densities and with larger numbers of chromophores. Simulations were allowed to equilibrate against 1 atm of pressure; the density of each simulation during the final 3.0 ns of the 5 ns production phase of each simulation is shown in Figure 4.13.

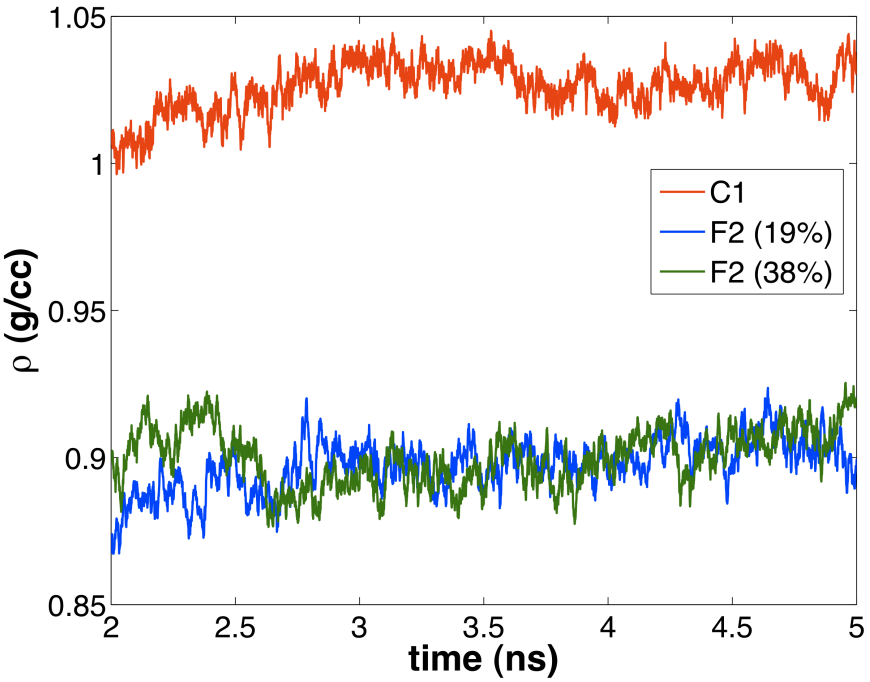


**Figure 4.13.** Equilibrium densities of C1 and F2/PMMA at 353K and 1 atm external pressure simulated with the MMFF94 force field and Tinker 5.1. (Pending publication in Benight, S. J.; Daniel B. Knorr, J.; Johnson, L. E.; Sullivan, P. A.; Lao, D.; Sun, J.; Kocherlakota, L. S.; Elangovan, A.; Robinson, B. H.; Overney, R. M.; Dalton, L. R., Nano-Engineering Soft Matter Lattice Dimensionality for an Organic Electro-Optic Material. *Advanced Materials* **2012**. ©2012 Wiley-VCH, used with permission)

Calculated densities ended up being very close to those expected from experiment (e.g. 0.92 g/cc for YLD-124 in PMMA)[5] and ~1.0 for C1.[8] This is remarkable given that the simulations were run with an unmodified force field primarily intended for conformational analysis and without using molecule-specific partial charges from electronic structure calculations, unlike several other such simulations.[21, 31]

Additionally, the radial distribution functions obtained from the longer, chromophore/polymer simulations were substantially less noisy. Results appear in Figure 4.14.

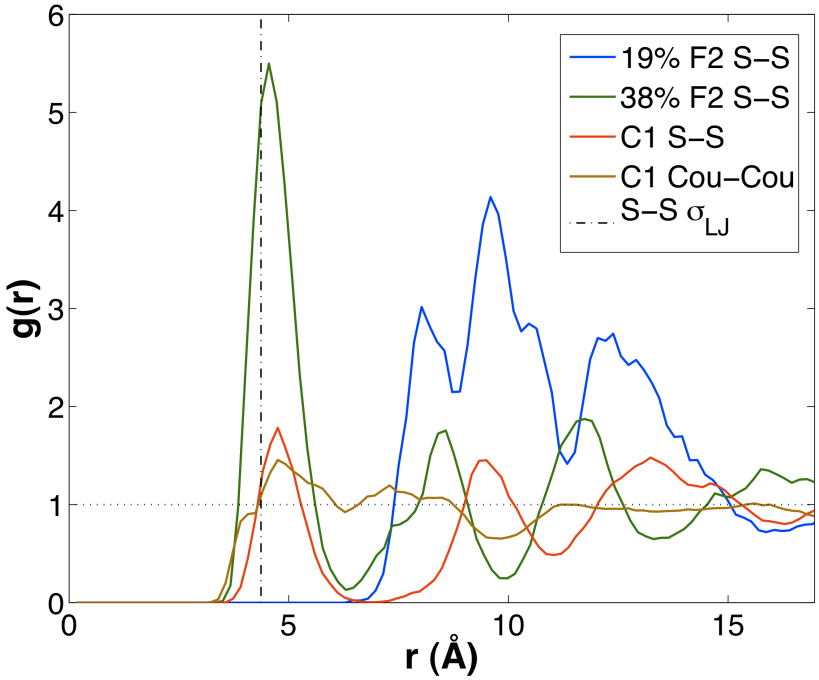


**Figure 4.14.** Radial distribution functions for C1 and F2/PMMA at 353K and 1 atm external pressure, averaging over 3.0 ns (6000 frames). The Lennard-Jones diameter for sulfur is shown to indicate closest contact. (Pending publication in Benight, S. J.; Daniel B. Knorr, J.; Johnson, L. E.; Sullivan, P. A.; Lao, D.; Sun, J.; Kocherlakota, L. S.; Elangovan, A.; Robinson, B. H.; Overney, R. M.; Dalton, L. R., Nano-Engineering Soft Matter Lattice Dimensionality for an Organic Electro-Optic Material. *Advanced Materials* **2012**. ©2012 Wiley-VCH, used with permission)

Here, strong correlation between the sulfurs in the chromophore bridge can be seen in the 38% F2 simulations at close contact, indicative of chromophore-chromophore stacking. In addition to being strong and sharp, the peak is also followed by weaker repeats at 8, 12, and 16 Å from additional shells of neighbors. A strong but broader and noisier peak appears for the lower-density F2, and much less chromophore-chromophore stacking is seen in C1; furthermore, the region between 6 and 8 Å is strongly excluded in the C1 simulation. Weak correlation between coumarins occurs between 5 and 8 Å. Visual inspection of simulations verified the presence of closely paired coumarins. A representative example is shown in Figure 4.15.

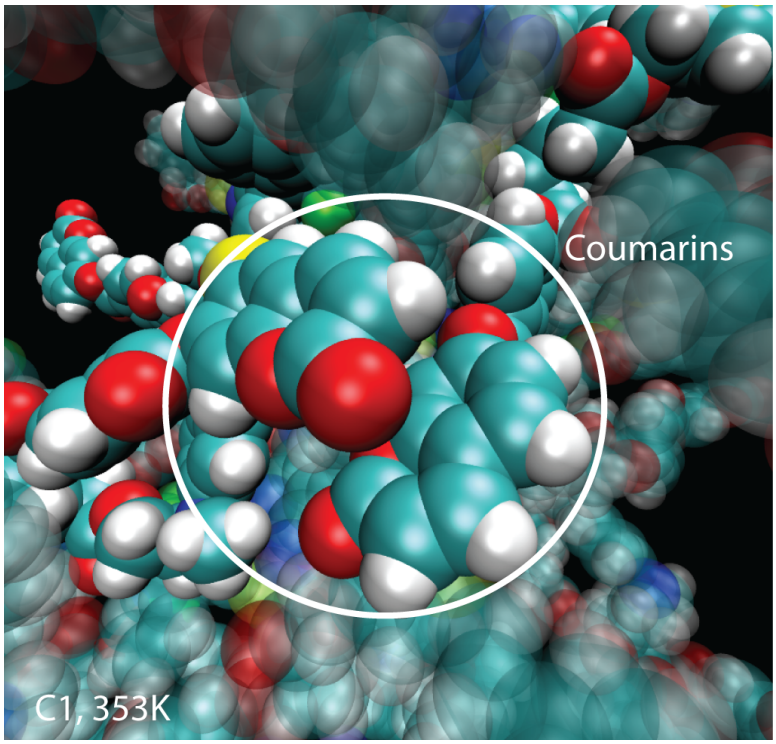


**Figure 4.15.** Coumarin-coumarin interaction in C1 (Pending publication in Benight, S. J.; Daniel B. Knorr, J.; Johnson, L. E.; Sullivan, P. A.; Lao, D.; Sun, J.; Kocherlakota, L. S.; Elangovan, A.; Robinson, B. H.; Overney, R. M.; Dalton, L. R., Nano-Engineering Soft Matter Lattice Dimensionality for an Organic Electro-Optic Material. *Advanced Materials* **2012**. ©2012 Wiley-VCH, used with permission)

Coumarin-coumarin interactions were further analyzed by means of the orientational correlation functions $g_{\mu}(r)$ and $g_{\mu}^{2}(r)$ (Equation 13); results are shown in Figure 4.16.

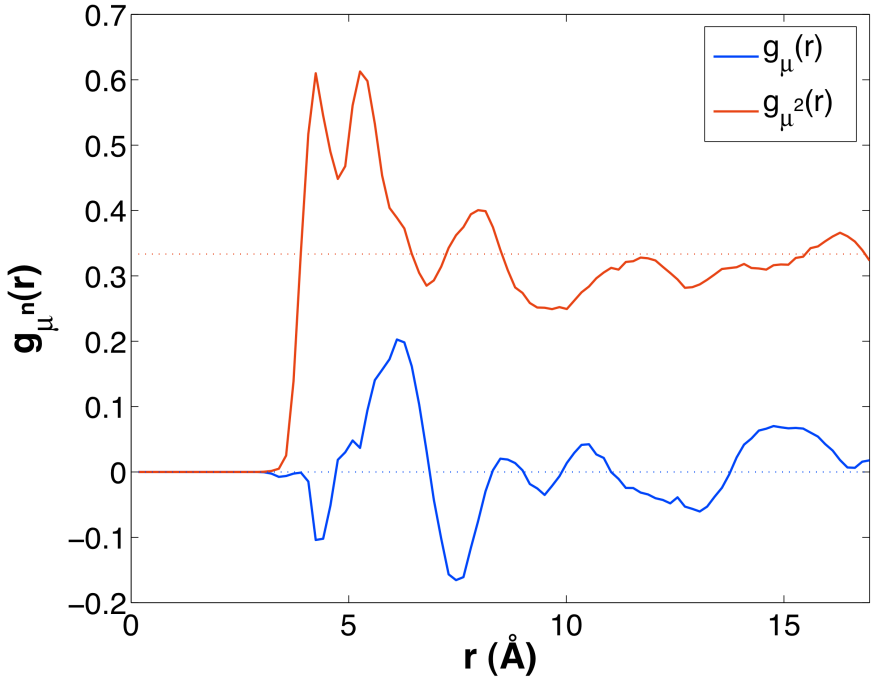


**Figure 4.16.** First and second-order dipole correlation functions for coumarins in C1 at 353K and 1 atm external pressure, averaging over 3.0 ns (6000 frames). The dotted lines indicate the isotropic value for each function. (Pending publiction in Benight, S. J.; Daniel B. Knorr, J.; Johnson, L. E.; Sullivan, P. A.; Lao, D.; Sun, J.; Kocherlakota, L. S.; Elangovan, A.; Robinson, B. H.; Overney, R. M.; Dalton, L. R., Nano-Engineering Soft Matter Lattice Dimensionality for an Organic Electro-Optic Material. *Advanced Materials* **2012**. ©2012 Wiley-VCH, used with permission)

Weak anti-correlation between the dipole moments of the coumarins can be seen in the first-order orientational correlation function at ~4 Å, followed by weak correlation at ~7 Å, immediately followed by another anti-correlated peak. Somewhat stronger pairing is seen in the second-order (centrosymmetric) correlation function between 4 and 7 Å, indicating that the dipole moments are more likely to be anti-aligned as would be predicted from classical electrostatics.

### *4.3.4. Phase behavior of MAP material C1*

While identifying the presence of coumarin-coumarin pairing in C1 at its standard poling temperature of 353 K, the interactions in the previous simulations were weak, and the use of a single temperature and relatively short time scale limited insight into their effect on the bulk thermal behavior of the material. Consequently, a cooling study was run on C1 using methods similar to prior work involving chromophores functionalized with aryl and perfluoroaryl groups[30] or chromophores in PMMA[21]. While operating on time scales substantially longer than any of the prior studies listed, the cooling rate was still very fast ($1.18 \times 10^{10}$ K/s). As the simulation was run in the NPT ensemble, the volume, and consequently density could change with temperature. Changes in $\partial\rho/\partial T$ (the coefficient of thermal expansion) would indicate the presence of a glass transition at that temperature ($T_g$). In the studies mentioned above, only a single $T_g$ was seen for each system. Molecular dynamics results for C1 appear in Figure 4.17; experimental SM-FM data by Stephanie Benight appears in Figure 4.18.

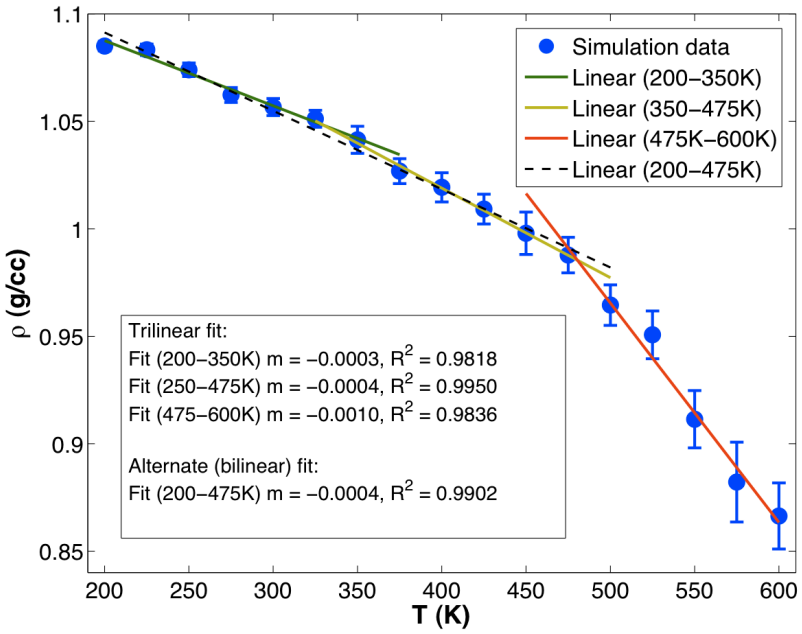


**Figure 4.17.** Density of C1 as a function of temperature at an external pressure of 1 atm and a cooling rate of $1.18 \times 10^{10}$ K/s. Fit lines were calculated using linear least squares; the dashed black line assumes no second transition near 350K.

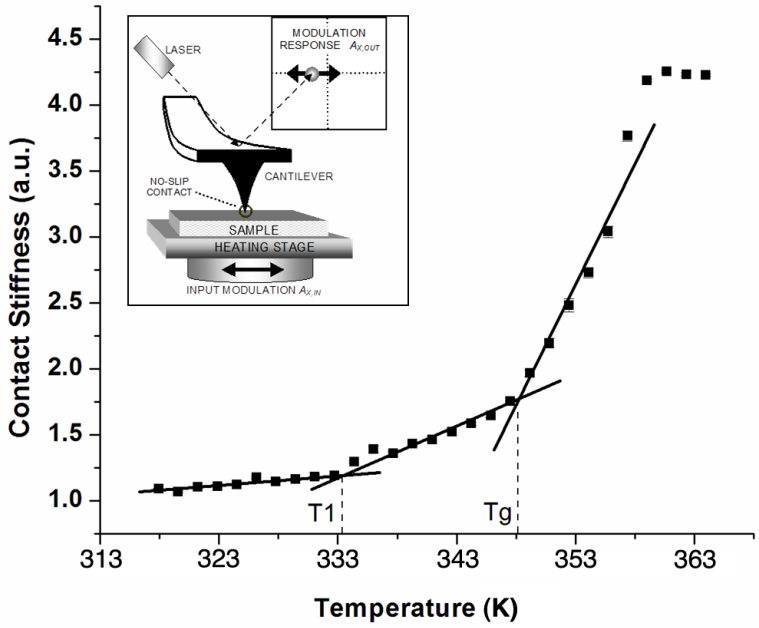


**Figure 4.18.** Shear-Modulation Force Microscopy data on C1 recorded and analyzed by Stephanie Benight; the $T_g$ is indicated along with the secondary transition (T1). Figure used under Creative Commons-Attribution license v3.0., from Benight, S. J.; Robinson, B. H.; Dalton, L. R., Nano-Engineering of Molecular Interactions in Organic Electro-Optic Materials. In *Molecular Interactions*, Meghea, A., Ed. Intech: Rijeka, Croatia, 2011.

A strong glass transition can be seen at 475K in the MD data; while much higher than the SMFM value[11] of ~353K. The discrepancy is typical for molecular dynamics simulations of similar systems and likely either represents overestimation of intermolecular interactions strength by the force field or is an artifact of the high cooling rate[21]. The glass transition temperature is similar to that observed for simulations of 24% DR1 in PMMA using the GAFF force field (480K)[31] or simulations of 9% EZ-FTC in PMMA (520K).[21] However, an additional, weak change in the slope of the curve can be seen near 325 K. Experimental work[11-12] by Stephanie Benight and Dan Knorr using SM-FM found a second, weak change in the stiffness of C1 at 334 K (seen in Figure 4.18) attributed to inter-coumarin interactions. While the temperature gap between the transitions in the MD simulations is much larger than that seen experimentally, it is possible that the same transition is being reflected in the molecular dynamics simulations. To further analyze this possibility, radial distribution functions (sulfur-sulfur, coumarin-coumarin, and sulfur-coumarin) were calculated at five temperatures to test this possibility. Results are shown in Figure 4.19.

**4.19a.** Sulfur-Sulfur

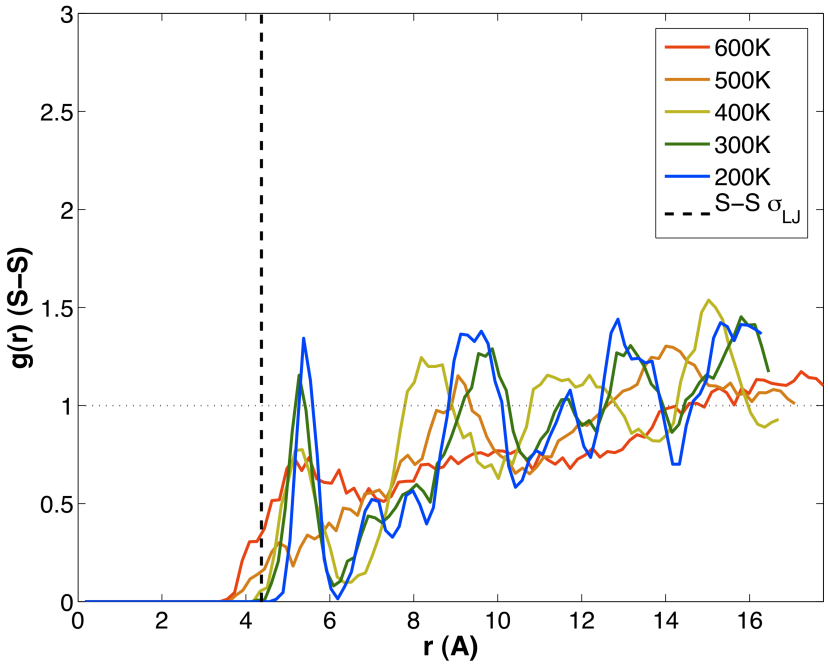


**4.19b.** Coumarin-Coumarin

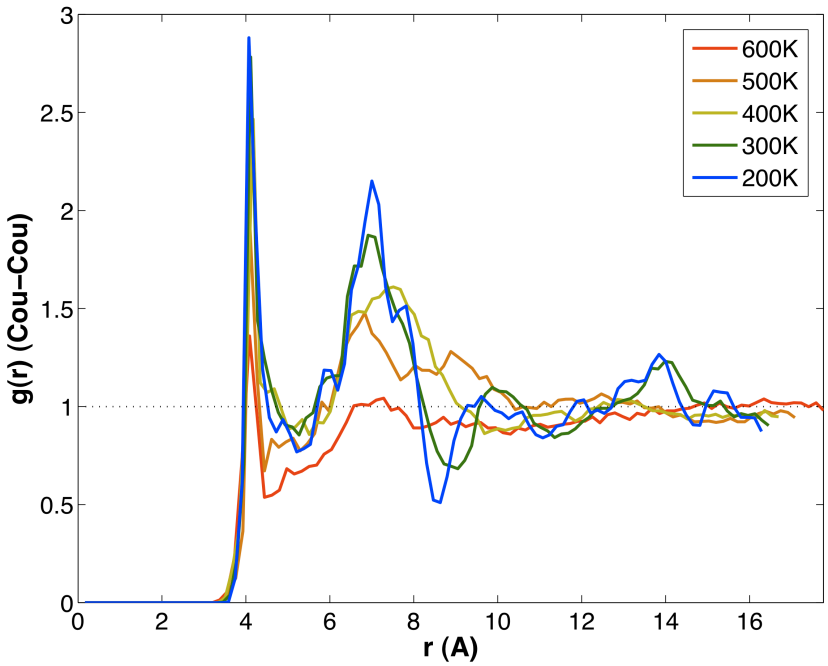

**4.19c.** Sulfur-Coumarin

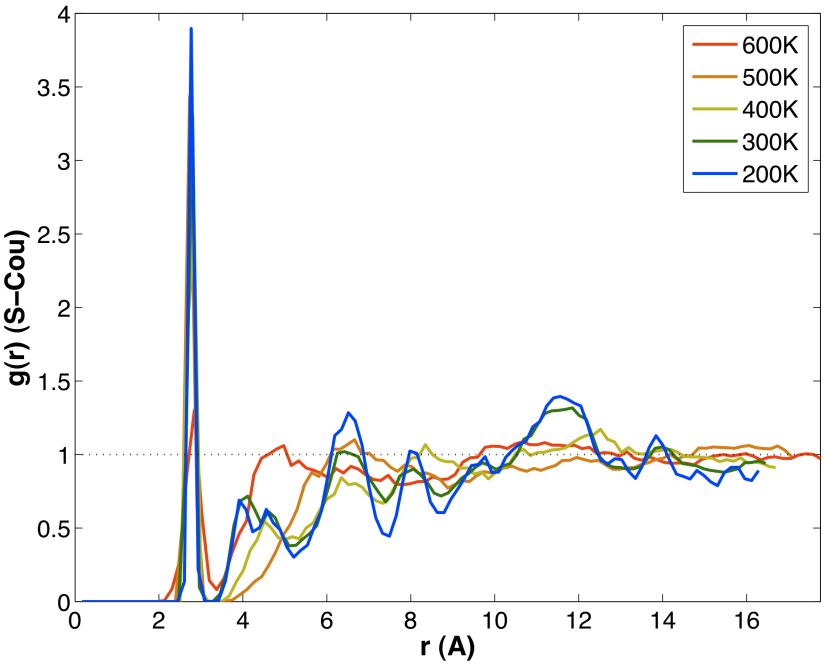


**Figure 4.19.** Sulfur-Sulfur (4.19a), Coumarin-Coumarin (4.19b), and Sulfur-Coumarin (4.19c) radial distribution functions for C1 at 200-500K and 1 atm external pressure. Each function is calculated from 1.0 ns of data (1000 frames).

Sulfur-sulfur correlations were weak at all temperatures, but particularly so at higher temperatures. As the temperature dropped, g(r) tended to oscillate around unity except for the previously observed excluded region near 6 Å. Given time to equilibrate, little chromophore-chromophore pairing occurred. For coumarin-coumarin interactions, however, the shape of g(r) varied greatly with temperature. At 600K, it remained near unity, with a broad peak developing near 7 Å between 500 and 400K, replaced by a much sharper peak with a repeat at 14 Å at lower temperatures. Additionally, the sharp peak near 3 Å monotonically grew as the temperature was reduced. The presence of two sharp, positive, peaks at low temperatures indicates the presence of two probable contact orientations for the coumarins. Finally, the sulfur-coumarin radial distribution function remained near unity at all temperatures except for sharp peak near 3 Å;

examination of the energies of individual interactions in the simulation indicated that this peak was due to a few high-energy close contacts that were likely frozen in during the cooling process.

In comparing all three sets of radial distribution functions, only the coumarin-coumarin radial distribution function shows qualitative changes below 400K. Consequentially, it is likely that if the weak transition at ~325K is real, it likely involves a change in the interactions between the coumarins. However, further work involving larger and longer simulations would be needed to verify the presence of this transition, and electrostatics from electronic structure calculations could be used to attempt to improve the absolute values of the transitions compared to experiment.

## 4.4. Conclusion

The combination of coarse-grained and atomistic techniques can provide useful predictions about a variety of systems relevant to organic electro-optic materials. While highly idealized, RBMC calculations can be used to provide reasonable estimates of ordering in organic EO materials, which is typically lower than that predicted by the 3D non-interacting rigid gas model. Furthermore, they can be used to demonstrate that the relationship between acentric and centrosymmetric order parameters under poling conditions does not remain constant with density or with molecular shape/size. The lattice dimensionality model developed for chromophores with mobility-restricting side chains provided a method to examine the relationship between these order parameters. Molecular dynamics simulations also provided insight on the role of coumarins in reducing the dimensionality of the C1 chromophore. The presence

of the coumarins disrupted pairing of chromophores at poling temperatures, and coumarins were found to pair weakly. The interactions appeared more strongly during rapid cooling, along with a weak change in $\partial\rho/\partial T$ that may be related to pairing of coumarins.

## 4.5. Acknowledgements for Chapter 4

Thanks to Stephanie J. Benight for extensive collaboration on this project, Larry R. Dalton, Bruce E. Eichinger, L. Michael Hayden, and Andreas F. Tillack for useful discussion, Benjamin C. Olbricht for his work on the VAPRAS technique, Benjamin H. Sibelman for developing the software used to visualize the RBMC simulations in this chapter, Jay Ponder for technical support regarding Tinker, as well as the National Science Foundation (STC-MDITR DMR-0120967 and DMR-0905686), the Air Force Office of Scientific Research (FA9550-09-1-0589), and the University of Washington Student Technology Fund for financial support.

## 4.6. References for Chapter 4

1. (a) Dalton, L. R.; Harper, A. W.; Robinson, B. H., The role of London forces in defining noncentrosymmetric order of high dipole moment–high hyperpolarizability chromophores in electrically poled polymeric thin films. *Proceedings of the National Academy of Sciences* **1997,** *94*, 4842-4847; (b) Robinson, B. H.; Dalton, L. R., Monte Carlo statistical mechanical simulations of the competition of intermolecular electrostatic and poling-field interactions in defining macroscopic electro-optic activity for organic chromophore/polymer materials. *Journal of Physical Chemistry A* **2000,** *104* (20), 4785-4795; (c) Dalton, L. R.; Benight, S. J.; Johnson, L. E.; Knorr, D. B.; Kosilkin, I.; Eichinger, B. E.; Robinson, B. H.; Jen, A. K. Y.; Overney, R. M., Systematic Nanoengineering of Soft Matter Organic Electro-optic Materials. *Chemistry of Materials* **2011,** *23* (3), 430-445; (d) Rommel, H. L.; Robinson, B. H., Orientation of Electro-optic Chromophores under Poling Conditions: A Spheroidal Model. *Journal of Physical Chemistry C* **2007,** *111* (50), 18765-18777; (e) Nielsen, R. D.; Rommel, H. L.;

Robinson, B. H., Simulation of the Loading Parameter in Organic Nonlinear Optical Materials. *Journal of Physical Chemistry B* **2004,** *108* (25), 8659-8667.
2. Pan, F.; Wong, M. S.; Bosshard, C.; Günter, P., Crystal Growth and Characterization of the Organic Salt 4-N,N-Dimethylamino-4'-N'- methyl-stilbazolium Tosylate (DAST). *Advanced Materials* **1996,** *8* (7), 592-595.
3. (a) Dalton, L. R.; Harper, A. W.; Ghosn, R.; Steier, W. H.; Ziari, M.; Fetterman, H.; Shi, Y.; Mustachich, R. V.; Jen, A. K.-Y.; Shea, K. J., Synthesis and Processing of Improved Organic Second-Order Nonlinear Optical Materials for Applications in Photonics. *Chemistry of Materials* **1995,** *7* (6), 1060-1081; (b) Facchetti, A.; Abbotto, A.; Beverina, L.; Boom, M. E. v. d.; Dutta, P.; Evmenenko, G.; Pagani, G. A.; Marks, T. J., Layer-by-Layer Self-Assembled Pyrrole-Based Donor-Acceptor Chromophores as Electro-Optic Materials. *Chemistry of Materials* **2003,** *15* (5), 1064-1072.
4. Dalton, L. R.; Sullivan, P. A.; Bale, D. H., Electric Field Poled Organic Electro-optic Materials: State of the Art and Future Prospects. *Chemical Reviews* **2010,** *110* (1), 25-55.
5. Olbricht, B. C.; Sullivan, P. A.; Dennis, P. C.; Hurst, J. T.; Johnson, L. E.; Benight, S. J.; Davies, J. A.; Chen, A.; Eichinger, B. E.; Reid, P. J.; Dalton, L. R.; Robinson, B. H., Measuring Order in Contact-Poled Organic Electrooptic Materials with Variable-Angle Polarization-Referenced Absorption Spectroscopy (VAPRAS). *Journal of Physical Chemistry B* **2011,** *115* (2), 231-241.
6. (a) Sullivan, P. A.; Rommel, H. L.; Takimoto, Y.; Hammond, S. R.; Bale, D. H.; Olbricht, B. C.; Liao, Y.; Rehr, J.; Eichinger, B. E.; Jen, A. K.-Y.; Reid, P. J.; Dalton, L. R.; Robinson, B. H., Modeling the Optical Behavior of Complex Organic Media: From Molecules to Materials. *Journal of Physical Chemistry B* **2009,** *113* (47), 15581-15588; (b) Sullivan, P. A.; Dalton, L. R., Theory-Inspired Development of Organic Electro-optic Materials. *Accounts of Chemical Research* **2009,** *43* (1), 10-18.
7. (a) Mortazavi, M. A.; Knoesen, A.; Kowel, S. T.; Higgins, B. G.; Dienes, A., Second-harmonic generation and absorption studies of polymer-dye films oriented by corona-onset poling at elevated temperatures. *Journal of the Optical Society of America B* **1989,** *6* (4), 733-741; (b) Onsager, L., Electric moments of molecules in liquids. *Journal of the American Chemical Society* **1936,** *58*, 1486-93.
8. Benight, S. J.; Johnson, L. E.; Barnes, R.; Olbricht, B. C.; Bale, D. H.; Reid, P. J.; Eichinger, B. E.; Dalton, L. R.; Sullivan, P. A.; Robinson, B. H., Reduced Dimensionality in Organic Electro-Optic Materials: Theory and Defined Order. *Journal of Physical Chemistry B* **2010,** *114* (37), 11949-11956.
9. (a) March, N. H.; Tosi, M. P., *Atomic Dynamics in Liquids*. Dover Publications, Inc.: New York, NY, 1976; (b) Singer, K. D.; Kuzyk, M. G.; Sohn, J. E., Second-order nonlinear-optical processes in orientationally ordered materials: relationship between molecular and macroscopic properties. *Journal of the Optical Society of America B* **1987,** *4* (6), 968-976.
10. Kuzyk, M. G.; Singer, K. D.; Zahn, H. E.; King, L. A., Second-order nonlinear-optical tensor properties of poled films under stress. *Journal of the Optical Society of America B* **1989,** *6* (4), 742-752.
11. Benight, S. J.; Robinson, B. H.; Dalton, L. R., Nano-Engineering of Molecular Interactions in Organic Electro-Optic Materials. In *Molecular Interactions*, Meghea, A., Ed. Intech: Rijeka, Croatia, 2011.

12. Benight, S. J.; Daniel B. Knorr, J.; Johnson, L. E.; Sullivan, P. A.; Lao, D.; Sun, J.; Kocherlakota, L. S.; Elangovan, A.; Robinson, B. H.; Overney, R. M.; Dalton, L. R., Nano-Engineering Soft Matter Lattice Dimensionality for an Organic Electro-Optic Material. *Advanced Materials* **2012,** *IN PRESS*.
13. Sullivan, P. A.; Rommel, H.; Liao, Y.; Olbricht, B. C.; Akelaitis, A. J. P.; Firestone, K. A.; Kang, J.-W.; Luo, J.; Davies, J. A.; Choi, D. H.; Eichinger, B. E.; Reid, P. J.; Chen, A.; Jen, A. K. Y.; Robinson, B. H.; Dalton, L. R., Theory-Guided Design and Synthesis of Multichromophore Dendrimers: An Analysis of the Electro-optic Effect. *Journal of the American Chemical Society* **2007,** *129* (24), 7523-7530.
14. Johnson, L. E.; Barnes, R.; Draxler, T. W.; Eichinger, B. E.; Robinson, B. H., Dielectric Constants of Simple Liquids: Stockmayer and Ellipsoidal Fluids. *Journal of Physical Chemistry B* **2010,** *114* (25), 8431-8440.
15. Lee, S.; Park, S. S., Dielectric properties of organic solvents from non-polarizable molecular dynamics simulation with electronic continuum model and density functional theory. *J Phys Chem B* **2011,** *115* (43), 12571-6.
16. Perram, J. W.; Wertheim, M. S., Statistical mechanics of hard ellipsoids. I. Overlap algorithm and the contact function. *Journal of Computational Physics* **1985,** *58* (3), 409-16.
17. (a) Neumann, M., Dipole moment fluctuation formulas in computer simulations of polar systems. *Molecular Physics* **1983,** *50* (4), 841-58; (b) Allen, M. P., Tildesley, D.J., *Computer Simulations of Liquids*. Clarendon: Oxford (UK), 1987.
18. *Spartan '08*, 1.2.0; Wavefunction, Inc.: Irvine, CA, 2008.
19. Frisch, M. J.; Trucks, G. W.; Schlegel, H. B.; Scuseria, G. E.; Robb, M. A.; Cheeseman, J. R.; G. Scalmani, V. B.; Mennucci, B.; Petersson, G. A.; Nakatsuji, H.; Caricato, M.; Li, X.; Hratchian, H. P.; Izmaylov, A. F.; Bloino, J.; Zheng, G.; Sonnenberg, J. L.; Hada, M.; Ehara, M.; Toyota, K.; Fukuda, R.; Hasegawa, J.; Ishida, M.; Nakajima, T.; Honda, Y.; Kitao, O.; Nakai, H.; Vreven, T.; J. A. Montgomery, J.; Peralta, J. E.; Ogliaro, F.; Bearpark, M.; Heyd, J. J.; Brothers, E.; Kudin, K. N.; Staroverov, V. N.; Kobayashi, R.; Normand, J.; Raghavachari, K.; Rendell, A.; Burant, J. C.; Iyengar, S. S.; Tomasi, J.; Cossi, M.; Rega, N.; Millam, J. M.; Klene, M.; Knox, J. E.; Cross, J. B.; Bakken, V.; Adamo, C.; Jaramillo, J.; Gomperts, R.; Stratmann, R. E.; Yazyev, O.; Austin, A. J.; Cammi, R.; Pomelli, C.; Ochterski, J. W.; Martin, R. L.; Morokuma, K.; Zakrzewski, V. G.; Voth, G. A.; Salvador, P.; Dannenberg, J. J.; Dapprich, S.; Daniels, A. D.; Farkas, Ö.; Foresman, J. B.; Ortiz, J. V.; Cioslowski, J.; Fox, D. J. *Gaussian 09*, Revision C.01; Gaussian, Inc.: Wallingford, CT, 2009.
20. Press, W. H., Teukolsky, S.A., Vetterling, W.T., Flannery, B.P., *Numerical Recipes*. 3rd ed.; Cambridge University Press: Cambridge (UK), 2007.
21. Leahy-Hoppa, M. R.; Cunningham, P. D.; French, J. A.; Hayden, L. M., Atomistic Molecular Modeling of the Effect of Chromophore Concentration on the Electro-optic Coefficient in Nonlinear Optical Polymers. *The Journal of Physical Chemistry A* **2006,** *110* (17), 5792-5797.
22. Ponder, J. *TINKER*, 5.1; Washington University: St. Louis MO, 2010.
23. Halgren, T. A., Merck Molecular Force Field. I. Basis, Form, Scope, Parameterization, and Performance of MMFF94. *Journal of Computational Chemistry* **1996,** *17* (5), 490-519.

24. Darden, T.; York, D.; Pedersen, L., Particle mesh Ewald: An N•log(N) method for Ewald sums in large systems. *The Journal of Chemical Physics* **1993,** *98* (12), 10089-10092.
25. Berendsen, H. J. C.; Postma, J. P. M.; van Gunsteren, W. F.; DiNola, A.; Haak, J. R., Molecular dynamics with coupling to an external bath. *The Journal of Chemical Physics* **1984,** *81* (8), 3684.
26. (a) McQuarrie, D. A., *Statistical Mechanics*. University Science Books: Sausalito, CA, 2000; (b) Leach, A. R., *Molecular Modeling: Principles and Applications*. 2nd ed.; Pearson Education: Harlow (UK), 2001; (c) Frenkel, D., Smidt, B., *Understanding Molecular Simulation: From Algorithms to Applications*. Elsevier: Amsterdam (ND), 2002.
27. Barker, J. A.; Watts, R. O., Monte-Carlo studies of the dielectric properties of water-like models. *Molecular Physics* **1973,** *26* (3), 789-92.
28. Weis, J. J.; Levesque, D., Ferroelectric phases of dipolar hard spheres. *Physical Review E* **1993,** *48* (5), 3728.
29. de Gennes, P. G.; Prost, J., *The Physics of Liquid Crystals*. Oxford University Press: Oxford, UK, 1993.
30. Knorr, D. B., Jr.; Zhou, X. H.; Shi, Z.; Luo, J.; Jang, S. H.; Jen, A. K.; Overney, R. M., Molecular mobility in self-assembled dendritic chromophore glasses. *J Phys Chem B* **2009,** *113* (43), 14180-8.
31. Tu, Y.; Zhang, Q.; Ågren, H., Electric Field Poled Polymeric Nonlinear Optical Systems: Molecular Dynamics Simulations of Poly(methyl methacrylate) Doped with Disperse Red Chromophores. *Journal of Physical Chemistry B* **2007,** *111* (14), 3591-3598.
32. (a) Kim, W.-K.; Hayden, L. M., Fully atomistic modeling of an electric field poled guest-host nonlinear optical polymer. *Journal of Chemical Physics* **1999,** *111* (11), 5212-5222; (b) Makowska-Janusik, M.; Reis, H.; Papadopoulos, M. G.; Economou, I. G.; Zacharopoulos, N., Molecular Dynamics Simulations of Electric Field Poled Nonlinear Optical Chromophores Incorporated in a Polymer Matrix. *Journal of Physical Chemistry B* **2004,** *108* (2), 588-596.

# 5. Accurate Calculation of Electronic Excitations and Relative Hyperpolarizabilities of High-Performance Organic Electro-Optic Chromophores

## 5.1. Introduction

Systematic improvement of electro-optic performance through theory-aided design requires accurate calculation of both linear and nonlinear optical properties of candidate chromophores.[1] Such calculations are important for pre-synthesis screening[2], to provide insight on whether a difficult synthesis may be worth pursuing, and for assisting in deconvoluting the effects of molecular nonlinearity (as quantified by the first hyperpolarizability, β) versus ordering in contributing to the electro-optic behavior of a material[3]. Measurements of the electro-optic coefficient[1a]

$$r_{33} \propto \rho_N \beta_{zzz}(-\omega,0,\omega)\left\langle \cos^3\theta \right\rangle \qquad (5\text{-}1)$$

where $\rho_N$ is the number density of the chromophores, $\beta_{zzz}(-\omega,0,\omega)$ is the component of the molecular first hyperpolarizability along the dipole moment for interacting low-frequency and optical fields, and $\left\langle \cos^3\theta \right\rangle$ is the bulk acentric order parameter, measure an aggregate of several properties,[4] complicating their use in uniquely determining β.

While hyperpolarizability can directly be measured using hyper-Rayleigh scattering,[4-5] the quantity measured is the rotationally averaged second-harmonic hyperpolarizability[6]

$$\beta_{HRS}(-2\omega,\omega,\omega) = \sqrt{\frac{6}{35}\sum_i \beta_{iii}^2 + \frac{16}{105}\sum_{i\neq j}\beta_{iii}\beta_{jij} + \frac{38}{105}\sum_{i\neq j}\beta_{ij}^2 + \frac{16}{105}\sum_{ijk,cyclic}\beta_{iij}\beta_{jkk} + \frac{20}{35}\beta_{ijk}^2} \qquad (5\text{-}2)$$

where all of the hyperpolarizability components are $\beta(-2\omega,\omega,\omega)$ and the cyclic sum is over the components $\beta_{xxy}$, $\beta_{yzz}$, $\beta_{yyz}$, $\beta_{zxx}$, $\beta_{xxz}$, and $\beta_{xyy}$. If the hyperpolarizability tensor is dominated by a single component along the molecular dipole axis[7] (arbitrarily defined as the z-axis), Equation 5-2 can be approximated as

$$\beta_{HRS}(-2\omega,\omega,\omega) \approx \sqrt{\frac{6}{35}}\beta_{zzz}(-2\omega,\omega,\omega) \qquad (5\text{-}3)$$

which allows for estimating the component relative to EO activity.[5a] However, the frequency dispersion of the hyperpolarizability must still be adjusted using the two-level model[8] expressions[3]

$$\begin{aligned}\beta(-2\omega,\omega,\omega) &\approx \left|\frac{\omega_{\max}^4}{\left(\omega^2-\omega_{\max}^2\right)\left(\omega^2-4\omega_{\max}^2\right)}\right|\beta(0)\\ \beta(-\omega,0,\omega) &\approx \frac{3\omega_{\max}^2-\omega^2}{3\left(\omega_{\max}^2-\omega^2\right)^2}\beta(0)\end{aligned} \qquad (5\text{-}4)$$

where $\omega$ is the frequency of the light field, and $\omega_{max}$ is the frequency of the lowest charge-transfer excitation of the chromophore. However, the two-level model is an incomplete description of the frequency dependence of hyperpolarizability due to transition linewidths, contributions from other electronic states, and solvent dielectric effects.[1a, 5b, 9]

In contrast, calculations using Coupled-Perturbed Hartree-Fock (CPHF),[10] Real-Time Time-Dependent Density Functional Theory (RT-TDDFT),[11] Sum-over-States[12] (SOS), or Coupled-Cluster response theory[13] calculation methods can obtain frequency-dependent hyperpolarizabilities directly for applied fields of arbitrary frequency. Static hyperpolarizabilities can also be obtained using finite-field (FF) techniques from many different electronic structure methods.[1c]

Previous computational studies have provided significant insight into general trends in chromophore hyperpolarizabilities,[1c, 12] relative hyperpolarizabilities of common chromophores versus experimental standards,[14] frequency dispersion of high-performance chromophores,[11] hyperpolarizabilities of small solvent molecules,[15] solvent dependence of hyperpolarizability,[5b, 16] and performace of unusual chromophore donor[17] (e.g. ferrocence) and bridge[18] (e.g. tictoid) structures. However, quantitative comparsison of calculated absolute hyperpolarizabilities remains difficult due to the variety of approximations and calibration standards used in the literature.[19]

One significant challenge is reliably and efficiently predicting the relative hyperpolarizabilities of high-performance chromophores, such as those based on variants the TCF acceptor. For reasons of computational efficiency, routine calculations of optical properties of chromophores are typically conducted using Density-Functional Theory[1b, 20] (DFT) or semi-empirical Hartree-Fock based methods such as INDO[12, 21] due to their favorable scaling with number of basis functions. Coupled-Cluster theory, while highly accurate, is currently barely tractable on large compute clusters for small chromophores such as p-nitroaniline with adequate-sized basis sets.[15a] Second-order Møller-Plesset perturbation theory[22] (MP2) has been reported to give reasonable estimates of hyperpolarizabilities at lower costs than Coupled-Cluster theory.[23] However, until recently, it has been considered to be too computationally expensive for larger chromophores.[1c, 14] It is now tractable on modest hardware, but consumes far more computing resources than DFT. Unfortunately, both DFT and semi-empirical HF methods are parameterization-dependent, and some DFT methods such as the commonly-used B3LYP[24] functional are insensitive to changes in

chromophore structure that produce large differences in experimentally-determined hyperpolarizability and EO activity. A particularly striking example is of TCF-based chromophores CLD-1 and EZ-FTC, where CLD-1 has been experimentally shown to have approximately 1.8 times the hyperpolarizability[5b] and poling efficiency ($r_{33}/E_p$) of EZ-FTC.[25] The structures of the two chromophores are shown in Figure 5.1.

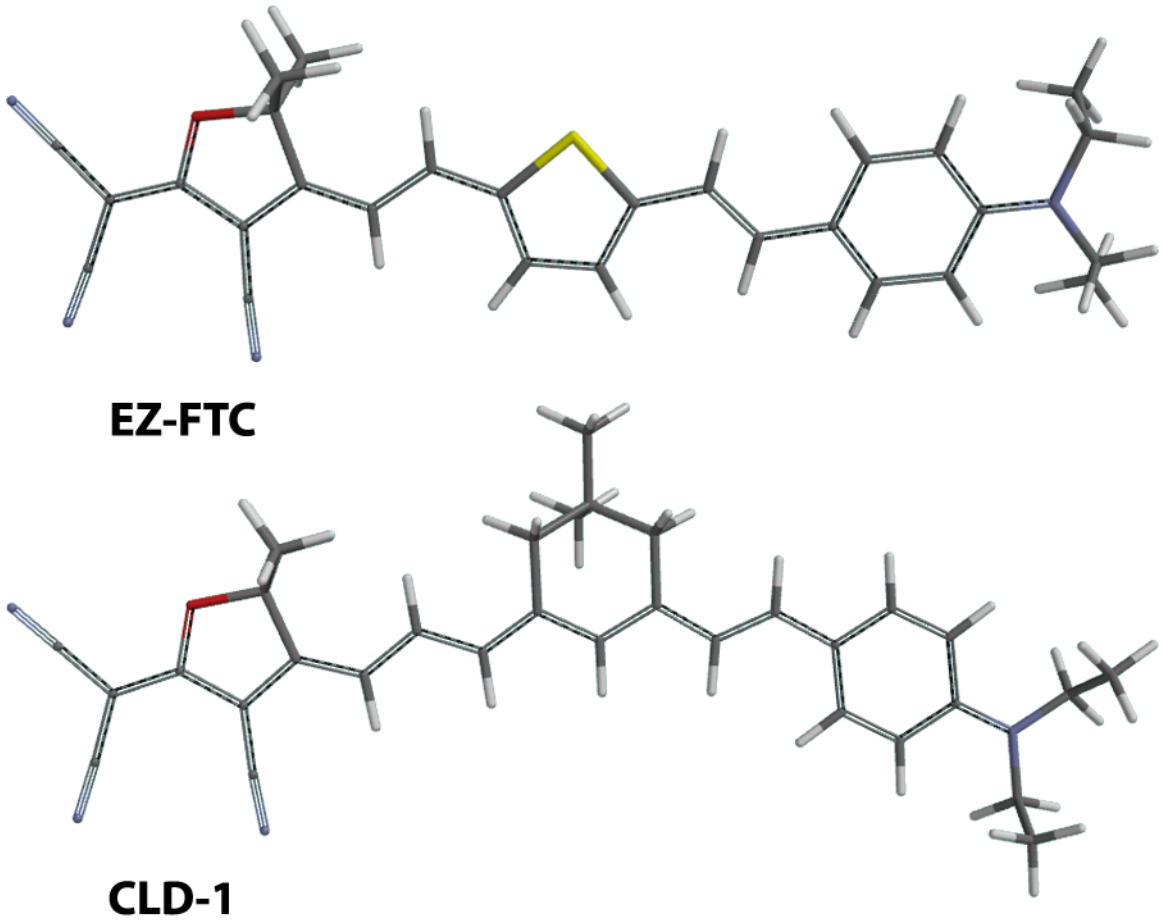


**Figure 5.1.** Optimized geometries of EZ-FTC and CLD-1 chromophores at the B3LYP/6-31+G(d) level. Alkyl chains have been truncated at two carbons for reasons of computational efficiency. Structures were optimized using Gaussian '09[26]; graphics produced using Spartan '08[27]. Both chromophores use dialkylaniline donors and a dimethyl variant of the TCF acceptor, differing only in the bridge.

A related issue is the prediction of excitation energies, which are critical for both understanding frequency dispersion of hyperpolarizability[3] and optical loss in device applications.[28] Here, common DFT functionals such as PBE0[29] and B3LYP often perform very well[28, 30]. An ideal calculation method for hyperpolarizabilities would also provide a reasonable treatment of electronic excitation energies, and consequently, the linear absorbance spectrum of the chromophore.

Finally, calculation methods used in screening chromophore hyperpolarizabilities would optimally have minimal dependence on empirical parameterization. Many of the DFT methods currently in use for molecular systems are so-called hybrid functionals,[24b, 31] which combine electron exchange and correlation approximated from local electron density and its gradient (the Generalized Gradient Approximation, or GGA)[20a] with non-local Hartree-Fock (HF) exchange. The exchange-correlation energy obtained from a hybrid functional is[31b]

$$E_{XC}^{hybrid} = E_{XC}^{GGA} + a_0\left(E_X^{HF} - E_X^{GGA}\right) \qquad (5\text{-}5)$$

Where $E_{XC}^{GGA}$ is the pure-GGA exchange-correlation energy, $E_X^{HF}$ is the HF exchange energy, $E_X^{GGA}$ is the GGA exchange energy, and $a_0$ is the fraction of HF exchange used. This is done in order to cancel out the tendency for DFT to be insensitive to longer-range interaction between orbital due to self-interaction error,[32] and partially correct for Hartree-Fock's neglect of electron correlation.[23, 33] While often providing an improvement over both parent techniques, hybrid DFT is inherently a semi-empirical approximation, albeit with fewer parameters than 'typical' semi-empirical methods such as INDO,[21] PM3[34] and PM6.[35] In common

formulations such as B3LYP and PBE0 (mild hybrids), the amount of Hartree-Fock exchange used is on the order of 25% or less. While this partially mitigates the issue of over-localization of electron density, mild hybrid functionals still provide an incorrect estimate of long-range Coulomb interactions and have difficulty in predicting energies of charge-transfer states,[32a] including sometimes predicting spurious low-lying states.[32a, 36] This problem can be mitigated by use of hybrids with larger quantities of HF exchange,[37] albeit at the expense of substantially blue-shifting electronic excitations.[36a] Other methods have been used to mitigate the over-localization in typical DFT methods, such as invocation of higher derivatives of the local density,[38] (Meta-GGA) adding MP2 correlation to the functional,[39] or extensive empirical parameterization (dozens of adjustable parameters), as used in the Truhlar[40] (Minnesota) functionals.

Another common method used for empirically correcting the long-range behavior of DFT functionals is by making the amount of Hartree-Fock exchange a distance dependent property[41]

$$\frac{1}{r_{12}} = \frac{1-\left[a+b\,\mathrm{erf}\left(cr_{12}\right)\right]}{r_{12}} + \frac{a+b\,\mathrm{erf}\left(cr_{12}\right)}{r_{12}} \qquad (5\text{-}6)$$

similar to the partitioning scheme used in Ewald sums[42]. Here, $r_{12}$ is the electron-electron distance in the exchange integrals[43] $\langle ij \mid ji \rangle$, $a$ is the fraction of HF exchange used at short range, $a + b$ is the fraction of HF exchange, and $c$ is a parameter related to the slope of the switching function. The incorporation of additional long-Range Hartree-Fock exchange improves screening of electron density over long distances, and reduces the over-localization[44] of electron density.[45] Range-separated functions such as LC-BLYP[41] and CAM-B3LYP[46] have

resulted in improved treatment of charge-transfer states,[32b, 37, 47] albeit sometimes at the expense of absolute excitation energies.

The following work will compare seven hybrid functionals, the already mentioned B3LYP, PBE0, CAM-B3LYP, and LC-BLYP, as well as the higher-HF B3LYP-like functional BHandHLYP,[48] the heavily parameterized, high-HF meta-GGA M062X functional,[49] and the newer-generation ωB97X range-separated functional.[50] Three wavefunction-based methods; Hartree-Fock, the computationally inexpensive semi-empirical PM6 method, combined with electronic excitations calculated with the ZINDO[51] semi-empirical method, and the more accurate but expensive MP2 method, were used for comparison. Methods used are shown in Table 1, along with the amount of Hartree-Fock exchange at zero and infinite distance.

**Table 5.1.** Methods used for comparison of hyperpolarizabilities, excitation energies, and dipole moments, showing amounts of short-range (SR) and long-range (LR) Hartree-Fock exchange

| **Name** | **Type** | **% HF exch. (SR)** | **% HF exch. (LR)** |
|---|---|---|---|
| B3LYP | Hybrid GGA | 20 | 20 |
| PBE0 | Hybrid GGA | 25 | 25 |
| BHandHLYP | Hybrid GGA | 50 | 50 |
| M062X | Hybrid Meta-GGA | 54 | 54 |
| CAM-B3LYP | Range-separated GGA | 19 | 65 |
| LC-BLYP | Range-separated GGA | 0 | 100 |
| wB97X | Range-separated GGA | 0 | 100 |
| Hartree-Fock | *Ab initio* wavefunction | 100 | 100 |
| PM6 | Semi-empirical HF | 100 | 100 |
| ZINDO | Semi-emprical HF | 100 | 100 |
| MP2 | Post-HF wavefunction | 100 | 100 |

Experimental UV/Vis and HRS data is shown in Table 5.2. The relative hyperpolarizability of CLD-1 versus EZ-FTC was used as a metric due to available data[52] on $\beta_{HRS}$ of EZ-FTC at 1907nm (off-resonance) having large

uncertainty, and HRS experiments typically being conducted against standard chromophore,[4, 14] such as EZ-FTC in this case.[5b]

**Table 5.2.** Experimental reference data used as benchmarks for calculations

| Property | Ref. Value | Solvent | Source |
|---|---|---|---|
| $\lambda_{max}$ (EZ-FTC) | 676 nm | Chloroform | Firestone 2005 |
| $\lambda_{max}$ (CLD-1) | 691 nm | Chloroform | Bale 2011 |
| $\beta_{HRS}$ CLD-1/EZFTC (1907nm) | 1.80 ± 0.08 | Chloroform | Bale 2011 |

The metrics used for comparing the functionals were the relative static hyperpolarizability, relative Pockels hyperpolarizabilities at 1310nm, and relative HRS hyperpolarizabilities at 1906 nm, as well as the dominant (lowest charge transfer) excitation energies of both chromophores. Static and Pockels hyperpolarizabilities were extrapolated with the two-level model. The degree of correlation between each property and the amount of Hartree-Fock exchange in each functional was also explored.

## 5.2. Computational Methods

All calculations were performed with the commercially available version of Gaussian 09 (rev. A, B, or C).[26] All DFT calculations used the Pople[53] 6-31+G(d) basis set (diffuse and polarization functions on heavy atoms), which had previously been determined to provide reasonable performance at low cost for larger ONLO chromophores,[16] albeit not for smaller molecules.[15a] All calculations (geometry and properties) were run in PCM[54] chloroform, starting from an initial gas-phase geometry optimized using the same method, which was in turn based on a rough PM3 geometry. Properties calculations were performed on structures optimized using the same method as the properties calculation, which used DFT geometries. Such calculations are indicated using double-slash notation such that

MP2//B3LYP means a MP2 properties calculation on a B3LYP geometry. Geometries were optimized to default convergence criteria, and wavefunctions were optimized to a SCF convergence criterion of $< 10^{-10}$ au RMS error in the density matrix, except for MP2 calculations, which were optimized to $<10^{-8}$ au RMS error in the density matrix. Two-electron integrals were calculated to a precision of $10^{-13}$ au.

Hyperpolarizabilities were calculated by differentiation of electronic energy with respect to an applied electric field. By the Hellman-Feynman theorem,[42]

$$\frac{\partial W}{dx} = \left\langle \frac{\partial H}{\partial x} \right\rangle \quad (5\text{-}7)$$

where $W$ is the total electronic energy of the molecule, $H$ is the corresponding Hamiltonian, and $x$ the parameter being differentiated with respect to, the dipole moment of a molecule can be calculated as

$$\mu_i = \frac{\partial W}{\partial E_i} \qquad (5\text{-}8)$$

by treating the applied field as a weak perturbation to the Hamiltonian.[43] The same treatment can be expanded to higher derivatives such that[10a, 43]

$$W(E) = W_0 + \frac{\partial W}{\partial E_i} E_i + \frac{1}{2} \frac{\partial^2 W}{\partial E_i E} E_i E_j + \frac{1}{6} \frac{\partial^3 W}{\partial E_i E_j E_k} E_i E_j E_k \ldots \quad (5\text{-}9)$$

which is equivalent to

$$W(E) = W_0 + \mu_i E_i + \alpha_{ij} E_i E_j + \beta_{ijk} E_i E_j E_k \ldots \quad (5\text{-}10)$$

These derivatives can be calculated with respect to either a static or time-varying field, and can be calculated numerically and/or analytically.[1b, 10a] Calculations used in this work used a mixed differentiation scheme, where HF, DFT, and PM6

hyperpolarizabilities were calculated by numerical differentiation of analytic polarizabilities (polar=cubic option in Gaussian), and MP2 hyperpolarizabilities were calculated by double numerical differentiation of analytic dipole moments (polar=doublenumer option in Gaussian) for reasons of computational efficiency. Both linear hyperpolarizabilities, $\beta(-\omega,0,\omega)$, and second-harmonic hyperpolarizabilities, $\beta(-2\omega,\omega,\omega)$, were calculated (polar=dcshg option in Gaussian). Calculated hyperpolarizability tensors were rotated such that $\beta_{zzz}$ was aligned with the molecular dipole moment and scaled such that they used the perturbation series convention (Equation 10) instead of the Taylor series convention (as implemented by default in Gaussian), in which calculated hyperpolarizabilities have twice the magnitude of those calculated using the perturbation convention.[1c] Data processing was performed using in-house MATLAB code developed by Bruce Eichinger.

Optical transitions were calculated using the time-dependent variant[32b] (TDDFT or TDHF) of the method used for the geometry calculation for each molecule, except for the PM6 semi-empirical model, where the ZINDO method, which is optimized for excited state calculations,[51b] was used instead. Corresponding optical transition calculations were not run for the MP2 calculations, due to limitations on Gaussian's implementation of the CIS(D)[55] (excited state analogue to MP2) method for calculations in PCM solvent environments.

## 5.3. Results and Discussion

### *5.3.1. Electronic excitations*

Calculated excitation energies for EZ-FTC and CLD-1 are compared in Table 5.3. Higher-level CIS(D) calculations were not run due to computational limitations.

**Table 5.3.** Wavelength of lowest-energy charge transfer excitation for EZ-FTC and CLD-1

| **Method** | **EZ-FTC $\lambda_{max}$ (nm)** | **CLD-1 $\lambda_{max}$ (nm)** |
|---|---|---|
| B3LYP | 707 | 715 |
| PBE0 | 677 | 692 |
| BHandHLYP | 558 | 581 |
| M062X | 564 | 592 |
| CAM-B3LYP | 554 | 582 |
| LC-BLYP | 432 | 445 |
| ωB97X | 469 | 493 |
| HF | 398 | 406 |
| ZINDO//PM6 | 622 | 628 |
| ***Experiment*** | ***676*** | ***691*** |

While absolute values were strongly method-depenent, the relative energies were strongly correlated with each other, as were the relative errors compared to experiment. Errors in the excitation energies are graphically compared in Figure 5.2.

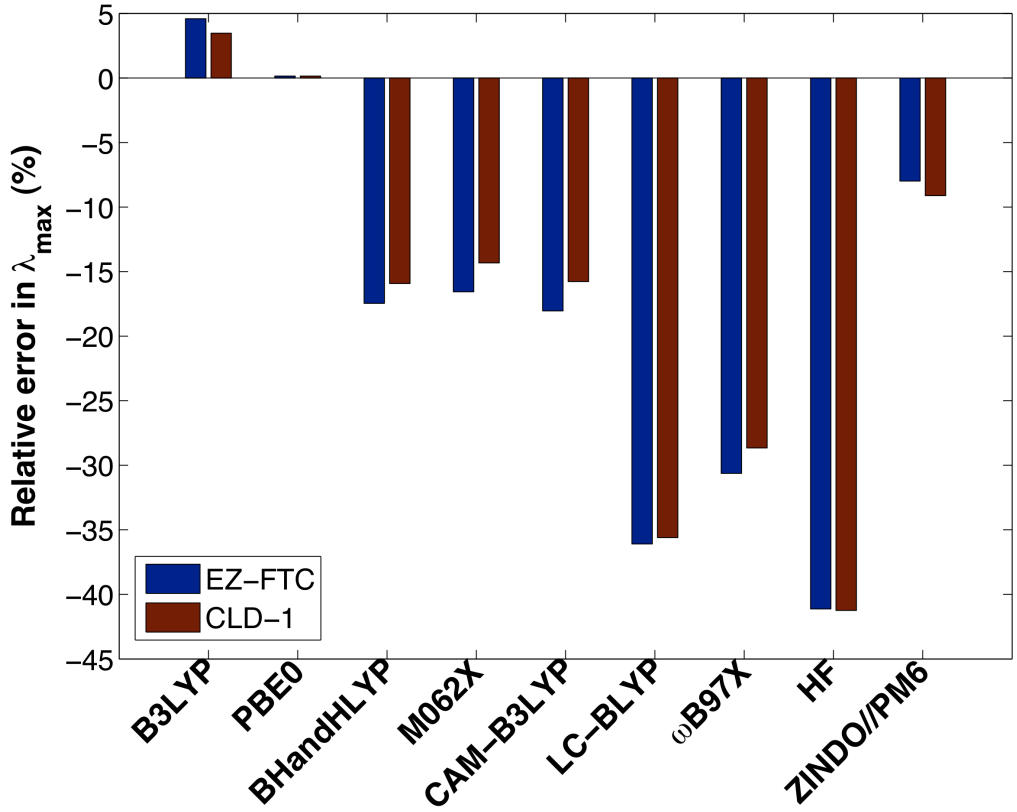


**Figure 5.2.** Relative errors in lowest charge-transfer excitation energies of EZ-FTC and CLD-1 in chloroform

Here, the mild hybrids (especially PBE0) are the strongest performers, followed by ZINDO. The latter is not surprising given that ZINDO was specifically parameterized to reproduce UV/Vis spectra.[51b] The performance of the mild hybrids is consistent with prior calculations on TCF-based chromophores,[28] as well as a variety of other small-molecule dyes[30] and conjugated polymers.[56] The range-separated functionals performed poorly, with errors on the order of those from TDHF, which typically significantly overestimates excitation energies.[32b] This likely indicates that the charge transfer distance is sufficiently long that the short-range portion of the exchange functional plays a relatively small role compared to the long-range (pure HF) portion. The only range-separated functional that performed well was CAM-B3LYP, which limits to 65% HF

exchange at long distance, instead of 100% as in the other two range-separated functionals.

Excitation energies were also compared with the amount of long-range Hartree-Fock exchange in the hybrid DFT methods used; results appear in Figure 5.3.

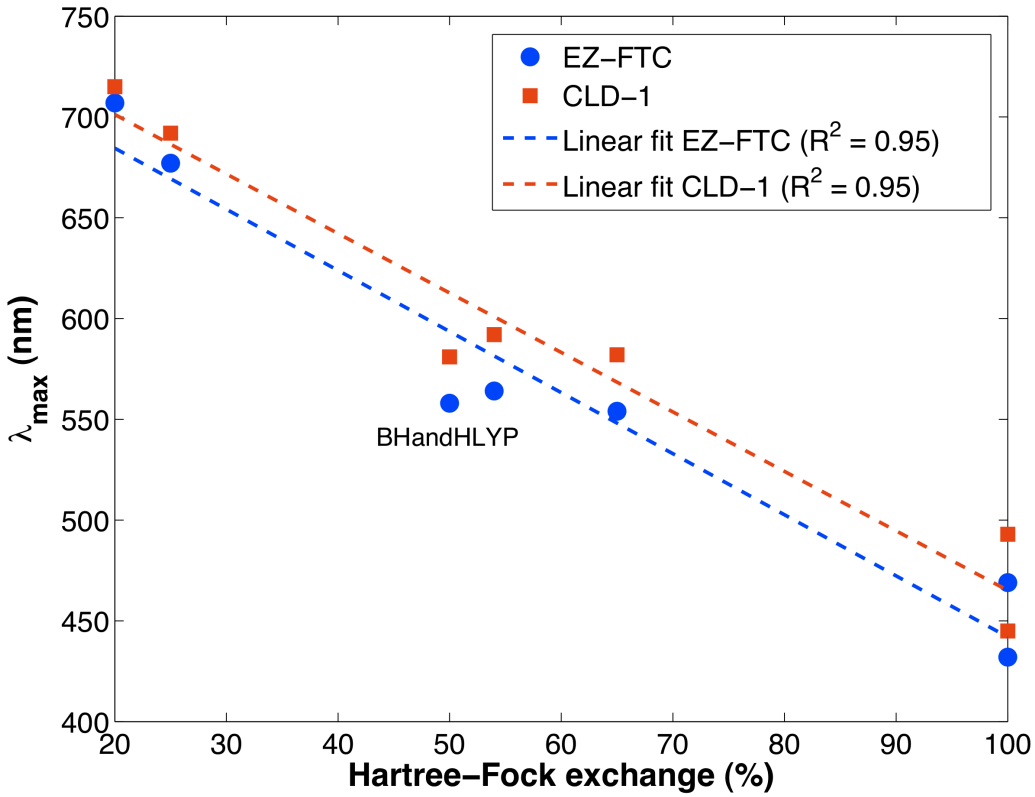


**Figure 5.3.** First charge-transfer excitation energy of EZ-FTC and CLD-1 in chloroform as a function of long-range Hartree-Fock exchange in hybrid DFT methods

Excitation energies of both EZ-FTC and CLD-1 were strongly and linearly correlated with the long-range HF exchange in the functionals used, consistent with results by Brédas and co-workers.[37] The BHandHLYP functional is a slight outlier. Given that dependence on the amount of HF exchange over the range of functionals examined is over an order of magnitude larger than the difference

between the two chromophores, it is important that calculations within a test set of molecules be compared only with those calculated by the same method, and that absolute values of the excitation energies be treated with caution.

### *5.3.2 Dipole moment*

Calculations of dipole moments of EZ-FTC and CLD-1 were compared to the amount of long-range HF exchange used in the calculation in a similar manner to calculations of electronic excitations. Dipole moments for each chromophore are shown in Table 5.4.

**Table 5.4.** Dipole moments for EZ-FTC and CLD-1

| Method | EZ-FTC μ (D) | CLD-1 μ (D) |
|---|---|---|
| B3LYP | 33.45 | 36.96 |
| PBE0 | 32.18 | 35.91 |
| BHandHLYP | 28.02 | 30.67 |
| M062X | 25.89 | 27.84 |
| CAM-B3LYP | 26.65 | 29.08 |
| LC-BLYP | 22.44 | 23.92 |
| ωB97X | 23.57 | 25.34 |
| HF | 23.21 | 25.08 |
| PM6 | 23.25 | 28.69 |
| MP2//B3LYP | 25.20 | 28.05 |
| MP2//M062X | 22.43 | 23.44 |

Mild hybrid DFT results resulted in the largest dipole moments, and MP2 the smallest when using the M062X geometry; the MP2 dipole moments showed substantial dependence on geometry. The high-HF functionals produced results similar to those obtained with purely HF-based methods. The DFT methods are compared as a function of long-range HF exchange in Figure 5.4.

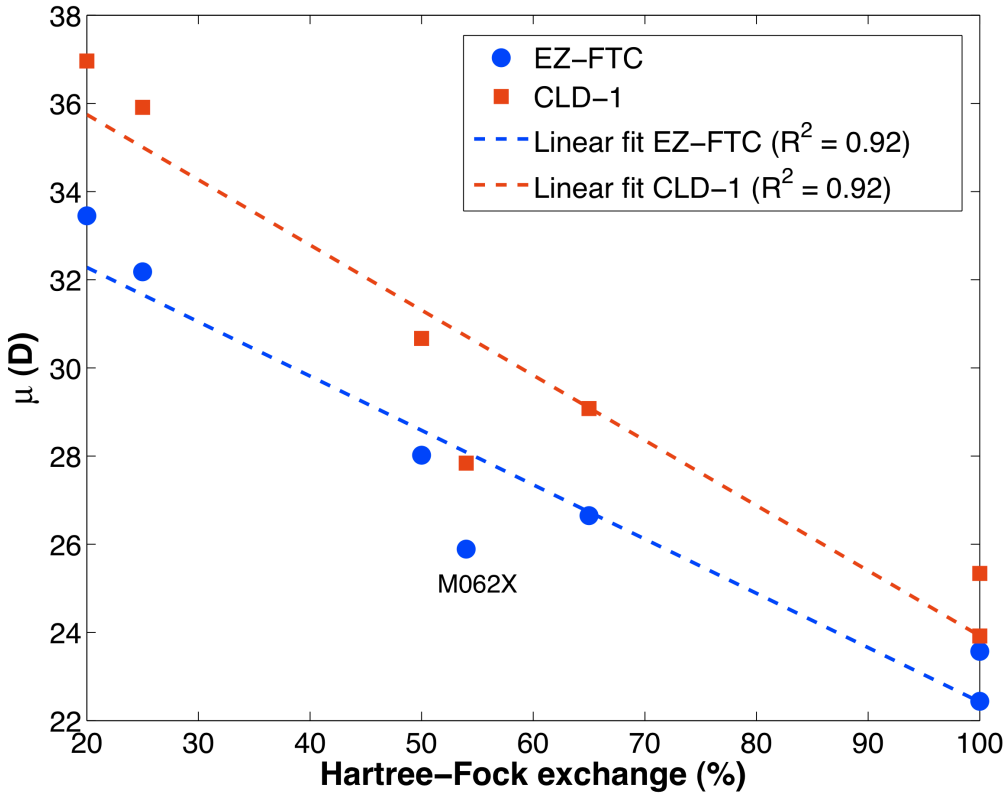


**Figure 5.4.** Dipole moment of EZ-FTC and CLD-1 in chloroform as a function of long-range Hartree-Fock exchange in hybrid DFT methods

As with the electronic excitations, the dipole moment is strongly and linearly correlated with the amount of Hartree-Fock exchange in the functional, decreasing by over a third between B3LYP and ωB97X. This is consistent with calculations[57] by Champagne *et al*. on smaller chromophores; they had also found that DFT methods (particularly those containing little or no HF exchange) produced much smaller dipole moments than high-level MP4 (fourth-order Møller-Plesset theory) calculations. It is also possible that the use of mild hybrids is one of the causes of the discrepancy[58] between experimental and computed dipole moments for high-performance chromophores. Interestingly, the dipole moments calculated with the HF-based and high-HF DFT methods in chloroform are similar to those calculated using B3LYP in the gas phase, possibly giving a

reason for the high efficacy of gas-phase B3LYP dipole moments in calculations of chromophore ordering (See Chapter 4). The M062X functional is a notable outlier, predicting substantially lower dipole moments than the BHandHLYP functional despite a similar quantity of HF exchange; this is likely due to it having been parameterized against high-level QCISD (a method similar[59] to Coupled-Cluster theory) calculations.[40a, 49]

### *5.3.3 Hyperpolarizability*

The relative hyperpolarizability of CLD-1 compared to EZ-FTC was calculated in both the static limit and at two experimentally relevant frequencies; 1906nm and 1310nm, the latter being within one of two common telecom frequency bands.[60] Static results appear in Table 5.5. Experimental results used for comparison were extrapolated to the static limit using the two-level model (Equation 5.4) and the experimental absorption maxima for the dyes.

**Table 5.5.** Static hyperpolarizability ratios (CLD-1/EZ-FTC)

| **Method** | **$\beta_{HRS}(0)$ ratio** | **$\beta_{zzz}(0)$ ratio** |
|---|---|---|
| B3LYP | 0.91 | 0.74 |
| PBE0 | 1.02 | 0.85 |
| BHandHLYP | 1.23 | 1.06 |
| M062X | 1.33 | 1.23 |
| CAM-B3LYP | 1.32 | 1.18 |
| LC-BLYP | 1.30 | 1.22 |
| ωB97X | 1.41 | 1.33 |
| HF | 1.22 | 1.07 |
| PM6 | 1.05 | 0.74 |
| MP2//B3LYP | 1.51 | 1.47 |
| MP2//M062X | 1.40 | 1.39 |
| ***Experiment (TLM)*** | ***1.71 ± 0.076*** | |

Rotationally-averaged hyperpolarizabilities, comparable with HRS experiments, are shown in Figure 5.5 at both the static limit and the wavelength

of the reference HRS measurement; the dotted red bands indicate the range of experimental uncertainty in the ratio.

**5.5a** ($\beta_{HRS}(0)$)

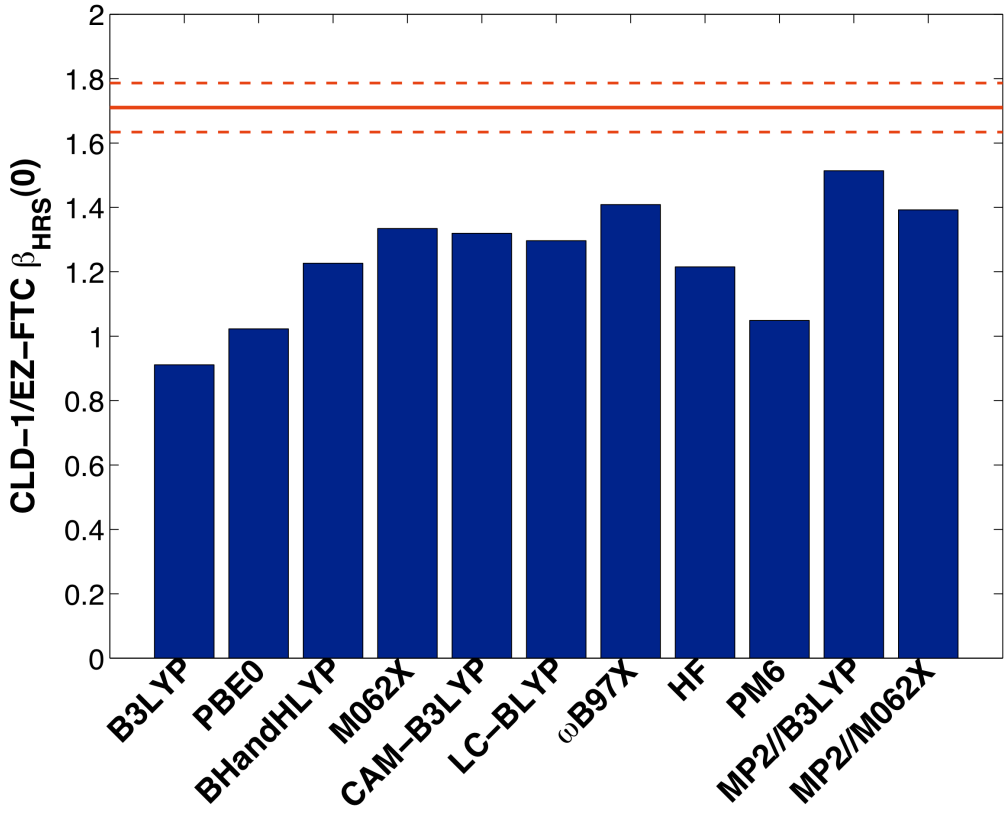

**5.5b** ($\beta_{HRS}(-2\omega,\omega,\omega)$ (1906 nm))

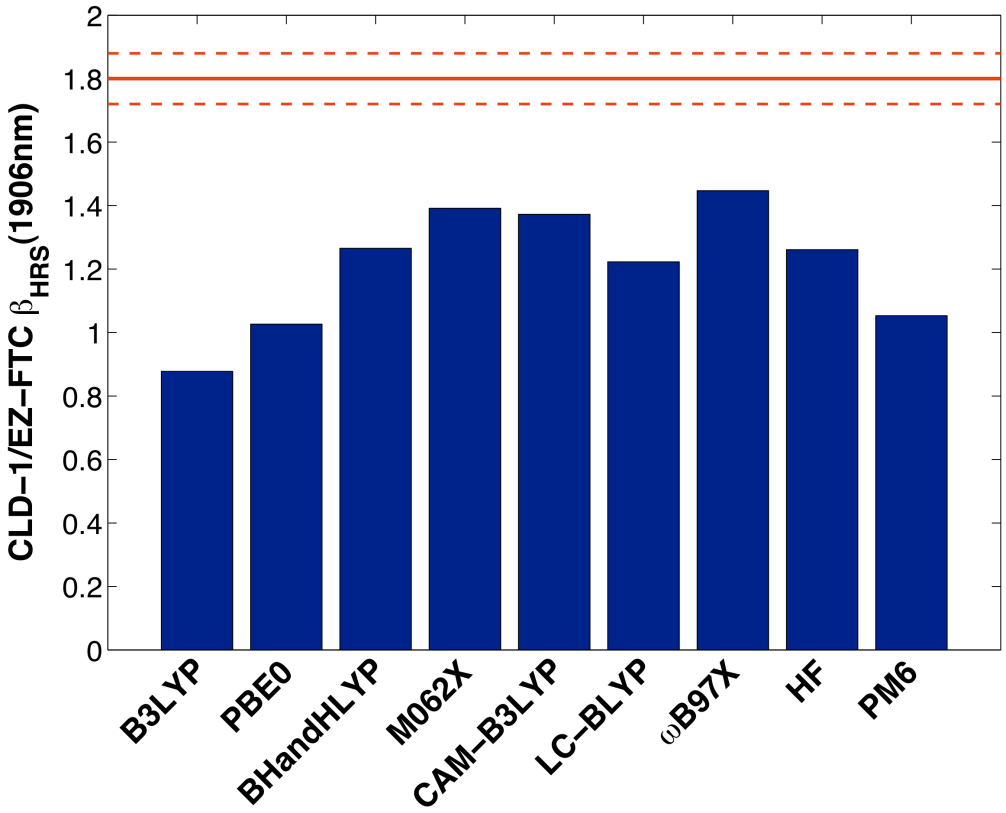


**Figure 5.5.** Comparsion of $\beta_{HRS}$ (CLD-1) / $\beta_{HRS}$ (EZ-FTC) in the static limit (5a) and at 1906 nm (5b) in chloroform versus the experimental ratio (red lines; dashed lines are ± standard error). The static limit for the experimental data was estimated using the two-level model (Equation 5-4).

Here, the two mild hybrids indicate little difference in hyperpolarizability between the two chromophores, with B3LYP predicting higher performance for EZ-FTC than CLD-1 and performing worse than even the semi-empirical PM6 method. Hartree-Fock does only moderately better. All of these results are consistent with prior results using the same methods *in vacuo*.[1c] The range-separated functionals perform well, especially ωB97X, which has recently been successfully used to model several charge transfer systems.[37, 47] M062X also performs well, consistent with prior work[14] by Liao and Masunov using the earlier M052X functional.[40a] The MP2 method using the B3LYP geometry was

closest to experiment, and consistent with MP2's relative accuracy compared to higher-order wavefunction-based methods[23, 44, 61] such as MP4. While little literature has yet appeared on the calculation of hyperpolarizabilty using range-separated functionals, CAM-B3LYP was found to perform well for predicting hyperpolarizabilities of polyacetylenes,[62] as well as of exotic annulenes.[63] In the latter case, the M052X and BHandHLYP functionals also performed well. Range-separated functionals were also found to closely track MP2 calculations for polymethineimine[45] and for substituted (E)-benzaldehyde phenylhydrazones.[64] In the latter case, BHandHLYP als performed well.

While the absolute values of the hyperpolarizabilities of EZ-FTC and CLD-1 at 1906nm varied significantly from the static limit, the ratios calculated at 1906nm were nearly identical to those observed in the static limit. This is likely a consequence of the similarity in absorbance maxima of the two chromophores and the strong correlation between their predicted absorbance maxima (see Figure 5-3), and indicates that dispersion plays a small role in the relative hyperpolarizabilities of these chromophores at long wavelengths.

The relationship between $\beta_{HRS}$ and the amount of Hartree-Fock exchange used in the DFT functionals was also analyzed in a similar manner to that used for the dipole moment and excitation energies. Calculated absolute static hyperpolarizabilities for each chromophore are shown in Figure 5.6.

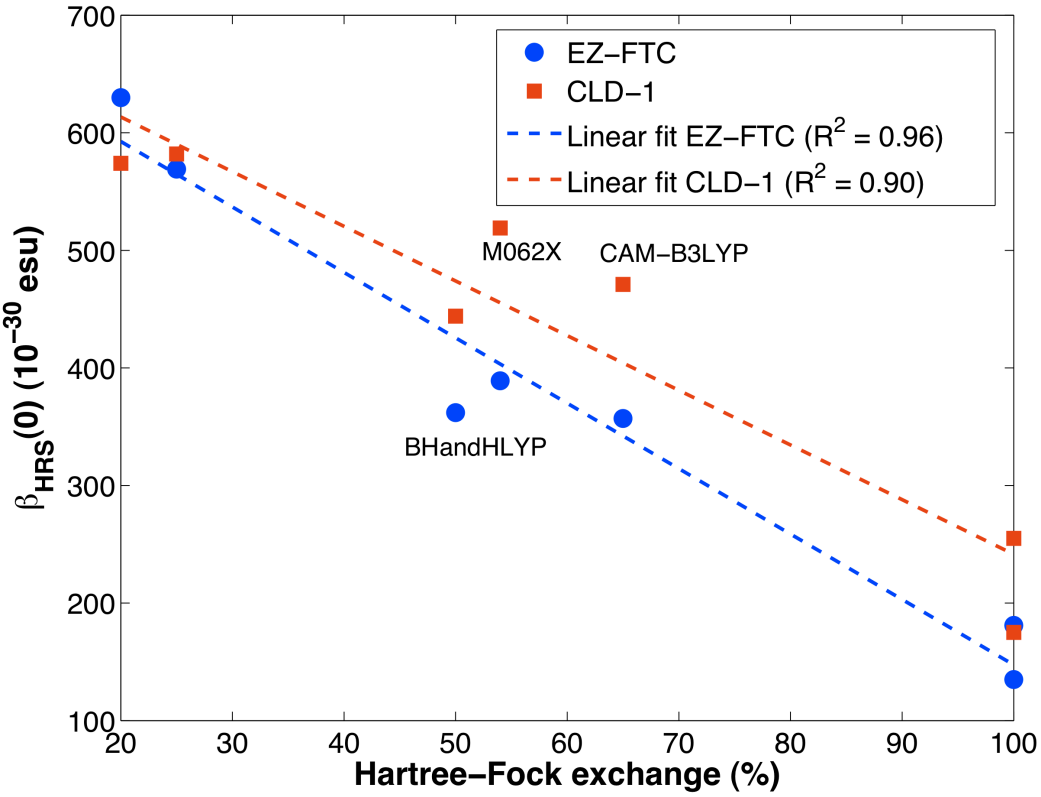


**Figure 5.6.** $\beta_{HRS}(0)$ of EZ-FTC and CLD-1 in chloroform as a function of long-range Hartree-Fock exchange in hybrid DFT methods

Once again, a strong linear trend is observed, albeit with a discontinuity between BHandHLYP and M062X, with CAM-B3LYP results being similar to those calculated using M062X. This is again likely due to the heavy parameterization of the M062X functional, and may indicate some effects from the smaller amount of short-range HF exchange used in CAM-B3LYP.

Results for the component of β along the dipole moment of the chromophores was compared in a similar manner to the rotationally-averaged hyperpolarizability. Results appear in Figure 5.7.

**5.7a** ($\beta_{zzz}(0)$)

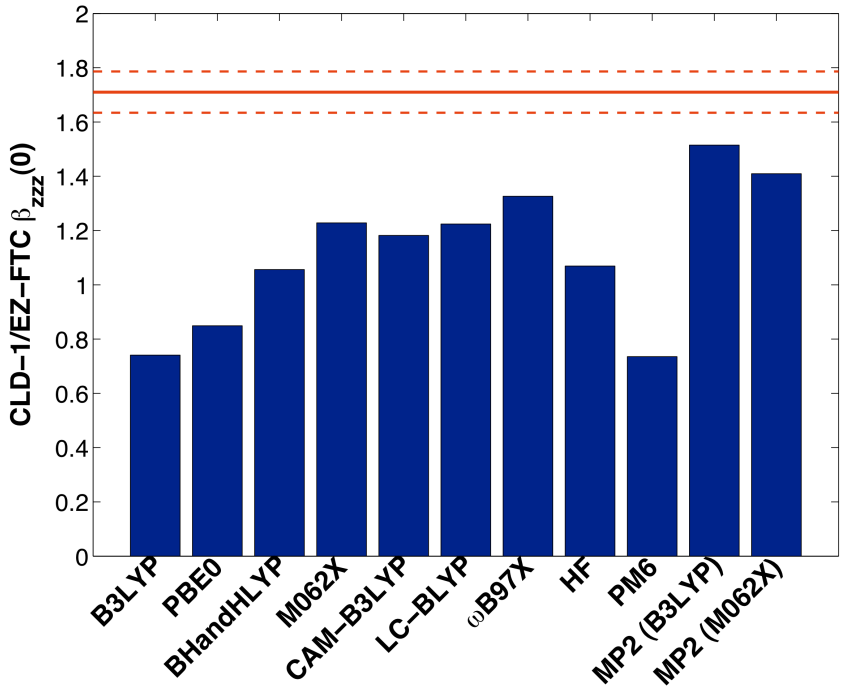


**5.7b** ($\beta_{zzz}(-\omega,0,\omega)$ (1310nm))

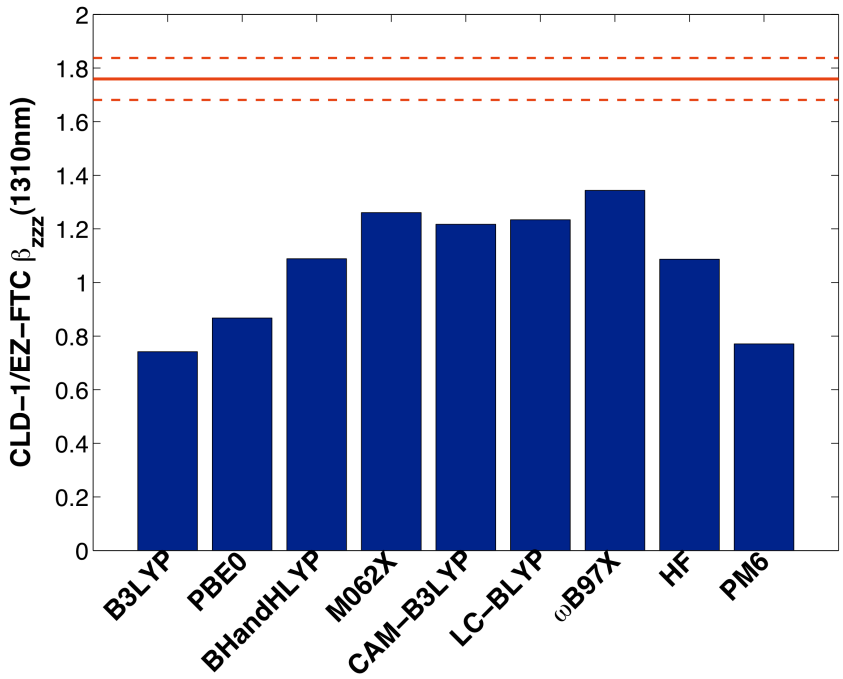


**Figure 5.7.** Comparison of $\beta_{zzz}$ (CLD-1) / $\beta_{zzz}$ (EZ-FTC) in the static limit (5a) and at 1906 nm (5b) in chloroform versus the experimental ratio (red lines; dashed lines are ± standard error). The static limit for the experimental data was estimated using the two-level model (Equation 5-4).

Trends were very similar to those for $\beta_{HRS}$, except that the PM6 and PBE0 predicted qualitatively inaccurate hyperpolarizability ratios (EZ-FTC > CLD-1). The difference from the $\beta_{HRS}$ calculations here is due to a large difference in the second-largest tensor component ($\beta_{yzz}$); that component is 4.24 times as large in CLD-1 compared to EZ-FTC in the calculations using the PBE0 functional, but only 1.92 times as large in those using the ωB97X functional. The relative contribution of different hyperpolarizability tensor components has previously been observed to substantial undergo calculation method-dependent shifts, with cancellation of error between components potentially explaining the relatively good performance of mild hybrids for small dyes such as p-nitroaniline.[15a] To further examine the contribution from minor tensor components, estimated $\beta_{zzz}$ values were calculated from the $\beta_{HRS}$ from each functional using Equation 5-3, and compared with the $\beta_{zzz}$ value directly from the (rotated) hyperpolarizability tensor as a function of Hartree-Fock exchange. Results appear in Figure 5.8.

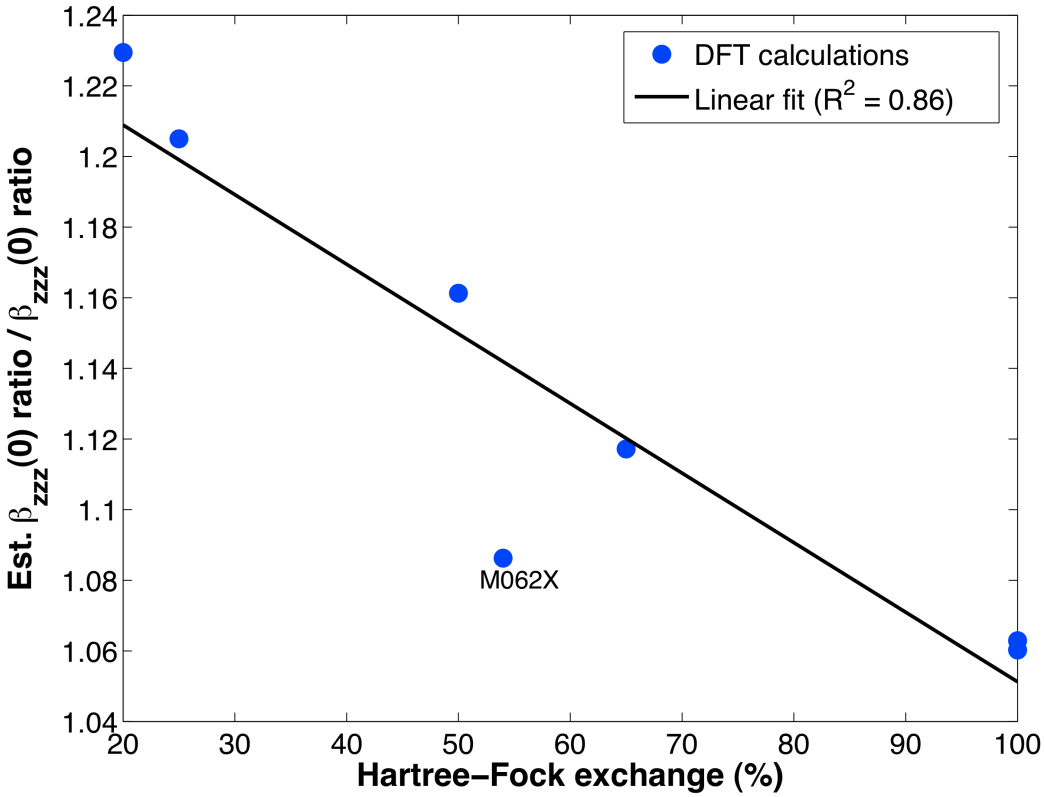


**Figure 5.8.** Comparison of $\beta_{zzz}$ versus the estimate of $\beta_{zzz}$ obtained from $\beta_{HRS}$ using Equation 5-3, assuming the zzz component is the only nonzero element of the β tensor

Once again, a strong linear trend is observed, with the minor tensor components making larger contributions to the hyperpolarizability for mild hybrids than for the higher-HF functionals. This would indicate that increased delocalization tends to encourage charge-transfer along the dipole (π-conjugated) axis of the molecule relative to the (much shorter) minor axes. M062X is once again an outlier, predicting minor tensor components of much smaller relative magnitude than BHandHLYP. Once again, this is likely a consequence of M062X having been parameterized to reproduce QCISD calculations. Given the relative accuracy of the high-HF range separated functionals for the CLD-1/EZ-FTC ratio, this data also indicates that Equation 5-3 is likely a reasonable

approximation to use with TCF-based chromophores with structures similar to CLD-1 and EZ-FTC.

### *5.3.4. Overall accuracy*

While the accuracy of the functionals varied depending on the property calculated, overall accuracy was assessed using two metrics. First, the relative difference in the dipole moment and static hyperpolarizability were compared with the MP2//B3LYP method, which was found (See Figure 5.5) to most closely reproduce the experimental hyperpolarizability ratio. Results are shown in Figure 5-9.

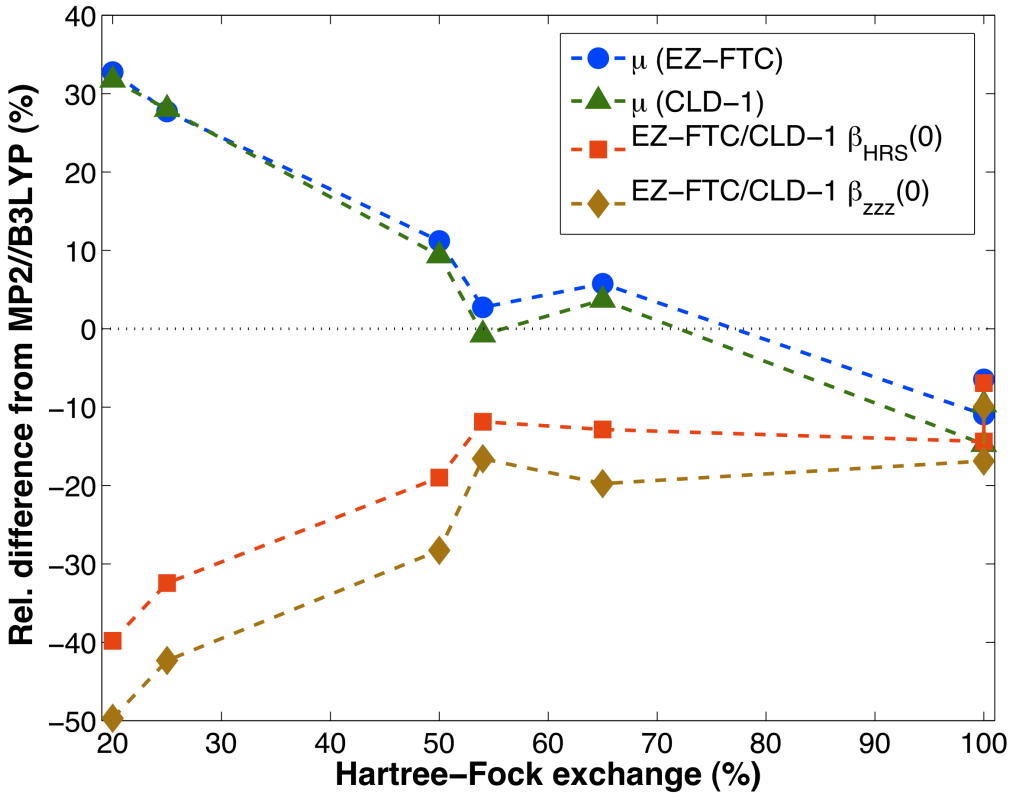


**Figure 5.9.** Comparison of DFT and MP2 methods. Relative difference between dipole moments and between $\beta_{HRS}(0)$ values obtained from hybrid DFT methods and those obtained using the MP2//B3LYP method, as a function of long-range Hartree-Fock exchange in the DFT functional.

DFT results converged to near the MP2 value as Hartree-Fock exchange was increased, most likely due MP2 being calculated as a perturbation off a Hartree-Fock wavefunction,[43] and therefore incorporating the exact HF exchange. These results indicate that the exchange energy is likely the main factor in differences between functionals. However, the similarity of the M062X results with the MP2 results indicates that exchange is likely not the only factor, as previously observed[44] by Champagne *et al*. The parameterzation of the M062X exchange-correlation functional may also provide significant improvements in calculation of the electron correlation component as well.

Secondly, the relative errors in the static hyperpolarizability ratio and in the excitation energy of CLD-1 were compared in a two-dimensional error space to further analyze trends based on general type of functional and determine the feasibility of using a single method to minimize total error. Results are shown in Figure 5.10.

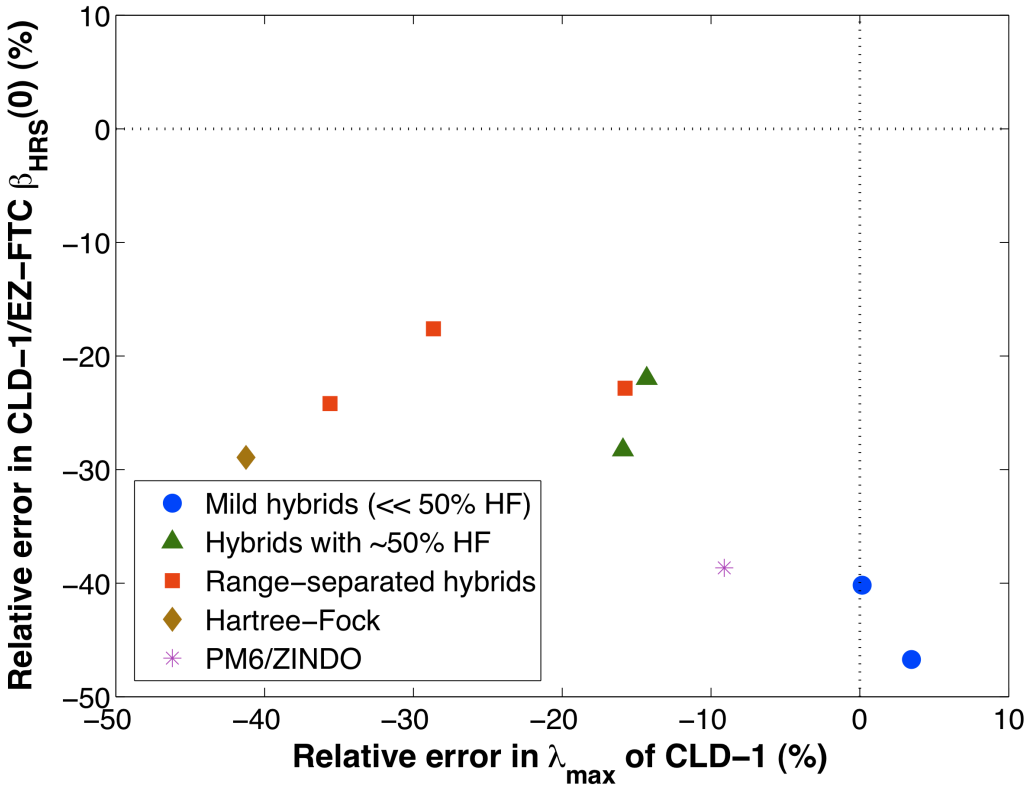


**Figure 5.10.** Two-dimensional error plot showing errors in $\beta_{HRS}(0)$ (CLD-1) / $\beta_{HRS}(0)$ (EZ-FTC) versus errors in the lowest charge-transfer excitation energy of CLD-1. DFT methods are divided into three families (mild hybrids, hybrids with ~50% HF exchange, and range-separated hybrids; HF and PM6/ZINDO are shown for comparison.

Errors in the absolute excitation energy and relative hyperpolarizability trended in opposite directions as the amount of Hartree-Fock exchange was varied; mild-hybrids predicted excitation energies well at the expense of predicting relative hyperpolarizabilities, and the high-HF hybrids predicted the hyperpolarizability ratio well at the expense of quantitative excitation energies. Hartree-Fock itself did not perform well for either metric, and PM6 severely underestimated the hyperpolarizability ratio. Results were quantified using the length of the two-dimensional error vector as a figure of merit

$$FOM = \sqrt{\left(\frac{\beta_{HRS}(comp) - \beta_{HRS}(exp)}{\beta_{HRS}(exp)}\right)^2 + \left(\frac{\lambda_{max}(comp) - \lambda_{max}(exp)}{\lambda_{max}(exp)}\right)^2} \qquad (5\text{-}11)$$

to provide an estimate of the total deviation from experiment. Results using this figure of merit, along with rankings of performance for excitations and hyperpolarizability alone are shown in Table 5.6.

**Table 5.6.** Accuracy ranking of DFT, HF, and MP2 methods

| Method | $\lambda_{max}$ rank | $\beta_{HRS}(0)$ rank | FOM | FOM rank |
|---|---|---|---|---|
| B3LYP | 2 | 11 | 0.468 | 8 |
| PBE0 | **1** | 10 | 0.402 | 6 |
| BHandHLYP | 6 | 7 | 0.324 | 3 |
| M062X | 4 | 4 | **0.262** | **1** |
| CAM-B3LYP | 5 | 5 | 0.278 | 2 |
| LC-BLYP | 8 | 6 | 0.430 | 7 |
| ωB97X | 7 | 2 | 0.336 | 4 |
| HF | 9 | 8 | 0.504 | 9 |
| PM6/ZINDO | 3 | 9 | 0.397 | 5 |
| MP2//B3LYP | N/A | **1** | N/A | N/A |
| MP2//M062X | N/A | 3 | N/A | N/A |

Despite not being the best performer for either property alone, the M062X functional minimizes the combined error, with the CAM-B3LYP functional being a close second. While the MP2 methods performed very well for hyperpolarizability, they did not receive an overall rank due to the lack of an excitation calculation, but should still be considered for calculating ground-state properties. The Hartree-Fock method was the worst overall performer, likely due to its complete neglect of electron correlation,[43] followed by the B3LYP functional, despite its high rank for calculating excitation energies alone. The BHandHLYP and ωB97X methods were reasonable performers, but not particularly distinguished compared to the CAM-B3LYP and M062X functionals.

Based on these aggregate results, the M062X and CAM-B3LYP functionals are recommended for routine calculations on TCF-based chromophores, assuming that relative properties are of interest, given their tendency to blueshift absolute excitation energies. Neither the Hartree-Fock nor B3LYP method are recommended due to large overall error in the former case, and qualitatively inaccurate prediction of the relative hyperpolarizability of CLD-1 and EZ-FTC in the latter case. Due to its superior performance in calculating electronic excitations in CLD-1 and EZ-FTC, the PBE0 functional is recommended for electronic spectra calculations on TCF-based chromophores with the caveat that it may not provide adequate information on hyperpolarizabilties.

## 5.4. Conclusion

Based on both static and frequency-dependent calculations on the high-performance chromophores CLD-1 and EZ-FTC, mild hybrid functionals (< 50% Hartree-Fock exchange) are inadequate for reliably predicting trends in the relative hyperpolarizabilities of chromophores with long bridges and strong acceptors (such as TCF variants), despite their reasonable performance for smaller molecules[1c, 65], including shorter TCF-based chromophores.[17] However, despite its lower performance for hyperpolarizabilities, the mild-hybrid PBE0 functional performs well for electronic excitation energies. Functionals with more than 50% Hartree-Fock exchange, as well as those incorporating distance-dependent Hartree-Fock exchange, perform better for hyperpolarizabilities at the expense of severely blueshifted excitation energies. The trade-off between these properties complicates the calculation of the dispersion of absolute hyperpolarizabilities. However, given that the relative excitation energies

between CLD-1 and EZ-FTC remain nearly constant, such functionals may still be useful in predicting relative trends in excitation energies.

Additionally, all three properties considered (μ, β, and $\lambda_{max}$) were strongly correlated with the amount of Hartree-Fock exchange in the functionals used, making prediction of absolute properties using DFT alone difficult. This issue could be mitigated by using calculated ratios against standard chromophores and obtaining estimates of absolute properties based on high-level calculations or experiments on the standards. The trends in relative values indicate that DFT with more long-range Hartree-Fock exchange typically perform closer to experiment and higher-level MP2 calculations, although Hartree-Fock itself does not perform well.

None of the methods provide an ideal combination of low error in hyperpolarizability and in electronic excitations, although the M062X and CAM-B3LYP functionals come the closest. Possible routes for improvement include tuning a range-separated functional such as CAM-B3LYP specifically for calculations on organic EO chromophores, as Autschbach and co-workers have done for circular dichroism spectra[66], or using a composite method (e.g. using CAM-B3LYP for geometry and hyperpolarizability, but PBE0 for frequency dispersion). Alternately, faster, approximate MP2 methods such as RI-MP2,[67] Density-Fitting MP2,[68] or SOS-MP2[69] could be used to enable more routine use of MP2 calculations.

However, despite imperfect accuracy, functionals such as M062X and CAM-B3LYP provide a reasonably good approximation of the trends in hyperpolarizability and electronic excitations between EZ-FTC and CLD-1 and,

with calibration against experiment, could still rapidly provide semi-quantitative insight on trends in chromophore properties relative to theory-aided design. However, further exploration of this hypothesis would require calibration against a larger set of chromophores than the two explored here, and ideally either highly-accurate HRS data on the reference chromophores and/or very high-level (i.e. Coupled Cluster) calculations for verification.

## 5.5. Acknowledgements for Chapter 5

Thanks to Bruce E. Eichinger, Larry R. Dalton, and Xiaosong Li for many useful discussions, Wenkel Liang and Richard Ketcham for technical support, as well as the National Science Foundation (STC-MDITR DMR-0120967 and DMR-0905686), the Air Force Office of Scientific Research (FA9550-09-1-0589), and the University of Washington Student Technology Fund for financial support.

## 5.6. Supplemental information for Chapter 5

Tables containing calculated $\mu$, $\lambda_{max}$, $\beta_{HRS}$, and $\beta_{zzz}$ values for EZ-FTC and CLD-1 are included in Appendix C.

## 5.7. References for Chapter 5

1. (a) Dalton, L. R.; Sullivan, P. A.; Bale, D. H., Electric Field Poled Organic Electro-optic Materials: State of the Art and Future Prospects. *Chemical Reviews* **2010,** *110* (1), 25-55; (b) Dalton, L. R.; Benight, S. J.; Johnson, L. E.; Knorr, D. B.; Kosilkin, I.; Eichinger, B. E.; Robinson, B. H.; Jen, A. K. Y.; Overney, R. M., Systematic Nanoengineering of Soft Matter Organic Electro-optic Materials. *Chemistry of Materials* **2011,** *23* (3), 430-445; (c) Isborn, C. M.; Leclercq, A.; Vila, F. D.; Dalton, L. R.; Brédas, J. L.; Eichinger, B. E.; Robinson, B. H., Comparison of Static First Hyperpolarizabilities Calculated with Various Quantum Mechanical Methods. *Journal of Physical Chemistry A* **2007,** *111* (7), 1319-1327.
2. Sullivan, P. A.; Dalton, L. R., Theory-Inspired Development of Organic Electro-optic Materials. *Accounts of Chemical Research* **2009,** *43* (1), 10-18.

3. Sullivan, P. A.; Rommel, H. L.; Takimoto, Y.; Hammond, S. R.; Bale, D. H.; Olbricht, B. C.; Liao, Y.; Rehr, J.; Eichinger, B. E.; Jen, A. K.-Y.; Reid, P. J.; Dalton, L. R.; Robinson, B. H., Modeling the Optical Behavior of Complex Organic Media: From Molecules to Materials. *Journal of Physical Chemistry B* **2009,** *113* (47), 15581-15588.
4. Firestone, K. A.; Lao, D. B.; Casmier, D. M.; Clot, O.; Dalton, L. R.; Reid, P. J., Frequency-agile hyper-Rayleigh scattering studies of electro-optic chromophores. *Proceedings of SPIE* **2005,** *5395*, 59350P.
5. (a) Clays, K.; Persoons, A., Hyper-Rayleigh scattering in solution. *Review of Scientific Instruments* **1992,** *63* (6), 3285; (b) Bale, D. H.; Eichinger, B. E.; Liang, W.; Li, X.; Dalton, L. R.; Robinson, B. H.; Reid, P. J., Dielectric dependence of the first molecular hyperpolarizability for electro-optic chromophores. *J Phys Chem B* **2011,** *115* (13), 3505-13.
6. (a) Cyvin, S. J.; Rauch, J. E.; Decius, J. C., Theory of Hyper-Raman Effects (Nonlinear Inelastic Light Scattering): Selection Rules and Depolarization Ratios for the Second-Order Polarizability. *The Journal of Chemical Physics* **1965,** *43* (11), 4083; (b) Takimoto, Y. A real-time time-dependent density functional theory method for calculating linear and nonlinear dynamic optical response. University of Washington, Seattle, WA, 2008.
7. Williams, D. J., Organic Polymeric and Non-Polymeric Materials with Large Optical Nonlinearities. *Agnewandte Chemie International Edition English* **1984,** *23*, 690-703.
8. Oudar, J. L.; Chemla, D. S., Hyperpolarizabilities of the nitroanilines and their relations to the excited state dipole moment. *The Journal of Chemical Physics* **1977,** *66* (6), 2664-2668.
9. Campo, J.; Painelli, A.; Terenziani, F.; Regemorter, T. V.; Beljonne, D.; Goovaerts, E.; Wenseleers, W., First Hyperpolarizability Dispersion of the Octupolar Molecule Crystal Violet: Multiple Resonances and Vibrational and Solvation Effects. *J Am Chem Soc* **2010,** *132* (46), 16467-16478.
10. (a) Rice, J. E.; Handy, N. C., The calculation of frequency-dependent polarizabilities as pseudo-energy derivatives. *Journal of Chemical Physics* **1991,** *94* (7), 4959-4971; (b) Gerratt, J.; Mills, I. M., Force Constants and Dipole-Moment Derivatives of Molecules from Perturbed Hartree-Fock Calculations. I. *The Journal of Chemical Physics* **1968,** *49* (4), 1719-1729.
11. Takimoto, Y.; Isborn, C. M.; Eichinger, B. E.; Rehr, J. J.; Robinson, B. H., Frequency and Solvent Dependence of Nonlinear Optical Properties of Molecules. *Journal of Physical Chemistry C* **2008,** *112* (21), 8016-8021.
12. Meyers, F.; Marder, S. R.; Pierce, B. M.; Brédas, J. L., Electric Field Modulated Nonlinear Optical Properties of Donor- Acceptor Polyenes: Sum-Over-States Investigation of the Relationship between Molecular Polarizabilities (α,β, and γ) and Bond Length Alternation. *J Am Chem Soc* **1994,** *116* (23), 10703-10714.
13. (a) Kobayashi, R.; Koch, H.; Jørgensen, P., Calculation of frequency-dependent polarizabilities using coupled-cluster response theory. *Chemical Physics Letters* **1994,** *219*, 30-35; (b) O'Neill, D. P.; Kallay, M.; Gauss, J., Calculation of frequency-dependent hyperpolarizabilities using general coupled-cluster models. *The Journal of Chemical Physics* **2007,** *127* (13), 134109.

14. Suponitsky, K. Y.; Liao, Y.; Masunov, A. E., Electronic Hyperpolarizabilities for Donor-Acceptor Molecules with Long Conjugated Bridges: Calculations versus Experiment. *Journal of Physical Chemistry A* **2009,** *113* (41), 10994-11001.
15. (a) Hammond, J. R.; Kowalski, K., Parallel computation of coupled-cluster hyperpolarizabilities. *The Journal of Chemical Physics* **2009,** *130* (19), 194108; (b) Davidson, E. R.; Eichinger, B. E.; Robinson, B. H., Hyperpolarizability: Calibration of theoretical methods for chloroform, water, acetonitrile, and p-nitroaniline. *Optical Materials* **2006,** *29* (4), 360-364.
16. Suponitsky, K. Y.; Tafur, S.; Masunov, A. E., Applicability of hybrid density functional theory methods to calculation of molecular hyperpolarizability. *The Journal of Chemical Physics* **2008,** *129* (4), 044109.
17. Liao, Y.; Eichinger, B. E.; Firestone, K. A.; Haller, M.; Luo, J.; Kaminsky, W.; Benedict, J. B.; Reid, P. J.; Jen, A. K.-Y.; Dalton, L. R.; Robinson, B. H., Systematic Study of the Structure-Property Relationship of a Series of Ferrocenyl Nonlinear Optical Chromophores. *J Am Chem Soc* **2005,** *127* (8), 2758-2766.
18. (a) Isborn, C. M.; Davidson, E. R.; Robinson, B. H., Ab Initio Diradical/Zwitterionic Polarizabilities and Hyperpolarizabilities in Twisted Double Bonds. *Journal of Physical Chemistry A* **2006,** *110* (22), 7189-7196; (b) Panja, N.; Ghanty, T. K.; Nandi, P. K., A sum-over-state scheme of analysis of hyperpolarizabilities and its application to spiroconjugated molecular system. *Theoretical Chemistry Accounts* **2009,** *126* (5-6), 323-337.
19. Reis, H., Problems in the comparison of theoretical and experimental hyperpolarizabilities revisited. *The Journal of Chemical Physics* **2006,** *125* (1), 014506.
20. (a) Hohenberg, P., Inhomogeneous Electron Gas. *Physical Review* **1964,** *136* (3B), B864-B871; (b) Kohn, W.; Sham, L. J., Self-Consistent Equations Including Exchange and Correlation Effects. *Physical Review* **1965,** *140* (4A), A1133-A1138.
21. Pople, J. A.; Beveridge, D. L.; Dobosh, P. A., Approximate Self-Consistent Molecular-Orbital Theory. V. Intermediate Neglect of Differential Overlap. *Journal of Chemical Physics* **1967,** *47* (6), 2026-2033.
22. Møller, C.; Plesset, M. S., Note on an Approximation Treatment for Many-Electron Systems. *Physical Review* **1934,** *46* (7), 618-622.
23. Jacquemin, D.; Champagne, B.; Hättig, C., Correlated frequency-dependent electronic first hyperpolarizability of small push–pull conjugated chains. *Chemical Physics Letters* **2000,** *319*, 327-334.
24. (a) Stephens, P. J.; Devlin, F. J.; Chabalowski, C. F.; Frisch, M. J., Ab Initio Calculation of Vibrational Absorption and Circular Dichroism Spectra Using Density Functional Force Fields. *Journal of Physical Chemistry* **1994,** *98* (45), 11623-11627; (b) Becke, A. D., A new mixing of Hartree-Fock and local density-functional theories. *Journal of Chemical Physics* **1993,** *98* (2), 1372-1377.
25. Shi, Y., Low (Sub-1-Volt) Halfwave Voltage Polymeric Electro-optic Modulators Achieved by Controlling Chromophore Shape. *Science* **2000,** *288* (5463), 119-122.
26. Frisch, M. J.; Trucks, G. W.; Schlegel, H. B.; Scuseria, G. E.; Robb, M. A.; Cheeseman, J. R.; G. Scalmani, V. B.; Mennucci, B.; Petersson, G. A.; Nakatsuji, H.; Caricato, M.; Li, X.; Hratchian, H. P.; Izmaylov, A. F.; Bloino, J.; Zheng, G.; Sonnenberg, J. L.; Hada, M.; Ehara, M.; Toyota, K.; Fukuda, R.; Hasegawa, J.; Ishida, M.; Nakajima, T.; Honda, Y.; Kitao, O.; Nakai, H.; Vreven, T.; J. A.

Montgomery, J.; Peralta, J. E.; Ogliaro, F.; Bearpark, M.; Heyd, J. J.; Brothers, E.; Kudin, K. N.; Staroverov, V. N.; Kobayashi, R.; Normand, J.; Raghavachari, K.; Rendell, A.; Burant, J. C.; Iyengar, S. S.; Tomasi, J.; Cossi, M.; Rega, N.; Millam, J. M.; Klene, M.; Knox, J. E.; Cross, J. B.; Bakken, V.; Adamo, C.; Jaramillo, J.; Gomperts, R.; Stratmann, R. E.; Yazyev, O.; Austin, A. J.; Cammi, R.; Pomelli, C.; Ochterski, J. W.; Martin, R. L.; Morokuma, K.; Zakrzewski, V. G.; Voth, G. A.; Salvador, P.; Dannenberg, J. J.; Dapprich, S.; Daniels, A. D.; Farkas, Ö.; Foresman, J. B.; Ortiz, J. V.; Cioslowski, J.; Fox, D. J. *Gaussian 09*, Revision C.01; Gaussian, Inc.: Wallingford, CT, 2009.
27. *Spartan '08*, 1.2.0; Wavefunction, Inc.: Irvine, CA, 2008.
28. Andzelm, J.; Rinderspacher, B. C.; Rawlett, A.; Dougherty, J.; Baer, R.; Govind, N., Performance of DFT Methods in the Calculation of Optical Spectra of TCF-Chromophores. *Journal of Chemical Theory and Computation* **2009,** *5* (10), 2835-2846.
29. Adamo, C.; Barone, V., Toward reliable density functional methods without adjustable parameters: The PBE0 model. *The Journal of Chemical Physics* **1999,** *110* (13), 6158.
30. Jacquemin, D.; Perpéte, E. A.; Scuseria, G. E.; Ciofini, I.; Adamo, C., TD-DFT Performance for the Visible Absorption Spectra of Organic Dyes: Conventional versus Long-Range Hybrids. *Journal of Chemical Theory and Computation* **2008,** *4* (1), 123-135.
31. (a) Becke, A. D., Density-functional thermochemistry. III. The role of exact exchange. *The Journal of Chemical Physics* **1993,** *98* (7), 5648; (b) Perdew, J. P.; Ernzerhof, M.; Burke, K., Rationale for mixing exact exchange with density functional approximations. *Journal of Chemical Physics* **1996,** *105* (22), 9982-9985.
32. (a) Dreuw, A.; Head-Gordon, M., Failure of Time-Dependent Density Functional Theory for Long-Range Charge-Transfer Excited States: The Zincbacteriochlorin-Bacteriochlorin and Bacteriochlorophyll-Spheroidene Complexes. *J Am Chem Soc* **2004,** *126* (12), 4007-4016; (b) Dreuw, A.; Head-Gordon, M., Single-Reference ab Initio Methods for the Calculation of Excited States of Large Molecules. *Chemical Reviews* **2005,** *105* (11), 4009-4037.
33. (a) Sim, F.; Chin, S.; Dupuis, M., Electron Correlation Effects in Hyperpolarizabilities of p-Nitroaniline. *Journal of Physical Chemistry* **1993,** *97* (6), 1158-1163; (b) Jacquemin, D.; Champagne, B.; Andre, J.-M., Møller–Plesset evaluation of the static first hyperpolarizability of polymethineimine. *Chemical Physics Letters* **1998,** *284* (24-30).
34. Stewart, J. J. P., Optimization of parameters for semiempirical methods I. Method. *Journal of Computational Chemistry* **1989,** *10* (2), 209-220.
35. Stewart, J. J., Optimization of parameters for semiempirical methods V: modification of NDDO approximations and application to 70 elements. *J Mol Model* **2007,** *13* (12), 1173-213.
36. (a) Magyar, R. J.; Tretiak, S., Dependence of Spurious Charge-Transfer Excited States on Orbital Exchange in TDDFT: Large Molecules and Clusters. *Journal of Chemical Theory and Computation* **2007,** *3* (3), 976-987; (b) Lange, A.; Herbert, J. M., Simple Methods To Reduce Charge-Transfer Contamination in Time-Dependent Density-Functional Calculations of Clusters and Liquids. *Journal of Chemical Theory and Computation* **2007,** *3* (5), 1680-1690.
37. Sini, G.; Sears, J. S.; Brédas, J.-L., Evaluating the Performance of DFT Functionals in Assessing the Interaction Energy and Ground-State Charge

Transfer of Donor/Acceptor Complexes: Tetrathiafulvalene−Tetracyanoquinodimethane (TTF−TCNQ) as a Model Case. *Journal of Chemical Theory and Computation* **2011,** *7* (3), 602-609.
38. (a) Tao, J.; Perdew, J.; Staroverov, V.; Scuseria, G., Climbing the Density Functional Ladder: Nonempirical Meta–Generalized Gradient Approximation Designed for Molecules and Solids. *Physical Review Letters* **2003,** *91* (14); (b) Tao, J.; Perdew, J., Nonempirical Construction of Current-Density Functionals from Conventional Density-Functional Approximations. *Physical Review Letters* **2005,** *95* (19).
39. Schwabe, T.; Grimme, S., Towards chemical accuracy for the thermodynamics of large molecules: new hybrid density functionals including non-local correlation effects. *Phys Chem Chem Phys* **2006,** *8* (38), 4398-401.
40. (a) Zhao, Y.; Schultz, N. E.; Truhlar, D. G., Design of Density Functionals by Combining the Method of Constraint Satisfaction with Parametrization for Thermochemistry, Thermochemical Kinetics, and Noncovalent Interactions. *Journal of Chemical Theory and Computation* **2006,** *2* (2), 364-382; (b) Zhao, Y.; Truhlar, D. G., Density Functionals with Broad Applicability in Chemistry. *Accounts of Chemical Research* **2007,** *41* (2), 157-167.
41. Tawada, Y.; Tsuneda, T.; Yanagisawa, S.; Yanai, T.; Hirao, K., A long-range-corrected time-dependent density functional theory. *The Journal of Chemical Physics* **2004,** *120* (18), 8425-33.
42. Leach, A. R., *Molecular Modeling: Principles and Applications*. 2nd ed.; Pearson Education: Harlow (UK), 2001.
43. Szabo, A.; Ostlund, N. S., *Modern Quantum Chemistry: Introduction to Advanced Electronic Structure Theory*. 1st (revised) ed.; Dover Publications, Inc.: New York, NY, 1989.
44. Champagne, B.; Perpéte, E. A.; Gisbergen, S. J. A. v.; Baerends, E.-J.; Snijders, J. G.; Soubra-Ghaoui, C.; Robins, K. A.; Kirtman, B., Assessment of conventional density functional schemes for computing the polarizabilities and hyperpolarizabilities of conjugated oligomers: An ab initio investigation of polyacetylene chains. *Journal of Chemical Physics* **1998,** *109* (23), 10489-10498.
45. Jacquemin, D.; Perpete, E. A.; Medved, M.; Scalmani, G.; Frisch, M. J.; Kobayashi, R.; Adamo, C., First hyperpolarizability of polymethineimine with long-range corrected functionals. *The Journal of Chemical Physics* **2007,** *126* (19), 191108.
46. Yanai, T.; Tew, D. P.; Handy, N. C., A new hybrid exchange–correlation functional using the Coulomb-attenuating method (CAM-B3LYP). *Chemical Physics Letters* **2004,** *393* (1-3), 51-57.
47. Aragó, J.; Sancho-Garcîa, J. C.; Ortî, E.; Beljonne, D., Ab Initio Modeling of Donor–Acceptor Interactions and Charge-Transfer Excitations in Molecular Complexes: The Case of Terthiophene–Tetracyanoquinodimethane. *Journal of Chemical Theory and Computation* **2011,** *7* (7), 2068-2077.
48. Gaussian 09 User's Reference. Gaussian, Inc.: Wallingford, CT, 2011. http://www.gaussian.com/g_tech/g_ur/k_dft.htm (accessed 03/26/2012).
49. Zhao, Y.; Truhlar, D. G., The M06 suite of density functionals for main group thermochemistry, thermochemical kinetics, noncovalent interactions, excited states, and transition elements: two new functionals and systematic testing of four M06-class functionals and 12 other functionals. *Theoretical Chemistry Accounts* **2007,** *120* (1-3), 215-241.

50. Chai, J. D.; Head-Gordon, M., Systematic optimization of long-range corrected hybrid density functionals. *The Journal of Chemical Physics* **2008,** *128* (8), 084106.
51. (a) Zerner, M., An approximate molecular orbital method. *Journal of Chemical Physics* **1975,** *62* (7), 2788-2799; (b) Caricato, M.; Mennucci, B.; Tomasi, J., Solvent Effects on the Electronic Spectra: An Extension of the Polarizable Continuum Model to the ZINDO Method. *Journal of Physical Chemistry A* **2004,** *108* (29), 6248-6256.
52. (a) Firestone, K. A. Frequency-agile hyper-Rayleigh scattering studies of nonlinear optical chromophores. University of Washington, Seattle, 2005; (b) Bale, D. H. Nonlinear optical materials characterization studies employing photostability, hyper-Rayleigh scattering, and electric field induced second harmonic generation techniques. University of Washington, Seattle, WA, 2008.
53. Francl, M. M.; Pietro, W. J.; Hehre, W. J.; Binkley, J. S.; Gordon, M. S.; DeFrees, D. J.; Pople, J. A., Self-consistent molecular orbital methods. XXIII. A polarization-type basis set for second-row elements. *Journal of Chemical Physics* **1982,** *77* (7), 3564-3665.
54. Tomasi, J.; Mennucci, B.; Cammi, R., Quantum Mechanical Continuum Solvation Models. *Chemical Reviews* **2005,** *105* (8), 2999-3093.
55. Head-Gordon, M.; Rico, R. J.; Oumi, M.; Lee, T. J., A doubles correction to electronic excited states from configuration interaction in the space of single substitutions. *Chemical Physics Letters* **1994,** *219*, 21-29.
56. Risko, C.; McGehee, M. D.; Brédas, J.-L., A quantum-chemical perspective into low optical-gap polymers for highly-efficient organic solar cells. *Chemical Science* **2011,** *2* (7), 1200.
57. Champagne, B.; Perpéte, E. A.; Jacquemin, D.; Gisbergen, S. J. A. v.; Baerends, E.-J.; Soubra-Ghaoui, C.; Robins, K. A.; Kirtman, B., Assessment of Conventional Density Functional Schemes for Computing the Dipole Moment and (Hyper)polarizabilities of Push-Pull π-Conjugated Systems. *Journal of Physical Chemistry A* **2000,** *104* (20), 4755-4763.
58. Liang, W.; Li, X.; Dalton, L. R.; Robinson, B. H.; Eichinger, B. E., Solvents level dipole moments. *J Phys Chem B* **2011,** *115* (43), 12566-70.
59. Paldus, J.; Čížek, J.; Jeziorski, B., Coupled cluster approach or quadratic configuration interaction? *The Journal of Chemical Physics* **1989,** *90* (8), 4356.
60. Dalton, L. R.; Steier, W. H.; Robinson, B. H.; Zhang, C.; Ren, A.; Garner, S.; Chen, A.; Londergan, T.; Irwin, L.; Carlson, B.; Fifield, L.; Phelan, G.; Kincaid, C.; Amend, J.; Jen, A., From molecules to opto-chips: organic electro-optic materials. *Journal of Materials Chemistry* **1999,** *9* (9), 1905-1920.
61. Champagne, B.; Bulat, F. A.; Yang, W.; Bonness, S.; Kirtman, B., Density functional theory investigation of the polarizability and second hyperpolarizability of polydiacetylene and polybutatriene chains: treatment of exact exchange and role of correlation. *The Journal of Chemical Physics* **2006,** *125* (19), 194114.
62. Borini, S.; Limacher, P. A.; Luthi, H. P., A systematic analysis of the structure and (hyper)polarizability of donor-acceptor substituted polyacetylenes using a Coulomb-attenuating density functional. *The Journal of Chemical Physics* **2009,** *131* (12), 124105.

63. Torrent-Sucarrat, M.; Anglada, J. M.; Luis, J. M., Evaluation of the Nonlinear Optical Properties for Annulenes with Hückel and Möbius Topologies. *Journal of Chemical Theory and Computation* **2011,** *7* (12), 3935-3943.
64. Lu, S. I., Computational study of static first hyperpolarizability of donor-acceptor substituted (E)-benzaldehyde phenylhydrazone. *Journal of Computational Chemistry* **2011,** *32* (4), 730-6.
65. Millefiori, S.; Alparone, A., Second hyperpolarisability of furan homologues C4H4X (X = O, S, Se, Te): ab initio HF and DFT study. *Chemical Physics Letters* **2000,** *332*, 175-180.
66. Srebro, M.; Autschbach, J., Tuned Range-Separated Time-Dependent Density Functional Theory Applied to Optical Rotation. *Journal of Chemical Theory and Computation* **2012,** *8* (1), 245-256.
67. Weigend, F.; Häser, M.; Patzelt, H.; Ahlrichs, R., RI-MP2: optimized auxiliary basis sets and demonstration of efficiency. *Chemical Physics Letters* **1998,** *1294*, 143-152.
68. Werner, H.-J.; Manby, F. R.; Knowles, P. J., Fast linear scaling second-order Møller-Plesset perturbation theory (MP2) using local and density fitting approximations. *The Journal of Chemical Physics* **2003,** *118* (18), 8149.
69. Jung, Y.; Lochan, R. C.; Dutoi, A. D.; Head-Gordon, M., Scaled opposite-spin second order Moller-Plesset correlation energy: an economical electronic structure method. *The Journal of Chemical Physics* **2004,** *121* (20), 9793-802.

# 6. Design and Synthesis of a Cationic ONLO Chromophore for DNA-Based Biophotonics

## 6.1. Introduction

Organic nonlinear optical (ONLO) dyes are typically blended into a host polymer matrix such as poly(methylmethacrylate) or amorphous polycarbonate for device applications in electro-optics, or alternately, functionalized to form a neat organic glass containing a large fraction of chromophores[1]. However, biopolymers such as DNA can be combined with surfactants such as CTAB or CTMA[2] and ONLO dyes to form an ordered host material with favorable optical properties (low loss, tunable refractive index).[3] Furthermore, bulk DNA has the advantage of being abundant and inexpensive, obtainable from fisheries and agricultural waste[2]. Finally, local ordering of base pairs and specific binding modes (intercalation and minor/major groove binding) present the potential for reduction of lattice dimensionality during poling, potentially increasing achievable acentric order at a given applied field strength.[1a, 4] The electro-optic coefficient is represented in Equation 6-1.

$$r_{33} = \rho_N \beta_{zzz} \left\langle \cos^3 \theta \right\rangle \quad (1)$$

Here, $\rho_N$ is the number density of chromophores, $\beta_{zzz}$ is molecular hyperpolarizability along the dipole moment of the active chromophore, and $\left\langle \cos^3 \theta \right\rangle$ is the acentric order parameter. The angle, θ, is the angle between the chromophore dipole moment and the poling field axis (arbitrarily defined as the z-axis).

An approach toward improved $r_{33}$ and hence, device performance has involved improving the ordered environment of the DNA. Most previous

experiments[5] related to developing DNA-based electro-optic devices, such as the first-ever demonstration of an all-biopolymer EO waveguide modulator developed at Wright-Patterson Air Force Research Laboratories (AFRL).[5a] have used Disperse Red 1 (DR1) as the active ONLO dye. However, despite being well-characterized[6] and commercially abundant, DR1 has several drawbacks that limit device performance. Firstly, its hyperpolarizability is far lower than newer chromophores[4, 6a, 7] using tricyanofuran (TCF) acceptors and longer polyene or thiophene-containing bridges, limiting achievable $r_{33}$. Secondly, while miscible with CTMA-DNA, neither DR1 nor high-performance chromophores such as FTC have been found to directly bind to DNA,[8] but instead are likely "semi-intercalating" into the surfactant layer.[9] However, most dyes known to intercalate into DNA, such as ethidium bromide[10] and methylene blue[11], lack substantial optical nonlinearity (i.e. have negligible hyperpolarizability). Crystal Violet, another common dye known to bind to DNA, does possess a reasonably high hyperpolarizability due to its octupolar structure,[12] although its mode of binding is not well characterized.[13] An optimal dye for DNA-based biophotonics would bind strongly to DNA with a well-characterized binding mode, possess optical nonlinearity in excess of that of DR1, and would be both stable and soluble in buffered aqueous solutions (for binding to Na-DNA) or alcohols[14], for binding to surfactant-coated DNA. A novel dye possessing these properties will be presented in this chapter.

## 6.2. Design and Synthesis

Dyes with high affinity for DNA are typically cationic and contain multiple aromatic rings, while intercalators tend to have aromatic systems with low aspect ratios (nearly rectangular).[13] Most dyes for EO applications, however, are uncharged and highly prolate in order to maximize the length of the π-system, and consequently, hyperpolarizability.[15] Developing an ONLO dye capable of binding to DNA requires compromising between these characteristics. However, cationic ONLO dyes have been used to grow crystals for photonic applications, with the most successful of these dyes thus far being DAST (*trans*-4-[4-(Dimethylamino)styryl]-1-methylpyridinium toluenesulfonate).[16] DAST has a structure analogous to DR1, but with a stilbene bridge instead of an azobenzene bridge, and a pyridinium acceptor instead of a nitro group. Both structures are shown in Scheme 1. However, as DAST is quite prolate, we sought to lower its aspect ratio and increase the size of its aromatic system, increasing its structural similarity to known intercalator[10, 13, 17] ethidium bromide while maintaining its optical nonlinearity. Structures of all three dyes are shown in Figure 6.1.

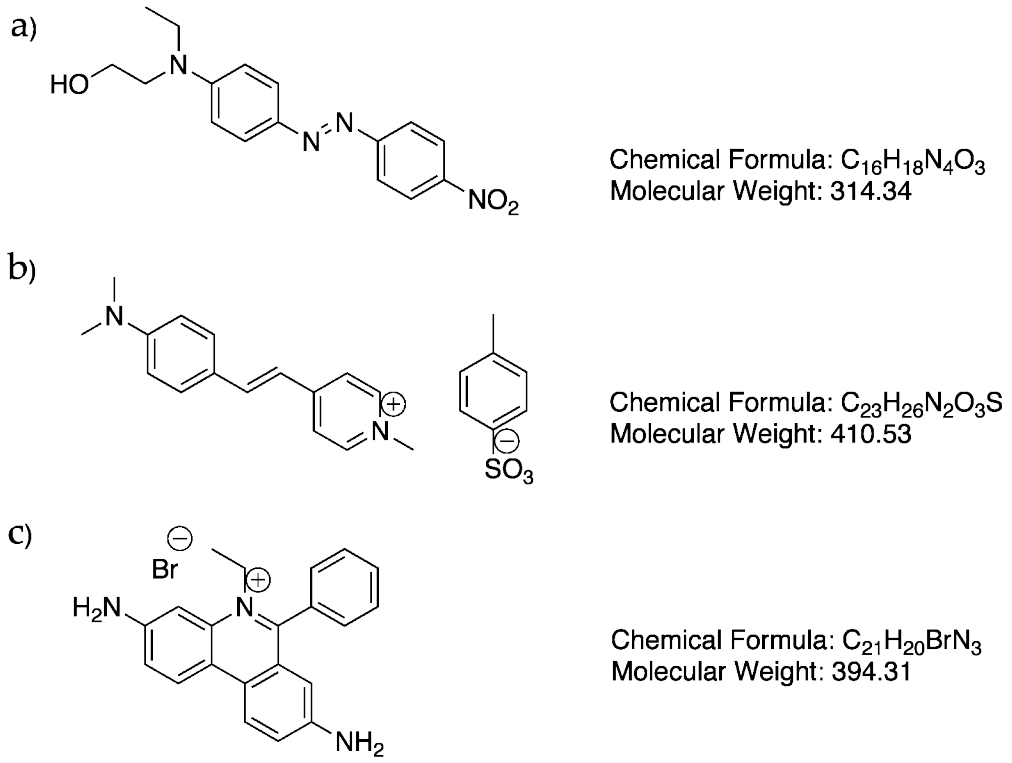


**Figure 6.1.** Comparison of (a) DR1, (b) DAST, and (c) ethidium bromide

Our goal was to design a structure based on the shape of ethidium bromide and DAST that would exhibit nonlinearity and bind to DNA. We examined many novel and known candidate structures by means of DFT calculations, including the structures shown in Figure 6.2, comparing their hyperpolarizabilities and excitation energies to those of DAST. Preliminary calculations were run at the B3LYP/6-31G(d) level *in vacuo* using Gaussian '09,[18] with hyperpolarizabilities calculated by analytic differentiation.[1a, 19]

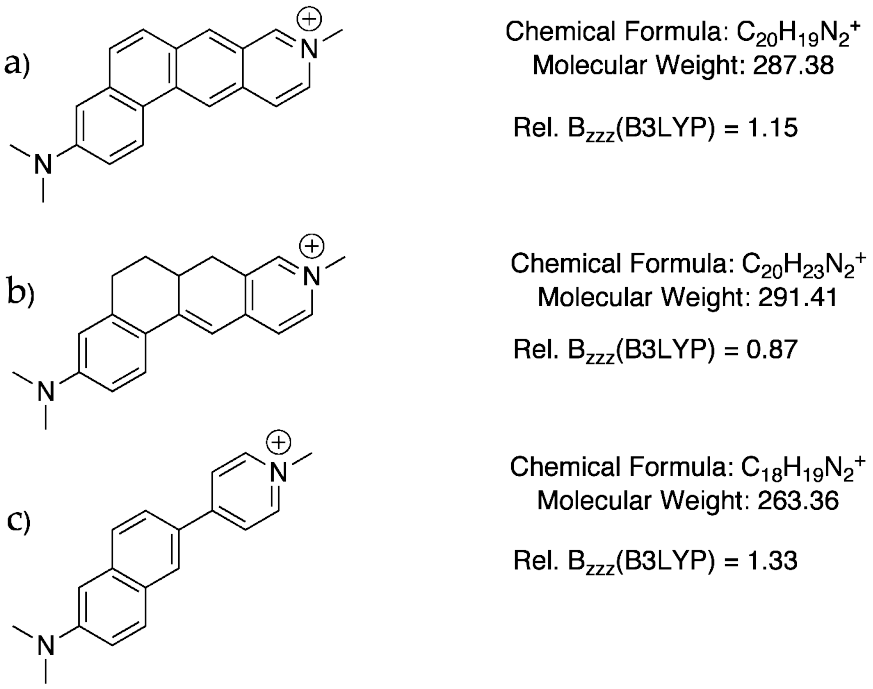


**Figure 6.2.** Candidate DAST analogues

Of the structures shown, structure **c** had the largest hyperpolarizability relative to DAST and could be synthesized from commercially available starting materials in few steps. It resembles the zwitterionic fluorescent dye BNBP,[20] but without a captive anion and with shorter alkyl chains to reduce steric hinderance when approaching DNA.

This dye, internally called LL-1, but likely to be renamed DANPY, is synthesized by means of a Suzuki coupling[21] to form (**1**), followed by methylation[22] of both the pyridine and the aniline moieties to form an iodide salt (**2**). The iodide counter-ion can be replaced with a counter-ion of choice by varying the acid used in the purification of (**3**). Acetic acid was chosen for reasons of solvent compatibility, volatility, and convenience. The synthesis is shown in Scheme 6.1.

**Scheme 6.1.** Synthesis of intercalating dye LL-1

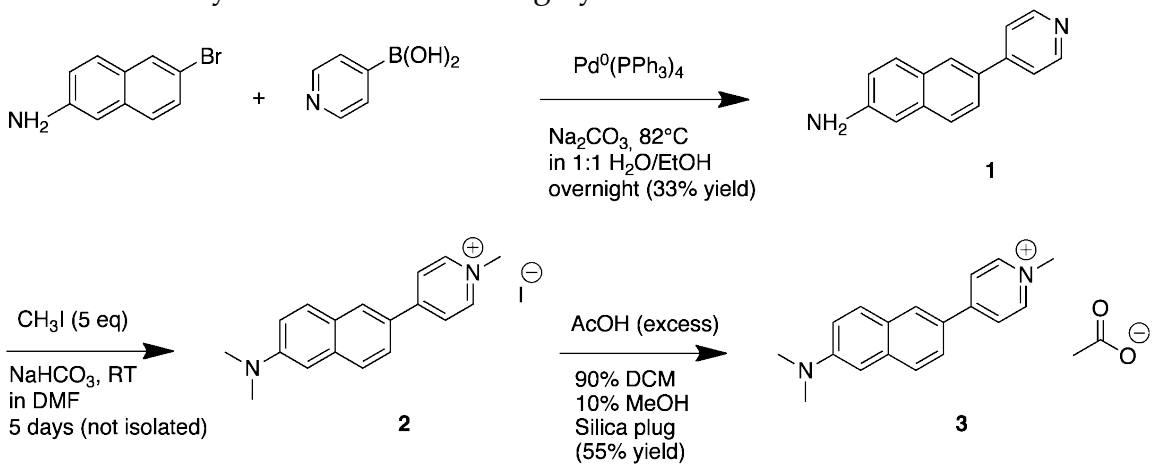


Both steps in the synthesis are highly sensitive to the solvent used. In the methylation step, trimethylation occurred in DMF far more readily than in other polar, aprotic solvents. However, after five days, some dimethyl product remained, and an additional equivalent of methyl iodide was added on the final day to push the reaction toward completion. Instead of having the intended effect of converting remaining dimethylated **1** to **2**, this resulted in formation of a blue-fluorescent baseline peak by TLC and corresponding appearance of a doubly ionized, tetramethylated peak ($m/z = 139.1$) by mass spectrometry. As such, increasing the amount of methyl iodide used is not recommended for further synthetic pursuits.

Chromatographic separation of **3** proved difficult. Reasons for difficulty included low solubility in non-alcohol solvents, low mobility on normal phase silica gel, and close spacing in the elution of compounds differing by a single methyl group. However, a heavily acidified mixture of dichloromethane and methanol allowed for reasonable separation through a short column of normal phase silica gel. The high efficacy of the silica plug likely renders the other purification methods used for this step (filtration, solvent washes) redundant.

## 6.3. Experimental Methods

### *6.3.1. General characterization methodology*

UV/Vis spectra were recorded on a Varian Cary 5000 spectrophotometer using paired 1cm fused quartz cuvettes and referenced against solvent. Fluorescence spectra were recorded on a Perkins-Elmer LS50B Luminescence Spectrophotometer using a 1cm fused quartz fluorescence cuvette and an excitation wavelength of 400nm. Circular dichroism spectra were recorded on a JASCO 720 Circular Dichroism Spectrophotometer using paired 100mm fused quartz cuvettes and referenced against solvent. $^{1}$H NMR spectra were recorded on either a Bruker AV300 or AV301 spectrometer. Medium-resolution mass spectra were recorded on a Bruker Esquire ion trap mass spectrometer using electrospray ionization (ESI), and high-resolution mass spectra were recorded on a JEOL HX-110 double focusing mass spectrometer using fast atom bombardment (FAB) in a 3-nitrobenzyl alcohol matrix. Fluorescence images were recorded using Zeiss Fluorescent microscope with a BP 450-490 FT 510 LP 515 filter cube.

### *6.3.2. Titration methodology*

Dyes were evaluated for their DNA-binding properties by means of colorimetric titrations in buffered aqueous solution (1X TE buffer titrated to pH 7.2 with HCl). All titrations were run using an Ocean Optics diode-array UV/Vis spectrometer connected to a temperature control system. The thermal bath temperature was set to 25.0 ± 0.1 °C (298 K). Initial dye solutions were typically 2.5 ml or 3.0 mL, with the concentration of the dye adjusted such that the optical density of the solution was between 0.60 and 0.90. DNA solution was added to

the dye solution in 30 µL aliquots. Solutions were mixed by *in-situ* magnetic stirring, as well as manually shaking the cuvette after each addition. After allowing the solution to mix for about one minute, the stirrer was stopped and a spectrum was recorded. If the initial absorbance of the dye was ≥ 1, the dye solution was diluted with the appropriate solvent (TE buffer, methanol, or butanol) until the initial absorbance was < 1. Runs continued until changes in absorbance became small (dilution only) or 450 µL of titrant was added, whichever was longer.

Spectra were then examined to determine the wavelength at which the dye's absorbance changed most over the course of the titration. The reduced absorbance change

$$Y = \frac{A - A_f}{A_b - A} \qquad (6\text{-}2)$$

was calculated at the selected wavelength for each point in the titration. The absorbance of the free dye ($A_f$) was obtained from the initial absorbance value, and the absorbance of the bound dye ($A_b$) was obtained from linear regression of the absorbance values at the three highest measured concentrations of dye versus 1/[DNA]. This parameter was then used to calculate the fraction of dye bound,

$$f_b = \frac{Y}{Y + 1} \qquad (6\text{-}3)$$

at each titrant concentration. Assuming an identical-and-independent-site binding model, this fraction can also be written as

$$f_b = \frac{[LN]}{[L] + [LN]} \qquad (6\text{-}4)$$

where [$L$] is the concentration of unbound dye and [$LN$] is the concentration of bound dye. These can be determined from the equilibrium expression

$$K = \frac{[LN]}{[L][N]} \quad (6\text{-}5)$$

and mass balance equations

$$\begin{aligned} [L_0] &= [L] + [LN] \\ [N_0] &= [N] + [LN] \end{aligned} \quad (6\text{-}6)$$

where [$N$] is the concentration of unbound DNA base pairs, [$L_0$] is the total concentration of dye, and [$N_0$] is the total concentration of dye. If it is further assumed that each dye requires $n$ sites (i.e. binding blocks access to adjacent sites), the fraction bound can be written in terms of two parameters, $[L_0]_i$ and $[N_0]_I$ for the $i$th measurement in a titration, and two variables, $n$ and $K$:

$$f_{b,i} = \frac{1 + nK[L_0]_i[N_0]_i - \sqrt{\left(-nK[L_0]_i - K[L_0]_i - 1\right)^2 - 4nK^2[L_0]_i[N_0]_i}}{2nK[L_0]_i} \quad (6\text{-}7)$$

The resulting system of quadratic equations (one per point) can be solved by non-linear least-squares regression to find $K$ and $n$. The fitting was done using an in-house, simulated-annealing[23] based algorithm.

### *6.3.3. Hyper-Rayleigh scattering methodology*

Hyper-Rayleigh scattering[24] (HRS) measurements of the hyperpolarizability of LL-1 were performed by Griet Depotter and Koen Clays at Katholieke Universiteit Leuven. Spectra were recorded in dichloromethane using a Ti:Sapphire laser with a fundamental wavelength of 800nm, and referenced against Crystal Violet.[25] Signal contamination from two-photon fluorescence was

suppressed using high-frequency demodulation,[26] and the hyperpolarizability was extrapolated to zero frequency using the two-level model,[27] with component along the chromophore dipole assumed to be the dominant tensor element. See Chapter 5 for more details.

## 6.4. Results and Discussion

### *6.4.1. Linear photophysics*

Absorbance and fluorescence spectra of LL-1 were recorded in four solvents (TE buffer at pH 7.2, methanol, dimethyl sulfoxide, and chloroform). Obtaining quantitative extinction coefficients required sample preparation to be carried out in a glovebox under dry nitrogen, as the dye was very hygroscopic. However, the extinction coefficients obtained compare favorably to that of ethidium bromide (5800 ± 200 $M^{-1}cm^{-1}$ at 480nm in aqueous solution[17]) and are consistent with dyes with similar structures [20] to LL-1. Absorbance and emission maxima are listed in Table 6.1.

**Table 6.1.** Linear optical properties of LL-1

| **Solvent** | **ε** (dielectric) | $\lambda_{max}$ (abs, nm) | $\varepsilon_{max}$ ($M^{-1}$ $cm^{-1}$) | $\lambda_{max}$ (fluor, nm) |
|---|---|---|---|---|
| TE buffer | 80.1 (water) | 409 | 17000 | 611 |
| Methanol | 33.0 | 445 | 20000 | 604 |
| DMSO | 47.24 | 442 | qualitative | 614 |
| Chloroform | 4.8064 | 468 | qualitative | 556 |

LL-1 exhibits strong negative solvatochromism in its absorbance maximum, with a hypsochromic shift of 59 nm between chloroform and water. However, it shows positive solvatochromism in its fluorescence maximum. These shifts are consistent with those observed for similar hemicyanine dyes with aryl-aryl linkages.[20] Fromherz explains this symmetrical solvatochromism by reversal of the molecular dipole moment between the ground and excited states[28]. The dye exhibits a large Stokes shift in all solvents, peaking at 202nm in TE buffer, although it is substantially reduced in less polar solvents by the symmetrical solvatochromism. Spectra are shown in Figure 6.3.

**6.3a.** LL-1 in protic solvents

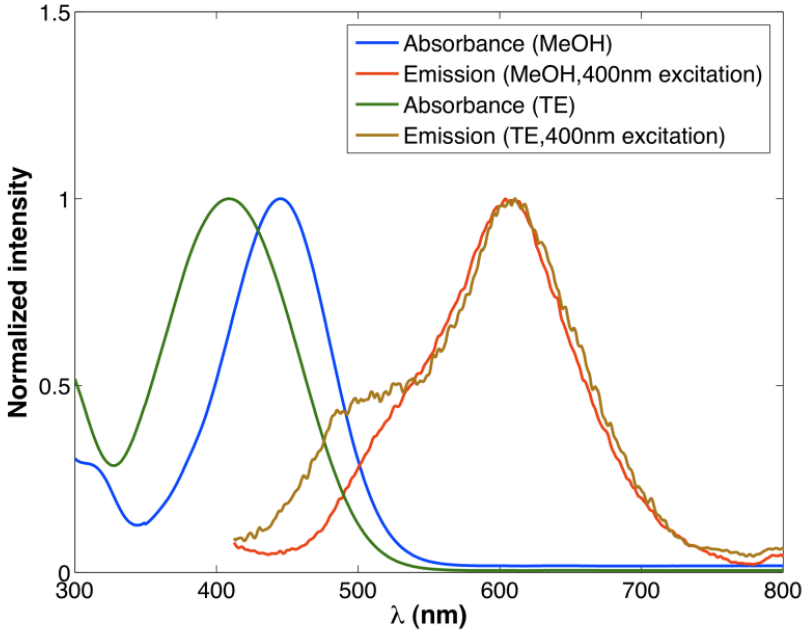


**6.3b.** LL-1 in aprotic solvents

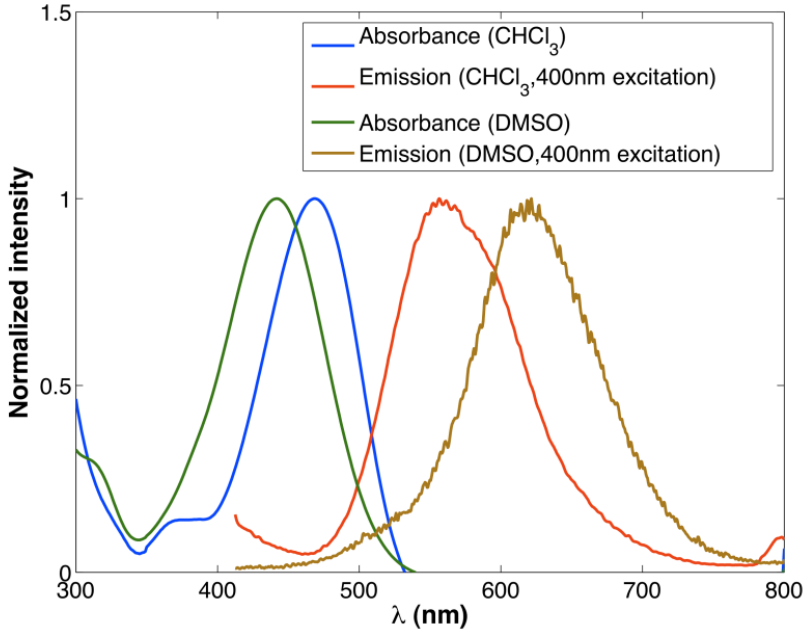


**Figure 6.3.** Normalized UV/Vis and fluorescence spectra of LL-1 in (a) TE buffer and methanol and (b) DMSO and chloroform. Fluorescence spectra are truncated near 410nm to remove the Rayleigh scattering peak at the excitation wavelength of 400nm.

The shape of the absorbance spectra is similar in all four solvents, with a single broad peak in the visible and a shoulder leading into a peak in the ultraviolet. The fluorescence spectra all exhibit a single broad peak, with the exception of the measurement in TE buffer, which shows a shoulder at about 500nm and about half the intensity of the primary peak. As the solution in TE buffer is the only one containing substantial concentrations of other ionic species, this peak could be due to complexation with the Tris or EDTA in the buffer.

### *6.4.2. Nonlinear optical properties*

The hyperpolarizability of LL-1 was investigated computationally, as well as experimentally by Hyper-Rayleigh scattering. As the B3LYP functional used for preliminary screening of molecular hyperpolarizabilities is known to overestimate charge transfer over long distances[29], additional electronic structure calculations were run using the heavily parameterized M062X functional,[30] which has previously shown good performance for calculating relative hyperpolarizabilities,[31] as well as with *ab initio* second-order Møller-Plesset Perturbation Theory (MP2). All calculations were run with Gaussian 09,[18] and hyperpolarizabilities were obtained by numerical (finite-field) differentiation of polarizabilities that were calculated by analytic differentiation. Results are listed in Table 6.2.

**Table 6.2.** Static hyperpolarizability along the molecular dipole axis ($\beta_{zzz}$, $10^{-30}$ esu, perturbation convention) of LL-1 in different dielectric environments.

| Method | Vacuum | Chloroform | Methanol |
|---|---|---|---|
| B3LYP/6-31+g(d) | -107 | -184 | -290 |
| M062X/6-31+g(d) | -111 | -157 | -151 |
| MP2/6-31+g(d)//MP2/6-31g(d) | -128 | -104 | -86 |

In all cases, LL-1 exhibits a negative $\beta_{zzz}$, a characteristic typically seen in zwitterionic chromophores[32], which indicates that charge transfer occurs in the direction opposite the molecular dipole moment. The magnitude of the static hyperpolarizability ($\beta_{zzz}(0)$) compares favorably in all three solvent environments with that of DR1[26] ($54 \pm 5 \times 10^{-30}$ esu in chloroform, extrapolated to zero frequency). Interestingly, while both DFT methods predict that hyperpolarizability will increase with solvent polarity, consistent with most neutral ground state ONLO chromophores, the MP2 calculations predict that the hyperpolarizability will decrease as solvent polarity is increased.

Experimental HRS data closely resembled the MP2 predicted value, with an extrapolated $\beta_{zzz}(0)$ of $90 \pm 3$ in dichloromethane. As HRS measurements are derived from a rotational average, the sign of beta cannot be determined. Follow-up calculations at the MP2/6-31+g(d) level in dichloromethane obtained a $\beta_{zzz}(0)$ of -95; calculations with a larger (aug-cc-pVDZ) basis set obtained a slightly larger $\beta_{zzz}(0)$ of -114. Additionally, the hyperpolarizability is comparable to measurements DAST variant MO by Clays and co-workers ($140 \pm 10 \times 10^{-30}$ esu in chloroform,[26] extrapolated to zero frequency), providing further evidence for similar optical nonlinearity between LL-1 and DAST.

### *6.4.3. Binding titrations*

Binding titrations were run for LL-1, DAST, and ethidium bromide as a control and are shown in Figure 6.4. All three exhibited a shift in absorbance maximum upon addition of DNA and show a single isosbestic point in the visible region of the spectrum, supporting the use of the two-species (bound and

unbound) model.[33] As DR1 is not sufficiently soluble in water, an exact comparison with the other three dyes was not possible, but a titration in 1:1 TE buffer and ethanol showed no substantial change in the absorbance peak.

**6.4a.** Ethidium bromide

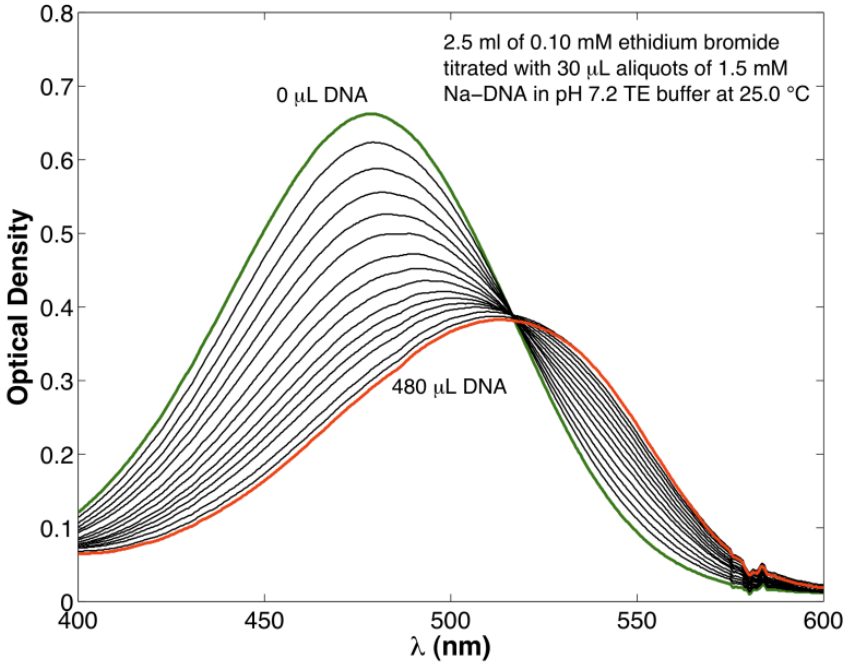

**6.4b.** DAST

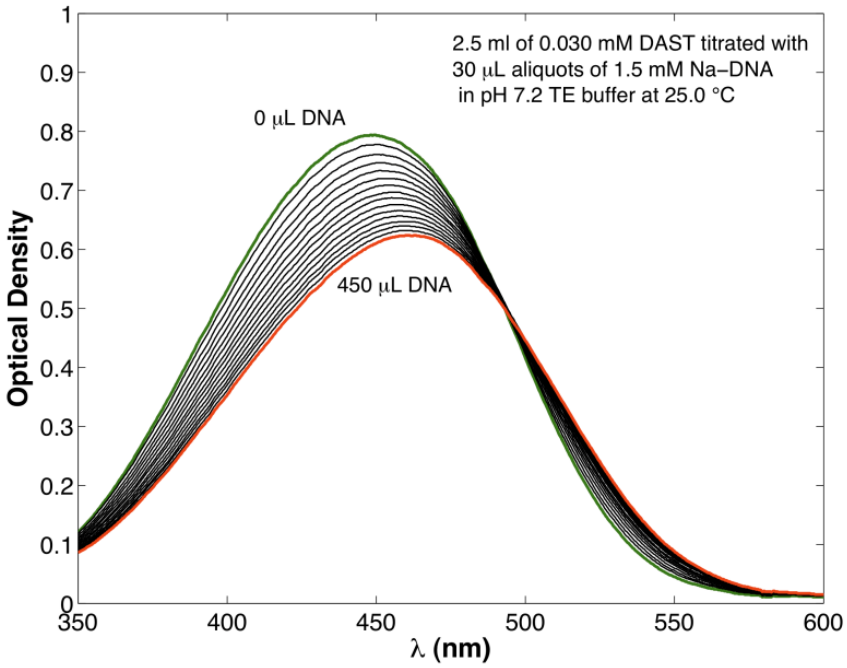


**6.4c.** LL-1

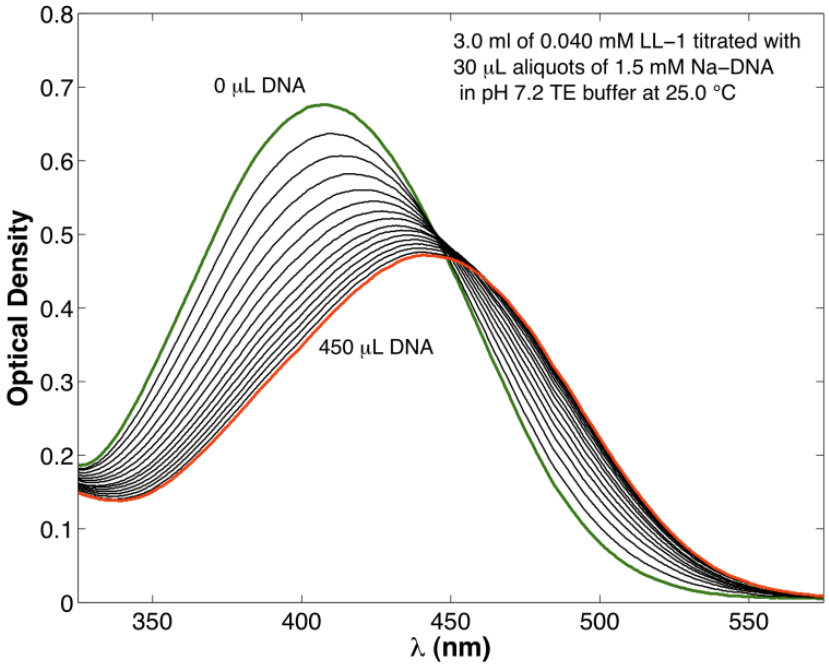


**Figure 6.4.** Overlay of spectra from titration of (a) ethidium bromide, (b) DAST, and (c) LL-1 with Na-DNA. The initial and final spectra are indicated with green and red lines, respectively.

The magnitude of the change in wavelength as DNA is added is far greater for LL-1 and ethidium bromide. Data for both of these dyes was fit using eqs. (2), (3), and (8) to produce binding curves. The control run for ethidium bromide produced data reasonably consistent with prior experiments, with $n$ = 1.91 ± 0.015, compared to 2.17 (using our convention of base pairs/dye) at 20°C in a CsCl/EDTA solution.[33] The $n$=2 binding model for DNA is often indicative of intercalation, as an intercalated dye molecule is inserted between two base pairs, distorting the shape of the DNA helix[10]. The binding curve for ethidium bromide is shown in Figure 6.5.

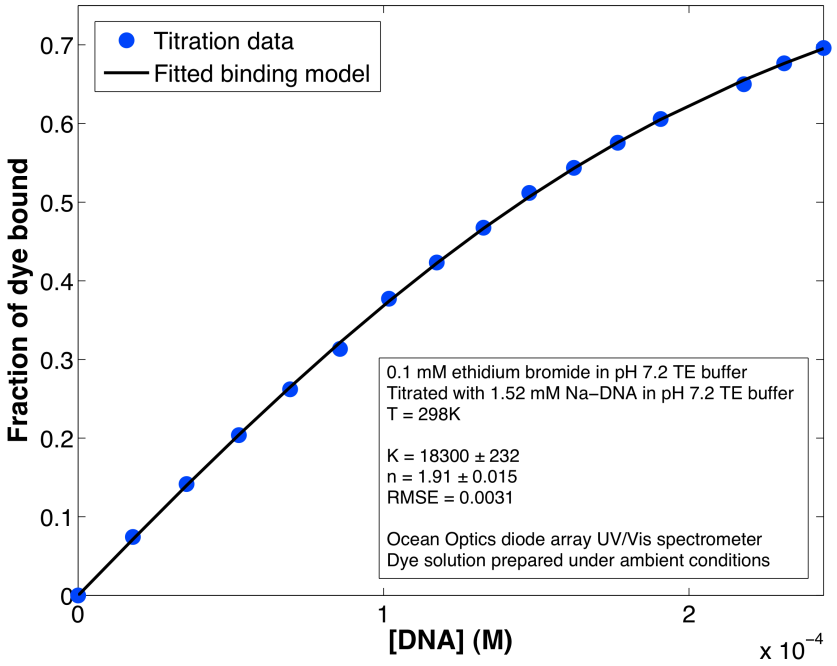


**Figure 6.5.** Binding curve for ethidium bromide in TE buffer at 298 K.

Binding curves for LL-1 were also fit best by the $n$ = 2 model, although the slope of the $n$-$K$ error surface was shallow near the minimum. Combined with the large red shift (indicative of a lower dielectric environment), these data illustrate that LL-1 likely intercalates into DNA. Results are shown in Figure 6.6.

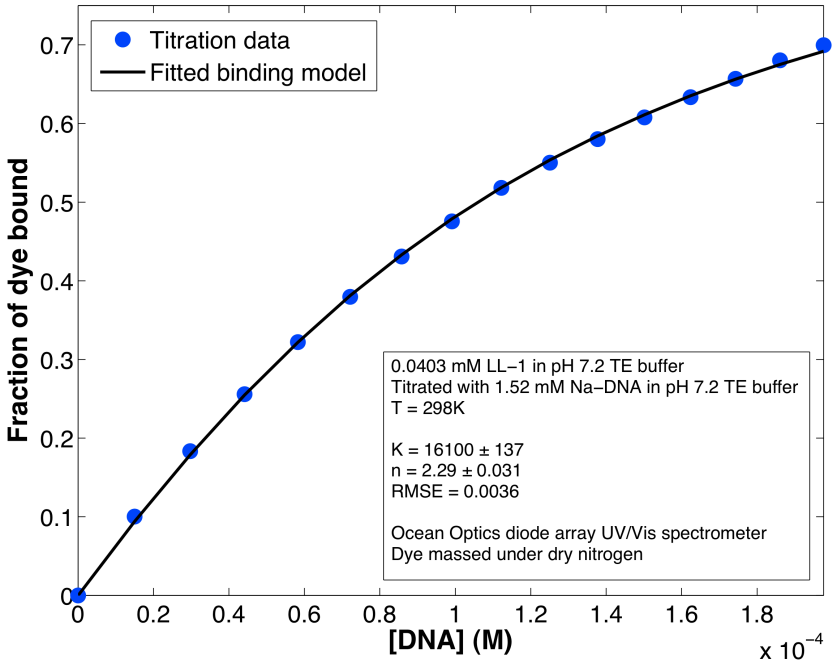


**Figure 6.6.** Binding curve for LL-1 in TE buffer at 298 K.

However, as the binding curves only indicate the number of base pairs needed to bind one dye molecule, without suggesting any particular ordering of the dye molecules, the electronic circular dichroism in the UV of both LL-1 and ethidium bromide was measured. In circular dichroism measurements, unperturbed DNA exhibits a positive peak about 275nm and a negative peak about 245nm. When ethidium bromide is added to the DNA solution, the peak is not only distorted, but an additional peak appears in a wavelength range corresponding to the UV absorbance of ethidium bromide[10a]. No such peak is observed for LL-1, although this does not rule out intercalation; steric characteristics may cause the difference in results between ethidium bromide and LL-1. Unlike LL-1, ethidium bromide has a bulky phenyl group projecting out from the plane of the main aromatic system. Thus, this side group may bias

the direction in which ethidium intercalates and enhance its response to circularly polarized light. Circular dichroism spectra are shown in Figure 6.7.

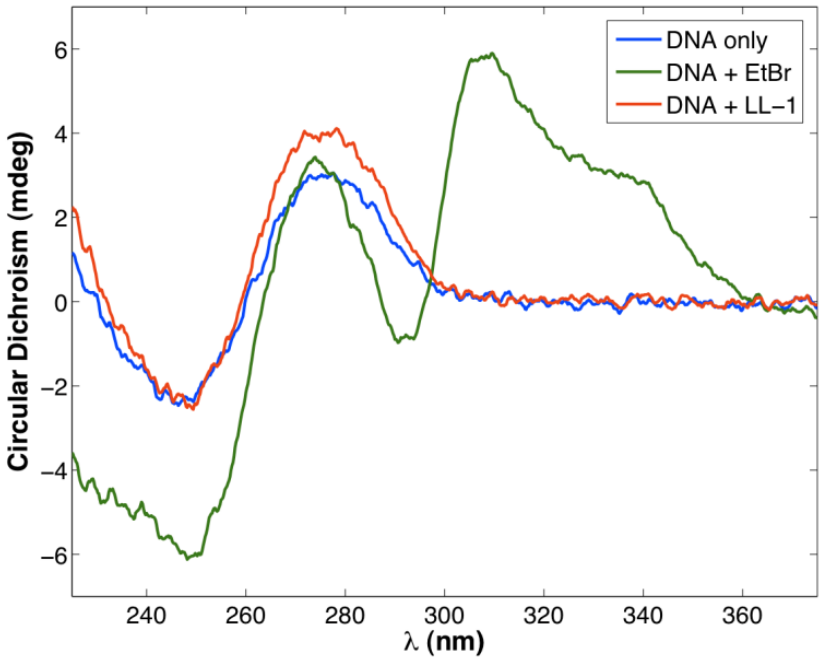


**Figure 6.7.** Electronic circular dichroism spectra of LL-1 and ethidium bromide in pH 7.2 TE buffer.

### *6.4.4. Fluorescence imaging*

In addition to the *in vitro* experiments mentioned above, LL-1 was also evaluated in living cells as a stain for fluorescence microscopy applications by William Hardin in the Cattolico group. When dissolved in DMSO, it proved capable of crossing the cell membrane of *Gymnodinium* sp[34] and accumulating in the nucleus, where it fluoresced yellow when excited by light in the 450-490nm range. A representative image is shown in Figure 6.8.

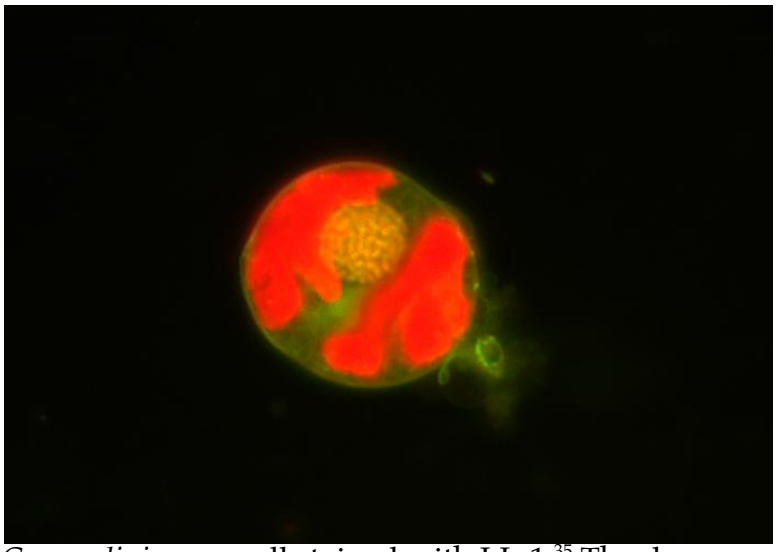

**Figure 6.8.** A *Gymnodinium* sp cell stained with LL-1.[35] The dye concentrates in the nucleus (orange region), where permanently condensed chromosomes are visible. The red regions are chloroplasts; the color is due to autofluorescence of chlorophyll. The cells is approximately 30 μm in diameter.

Extensive further characterization will be needed for imaging use, including testing selectivity between DNA and RNA, ability to penetrate thick cell walls, and sensitivity in organisms with smaller nuclei. Furthermore, should experimental characterization of optical nonlinearity yield positive results, characterization of two-photon fluorescence may also be worthwhile.

## 6.5. Conclusion and Outlook

By combining characteristics of common intercalators and the ONLO dye DAST, we designed a cationic ONLO dye capable of binding to DNA. It exhibits binding behavior similar to the common intercalator ethidium bromide. Both HRS measurments and electronic structure calculations at the MP2 level indicate that it has a hyperpolarizability similar to that of DAST. It also absorbs much more strongly than ethidium bromide, albeit at a shorter wavelength and away from telecommunications wavelengths. Furthermore, in addition to potential applications in electro-optics, it has demonstrated potential for use as a biological

stain for fluorescence imaging of nucleic acids in living cells. While further characterization will be required to assess incorporation of the dye into thin films, electro-optic performance, and quantitative performance of the dye in biological systems, LL-1 seems promising as an ONLO dye for biophotonic applications.

Finally, the structure of LL-1 lends itself to further functionalization for compatibility with a DNA host. One possible modification is to add a coumarin-containing side chain similar to that used in C1[4] in order to both avoid the need for a separate surfactant such as CTMA and allow for hardening of the film through photocrosslinking[36] of the coumarins. A proposed synthesis for such a modified dye is shown in Scheme 6.2.

**Scheme 6.2.** Proposed synthesis of coumarin-functionalized LL-1 variant

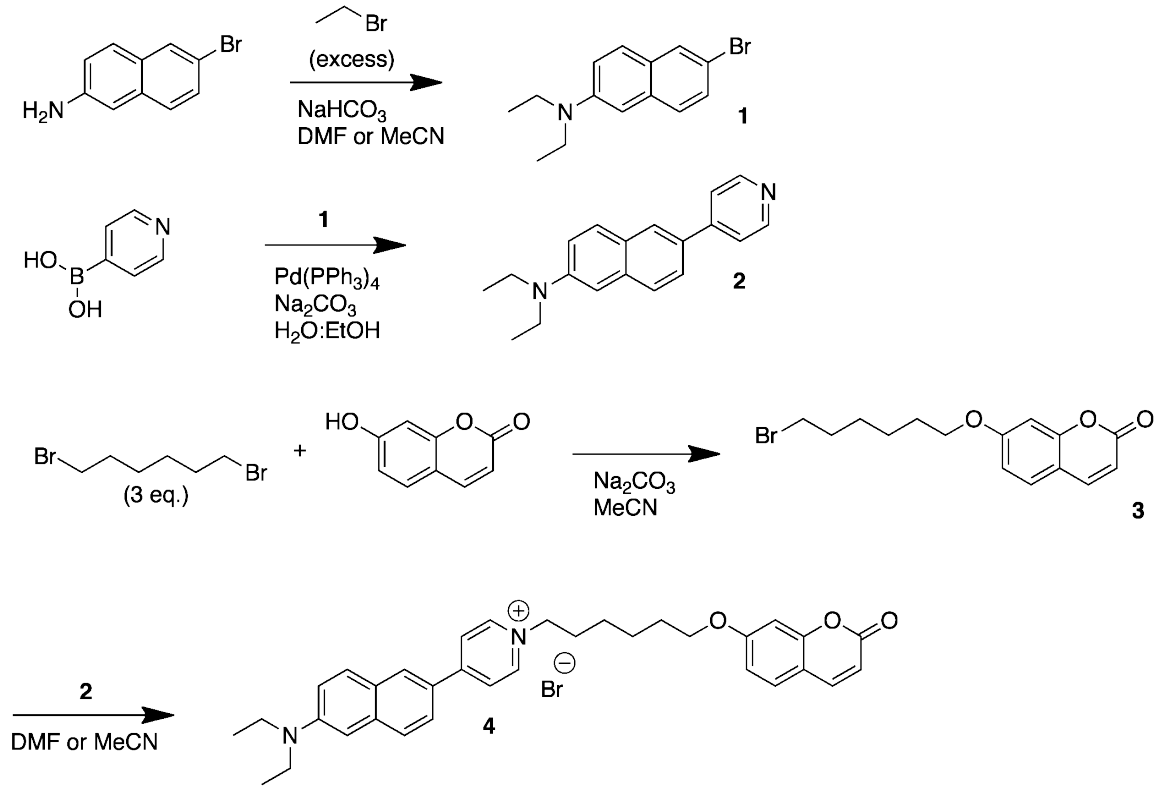

A coumarin-based crosslinker based on structure (**3**) attached to pyridine has already been synthesized (see Appendix D), based on an initial crosslinker concept by Stephanie Benight. Further synthetic work will explore covalently attaching such a crosslinker to LL-1, as well as effects from different attachment points. Photostability characterization will also be required to ensure that the ultraviolet light used for crosslinking does not adversely affect the chromophore.

## 6.6. Synthetic Details

### *6.6.1. General synthesis*

6-bromo-2-napthaleneamine was purchased from Astatech, and pyridine-4-boronic acid was purchased from Sigma-Aldrich, all other chemicals were purchased from Sigma Aldrich, Fisher Scientific, or Alfa Aesar. Commercially available chemicals, including solvents, were used as received. Solvents used for synthesis and chromatography were all of HPLC grade. Water used for making TE buffer was purified by reverse osmosis to a resistivity of > 18 MΩ $cm^{-1}$. Glassware was acid and base treated and oven dried before use.

### *6.6.2. Synthetic procedures*

(**1**) 6-bromo-2-napthaleneamine (1 eq), pyridine-4-boronic acid (1.1 eq), and sodium carbonate (3.7 eq) were added to a solution of 50% water and 50% ethanol in a double-necked round bottom flask. The solution was sparged with dry nitrogen for >30min, then degassed by four cycles of exposing to vacuum and flushing with dry nitrogen. Tetrakis(triphenylphosphine)palladium(0) (0.01 eq) was added as a catalyst and the mixture was stirred overnight at 82°C under dry nitrogen. Reaction progress was monitored by TLC and GC/MS. The

mixture was then transferred to a separatory funnel, extracted with ethyl acetate, and washed with saturated aqueous $NaHCO_3$ and brine. The organic phase was retained, dried with anhydrous magnesium sulfate, and the solvent was removed *in vacuo*. The crude mixture was purified using silica gel chromatography eluting with 95% ethyl acetate and 5% methanol to afford a yellow powder (33% yield). $C_{15}H_{12}N_2$, m/z 221.2 (M+H, ESI). $^1$H NMR (500 MHz, $CDCl_3$) δ 8.66 (d, *J* = 6.1 Hz, 1H), 7.99 (s, 1H), 7.75 (d, *J* = 8.5 Hz, 1H), 7.71 – 7.64 (m, 1H), 7.62 (d, *J* = 6.1 Hz, 1H), 7.47 (s, 0H), 7.26 (d, *J* = 0.6 Hz, 4H), 7.01 (s, 1H), 6.99 (d, *J* = 2.1 Hz, 0H), 3.96 (s, 1H), 1.56 (s, 2H).

(**2**) Purified **1** was re-dissolved in DMF in a single-necked round bottom flask, and methyl iodide (5 eq) and sodium bicarbonate (1.9 eq) were added. The flask was sealed with a rubber septum and stirred at ambient temperature for 5 days. The reaction was monitored by TLC and ESI-MS, and an additional equivalent of methyl iodide was added on the final day to push the reaction toward completion. Upon completion, the mixture was filtered, washed with methanol, then degassed by rotary evaporation. The DMF was removed by distillation under vacuum (max temperature of 80°C), and the crude product was dried *in vacuo* overnight to yield an orange powder. $C_{18}H_{19}N_2I$, m/z 263.2 (M+, ESI)

(**3**) Crude **2** was purified using a silica gel plug with 90% dichloromethane and 10% methanol, acidified with glacial acetic acid to yield an orange product. The purified product was dried by rotary evaporation followed by 48 hours *in*

*vacuo* at 90°C to form a red powder. (55% yield) $C_{20}H_{22}N_2O_2$, m/z 263.15471 (M+, FAB). $^1$H NMR (300 MHz, MeOD) δ 8.74 (t, *J* = 6.4 Hz, 2H), 8.42 (dd, *J* = 15.4, 8.7 Hz, 3H), 7.94 – 7.74 (m, 3H), 7.32 (dd, *J* = 9.2, 2.5 Hz, 1H), 7.00 (d, *J* = 2.6 Hz, 1H), 6.78 (d, *J* = 2.2 Hz, 0H), 4.89 (s, 8H), 4.34 (d, *J* = 3.1 Hz, 3H), 3.33 (dt, *J* = 3.3, 1.6 Hz, 10H), 3.15 (s, 4H), 2.94 (s, 1H), 2.71 (s, 2H), 1.94 (s, 5H), 1.39 (d, *J* = 6.6 Hz, 1H).

## 6.7. Acknowledgements for Chapter 6

Thanks to Luke Latimer (REU, 2010) for extensive collaboration on this project, including much of the early synthetic and characterization work, Zach Watanabe (REU, 2010) for computational work screening candidate molecules, Koen Clays and Griet Depotter for HRS measurements, William Hardin and Rose Ann Cattolico for *in vivo* characterization, Stephanie Benight and Delwin Elder for synthetic assistance and advice, Peter Johnston, Jinsheng Song, Ilya Kosilkin, and Meghana Rawal for further help with synthetic questions, and Emily Heckman for useful discussion. Additionally, thanks to Nicholas Bigelow for his early work on the project, Derek Frei (REU, 2009) and Todd Lien for work on optimization and testing of titration protocols, Wes Winn (REU, 2011) for running several test syntheses, Andreas F. Tillack for assistance with glovebox techniques, and Bill Cusworth, Angie Steuermann, and Chris Bingham for assistance in securing space and equipment for the titrations. Also, thanks to Martin Sadilek, Loren Kruse, and Paul Miller for instrument training, troubleshooting, and useful discussion, as well as Carolina Medrano at Rainbow Photonics for providing a sample of DAST. Finally, Air Force Research Laboratory (via subcontract through Optimetrix), the National Science

Foundation (STC-MDITR DMR-0120967), and the University of Washington Student Technology Fund are acknowledged for financial support.

## 6.8. Supplemental Information for Chapter 6

The synthesis and characterization of a coumarin-functionalized surfactant intended to be used in conjunction for LL-1 to produce crosslinkable EO films is described in Appendix D.

## 6.9. References for Chapter 6

1. (a) Dalton, L. R.; Benight, S. J.; Johnson, L. E.; Knorr, D. B.; Kosilkin, I.; Eichinger, B. E.; Robinson, B. H.; Jen, A. K. Y.; Overney, R. M., Systematic Nanoengineering of Soft Matter Organic Electro-optic Materials. *Chemistry of Materials* **2011,** *23* (3), 430-445; (b) Benight, S. J.; Bale, D. H.; Olbricht, B. C.; Dalton, L. R., Organic electro-optics: Understanding material structure/function relationships and device fabrication issues. *Journal of Materials Chemistry* **2009,** *19* (40), 7466-7475.
2. Grote, J. G.; Ogata, N.; Hagen, J. A.; Heckman, E.; Curley, M. J.; Yaney, P. P.; Stone, M. O.; Diggs, D. E.; Nelson, R. L.; Zetts, J. S.; Hopkins, F. K.; Dalton, L. R., Deoxyribonucleic Acid (DNA) based nonlinear optics. *Proceedings of SPIE* **2003,** *5211*, 53-62.
3. Heckman, E. M., Poling and optical studies of DNA NLO waveguides. *Proceedings of SPIE* **2005,** *5934*, 593408-593408-7.
4. Benight, S. J.; Johnson, L. E.; Barnes, R.; Olbricht, B. C.; Bale, D. H.; Reid, P. J.; Eichinger, B. E.; Dalton, L. R.; Sullivan, P. A.; Robinson, B. H., Reduced Dimensionality in Organic Electro-Optic Materials: Theory and Defined Order. *Journal of Physical Chemistry B* **2010,** *114* (37), 11949-11956.
5. (a) Heckman, E. M.; Yaney, P. P.; Grote, J. G.; Hopkins, F. K., Development and performance of an all-DNA-based electro-optic waveguide modulator. *Proceedings of SPIE* **2006,** *6401*, 640108-640108-10; (b) Heckman, E. The Development of an All-DNA-Based Electro-Optic Waveguide Modulator. University of Dayton, Dayton, OH
, 2006; (c) Samoc, M.; Samoc, A.; Miniewicz, A.; Przemyslaw, M. P.; Prasad, P. N.; Grote, J. G., Cubic nonlinear optical effects in deoxyribonucleic acid (DNA) based materials containing chromophores. **2007,** *6646*, 66460A-66460A-10.
6. (a) Dalton, L. R.; Steier, W. H.; Robinson, B. H.; Zhang, C.; Ren, A.; Garner, S.; Chen, A.; Londergan, T.; Irwin, L.; Carlson, B.; Fifield, L.; Phelan, G.; Kincaid, C.; Amend, J.; Jen, A., From molecules to opto-chips: organic electro-optic materials. *Journal of Materials Chemistry* **1999,** *9* (9), 1905-1920; (b) Singer, K. D.; Kuzyk, M. G.; Sohn, J. E., Second-order nonlinear-optical processes in

orientationally ordered materials: relationship between molecular and macroscopic properties. *Journal of the Optical Society of America B* **1987,** *4* (6), 968-976.
7. Luo, J.; Zhou, X.-H.; Jen, A. K. Y., Rational molecular design and supramolecular assembly of highly efficient organic electro-optic materials. *Journal of Materials Chemistry* **2009,** *19* (40), 7410.
8. Latimer, L.; Lien, T.; Chung, T.; Smith, A., Unpublished work in Robinson group. University of Washington: 2010.
9. (a) Mitus, A. C.; Pawlik, G.; Kochalska, A.; Mysliwiec, J.; Miniewicz, A.; Kajzar, F., Experimental and Monte Carlo studies of diffraction grating inscription in DNA-based materials. **2007,** *6646*, 66460I-66460I-8; (b) Pawlik, G.; Mitus, A. C.; Mysliwiec, J.; Miniewicz, A.; Grote, J. G., Photochromic dye semi-intercalation into DNA-based polymeric matrix: Computer modeling and experiment. *Chemical Physics Letters* **2010,** *484* (4-6), 321-323.
10. (a) Pohl, F. M.; Jovin, T. M.; Baehr, W.; Holbrook, J. J., Ethidium Bromide as a Cooperative Effector of a DNA Structure. *Proceedings of the National Academy of Sciences* **1972,** *69* (12), 3805-3809; (b) Nordmeier, E., Absorption spectroscopy and dynamic and static light-scattering studies of ethidium bromide binding to calf thymus DNA: implications for outside-binding and intercalation. *The Journal of Physical Chemistry* **1992,** *96* (14), 6045-6055.
11. Atherton, S. J.; Harriman, A., Photochemistry of Intercalated Methylene Blue: Photoinduced Hydrogen Atom Abstraction from Guanine and Adenine. *Journal of the American Chemical Society* **1993,** *115* (5), 1816-1822.
12. (a) Berbiest, T.; Clays, K.; Samyn, C.; Wolff, J.; Reinhoudt, D.; Persoons, A., Investigations of the Hyperpolarizabiltiy in Organic Molecules from Dipolar to Octupolar Systems. *Journal of the American Chemical Society* **1994,** *116* (20), 9320-9323; (b) Stadler, S.; Dietrich, R.; Bourhill, G.; Bräuchle, C., Long-wavelength first hyperpolarizability measurements by hyper-Rayleigh scattering. *Optics Letters* **1996,** *21* (4), 251-253.
13. Del Castillo, P.; Horobin, R. W.; Bláquez-Castro, A.; Stockert, J. C., Binding of cationic dyes to DNA: distinguishing intercalation and groove binding mechanisms using simple experimental and numerical models. *Biotechnic & Histochemistry* **2010,** *85* (4), 247-256.
14. Heckman, E. M.; Hagen, J. A.; Yaney, P. P.; Grote, J. G.; Hopkins, F. K., Processing techniques for deoxyribonucleic acid: Biopolymer for photonics applications. *Applied Physics Letters* **2005,** *87* (21), 211115.
15. Dalton, L. R.; Harper, A. W.; Robinson, B. H., The role of London forces in defining noncentrosymmetric order of high dipole moment–high hyperpolarizability chromophores in electrically poled polymeric thin films. *Proceedings of the National Academy of Sciences* **1997,** *94*, 4842-4847.
16. (a) Pan, F.; Wong, M. S.; Bosshard, C.; Günter, P., Crystal Growth and Characterization of the Organic Salt 4-N,N-Dimethylamino-4'-N'- methyl-stilbazolium Tosylate (DAST). *Advanced Materials* **1996,** *8* (7), 592-595; (b) Brahadeeswaran, S.; Onduka, S.; Takagi, M.; Takahashi, Y.; Adachi, H.; Kamimura, T.; Yoshimura, M.; Mori, Y.; Yoshida, K.; Sasaki, T., Twin-free and High-Quality DAST Crystals - Effected through Solutions of Lower Supersaturation Coupled with Isothermal Solvent Evaporation. *Crystal Growth & Design* **2006,** *6* (11), 2463-2468; (c) Ruiz, B.; Jazbinsek, M.; Günter, P., Crystal Growth of DAST. *Crystal Growth & Design* **2008,** *8* (11), 4173-4184.

17. Nelson, J. W.; Tinoco, I., Intercalation of Ethidium Ion into DNA and RNA Oligonucleotides. *Biopolymers* **1984,** *23* (2), 213-233.
18. Frisch, M. J.; Trucks, G. W.; Schlegel, H. B.; Scuseria, G. E.; Robb, M. A.; Cheeseman, J. R.; G. Scalmani, V. B.; Mennucci, B.; Petersson, G. A.; Nakatsuji, H.; Caricato, M.; Li, X.; Hratchian, H. P.; Izmaylov, A. F.; Bloino, J.; Zheng, G.; Sonnenberg, J. L.; Hada, M.; Ehara, M.; Toyota, K.; Fukuda, R.; Hasegawa, J.; Ishida, M.; Nakajima, T.; Honda, Y.; Kitao, O.; Nakai, H.; Vreven, T.; J. A. Montgomery, J.; Peralta, J. E.; Ogliaro, F.; Bearpark, M.; Heyd, J. J.; Brothers, E.; Kudin, K. N.; Staroverov, V. N.; Kobayashi, R.; Normand, J.; Raghavachari, K.; Rendell, A.; Burant, J. C.; Iyengar, S. S.; Tomasi, J.; Cossi, M.; Rega, N.; Millam, J. M.; Klene, M.; Knox, J. E.; Cross, J. B.; Bakken, V.; Adamo, C.; Jaramillo, J.; Gomperts, R.; Stratmann, R. E.; Yazyev, O.; Austin, A. J.; Cammi, R.; Pomelli, C.; Ochterski, J. W.; Martin, R. L.; Morokuma, K.; Zakrzewski, V. G.; Voth, G. A.; Salvador, P.; Dannenberg, J. J.; Dapprich, S.; Daniels, A. D.; Farkas, Ö.; Foresman, J. B.; Ortiz, J. V.; Cioslowski, J.; Fox, D. J. *Gaussian 09*, Revision A.1; Gaussian, Inc.: Wallingford, CT, 2009.
19. Rice, J. E.; Handy, N., The calculation of frequency-dependent polarizabilities as pseudo-energy derivatives. *Journal of Chemical Physics* **1991,** *94* (7), 4959-4971.
20. Ephardt, H.; Fromherz, P., Fluorescence of Amphiphilic Hemicyanine Dyes without Free Double Bonds. *Journal of Physical Chemistry* **1993,** *97* (17), 4540-4547.
21. (a) Leadbeater, N. E.; Williams, V. A.; Barnard, T. M.; Collins, M. J., Open-Vessel Microwave-Promoted Suzuki Reactions Using Low Levels of Palladium Catalyst: Optimization and Scale-Up. *Organic Process Research & Development* **2006,** *10* (4), 833-837; (b) Zhang, Y.; Xin, B.; Liu, L.; Wang, Y., Water-Promoted Suzuki Reaction in Room Temperature Ionic Liquids. *Synlett* **2005,** (20), 3083-3086; (c) Liu, L.; Zhang, Y.; Wang, Y., Phosphine-free palladium acetate catalyzed Suzuki reaction in water. *Journal of Organic Chemistry* **2005,** *70* (15), 6122-5; (d) Arvela, R. K.; Leadbeater, N. E., Suzuki Coupling of Aryl Chlorides with Phenylboronic Acid in Water, Using Microwave Heating with Simultaneous Cooling. *Organic Letters* **2005,** *7* (11), 2101-2104.
22. (a) Sommer, H. Z.; Lipp, H. I.; Jackson, L. L., Alkylation of Amines. A General Exhaustive Alkylation Method for the Synthesis of Quaternary Ammonium Compounds. *Journal of Organic Chemistry* **1971,** *36* (6), 824-828; (b) Chiappe, C.; Piccioli, P.; Pieraccini, D., Selective N-alkylation of anilines in ionic liquids. *Green Chemistry* **2006,** *8* (3), 277.
23. Press, W. H., Teukolsky, S.A., Vetterling, W.T., Flannery, B.P., *Numerical Recipes*. 3rd ed.; Cambridge University Press: Cambridge (UK), 2007.
24. Clays, K.; Persoons, A., Hyper-Rayleigh scattering in solution. *Review of Scientific Instruments* **1992,** *63* (6), 3285.
25. Clays, K., Personal communication (via email). 2012.
26. Olbrechts, G.; Wostyn, K.; Clays, K.; Persoons, A., High-frequency demodulation of multiphoton fluorescence in long-wavelength hyper-Rayleigh scattering. *Optics Letters* **1999,** *24* (6), 403-405.
27. Oudar, J. L.; Chemla, D. S., Hyperpolarizabilities of the nitroanilines and their relations to the excited state dipole moment. *J Chem Phys* **1977,** *66* (6), 2664-2668.

28. Fromherz, P., Monopole-Dipole Model for Symmetrical Solvatochromism of Hemicyanine Dyes. *Journal of Physical Chemistry* **1995,** *99* (18), 7188-9192.
29. Yanai, T.; Tew, D. P.; Handy, N. C., A new hybrid exchange–correlation functional using the Coulomb-attenuating method (CAM-B3LYP). *Chemical Physics Letters* **2004,** *393* (1-3), 51-57.
30. Zhao, Y.; Truhlar, D. G., The M06 suite of density functionals for main group thermochemistry, thermochemical kinetics, noncovalent interactions, excited states, and transition elements: two new functionals and systematic testing of four M06-class functionals and 12 other functionals. *Theoretical Chemistry Accounts* **2007,** *120* (1-3), 215-241.
31. Suponitsky, K. Y.; Liao, Y.; Masunov, A. E., Electronic Hyperpolarizabilities for Donor-Acceptor Molecules with Long Conjugated Bridges: Calculations versus Experiment. *Journal of Physical Chemistry A* **2009,** *113* (41), 10994-11001.
32. Szablewski, M.; Thomas, P. R.; Thornton, A.; Bloor, D.; Cross, G. H.; Cole, J. M.; Howard, J. A. K.; Malagoli, M.; Meyers, F.; Brédas, J.-L.; Wenseleers, W.; Goovaerts, E., Highly Dipolar, Optically Nonlinear Adducts of Tetracyano-p-quinodimethane: Synthesis, Physical Characterization, and Theoretical Aspects. *Journal of the American Chemical Society* **1997,** *119* (13), 3144-3154.
33. Tinoco, I.; Sauer, K.; Wang, J. C.; Puglisi, J. D., *Physical Chemistry: Principles and Applications in Biological Sciences*. 4th ed.; Prentice-Hall: Upper Saddle River, NJ, 2002.
34. Graham, H. W., Gymnodinium Catenatum, A New Dinoflagellate from the Gulf of California. *Transactions of the American Microscopical Society* **1943,** *62* (3), 259-261.
35. Hardin, W., Personal communication (via email). 2012.
36. Tian, Y.; Kong, X.; Nagase, Y.; Iyoda, T., Photocrosslinkable Liquid-Crystalline Block Copolymers with Coumarin Units Synthesized with Atom Transfer Radical Polymerization. *Journal of Polymer Science: Part A: Polymer Chemistry* **2003,** *41*, 2197-2206.

# Bibliography


1. NIST Chemistry WebBook. http://webbook.nist.gov (accessed 12/23/2009).

2. *Cisco Visual Networking Index: Forecast and Methodology, 2010–2015*; Cisco Systems: San Jose, CA, 2011.

3. Gaussian 09 User's Reference. Gaussian, Inc.: Wallingford, CT, 2011. http://www.gaussian.com/g_tech/g_ur/k_dft.htm (accessed 03/26/2012).

4. Adamo, C.; Barone, V., Toward reliable density functional methods without adjustable parameters: The PBE0 model. *Journal of Chemical Physics* **1999,** *110* (13), 6158.

5. Adams, D. J., Computer simulation of highly polar liquids. The hard sphere plus point dipole potential. *Molecular Physics* **1980,** *40* (5), 1261-71.

6. Alder, B. J., Wainright, T.E., Phase Transition for a Hard Sphere System. *Journal of Chemical Physics* **1957,** *27*, 1208-1209.

7. Alder, B. J.; Pollock, E. L., Simulation of Polar and Polarizable Fluids. *Annual Review of Physical Chemistry* **1981,** *32*, 311-329.

8. Allen, M. P., Tildesley, D.J., *Computer Simulations of Liquids*. Clarendon: Oxford (UK), 1987.

9. Alper, H. E.; Levy, R. M., Computer simulations of the dielectric properties of water: studies of the simple point charge and transferrable intermolecular potential models. *Journal of Chemical Physics* **1989,** *91* (2), 1242-51.

10. Andzelm, J.; Rinderspacher, B. C.; Rawlett, A.; Dougherty, J.; Baer, R.; Govind, N., Performance of DFT Methods in the Calculation of Optical Spectra of TCF-Chromophores. *Journal of Chemical Theory and Computation* **2009,** *5* (10), 2835-2846.

11. Anet, R., The Photodimers of Coumarin and Related Compounds. *Canadian Journal of Chemistry* **1962,** *40*, 1249-1256.

12. Aragó, J.; Sancho-García, J. C.; Ortí, E.; Beljonne, D., Ab Initio Modeling of Donor–Acceptor Interactions and Charge-Transfer Excitations in Molecular Complexes: The Case of Terthiophene–Tetracyanoquinodimethane. *Journal of Chemical Theory and Computation* **2011,** *7* (7), 2068-2077.

13. Arvela, R. K.; Leadbeater, N. E., Suzuki Coupling of Aryl Chlorides with Phenylboronic Acid in Water, Using Microwave Heating with Simultaneous Cooling. *Organic Letters* **2005,** *7* (11), 2101-2104.

14. Atherton, S. J.; Harriman, A., Photochemistry of Intercalated Methylene Blue: Photoinduced Hydrogen Atom Abstraction from Guanine and Adenine. *Journal of the American Chemical Society* **1993,** *115* (5), 1816-1822.

15. Ayton, G.; Patey, G. N., Ferroelectric Order in Model Discotic Nematic Liquid Crystals. *Physical Review Letters* **1996,** *76* (2), 239-242.

16. Ayton, G.; Wei, D. Q.; Patey, G. N., Liquid crystal phases of dipolar discotic particles. *Physical Review E* **1997,** *55* (1), 447-454.

17. Baehr-Jones, T. W.; Hochberg, M. J., Polymer Silicon Hybrid Systems: A Platform for Practical Nonlinear Optics. *Journal of Physical Chemistry C* **2008,** *112* (21), 8085-8090.

18. Bale, D. H. Nonlinear optical materials characterization studies employing photostability, hyper-Rayleigh scattering, and electric field induced second harmonic generation techniques. University of Washington, Seattle, WA, 2008.

19. Bale, D. H.; Eichinger, B. E.; Liang, W.; Li, X.; Dalton, L. R.; Robinson, B. H.; Reid, P. J., Dielectric dependence of the first molecular hyperpolarizability for electro-optic chromophores. *J Phys Chem B* **2011,** *115* (13), 3505-13.

20. Barker, J. A.; Watts, R. O., Structure of water; A Monte Carlo calculation. *Chemical Physics Letters* **1969,** *3* (3), 144-145.

21. Barker, J. A.; Watts, R. O., Monte-Carlo studies of the dielectric properties of water-like models. *Molecular Physics* **1973,** *26* (3), 789-92.

22. Bartke, J.; Hentschke, R., Dielectric properties and the ferroelectric transition of the Stockmayer-fluid via computer simulation. *Molecular Physics* **2006,** *104* (19), 3057-3068.

23. Bartke, J.; Hentschke, R., Phase behavior of the Stockmayer fluid via molecular dynamics simulation. *Physical Review E: Statistical, Nonlinear, and Soft Matter Physics* **2007,** *75* (6-1), 061503/1-061503/11.

24. Baus, M.; Colot, J.-L., Ferroelectric nematic liquid-crystal phases of dipolar hard ellipsoids. *Physical Review A* **1989,** *40* (9), 5444-5446.

25. Becke, A. D., A new mixing of Hartree-Fock and local density-functional theories. *Journal of Chemical Physics* **1993,** *98* (2), 1372-1377.

26. Becke, A. D., Density-functional thermochemistry. III. The role of exact exchange. *Journal of Chemical Physics* **1993,** *98* (7), 5648.

27. Behr, J. *Instant Player*, 2.00b5; Fraunhofer GmbH: 2008.

28. Benight, S. J. Nanoengineering of soft matter interactions in organic electro-optic materials. University of Washington, Seattle, WA, 2011.

29. Benight, S. J.; Bale, D. H.; Olbricht, B. C.; Dalton, L. R., Organic electro-optics: Understanding material structure/function relationships and device fabrication issues. *Journal of Materials Chemistry* **2009,** *19* (40), 7466.

30. Benight, S. J.; Daniel B. Knorr, J.; Johnson, L. E.; Sullivan, P. A.; Lao, D.; Sun, J.; Kocherlakota, L. S.; Elangovan, A.; Robinson, B. H.; Overney, R. M.; Dalton, L. R., Nano-Engineering Soft Matter Lattice Dimensionality for an Organic Electro-Optic Material. *Advanced Materials* **2012,** *IN PRESS*.

31. Benight, S. J.; Johnson, L. E.; Barnes, R.; Olbricht, B. C.; Bale, D. H.; Reid, P. J.; Eichinger, B. E.; Dalton, L. R.; Sullivan, P. A.; Robinson, B. H., Reduced Dimensionality in Organic Electro-Optic Materials: Theory and Defined Order. *Journal of Physical Chemistry B* **2010,** *114* (37), 11949-11956.

32. Benight, S. J.; Robinson, B. H.; Dalton, L. R., Nano-Engineering of Molecular Interactions in Organic Electro-Optic Materials. In *Molecular Interactions*, Meghea, A., Ed. Intech: Rijeka, Croatia, 2011.

33. Berardi, R.; Orlandi, S.; Zannoni, C., Monte Carlo simulation of discotic Gay–Berne mesogens with axial dipole. *Journal of the Chemical Society, Faraday Transactions* **1997,** *93* (8), 1493-1496.

34. Berardi, R.; Orlandi, S.; Zannoni, C., Columnar phases and field induced biaxiality of a Gay–Berne discotic liquid crystal. *Physical Chemistry Chemical Physics* **2000,** *2* (13), 2933-2942.

35. Berbiest, T.; Clays, K.; Samyn, C.; Wolff, J.; Reinhoudt, D.; Persoons, A., Investigations of the Hyperpolarizabiltiy in Organic Molecules from Dipolar to Octupolar Systems. *Journal of the American Chemical Society* **1994,** *116* (20), 9320-9323.

36. Berendsen, H. J. C.; Postma, J. P. M.; van Gunsteren, W. F.; DiNola, A.; Haak, J. R., Molecular dynamics with coupling to an external bath. *The Journal of Chemical Physics* **1984,** *81* (8), 3684.

37. Borini, S.; Limacher, P. A.; Luthi, H. P., A systematic analysis of the structure and (hyper)polarizability of donor-acceptor substituted polyacetylenes using a Coulomb-attenuating density functional. *Journal of Chemical Physics* **2009,** *131* (12), 124105.

38. Bortchagovsky, E. G., Ellipsometric method for investigation of the optical anisotropy of thin films: theory and calculations. *Thin Solid Films* **1997,** *307*, 192-199.

39. Böttcher, C. J. F., *Theory of Electric Polarization*. Elsevier: Amsterdam, Netherlands, 1952.

40. Brahadeeswaran, S.; Onduka, S.; Takagi, M.; Takahashi, Y.; Adachi, H.; Kamimura, T.; Yoshimura, M.; Mori, Y.; Yoshida, K.; Sasaki, T., Twin-free and High-Quality DAST Crystals - Effected through Solutions of Lower Supersaturation Coupled with Isothermal Solvent Evaporation. *Crystal Growth & Design* **2006,** *6* (11), 2463-2468.

41. Brunelle, D. J., Polycarbonates. In *Kirk-Othmer Encyclopedia of Chemical Technology*, John Wiley and Sons: Hoboken, NJ, 2001.

42. Campo, J.; Painelli, A.; Terenziani, F.; Regemorter, T. V.; Beljonne, D.; Goovaerts, E.; Wenseleers, W., First Hyperpolarizability Dispersion of the Octupolar Molecule Crystal Violet: Multiple Resonances and Vibrational and Solvation Effects. *Journal of the American Chemical Society* **2010,** *132* (46), 16467-16478.
43. Cao, J.; Berne, B. J., Theory and simulation of polar and nonpolar polarizable fluids. *Journal of Chemical Physics* **1993,** *99* (9), 6998-7011.

44. Cao, J.; Berne, B. J., Theory of polarizable liquid crystals: Optical birefringence. *Journal of Chemical Physics* **1993,** *99* (3), 2213-2220.

45. Caricato, M.; Mennucci, B.; Tomasi, J., Solvent Effects on the Electronic Spectra: An Extension of the Polarizable Continuum Model to the ZINDO Method. *Journal of Physical Chemistry A* **2004,** *108* (29), 6248-6256.

46. Chai, J. D.; Head-Gordon, M., Systematic optimization of long-range corrected hybrid density functionals. *Journal of Chemical Physics* **2008,** *128* (8), 084106.

47. Champagne, B.; Bulat, F. A.; Yang, W.; Bonness, S.; Kirtman, B., Density functional theory investigation of the polarizability and second hyperpolarizability of polydiacetylene and polybutatriene chains: treatment of exact exchange and role of correlation. *The Journal of Chemical Physics* **2006,** *125* (19), 194114.

48. Champagne, B.; Perpéte, E. A.; Gisbergen, S. J. A. v.; Baerends, E.-J.; Snijders, J. G.; Soubra-Ghaoui, C.; Robins, K. A.; Kirtman, B., Assessment of conventional density functional schemes for computing the polarizabilities and hyperpolarizabilities of conjugated oligomers: An ab initio investigation of polyacetylene chains. *Journal of Chemical Physics* **1998,** *109* (23), 10489-10498.

49. Champagne, B.; Perpéte, E. A.; Jacquemin, D.; Gisbergen, S. J. A. v.; Baerends, E.-J.; Soubra-Ghaoui, C.; Robins, K. A.; Kirtman, B., Assessment of Conventional Density Functional Schemes for Computing the Dipole Moment and (Hyper)polarizabilities of Push-Pull π-Conjugated Systems. *Journal of Physical Chemistry A* **2000,** *104* (20), 4755-4763.

50. Chen, A.; Chuyanov, V.; Garner, S.; Steier, W. H.; Dalton, L. R. In *Modified attenuated total reflection for the fast and routine electro-optic measurement of nonlinear optical polymer thin films*, Organic Thin Films for Photonics Applications, Long Beach, CA, Long Beach, CA, 1997; pp 158-160.

51. Chiappe, C.; Piccioli, P.; Pieraccini, D., Selective N-alkylation of anilines in ionic liquids. *Green Chemistry* **2006,** *8* (3), 277.

52. Čížek, J. i., On the Correlation Problem in Atomic and Molecular Systems. Calculation of Wavefunction Components in Ursell-Type Expansion Using Quantum-Field Theoretical Methods. *The Journal of Chemical Physics* **1966,** *45* (11), 4256.

53. Clark, J.; Lanzani, G., Organic photonics for communications. *Nature Photonics* **2010,** *4*, 438-446.

54. Clays, K.; Persoons, A., Hyper-Rayleigh Scattering in Solution. *Physical Review Letters* **1991,** *66* (23), 2980-2983.

55. Clays, K.; Persoons, A., Hyper-Rayleigh scattering in solution. *Review of Scientific Instruments* **1992,** *63* (6), 3285.

56. Cornell, W. D.; Cieplak, P.; Bayly, C. I.; Gould, I. R.; Kenneth M. Merz, J.; Ferguson, D. M.; Spellmeyer, D. C.; Fox, T.; Caldwell, J. W.; Kollman, P. A., A Second Generation Force Field for the Simulation of Proteins, Nucleic Acids, and Organic Molecules. *Journal of the American Chemical Society* **1995,** *117* (19), 5179-5197.

57. Cramer, C. J., *Essentials of Computational Chemistry: Theories and Models*. John Wiley & Sons Ltd.: Chinchester, UK, 2004.

58. Cyvin, S. J.; Rauch, J. E.; Decius, J. C., Theory of Hyper-Raman Effects (Nonlinear Inelastic Light Scattering): Selection Rules and Depolarization Ratios for the Second-Order Polarizability. *The Journal of Chemical Physics* **1965,** *43* (11), 4083.

59. Dalton, L. R.; Benight, S. J.; Johnson, L. E.; Knorr, D. B.; Kosilkin, I.; Eichinger, B. E.; Robinson, B. H.; Jen, A. K. Y.; Overney, R. M., Systematic Nanoengineering of Soft Matter Organic Electro-optic Materials. *Chemistry of Materials* **2011,** *23* (3), 430-445.

60. Dalton, L. R.; Harper, A. W.; Ghosn, R.; Steier, W. H.; Ziari, M.; Fetterman, H.; Shi, Y.; Mustachich, R. V.; Jen, A. K.-Y.; Shea, K. J., Synthesis and Processing of Improved Organic Second-Order Nonlinear Optical Materials for Applications in Photonics. *Chemistry of Materials* **1995,** *7* (6), 1060-1081.

61. Dalton, L. R.; Harper, A. W.; Robinson, B. H., The role of London forces in defining noncentrosymmetric order of high dipole moment–high hyperpolarizability chromophores in electrically poled polymeric thin films. *Proceedings of the National Academy of Sciences* **1997,** *94*, 4842-4847.

62. Dalton, L. R.; Steier, W. H.; Robinson, B. H.; Zhang, C.; Ren, A.; Garner, S.; Chen, A.; Londergan, T.; Irwin, L.; Carlson, B.; Fifield, L.; Phelan, G.; Kincaid, C.; Amend, J.; Jen, A., From molecules to opto-chips: organic electro-optic materials. *Journal of Materials Chemistry* **1999,** *9* (9), 1905-1920.

63. Dalton, L. R.; Sullivan, P. A.; Bale, D. H., Electric Field Poled Organic Electro-optic Materials: State of the Art and Future Prospects. *Chemical Reviews* **2010,** *110* (1), 25-55.

64. Darden, T.; York, D.; Pedersen, L., Particle mesh Ewald: An N•log(N) method for Ewald sums in large systems. *The Journal of Chemical Physics* **1993,** *98* (12), 10089-10092.

65. Davidson, E. R.; Eichinger, B. E.; Robinson, B. H., Hyperpolarizability: Calibration of theoretical methods for chloroform, water, acetonitrile, and p-nitroaniline. *Optical Materials* **2006,** *29* (4), 360-364.

66. Davies, J. A.; Elangovan, A.; Sullivan, P. A.; Olbricht, B. C.; Bale, D. H.; Ewy, T. R.; Isborn, C. M.; Eichinger, B. E.; Robinson, B. H.; Reid, P. J.; Li, X.; Dalton, L. R., Rational Enhancement of Second-Order Nonlinearity: Bis-(4-methoxyphenyl)hetero-aryl-amino Donor-Based Chromophores: Design, Synthesis, and Electrooptic Activity. *Journal of the American Chemical Society* **2008,** *130* (32), 10565-10575.
67. de Gennes, P. G.; Prost, J., *The Physics of Liquid Crystals*. Oxford University Press: Oxford, UK, 1993.

68. De Leeuw, S. W.; Perram, J. W.; Smith, E. R., Simulation of electrostatic systems in periodic boundary conditions. I. Lattice sums and dielectric constants. *Proceedings of the Royal Society of London, Series A: Mathematical, Physical and Engineering Sciences* **1980,** *373* (1752), 27-56.

69. De Leeuw, S. W.; Perram, J. W.; Smith, E. R., Computer Simulation of the Static Dielectric Constant of Systems with Permanent Electric Dipoles. *Annual Review of Physical Chemistry* **1986,** *37*, 245-270.

70. Debye, P., *Polar Molecules*. Dover Publications: New York, 1929.

71. Del Castillo, P.; Horobin, R. W.; Bláquez-Castro, A.; Stockert, J. C., Binding of cationic dyes to DNA: distinguishing intercalation and groove binding mechanisms using simple experimental and numerical models. *Biotechnic & Histochemistry* **2010,** *85* (4), 247-256.

72. Drenser, K. A.; Larsen, R. J.; Strohkendl, F. P.; Dalton, L. R., Femtosecond, Frequency-Agile, Phase-Sensitive-Detected, Multi-Wave-Mixing Nonlinear Optical Spectroscopy Applied to π-Electron Photonic Materials. *Journal of Physical Chemistry A* **1999,** *103* (14), 2290-2301.

73. Dreuw, A.; Head-Gordon, M., Failure of Time-Dependent Density Functional Theory for Long-Range Charge-Transfer Excited States: The Zincbacteriochlorin-Bacteriochlorin and Bacteriochlorophyll-Spheroidene Complexes. *Journal of the American Chemical Society* **2004,** *126* (12), 4007-4016.

74. Dreuw, A.; Head-Gordon, M., Single-Reference ab Initio Methods for the Calculation of Excited States of Large Molecules. *Chemical Reviews* **2005,** *105* (11), 4009-4037.

75. Edwards, D. M. F.; Madden, P. A., A computer simulation study of the dielectric properties of a model of methyl cyanide. II. The interference of permanent and induced dipoles. *Molecular Physics* **1984,** *51* (5), 1163-79.

76. Edwards, D. M. F.; Madden, P. A.; McDonald, I. R., A computer simulation study of the dielectric properties of a model of methyl cyanide. I. The rigid dipole case. *Molecular Physics* **1984,** *51* (5), 1141-61.

77. Ephardt, H.; Fromherz, P., Fluorescence of Amphiphilic Hemicyanine Dyes without Free Double Bonds. *Journal of Physical Chemistry* **1993,** *97* (17), 4540-4547.

78. Everaers, R.; Ejtehadi, M., Interaction potentials for soft and hard ellipsoids. *Physical Review E* **2003,** *67* (4).

79. Facchetti, A.; Abbotto, A.; Beverina, L.; Boom, M. E. v. d.; Dutta, P.; Evmenenko, G.; Pagani, G. A.; Marks, T. J., Layer-by-Layer Self-Assembled Pyrrole-Based Donor-Acceptor Chromophores as Electro-Optic Materials. *Chemistry of Materials* **2003,** *15* (5), 1064-1072.

80. Finn, R. S., Measurements of hyperpolarizabilities for some halogenated methanes. *The Journal of Chemical Physics* **1974,** *60* (2), 454.

81. Firestone, K. A. Frequency-agile hyper-Rayleigh scattering studies of nonlinear optical chromophores. University of Washington, Seattle, 2005.

82. Firestone, K. A.; Lao, D. B.; Casmier, D. M.; Clot, O.; Dalton, L. R.; Reid, P. J., Frequency-agile hyper-Rayleigh scattering studies of electro-optic chromophores. *Proceedings of SPIE* **2005,** *5395*, 59350P.

83. Firestone, K. A.; Reid, P.; Lawson, R.; Jang, S.-H.; Dalton, L. R., Advances in organic electro-optic materials and processing. *Inorganica Chimica Acta* **2004,** *357* (13), 3957-3966.

84. Firestone, M. A.; Ratner, M. A.; Marks, T. J., Electric Field Poling in Polymeric Nonlinear Optical Materials. Relaxation Dynamics, Model, and Experiment. *Macromolecules* **1995,** *28* (18), 6296-6310.

85. Francl, M. M.; Pietro, W. J.; Hehre, W. J.; Binkley, J. S.; Gordon, M. S.; DeFrees, D. J.; Pople, J. A., Self-consistent molecular orbital methods. XXIII. A polarization-type basis set for second-row elements. *Journal of Chemical Physics* **1982,** *77* (7), 3564-3665.

86. Frenkel, D., Computer simulations of hard-core models for liquid crystals. *Molecular Physics* **1987,** *60* (1), 1-20.

87. Frenkel, D., Onsager's Spherocylinders Revisited. *Journal of Physical Chemistry* **1987,** *91* (9), 4912-4916.

88. Frenkel, D., Smidt, B., *Understanding Molecular Simulation: From Algorithms to Applications*. Elsevier: Amsterdam (ND), 2002.

89. Frenkel, D.; Mulder, B.; McTague, J., Phase Diagram of a System of Hard Ellipsoids. *Physical Review Letters* **1984,** *52* (4), 287-290.

90. Frenkel, D.; Mulder, B. M., The hard ellipsoid-of-revolution fluid I. Monte Carlo simulations. *Molecular Physics* **1985,** *55* (5), 1171-1192.

91. Fries, P. H.; Richardi, J.; Krienke, H., Dielectric and structural results for liquid acetonitrile, acetone and chloroform from the hypernetted chain molecular integral equation. *Molecular Physics* **1997,** *90* (5), 841-853.

92. Fröhlich, H., *Theory of Dielectrics*. 2nd ed.; Clarendon Press: Oxford, UK, 1958.

93. Fromherz, P., Monopole-Dipole Model for Symmetrical Solvatochromism of Hemicyanine Dyes. *Journal of Physical Chemistry* **1995,** *99* (18), 7188-9192.

94. Gay, J. G., Modification of the overlap potential to mimic a linear site–site potential. *Journal of Chemical Physics* **1981,** *74* (6), 3316.

95. Gerratt, J.; Mills, I. M., Force Constants and Dipole-Moment Derivatives of Molecules from Perturbed Hartree-Fock Calculations. I. *The Journal of Chemical Physics* **1968,** *49* (4), 1719-1729.

96. Goldman, S., Determination of the static dielectric constant-temperature-density surfaces of a Stockmayer fluid by perturbation theory. *Molecular Physics* **1990,** *71* (3), 491-507.

97. Graham, H. W., Gymnodinium Catenatum, A New Dinoflagellate from the Gulf of California. *Transactions of the American Microscopical Society* **1943,** *62* (3), 259-261.

98. Gray, C. G.; Sainger, Y. S.; Joslin, C. G.; Cummings, P. T.; Goldman, S., Computer simulation of dipolar fluids. Dependence of the dielectric constant on system size: a comparative study of Ewald sum and reaction field approaches. *Journal of Chemical Physics* **1986,** *85* (3), 1502-4.

99. Greengard, L., Fast Algorithms for Classical Physics. *Science* **1994,** *265* (5174), 909-914.

100. Greenlee, C.; Guilmo, A.; Opadeyi, A.; Himmelhuber, R.; Norwood, R. A.; Fallahi, M.; Luo, J.; Huang, S.; Zhou, X.-H.; Jen, A. K. Y.; Peyghambarian, N., Mach-Zehnder interferometry method for decoupling electro-optic and piezoelectric tensor components in poled polymer films. **2010**, 77740D-77740D-10.

101. Groh, B.; Dietrich, S., Orientational order in dipolar fluids consisting of nonspherical hard particles. *Physical Review E: Statistical Physics, Plasmas, Fluids, and Related Interdisciplinary Topics* **1997,** *55* (3-A), 2892-2901.

102. Groh, B.; Dietrich, S., Spatial structures of dipolar ferromagnetic liquids. *Physical Review Letters* **1997,** *79* (4), 749-752.

103. Grote, J. G.; Diggs, D. E.; Nelson, R. L.; Zetts, J. S.; Hopkins, F. K.; Ogata, N.; Hagen, J. A.; Heckman, E.; Yaney, P. P.; Stone, M. O.; Dalton, L. R., DNA Photonics [Deoxyribonucleic Acid]. *Molecular Crystals and Liquid Crystals* **2005,** *426* (1), 3-17.

104. Grote, J. G.; Ogata, N.; Hagen, J. A.; Heckman, E.; Curley, M. J.; Yaney, P. P.; Stone, M. O.; Diggs, D. E.; Nelson, R. L.; Zetts, J. S.; Hopkins, F. K.; Dalton, L. R., Deoxyribonucleic Acid (DNA) based nonlinear optics. *Proceedings of SPIE* **2003,** *5211*, 53-62.

105. Halgren, T. A., Merck Molecular Force Field. I. Basis, Form, Scope, Parameterization, and Performance of MMFF94. *Journal of Computational Chemistry* **1996,** *17* (5), 490-519.

106. Hammond, J. R.; Kowalski, K., Parallel computation of coupled-cluster hyperpolarizabilities. *The Journal of Chemical Physics* **2009,** *130* (19), 194108.

107. Hammond, S. R.; Clot, O.; Firestone, K. A.; Bale, D. H.; Lao, D.; Haller, M.; Phelan, G. D.; Carlson, B.; Jen, A. K.-Y.; Reid, P. J.; Dalton, L. R., Site-Isolated Electro-optic Chromophores Based on Substituted 2,2′-Bis(3,4-propylenedioxythiophene) π-Conjugated Bridges. *Chemistry of Materials* **2008,** *20* (10), 3425-3434.

108. Handgraaf, J.-W.; Serral Gracia, R.; Nath, S. K.; Chen, Z.; Chou, S.-H.; Ross, R. B.; Schultz, N. E.; Fraaije, J. G. E. M., A Multiscale Modeling Protocol To Generate Realistic Polymer Surfaces. *Macromolecules* **2011,** *44* (4), 1053-1061.

109. Hansen, J.-P., McDonald, I.R., *Theory of Simple Liquids*. 3rd ed.; Elsevier: Amsterdam, Netherlands, 2006.

110. Hayden, L. M.; Sauter, G. F.; Ore, F. R.; Pasillas, P. L.; Hoover, J. M.; Lindsay, G. A.; Henry, R. A., Second-order nonlinear optical measurements in guest-host and side-chain polymers. *Journal of Applied Physics* **1990,** *68* (2), 456.

111. Head-Gordon, M.; Rico, R. J.; Oumi, M.; Lee, T. J., A doubles correction to electronic excited states from configuration interaction in the space of single substitutions. *Chemical Physics Letters* **1994,** *219*, 21-29.

112. Heckman, E. The Development of an All-DNA-Based Electro-Optic Waveguide Modulator. University of Dayton, Dayton, OH, 2006.

113. Heckman, E. M., Poling and optical studies of DNA NLO waveguides. *Proceedings of SPIE* **2005,** *5934*, 593408-593408-7.

114. Heckman, E. M.; Hagen, J. A.; Yaney, P. P.; Grote, J. G.; Hopkins, F. K., Processing techniques for deoxyribonucleic acid: Biopolymer for photonics applications. *Applied Physics Letters* **2005,** *87* (21), 211115.

115. Heckman, E. M.; Yaney, P. P.; Grote, J. G.; Hopkins, F. K., Development and performance of an all-DNA-based electro-optic waveguide modulator. *Proceedings of SPIE* **2006,** *6401*, 640108-640108-10.

116. Hohenberg, P.; Kohn, W., Inhomogeneous Electron Gas. *Physical Review* **1964,** *136* (3B), B864-B871.

117. Houssa, M.; Rull, L. F.; McGrother, S. C., Effect of dipolar interactions on the phase behavior of the Gay–Berne liquid crystal model. *The Journal of Chemical Physics* **1998,** *109* (21), 9529.

118. Isborn, C. M.; Davidson, E. R.; Robinson, B. H., Ab Initio Diradical/Zwitterionic Polarizabilities and Hyperpolarizabilities in Twisted Double Bonds. *Journal of Physical Chemistry A* **2006,** *110* (22), 7189-7196.

119. Isborn, C. M.; Leclercq, A.; Vila, F. D.; Dalton, L. R.; Brédas, J. L.; Eichinger, B. E.; Robinson, B. H., Comparison of Static First Hyperpolarizabilities Calculated with Various Quantum Mechanical Methods. *Journal of Physical Chemistry A* **2007,** *111* (7), 1319-1327.

120. Izvekov, S.; Voth, G. A., Multiscale coarse graining of liquid-state systems. *Journal of Chemical Physics* **2005,** *123* (13), 134105.

121. Jackson, P. O.; Karapinar, R.; O'Neill, M.; Hindmarsh, P.; J.Owen, G.; Kelly, S. M., Alignment models for coumarin-containing polymers for liquid crystal. *Proceedings of SPIE* **1999,** *3635*, 38-47.

122. Jacquemin, D.; Champagne, B.; Andre, J.-M., Møller–Plesset evaluation of the static first hyperpolarizability of polymethineimine. *Chemical Physics Letters* **1998,** *284* 24-30.

123. Jacquemin, D.; Champagne, B.; Hättig, C., Correlated frequency-dependent electronic first hyperpolarizability of small push–pull conjugated chains. *Chemical Physics Letters* **2000,** *319*, 327-334.

124. Jacquemin, D.; Perpete, E. A.; Medved, M.; Scalmani, G.; Frisch, M. J.; Kobayashi, R.; Adamo, C., First hyperpolarizability of polymethineimine with long-range corrected functionals. *The Journal of Chemical Physics* **2007,** *126* (19), 191108.

125. Jacquemin, D.; Perpéte, E. A.; Scuseria, G. E.; Ciofini, I.; Adamo, C., TD-DFT Performance for the Visible Absorption Spectra of Organic Dyes: Conventional versus Long-Range Hybrids. *Journal of Chemical Theory and Computation* **2008,** *4* (1), 123-135.

126. Jang, S.-H.; Luo, J.; Tucker, N. M.; Leclercq, A.; Zojer, E.; Haller, M. A.; Kim, T.-D.; Kang, J.-W.; Firestone, K.; Bale, D.; Lao, D.; Benedict, J. B.; Cohen, D.; Kaminsky, W.; Kahr, B.; Brédas, J.-L.; Reid, P.; Dalton, L. R.; Jen, A. K.-Y., Pyrroline Chromophores for Electro-Optics. *Chemistry of Materials* **2006,** *18* (13), 2982-2988.

127. Jia, R.; Hentschke, R., Dipolar particles in an external field: Molecular dynamics simulation and mean field theory. *Physical Review E: Statistical, Nonlinear, and Soft Matter Physics* **2009,** *80* (5-1), 051502/1-051502/9.

128. Johal, M. S., *Understanding Nanomaterials*. CRC Press: Boca Raton, FL, 2011.

129. Johnson, L. E.; Barnes, R.; Draxler, T. W.; Eichinger, B. E.; Robinson, B. H., Dielectric Constants of Simple Liquids: Stockmayer and Ellipsoidal Fluids. *Journal of Physical Chemistry B* **2010,** *114* (25), 8431-8440.

130. Johnson, L. E.; Benight, S. J.; Rawal, M.; Robinson, B. H. *NLO Chromophore/Surfactant Systems for Biophotonics Applications (Report to AFRL)*; University of Washington: 2010.

131. Jones, R. C., A New Calculus for the Treatment of Optical Systems. *Journal of the Optical Society of America* **1941,** *31*, 488-493.

132. Jorgensen, W. L.; Briggs, J. M.; Contreras, M. L., Relative partition coefficients for organic solutes from fluid simulations. *Journal of Physical Chemistry* **1990,** *94* (4), 1683-6.

133. Jorgensen, W. L.; Tirado-Rives, J., The OPLS Potential Functions for Proteins. Energy Minimizations for Crystals of Cyclic Peptides and Crambin. *Journal of the American Chemical Society* **1988,** *110* (6), 1657-1666.

134. Jung, Y.; Lochan, R. C.; Dutoi, A. D.; Head-Gordon, M., Scaled opposite-spin second order Moller-Plesset correlation energy: an economical electronic structure method. *Journal of Chemical Physics* **2004,** *121* (20), 9793-802.

135. Kaino, T.; Tomaru, S., Organic Materials for Nonlinear Optics. *Advanced Materials* **1993,** *5* (3), 172-178.

136. Kaminski, G.; Jorgensen, W. L., Performance of the AMBER94, MMFF94, and OPLS-AA Force Fields for Modeling Organic Liquids. *Journal of Physical Chemistry* **1996,** *100* (46), 18010-18013.

137. Karlstrom, G., Formation of ferroelectric domains observed in simulation of droplets of dipolar particles. *The journal of physical chemistry B* **2007,** *111* (36), 10745-58.

138. Kim, T.-D.; Kang, J.-W.; Luo, J.; Jang, S.-H.; Ka, J.-W.; Tucker, N.; Benedict, J. B.; Dalton, L. R.; Gray, T.; Overney, R. M.; Park, D. H.; Herman, W. N.; Jen, A. K.-Y., Ultralarge and Thermally Stable Electro-Optic Activities from Supramolecular Self-Assembled Molecular Glasses. *Journal of the American Chemical Society* **2007,** *129* (3), 488-489.

139. Kim, W.-K.; Hayden, L. M., Fully atomistic modeling of an electric field poled guest-host nonlinear optical polymer. *Journal of Chemical Physics* **1999,** *111* (11), 5212-5222.

140. Kirkwood, J. G., The dielectric polarization of polar liquids. *Journal of Chemical Physics* **1939,** *7*, 911-19.

141. Klapp, S. H. L.; Schoen, M., Spontaneous orientational order in confined dipolar fluid films. *Journal of Chemical Physics* **2002,** *117* (17), 8050-8062.

142. Knorr, D. B., Jr.; Zhou, X. H.; Shi, Z.; Luo, J.; Jang, S. H.; Jen, A. K.; Overney, R. M., Molecular mobility in self-assembled dendritic chromophore glasses. *J Phys Chem B* **2009,** *113* (43), 14180-8.

143. Kobayashi, R.; Koch, H.; Jørgensen, P., Calculation of frequency-dependent polarizabilities using coupled-cluster response theory. *Chemical Physics Letters* **1994,** *219*, 30-35.

144. Kohn, W.; Sham, L. J., Self-Consistent Equations Including Exchange and Correlation Effects. *Physical Review* **1965,** *140* (4A), A1133-A1138.

145. Koos, C.; Vorreau, P.; Vallaitis, T.; Dumon, P.; Bogaerts, W.; Baets, R.; Esembeson, B.; Biaggio, I.; Michinobu, T.; Diederich, F.; Freude, W.; Leuthold, J., All-optical high-speed signal processing with silicon–organic hybrid slot waveguides. *Nature Photonics* **2009,** *3* (4), 216-219.

146. Kumar, P.; Franzese, G.; Buldyrev, S. V.; Stanley, H. E., Molecular dynamics study of orientational cooperativity in water. *Physical Review E: Statistical, Nonlinear, and Soft Matter Physics* **2006,** *73* (4-1), 041505/1-041505/8.

147. Kusalik, P. G., Computer simulation results for the dielectric properties of a highly polar fluid. *The Journal of Chemical Physics* **1990,** *93* (5), 3520.

148. Kuzyk, M. G.; Singer, K. D.; Zahn, H. E.; King, L. A., Second-order nonlinear-optical tensor properties of poled films under stress. *Journal of the Optical Society of America B* **1989,** *6* (4), 742-752.

149. Kwon, O. P.; Kwon, S.-J.; Jazbinsek, M.; Brunner, F. D. J.; Seo, J.-I.; Hunziker, C.; Schneider, A.; Yun, H.; Lee, Y.-S.; Günter, P., Organic Phenolic Configurationally Locked Polyene Single Crystals for Electro-optic and Terahertz Wave Applications. *Advanced Functional Materials* **2008,** *18* (20), 3242-3250.

150. Lange, A.; Herbert, J. M., Simple Methods To Reduce Charge-Transfer Contamination in Time-Dependent Density-Functional Calculations of Clusters and Liquids. *Journal of Chemical Theory and Computation* **2007,** *3* (5), 1680-1690.

151. Leach, A. R., *Molecular Modeling: Principles and Applications*. 2nd ed.; Pearson Education: Harlow (UK), 2001.

152. Leadbeater, N. E.; Williams, V. A.; Barnard, T. M.; Collins, M. J., Open-Vessel Microwave-Promoted Suzuki Reactions Using Low Levels of Palladium Catalyst: Optimization and Scale-Up. *Organic Process Research & Development* **2006,** *10* (4), 833-837.

153. Leahy-Hoppa, M. R.; Cunningham, P. D.; French, J. A.; Hayden, L. M., Atomistic Molecular Modeling of the Effect of Chromophore Concentration on the Electro-optic Coefficient in Nonlinear Optical Polymers. *The Journal of Physical Chemistry A* **2006,** *110* (17), 5792-5797.

154. Lee, M.; Katz, H. E.; Erben, C.; Gill, D. M.; Gopalan, P.; Heber, J. D.; McGee, D. J., Broadband Modulation of Light by Using an Electro-Optic Polymer. *Science* **2002,** *298*, 1401-1403.

155. Lee, S.; Park, S. S., Dielectric properties of organic solvents from non-polarizable molecular dynamics simulation with electronic continuum model and density functional theory. *J Phys Chem B* **2011,** *115* (43), 12571-6.

156. Levesque, D.; Weis, J. J., On the Calculation of Dielectric Properties from Computer Simulations. *Physica A* **1984,** *125*, 270-274.

157. Levine, B. F., Absolute signs of hyperpolarizabilities in the liquid state. *The Journal of Chemical Physics* **1974,** *60* (10), 3856.

158. Levine, I. N., *Quantum Chemistry*. Prentice-Hall, Inc.: Upper Saddle River, NJ, 2000.

159. Liang, W.; Li, X.; Dalton, L. R.; Robinson, B. H.; Eichinger, B. E., Solvents level dipole moments. *J Phys Chem B* **2011,** *115* (43), 12566-70.

160. Liao, Y.; Anderson, C. A.; Sullivan, P. A.; Akelaitis, A. J. P.; Robinson, B. H.; Dalton, L. R., Electro-Optical Properties of Polymers Containing Alternating Nonlinear Optical Chromophores and Bulky Spacers. *Chemistry of Materials* **2006,** *18* (4), 1062-1067.

161. Liao, Y.; Bhattacharjee, S.; Firestone, K. A.; Eichinger, B. E.; Paranji, R.; Anderson, C. A.; Robinson, B. H.; Reid, P. J.; Dalton, L. R., Antiparallel-Aligned Neutral-Ground-State and Zwitterionic Chromophores as a Nonlinear Optical Material. *Journal of the American Chemical Society* **2005,** *128* (21), 6847-6853.

162. Liao, Y.; Eichinger, B. E.; Firestone, K. A.; Haller, M.; Luo, J.; Kaminsky, W.; Benedict, J. B.; Reid, P. J.; Jen, A. K.-Y.; Dalton, L. R.; Robinson, B. H., Systematic Study of the Structure-Property Relationship of a Series of Ferrocenyl Nonlinear Optical Chromophores. *Journal of the American Chemical Society* **2005,** *127* (8), 2758-2766.

163. Lide, D. R., *CRC Handbook of Chemistry and Physics*. 90th ed.; CRC Press: Baton Rouge, LA, 2009.

164. Liu, A.; Jones, R.; Liao, L.; Samara-Rubio, D.; Rubin, D.; Cohen, O.; Nicolaescu, R.; Paniccia, M., A high-speed silicon optical modulator based on a metal–oxide–semiconductor capacitor. *Nature* **2004,** *427*, 615-618.

165. Liu, L.; Zhang, Y.; Wang, Y., Phosphine-free palladium acetate catalyzed Suzuki reaction in water. *J Org Chem* **2005,** *70* (15), 6122-5.

166. Lu, S. I., Computational study of static first hyperpolarizability of donor-acceptor substituted (E)-benzaldehyde phenylhydrazone. *Journal of Computational Chemistry* **2011,** *32* (4), 730-6.

167. Luo, J.; Huang, S.; Shi, Z.; Polishak, B. M.; Zhou, X.-H.; Jen, A. K. Y., Tailored Organic Electro-optic Materials and Their Hybrid Systems for Device Applications. *Chemistry of Materials* **2011,** *23* (3), 544-553.

168. Luo, J.; Zhou, X.-H.; Jen, A. K. Y., Rational molecular design and supramolecular assembly of highly efficient organic electro-optic materials. *Journal of Materials Chemistry* **2009,** *19* (40), 7410.

169. Ma, H.; Chen, B.; Sassa, T.; Dalton, L. R.; Jen, A. K.-Y., Highly Efficient and Thermally Stable Nonlinear Optical Dendrimer for Electrooptics. *Journal of the American Chemical Society* **2001,** *123* (5), 986-987.

170. Magyar, R. J.; Tretiak, S., Dependence of Spurious Charge-Transfer Excited States on Orbital Exchange in TDDFT: Large Molecules and Clusters. *Journal of Chemical Theory and Computation* **2007,** *3* (3), 976-987.

171. Makowska-Janusik, M.; Reis, H.; Papadopoulos, M. G.; Economou, I. G.; Zacharopoulos, N., Molecular Dynamics Simulations of Electric Field Poled Nonlinear Optical Chromophores Incorporated in a Polymer Matrix. *Journal of Physical Chemistry B* **2004,** *108* (2), 588-596.

172. Mansuripur, M., Analysis of multilayer thin-film structures containing magneto-optic and anisotropic media at oblique incidence using 2×2 matrices. *Journal of Applied Physics* **1990,** *67* (10), 6466.

173. March, N. H.; Tosi, M. P., *Atomic Dynamics in Liquids*. Dover Publications, Inc.: New York, NY, 1976.

174. Maurer, R. D., Glass Fibers for Optical Communications. *Proceedings of the IEEE* **1973,** *61* (4), 452-462.

175. McGrother, S. C.; Gil-Villegas, A.; Jackson, G., The effect of dipolar interactions on the liquid crystalline phase transitions of hard spherocylinders with central longitudinal dipoles. *Molecular Physics* **1998,** *95* (3), 657-673.

176. McLachlan, A.; Ball, M., Time-Dependent Hartree—Fock Theory for Molecules. *Reviews of Modern Physics* **1964,** *36* (3), 844-855.

177. McQuarrie, D. A., *Statistical Mechanics*. University Science Books: Sausalito, CA, 2000.

178. McQuarrie, D. A.; Simon, J. D., *Physical Chemistry: A Molecular Approach*. University Science Books: Sausalito, CA, 1997.

179. Melikian, G.; Rouessac, F. P.; Alexandre, C., Synthesis of Substituted Dicyanomethylendihydrofurans. *Synthetic Communications* **1995,** *25*, 3045-3051.

180. Melnichuk, M.; Wood, L., Direct Kerr electro-optic effect in noncentrosymmetric materials. *Physical Review A* **2010,** *82* (1), 013821.

181. Metropolis, N., Rosenbluth, A. W., Rosenbluth, M. N., Teller, A H., Teller, E., Equation of State Calculations by Fast Computing Machines. *Journal of Chemical Physics* **1953,** *21* (6), 1087-1092.

182. Meyers, F.; Marder, S. R.; Pierce, B. M.; Brédas, J. L., Electric Field Modulated Nonlinear Optical Properties of Donor- Acceptor Polyenes: Sum-Over-States Investigation of the Relationship between Molecular Polarizabilities (α,β, and γ) and Bond Length Alternation. *Journal of the American Chemical Society* **1994,** *116* (23), 10703-10714.

183. Millefiori, S.; Alparone, A., Second hyperpolarisability of furan homologues C4H4X (X = O, S, Se, Te): ab initio HF and DFT study. *Chemical Physics Letters* **2000,** *332*, 175-180.

184. Mitus, A. C.; Pawlik, G.; Kochalska, A.; Mysliwiec, J.; Miniewicz, A.; Kajzar, F., Experimental and Monte Carlo studies of diffraction grating inscription in DNA-based materials. **2007,** *6646*, 66460I-66460I-8.

185. Møller, C.; Plesset, M. S., Note on an Approximation Treatment for Many-Electron Systems. *Physical Review* **1934,** *46* (7), 618-622.

186. Mortazavi, M. A.; Knoesen, A.; Kowel, S. T.; Higgins, B. G.; Dienes, A., Second-harmonic generation and absorption studies of polymer-dye films oriented by corona-onset poling at elevated temperatures. *Journal of the Optical Society of America B* **1989,** *6* (4), 733-741.

187. Nelson, J. W.; Tinoco, I., Intercalation of Ethidium Ion into DNA and RNA Oligonucleotides. *Biopolymers* **1984,** *23* (2), 213-233.

188. Neumann, M., Dipole moment fluctuation formulas in computer simulations of polar systems. *Molecular Physics* **1983,** *50* (4), 841-58.

189. Neumann, M.; Steinhauser, O., The influence of boundary conditions used in machine simulations on the structure of polar systems. *Molecular Physics* **1980,** *39* (2), 437-54.

190. Neumann, M.; Steinhauser, O.; Pawley, G. S., Consistent calculation of the static and frequency-dependent dielectric constant in computer simulations. *Molecular Physics* **1984,** *52* (1), 97-113.

191. Nielsen, R. D.; Rommel, H. L.; Robinson, B. H., Simulation of the Loading Parameter in Organic Nonlinear Optical Materials. *Journal of Physical Chemistry B* **2004,** *108* (25), 8659-8667.

192. Nordmeier, E., Absorption spectroscopy and dynamic and static light-scattering studies of ethidium bromide binding to calf thymus DNA: implications for outside-binding and intercalation. *Journal of Physical Chemistry* **1992,** *96* (14), 6045-6055.

193. O'Neill, D. P.; Kallay, M.; Gauss, J., Calculation of frequency-dependent hyperpolarizabilities using general coupled-cluster models. *The Journal of Chemical Physics* **2007,** *127* (13), 134109.

194. Olbrechts, G.; Wostyn, K.; Clays, K.; Persoons, A., High-frequency demodulation of multiphoton fluorescence in long-wavelength hyper-Rayleigh scattering. *Optics Letters* **1999,** *24* (6), 403-405.

195. Olbricht, B. C. Characterization and processing of organic nonlinear optical materials using ellipsometric, waveguiding, and absorption spectroscopy techniques. University of Washington, Seattle, WA, 2010.

196. Olbricht, B. C.; Sullivan, P. A.; Dennis, P. C.; Hurst, J. T.; Johnson, L. E.; Benight, S. J.; Davies, J. A.; Chen, A.; Eichinger, B. E.; Reid, P. J.; Dalton, L. R.; Robinson, B. H., Measuring Order in Contact-Poled Organic Electrooptic Materials with Variable-Angle Polarization-Referenced Absorption Spectroscopy (VAPRAS). *Journal of Physical Chemistry B* **2011,** *115* (2), 231-241.

197. Olbricht, B. C.; Sullivan, P. A.; Wen, G.-A.; Mistry, A. A.; Davies, J. A.; Ewy, T. R.; Eichinger, B. E.; Robinson, B. H.; Reid, P. J.; Dalton, L. R., Laser-Assisted Poling of Binary Chromophore Materials. *Journal of Physical Chemistry C* **2008,** *112* (21), 7983-7988.

198. Onodera, H.; Awal, I.; Ikenoue, J.-i., Refractive-index measurement of bulk materials: prism coupling method. *Applied Optics* **1983,** *22* (8), 1194-1197.

199. Onsager, L., Electric moments of molecules in liquids. *Journal of the American Chemical Society* **1936,** *58*, 1486-93.

200. Onsager, L., The Effects of Shape on the Interaction of Colloidal Particles. *Annals of the New York Academy of Sciences* **1949,** *51*, 627-659.

201. Oudar, J. L.; Chemla, D. S., Hyperpolarizabilities of the nitroanilines and their relations to the excited state dipole moment. *The Journal of Chemical Physics* **1977,** *66* (6), 2664-2668.

202. Ouyang, W.-Z.; Hentschke, R., From gas-liquid to liquid crystalline phase behavior via anisotropic attraction: A computer simulation study. *Journal of Chemical Physics* **2007,** *127* (16), 164501/1-164501/7.

203. Paldus, J.; Čížek, J.; Jeziorski, B., Coupled cluster approach or quadratic configuration interaction? *The Journal of Chemical Physics* **1989,** *90* (8), 4356.

204. Pan, F.; Wong, M. S.; Bosshard, C.; Günter, P., Crystal Growth and Characterization of the Organic Salt 4-N,N-Dimethylamino-4′-N′- methyl-stilbazolium Tosylate (DAST). *Advanced Materials* **1996,** *8* (7), 592-595.

205. Paniccia, M.; Krutul, V.; Koehl, S. *Introducing Intel's Advances in Silicon Photonics*; Intel Corp.: Santa Clara, CA, 2004.

206. Panja, N.; Ghanty, T. K.; Nandi, P. K., A sum-over-state scheme of analysis of hyperpolarizabilities and its application to spiroconjugated molecular system. *Theoretical Chemistry Accounts* **2009,** *126* (5-6), 323-337.

207. Patey, G. N.; Levesque, D.; Weis, J. J., On the theory and computer simulation of dipolar fluids. *Molecular Physics* **1982,** *45* (3), 733-46.

208. Pawlik, G.; Mitus, A. C.; Mysliwiec, J.; Miniewicz, A.; Grote, J. G., Photochromic dye semi-intercalation into DNA-based polymeric matrix: Computer modeling and experiment. *Chemical Physics Letters* **2010,** *484* (4-6), 321-323.

209. Perdew, J. P.; Ernzerhof, M.; Burke, K., Rationale for mixing exact exchange with density functional approximations. *Journal of Chemical Physics* **1996,** *105* (22), 9982-9985.

210. Perram, J. W.; Petersen, H. G.; De Leeuw, S. W., An algorithm for the simulation of condensed matter which grows as the 3/2 power of the number of particles. *Molecular Physics* **1988,** *65* (4), 875-93.

211. Perram, J. W.; Wertheim, M. S., Statistical mechanics of hard ellipsoids. I. Overlap algorithm and the contact function. *Journal of Computational Physics* **1985,** *58* (3), 409-16.

212. Peter, C.; Kremer, K., Multiscale simulation of soft matter systems – from the atomistic to the coarse-grained level and back. *Soft Matter* **2009,** *5* (22), 4357.

213. Peter, C.; Kremer, K., Multiscale simulation of soft matter systems. *Faraday Discussions* **2010,** *144*, 9.

214. Pohl, F. M.; Jovin, T. M.; Baehr, W.; Holbrook, J. J., Ethidium Bromide as a Cooperative Effector of a DNA Structure. *Proceedings of the National Academy of Sciences* **1972,** *69* (12), 3805-3809.

215. Ponder, J. W.; Wu, C.; Ren, P.; Pande, V. S.; Chodera, J. D.; Schnieders, M. J.; Haque, I.; Mobley, D. L.; Lambrecht, D. S.; DiStasio Jr., R. A.; Head-Gordon, M.; Clark, G. N. I.; Johnson, M. E.; Head-Gordon, T., Current Status of the AMOEBA Polarizable Force Field. *Journal of Physical Chemistry B* **2010,** *114* (8), 2549-2564.

216. Pople, J. A.; Beveridge, D. L.; Dobosh, P. A., Approximate Self-Consistent Molecular-Orbital Theory. V. Intermediate Neglect of Differential Overlap. *Journal of Chemical Physics* **1967,** *47* (6), 2026-2033.

217. Pounds, M. A.; Madden, P. A., Are dipolar liquids ferroelectric? Simulation studies. *Journal of Chemical Physics* **2007,** *126* (10), 104506/1-104506/7.

218. Praprotnik, M.; Site, L. D.; Kremer, K., Multiscale simulation of soft matter: from scale bridging to adaptive resolution. *Annual review of physical chemistry* **2008,** *59*, 545-71.

219. Press, W. H., Teukolsky, S.A., Vetterling, W.T., Flannery, B.P., *Numerical Recipes in C*. 2nd ed.; Cambridge University Press: Cambridge (UK), 1992.

220. Press, W. H., Teukolsky, S.A., Vetterling, W.T., Flannery, B.P., *Numerical Recipes*. 3rd ed.; Cambridge University Press: Cambridge (UK), 2007.

221. Reed, G. T.; Mashanovich, G.; Gardes, F. Y.; Thomson, D. J., Silicon optical modulators. *Nature Photonics* **2010,** *4* (8), 518-526.

222. Reis, H., Problems in the comparison of theoretical and experimental hyperpolarizabilities revisited. *Journal of Chemical Physics* **2006,** *125* (1), 014506.

223. Rice, J. E.; Handy, N., The calculation of frequency-dependent polarizabilities as pseudo-energy derivatives. *Journal of Chemical Physics* **1991,** *94* (7), 4959-4971.

224. Rice, J. E.; Handy, N. C., The calculation of frequency-dependent polarizabilities as pseudo-energy derivatives. *Journal of Chemical Physics* **1991,** *94* (7), 4959-4971.

225. Risko, C.; McGehee, M. D.; Brédas, J.-L., A quantum-chemical perspective into low optical-gap polymers for highly-efficient organic solar cells. *Chemical Science* **2011,** *2* (7), 1200.

226. Robinson, B. H.; Dalton, L. R., Monte Carlo statistical mechanical simulations of the competition of intermolecular electrostatic and poling-field interactions in defining macroscopic electro-optic activity for organic chromophore/polymer materials. *Journal of Physical Chemistry A* **2000,** *104* (20), 4785-4795.

227. Rommel, H. L.; Robinson, B. H., Orientation of Electro-optic Chromophores under Poling Conditions: A Spheroidal Model. *Journal of Physical Chemistry C* **2007,** *111* (50), 18765-18777.

228. Ruiz, B.; Jazbinsek, M.; Günter, P., Crystal Growth of DAST. *Crystal Growth & Design* **2008,** *8* (11), 4173-4184.

229. Runge, E.; Gross, E. K. U., Density-Functional Theory for Time-Dependent Systems. *Physical Review Letters* **1984,** *52* (12), 997-1000.

230. Saiz, L.; Guardia, E.; Padro, J.-A., Dielectric properties of liquid ethanol. A computer simulation study. *Journal of Chemical Physics* **2000,** *113* (7), 2814-2822.

231. Samoc, M.; Samoc, A.; Miniewicz, A.; Markowicz, P. P.; Prasad, P. N.; Grote, J. G., Cubic nonlinear optical effects in deoxyribonucleic acid (DNA) based materials containing chromophores. **2007,** *6646*, 66460A-66460A-10.

232. Schurr, J. M., Dielectric relaxation and depolarized dynamic light scattering of a generalized Debye model fluid. *Molecular Physics* **1980,** *40* (5), 1025-51.

233. Schwabe, T.; Grimme, S., Towards chemical accuracy for the thermodynamics of large molecules: new hybrid density functionals including non-local correlation effects. *Phys Chem Chem Phys* **2006,** *8* (38), 4398-401.

234. Schwegler, E.; Challacombe, M., Linear scaling computation of the Hartree–Fock exchange matrix. *Journal of Chemical Physics* **1996,** *105* (7), 2726-2734.

235. Shao, Y.; Molnar, L. F.; Jung, Y.; Kussmann, J.; Ochsenfeld, C.; Brown, S. T.; Gilbert, A. T.; Slipchenko, L. V.; Levchenko, S. V.; O'Neill, D. P.; DiStasio, R. A., Jr.; Lochan, R. C.; Wang, T.; Beran, G. J.; Besley, N. A.; Herbert, J. M.; Lin, C. Y.; Van Voorhis, T.; Chien, S. H.; Sodt, A.; Steele, R. P.; Rassolov, V. A.; Maslen, P. E.; Korambath, P. P.; Adamson, R. D.; Austin, B.; Baker, J.; Byrd, E. F.; Dachsel, H.; Doerksen, R. J.; Dreuw, A.; Dunietz, B. D.; Dutoi, A. D.; Furlani, T. R.; Gwaltney, S. R.; Heyden, A.; Hirata, S.; Hsu, C. P.; Kedziora, G.; Khalliulin, R. Z.; Klunzinger, P.; Lee, A. M.; Lee, M. S.; Liang, W.; Lotan, I.; Nair, N.; Peters, B.; Proynov, E. I.; Pieniazek, P. A.; Rhee, Y. M.; Ritchie, J.; Rosta, E.; Sherrill, C. D.; Simmonett, A. C.; Subotnik, J. E.; Woodcock, H. L., 3rd; Zhang, W.; Bell, A. T.; Chakraborty, A. K.; Chipman, D. M.; Keil, F. J.; Warshel, A.; Hehre, W. J.; Schaefer, H. F., 3rd; Kong, J.; Krylov, A. I.; Gill, P. M.; Head-Gordon, M., Advances in methods and algorithms in a modern quantum chemistry program package. *Phys Chem Chem Phys* **2006,** *8* (27), 3172-91.

236. Shelton, D. P., Are dipolar liquids ferroelectric? *Journal of Chemical Physics* **2005,** *123* (8), 084502/1-084502/8.

237. Shi, Q.; Izvekov, S.; Voth, G. A., Mixed Atomistic and Coarse-Grained Molecular Dynamics: Simulation of a Membrane-Bound Ion Channel. *Journal of Physical Chemistry B* **2006,** *110* (31), 15045-15048.

238. Shi, Y.; Zhang, C.; Zhang, H.; Bechtel, J. H.; Dalton, L. R.; Robinson, B. H.; Steier, W. H., Low (Sub-1-Volt) Halfwave Voltage Polymeric Electro-optic Modulators Achieved by Controlling Chromophore Shape. *Science* **2000,** *288* (5463), 119-122.

239. Sim, F.; Chin, S.; Dupuis, M., Electron Correlation Effects in Hyperpolarizabilities of p-Nitroaniline. *Journal of Physical Chemistry* **1993,** *97* (6), 1158-1163.

240. Singer, K. D.; Kuzyk, M. G.; Sohn, J. E., Second-order nonlinear-optical processes in orientationally ordered materials: relationship between molecular and macroscopic properties. *Journal of the Optical Society of America B* **1987,** *4* (6), 968-976.

241. Singer, K. D.; Sohn, J. E.; Lalama, S. J., Second harmonic generation in poled polymer films. *Applied Physics Letters* **1986,** *49* (5), 248.

242. Sini, G.; Sears, J. S.; Brédas, J.-L., Evaluating the Performance of DFT Functionals in Assessing the Interaction Energy and Ground-State Charge Transfer of Donor/Acceptor Complexes: Tetrathiafulvalene−Tetracyanoquinodimethane (TTF−TCNQ) as a Model Case. *Journal of Chemical Theory and Computation* **2011,** *7* (3), 602-609.

243. Skaf, M. S., Static dielectric properties of a model for liquid DMSO. *Molecular Physics* **1997,** *90* (1), 25-34.

244. Slone, R. V., Methacrylic Polymers. In *Kirk-Othmer Encyclopedia of Chemical Technology*, John Wiley and Sons: 2003.

245. Sommer, H. Z.; Lipp, H. I.; Jackson, L. L., Alkylation of Amines. A General Exhaustive Alkylation Method for the Synthesis of Quaternary Ammonium Compounds. *Journal of Organic Chemistry* **1971,** *36* (6), 824-828.

246. Srebro, M.; Autschbach, J., Tuned Range-Separated Time-Dependent Density Functional Theory Applied to Optical Rotation. *Journal of Chemical Theory and Computation* **2012,** *8* (1), 245-256.

247. Stadler, S.; Dietrich, R.; Bourhill, G.; Bräuchle, C., Long-wavelength first hyperpolarizability measurements by hyper-Rayleigh scattering. *Optics Letters* **1996,** *21* (4), 251-253.

248. Stephens, P. J.; Devlin, F. J.; Chabalowski, C. F.; Frisch, M. J., Ab Initio Calculation of Vibrational Absorption and Circular Dichroism Spectra Using Density Functional Force Fields. *Journal of Physical Chemistry* **1994,** *98* (45), 11623-11627.

249. Stewart, J. J., Optimization of parameters for semiempirical methods V: modification of NDDO approximations and application to 70 elements. *Journal of Molecular Modeling* **2007,** *13* (12), 1173-213.

250. Stewart, J. J. P., Optimization of parameters for semiempirical methods I. Method. *Journal of Computational Chemistry* **1989,** *10* (2), 209-220.

251. Sturm, J.; Tasch, S.; Niko, A.; Leising, G.; Toussaere, E.; Zyss, J.; Kowalczyk, T. C.; Singer, K. D.; Scherf, U.; Huber, J., Optical anisotropy in thin films of a blue electroluminescent conjugated polymer. *Thin Solid Films* **1997,** *298*, 138-142.

252. Sullivan, P. A.; Dalton, L. R., Theory-Inspired Development of Organic Electro-optic Materials. *Accounts of Chemical Research* **2009,** *43* (1), 10-18.

253. Sullivan, P. A.; Rommel, H.; Liao, Y.; Olbricht, B. C.; Akelaitis, A. J. P.; Firestone, K. A.; Kang, J.-W.; Luo, J.; Davies, J. A.; Choi, D. H.; Eichinger, B. E.; Reid, P. J.; Chen, A.; Jen, A. K. Y.; Robinson, B. H.; Dalton, L. R., Theory-Guided Design and Synthesis of Multichromophore Dendrimers: An Analysis of the Electro-optic Effect. *Journal of the American Chemical Society* **2007,** *129* (24), 7523-7530.

254. Sullivan, P. A.; Rommel, H. L.; Takimoto, Y.; Hammond, S. R.; Bale, D. H.; Olbricht, B. C.; Liao, Y.; Rehr, J.; Eichinger, B. E.; Jen, A. K.-Y.; Reid, P. J.; Dalton, L. R.; Robinson, B. H., Modeling the Optical Behavior of Complex Organic Media: From Molecules to Materials. *Journal of Physical Chemistry B* **2009,** *113* (47), 15581-15588.

255. Suponitsky, K. Y.; Liao, Y.; Masunov, A. E., Electronic Hyperpolarizabilities for Donor-Acceptor Molecules with Long Conjugated Bridges: Calculations versus Experiment. *Journal of Physical Chemistry A* **2009,** *113* (41), 10994-11001.

256. Suponitsky, K. Y.; Tafur, S.; Masunov, A. E., Applicability of hybrid density functional theory methods to calculation of molecular hyperpolarizability. *Journal of Chemical Physics* **2008,** *129* (4), 044109.

257. Szablewski, M.; Thomas, P. R.; Thornton, A.; Bloor, D.; Cross, G. H.; Cole, J. M.; Howard, J. A. K.; Malagoli, M.; Meyers, F.; Brédas, J.-L.; Wenseleers, W.; Goovaerts, E., Highly Dipolar, Optically Nonlinear Adducts of Tetracyano-p-quinodimethane: Synthesis, Physical Characterization, and Theoretical Aspects. *Journal of the American Chemical Society* **1997,** *119* (13), 3144-3154.

258. Szabo, A.; Ostlund, N. S., *Modern Quantum Chemistry: Introduction to Advanced Electronic Structure Theory*. 1st (revised) ed.; Dover Publications, Inc.: New York, NY, 1989.

259. Szalai, I.; Nagy, S.; Dietrich, S., Nonlinear dielectric effect of dipolar fluids. *Journal of Chemical Physics* **2009,** *131* (15), 154905-9.

260. Takimoto, Y. A real-time time-dependent density functional theory method for calculating linear and nonlinear dynamic optical response. University of Washington, Seattle, WA, 2008.

261. Takimoto, Y.; Isborn, C. M.; Eichinger, B. E.; Rehr, J. J.; Robinson, B. H., Frequency and Solvent Dependence of Nonlinear Optical Properties of Molecules. *Journal of Physical Chemistry C* **2008,** *112* (21), 8016-8021.

262. Tani, A.; Henderson, D.; Barker, J. A.; Hecht, C. E., Application of perturbation theory to the calculation of the dielectric constant of a dipolar hard sphere fluid. *Molecular Physics* **1983,** *48* (4), 863-9.

263. Tao, J.; Perdew, J., Nonempirical Construction of Current-Density Functionals from Conventional Density-Functional Approximations. *Physical Review Letters* **2005,** *95* (19).

264. Tao, J.; Perdew, J.; Staroverov, V.; Scuseria, G., Climbing the Density Functional Ladder: Nonempirical Meta–Generalized Gradient Approximation Designed for Molecules and Solids. *Physical Review Letters* **2003,** *91* (14).

265. Tawada, Y.; Tsuneda, T.; Yanagisawa, S.; Yanai, T.; Hirao, K., A long-range-corrected time-dependent density functional theory. *The Journal of Chemical Physics* **2004,** *120* (18), 8425-33.

266. Teng, C. C.; Man, H. T., Simple reflection technique for measuring the electro-optic coefficient of poled polymers. *Applied Physics Letters* **1990,** *56* (18), 1734.

267. Tian, Y.; Kong, X.; Nagase, Y.; Iyoda, T., Photocrosslinkable Liquid-Crystalline Block Copolymers with Coumarin Units Synthesized with Atom Transfer Radical Polymerization. *Journal of Polymer Science: Part A: Polymer Chemistry* **2003,** *41* (2197-2206).

268. Tinoco, I.; Sauer, K.; Wang, J. C.; Puglisi, J. D., *Physical Chemistry: Principles and Applications in Biological Sciences*. 4th ed.; Prentice-Hall: Upper Saddle River, NJ, 2002.

269. Tomasi, J.; Mennucci, B.; Cammi, R., Quantum Mechanical Continuum Solvation Models. *Chemical Reviews* **2005,** *105* (8), 2999-3093.

270. Torrent-Sucarrat, M.; Anglada, J. M.; Luis, J. M., Evaluation of the Nonlinear Optical Properties for Annulenes with Hückel and Möbius Topologies. *Journal of Chemical Theory and Computation* **2011,** *7* (12), 3935-3943.

271. Tu, Y.; Zhang, Q.; Ågren, H., Electric Field Poled Polymeric Nonlinear Optical Systems: Molecular Dynamics Simulations of Poly(methyl methacrylate) Doped with Disperse Red Chromophores. *Journal of Physical Chemistry B* **2007,** *111* (14), 3591-3598.

272. Valisko, M.; Boda, D., Relative Permittivity of Polar Liquids. Comparison of Theory, Experiment, and Simulation. *Journal of Physical Chemistry B* **2005,** *109* (13), 6355-6365.

273. Valisko, M.; Boda, D.; Liszi, J.; Szalai, I., A systematic Monte Carlo simulation and renormalized perturbation theoretical study of the dielectric constant of the polarizable Stockmayer fluid. *Molecular Physics* **2003,** *101* (14), 2309-2313.

274. Van Workum, K.; Douglas, J. F., Equilibrium polymerization in the Stockmayer fluid as a model of supermolecular self-organization. *Physical Review E*, *71* (3-1), 031502/1-031502/15.

275. Vreven, T.; Byun, K. S.; Komáromi, I.; Dapprich, S.; John A. Montgomery, J.; Morokuma, K.; Frisch, M. J., Combining Quantum Mechanics Methods with Molecular Mechanics Methods in ONIOM. *Journal of Chemical Theory and Computation* **2006,** *2* (3), 815-826.

276. Weigend, F.; Häser, M.; Patzelt, H.; Ahlrichs, R., RI-MP2: optimized auxiliary basis sets and demonstration of efficiency. *Chemical Physics Letters* **1998,** *1294*, 143-152.

277. Weis, J. J.; Levesque, D., Ferroelectric phases of dipolar hard spheres. *Physical Review E* **1993,** *48* (5), 3728.

278. Weis, J. J.; Levesque, D., Orientational order in high density dipolar hard sphere fluids. *Journal of Chemical Physics* **2006,** *125* (3), 034504-5.

279. Werner, H.-J.; Manby, F. R.; Knowles, P. J., Fast linear scaling second-order Møller-Plesset perturbation theory (MP2) using local and density fitting approximations. *Journal of Chemical Physics* **2003,** *118* (18), 8149.

280. Williams, D. J., Organic Polymeric and Non-Polymeric Materials with Large Optical Nonlinearities. *Agnewandte Chemie International Edition English* **1984,** *23*, 690-703.

281. Wolff, T.; Görner, H., Photodimerization of coumarin revisited: Effects of solvent polarity on the triplet reactivity and product pattern. **2004**.

282. Woodcock, H. L.; Miller, B. T.; Hodoscek, M.; Okur, A.; Larkin, J. D.; Ponder, J. W.; Brooks, B. R., MSCALE: A General Utility for Multiscale Modeling. *Journal of Chemical Theory and Computation* **2011,** *7* (4), 1208-1219.

283. Wyman, J., Jr., Polarization and dielectric constant of liquids. *Journal of the American Chemical Society* **1936,** *58*, 1482-6.

284. Yanai, T.; Tew, D. P.; Handy, N. C., A new hybrid exchange–correlation functional using the Coulomb-attenuating method (CAM-B3LYP). *Chemical Physics Letters* **2004,** *393* (1-3), 51-57.

285. Zarragoicoecha, G. J.; Levesque, D.; Weis, J. J., Monte Carlo study of dipolar ellipsoids. I. The isotropic phase. *Molecular Physics* **1991,** *74* (3), 629-637.

286. Zeng, Q. H.; Yu, A. B.; Lu, G. Q., Multiscale modeling and simulation of polymer nanocomposites. *Progress in Polymer Science* **2008,** *33* (2), 191-269.

287. Zerner, M., An approximate molecular orbital method. *Journal of Chemical Physics* **1975,** *62* (7), 2788-2799.

288. Zernike, F.; Midwinter, J. E., *Applied Nonlinear Optics*. Dover Publications, Inc.: Mineola, NY, 1973.

289. Zhang, C.; Dalton, L. R., Low Vπ Electrooptic Modulators from CLD-1: Chromophore Design and Synthesis, Material Processing, and Characterization. *Chemistry of Materials* **2001,** *13* (9), 3043-3050.

290. Zhang, Y.; Xin, B.; Liu, L.; Wang, Y., Water-Promoted Suzuki Reaction in Room Temperature Ionic Liquids. *Synlett* **2005,** (20), 3083-3086.

291. Zhao, Y.; Schultz, N. E.; Truhlar, D. G., Design of Density Functionals by Combining the Method of Constraint Satisfaction with Parametrization for Thermochemistry, Thermochemical Kinetics, and Noncovalent Interactions. *Journal of Chemical Theory and Computation* **2006,** *2* (2), 364-382.

292. Zhao, Y.; Truhlar, D. G., The M06 suite of density functionals for main group thermochemistry, thermochemical kinetics, noncovalent interactions, excited states, and transition elements: two new functionals and systematic testing of four M06-class functionals and 12 other functionals. *Theoretical Chemistry Accounts* **2007,** *120* (1-3), 215-241.

293. Zhao, Y.; Truhlar, D. G., Density Functionals with Broad Applicability in Chemistry. *Accounts of Chemical Research* **2007,** *41* (2), 157-167.

294. Zhou, J.; Thorpe, I. F.; Izvekov, S.; Voth, G. A., Coarse-grained peptide modeling using a systematic multiscale approach. *Biophys J* **2007,** *92* (12), 4289-303.

# Appendix A: Supplemental Methodological Details and Reference Data for Chapter 2



## A.1. Computational Details

The simulation code used for this paper is a C++ version of the prototype described in our 2007 paper;[1] it is about four orders of magnitude faster than the MATLAB code. The code contains a small math library optimized for three-dimensional linear algebra, and does not use any external libraries beyond the standard C++ library. It also lacks any system-specific language extensions, so it can run on Linux, Mac OS X, and Windows with a simple recompile. Random numbers were generated using the Ran2 algorithm from Numerical Recipes,[2] which has a period in excess of $2 \times 10^{18}$ deviates, and were seeded with either hand-selected negative integers (field-response and variable μ calculations), or the negative of the 64-bit integer representation of the number of seconds since Jan 1, 1970 via the time() function from the standard C++ library.[3]

Simulation code was compiled with ICC using the -fast optimization option, including auto-vectorization and interprocedural optimization. Simulations run prior to Summer 2009 (data in Figure 2.3 and Figure A.12) were compiled using version 9.1. All other simulations were compiled with version 11.1. Testing of one or more simulations with each compiler version and a range of optimization settings produced the same results. Results from simulations compiled and optimized with ICC were also consistent

with non-optimized code, and with code compiled with other compilers such as GCC[4] 4.2.

All simulations were implemented on ROCKS[5] clusters at the University of Washington Department of Chemistry, and all machines used x86-64 Intel processors. Output data from batches of simulations was processed with a variety of MATLAB[6] scripts to obtain means and correlation functions. Coordinate data from simulations was converted[7] into X3D markup for display using X3D players such as InstantPlayer.[8]

## A.2. Description of Mean-Field Dielectric Models

The Debye and Onsager models are the main mean-field models of dielectrics that rely only on macroscopic properties of the system. Here, both models will be discussed in the absence of any electronic polarizability ($\alpha = 0$). The Debye model ignores any effects on the material from the presence of dipoles in the cavity, and defines the cavity depolarization field purely in terms of the macroscopic polarization of the material, yielding a local electric field[9]

$$\mathbf{F} = \mathbf{E} + \frac{4\pi}{3}\frac{\mathbf{M}}{V} \qquad \text{(A-1)}$$

where **E** is the macroscopic electric field, **M** is the total permanent dipole moment of the material, and $V$ is the volume of the sample. As only macroscopic polarization, equivalent to averaging over all dipoles, is considered, Debye's theory assumes a high degree of correlation among molecules in the material.

Debye's equation[9]

$$\cdot\frac{\varepsilon - 1}{\varepsilon + 2}\mathbf{F} = \frac{4\pi\mathbf{M}}{3V}\cdot \qquad \text{(A-2)}$$

provided an adequate model for dilute gases and weakly polar liquids, but erroneously predicts that many polar liquids exhibit ferroelectric behavior.[10] Onsager argued that this behavior is not seen, and developed a theory in which the field acting on a polar molecule consists of additive contributions from the cavity field **G** and the reaction field **R**, where the former represents cavity depolarization effects and the latter represents the response of the material to the polarization of a single molecule. The local electric field was determined to be

$$\mathbf{F} = \mathbf{G} + \mathbf{R} = \frac{3\varepsilon}{2\varepsilon + 1}\mathbf{E} + \frac{2\left(\varepsilon - 1\right)}{\left(2\varepsilon + 1\right)a^3}\boldsymbol{\mu} \qquad \text{(S3)}$$

Here, $\varepsilon$ is the dielectric constant of the surrounding medium, $a$ is the radius of the cavity, and $\boldsymbol{\mu}$ is the gas-phase dipole moment of an individual molecule.

Since the reaction field is parallel to the dipole, it cannot exert a torque on it. The orienting field reduces to the cavity-corrected external field $\mathbf{E}_0$, which is equivalent to **G**. Onsager then used the relationship between **G** and **E** to scale the dipole moment of the molecule to an effective moment

$$.\boldsymbol{\mu}^* = \frac{3\varepsilon}{2\varepsilon + 1}\boldsymbol{\mu}\,. \qquad \text{(A-4)}$$

that interacts with **E**. However, using the gas-phase dipole moment and cavity field is equivalent since the Hamiltonian is dependent on the product of the field and the dipole moment ($\boldsymbol{\mu} \cdot \mathbf{E}_0$ and $\boldsymbol{\mu}^* \cdot \mathbf{E}$ are the same). Classical statistical mechanics can then be used to calculate $\langle \cos\theta \rangle$, the average of the angle between the molecular dipole and the external field. Assuming the particles are independent of each other yields the Langevin function

$$\left\langle \cos\theta \right\rangle = \frac{\int \cos\theta e^{x\cos\theta} \sin\theta d\theta d\phi}{\int e^{x\cos\theta} \sin\theta d\theta d\phi} = \coth\left(x\right) - \frac{1}{x} \approx \frac{x}{3} \quad \text{(A-5)}$$

where

$$x = \frac{\mu E_0}{kT} = \frac{\mu^* E}{kT} = \frac{3\varepsilon}{2\varepsilon + 1}\frac{\mu E}{kT} \quad \text{(A-6)}$$

On substituting the linearized version of Equation A-7 into Equation 2-2a, one obtains the well-known Onsager equation (without the electronic polarizability contribution),[11]

$$\frac{\left(\varepsilon - 1\right)\left(2\varepsilon + 1\right)}{3\varepsilon} = \frac{4\pi\rho_N \mu^2}{3kT} \quad \text{(A-7)}$$

While the Onsager equation avoids the ferroelectric catastrophe that occurs with the Debye equation, it is derived in the independent-particle limit, with all effects from other molecules modeled via the continuous medium. As it neglects local correlations among dipoles, it rigorously holds only for systems with low dipole density $y$.[12] A more extensive discussion of Debye and Onsager that includes electronic polarizability can be found in the paper of Bartke and Hentschke.[13]

## A.3. Reaction Field and SCRF Update Scheme

Simulations were run under reaction field boundary conditions, where the cavity radius $R_{cut}$ was defined as half of the length of the simulation cell. A diagram is shown in Figure A.1.

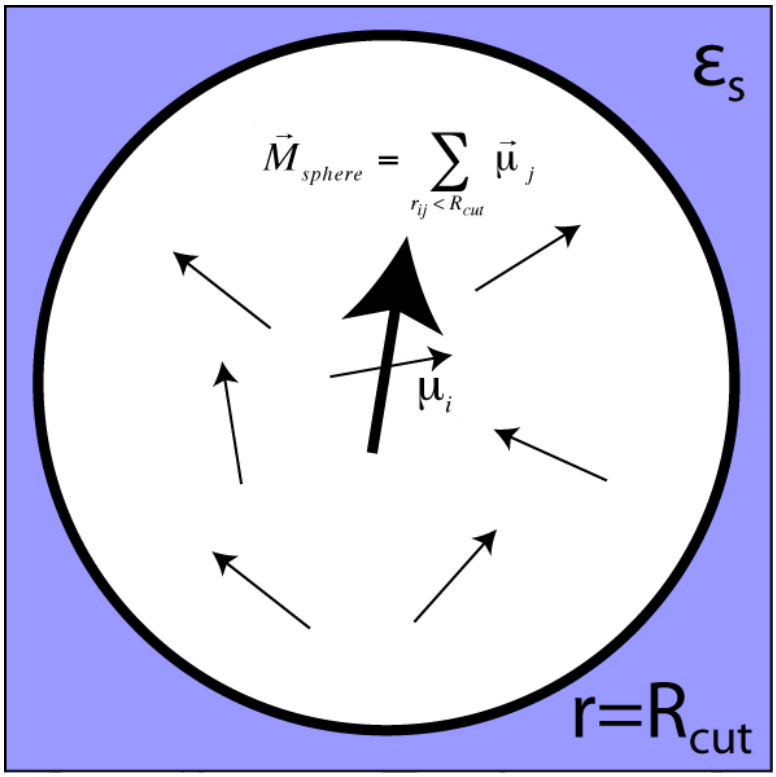


**Figure A.1.** Schematic of reaction field model. Dipole-dipole interactions between the *i*th particle and its neighbors are evaluated explicitly out to some distance $R_{cut}$, with the medium outside the cutoff treated as continuous media with a dielectric constant $\varepsilon_s$. The external continuum polarizes in response to the net dipole moment of the molecules within the cutoff sphere. The external dielectric constant may be defined as a constant or allowed to update self-consistently (SCRF) as the simulation runs. If $\varepsilon_s$ is set to unity, the reaction field vanishes and the boundary becomes a simple spherical cutoff. If $\varepsilon_s$ is very large (conductor-like boundary condition), the reaction field converges to $\mathbf{M}_{sphere} / R_{cut}^3$ . Figure based on Fig. 6.23 in A.R. Leach, *Molecular Modeling*[14] and Fig. 5.13 in M.P. Allen and D. J. Tildesley, *Computer Simulations of Liquids*.[15]

In simulations that used the self-consistent reaction field[13b, 14-15] (SCRF) boundary condition, the reaction field dielectric was updated at the beginning of each cycle (after $N$ trial moves, equal to the number of particles). The reaction field update used the instantaneous square of the total polarization $\mathbf{M}$ ($\mathbf{E}_0 = 0$) in the Kirkwood-Fröhlich equation (2-4), giving

$$\frac{(\varepsilon_s - 1)(2\varepsilon_s + 1)}{9\varepsilon_s} = \frac{4\pi \mathbf{M}^2}{9VkT} \qquad \text{(A-8)}$$

where $V$ is the volume of the simulation box. As instantaneous polarization was used, the instantaneous dielectric constant fluctuated more than the dielectric constant calculated from Var(**M**), though simulations still exhibited good convergence of energy and other properties, as shown in the body of the paper. The calculated reaction field dielectric constant was then used in the reaction field for every particle in the box for the remainder of that cycle. As changing the reaction field strength affects the energy of every molecule, total dipole-dipole interaction energy was recalculated after each reaction field update, since only the change in energy was calculated for ordinary moves.

Since the instantaneous dielectric constant was calculated using the instantaneous $\mathbf{M}^2$, while the final dielectric constant as calculated using Var(**M**) the condition $\varepsilon_s = \varepsilon$ did not always hold, since $\langle \mathbf{M} \rangle_0^2 > 0$. While the difference was much smaller for the EM1 fluid than for the SM1 fluid, we analyzed the SCRF data using a two-step process with Equation 2-10 and Equation 2-4, instead of just Equation 2-4. In the first step, we used Equation 4 with the one-term definition of $g_K$ to obtain $\langle \varepsilon_s \rangle$, where

$$\frac{(\langle \varepsilon_s \rangle - 1)(2\langle \varepsilon_s \rangle + 1)}{9\langle \varepsilon_s \rangle} = \frac{4\pi \langle \mathbf{M}^2 \rangle_{E_0=0}}{9VkT} \qquad \text{(A-9)}$$

We then substituted $\langle \varepsilon_s \rangle$ into eq. (10) to obtain the final expression for ε under the SCRF boundary condition,

$$\frac{1}{\varepsilon - 1} = \frac{1}{3yg_K} - \frac{1}{2\langle \varepsilon_S \rangle + 1} \qquad \text{(A-10)}$$

which converges to Equation 9 as $\langle \varepsilon_s \rangle$ approaches $\varepsilon$. Achieving complete self-consistency would likely require a longer averaging period in each simulation or use of a moving average of $\varepsilon_s$ during simulations to smooth out fluctuations and allow for using Var(M) instead of $\langle \mathbf{M}^2 \rangle$. Use of the method described above instead of assuming that $\varepsilon_s = \varepsilon$ resulted in a decrease in the calculated dielectric constant, as can be seen in Figure A.2, which was produced using the same MC trajectories as Figure 2.2.

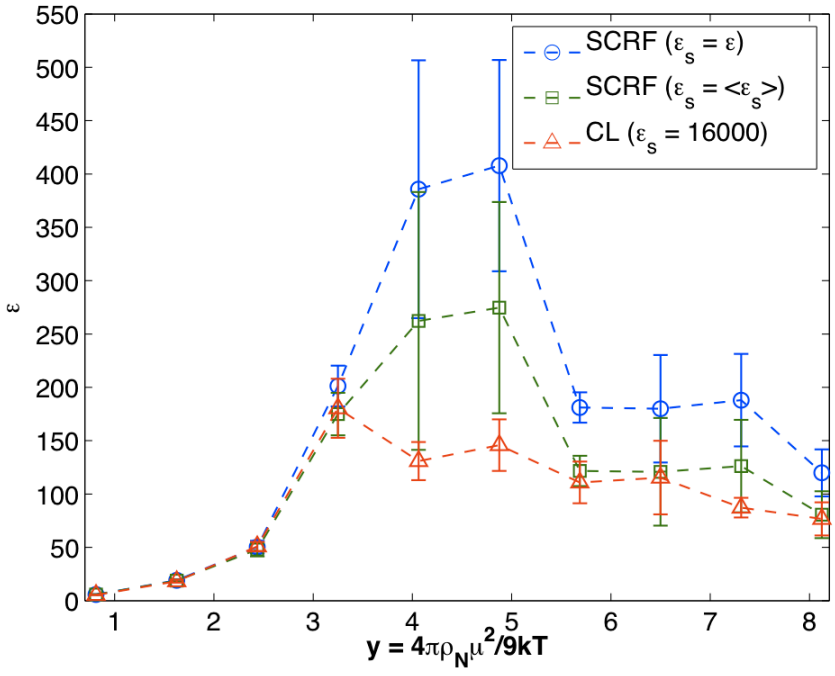


**Figure A.2.** Comparison of the data from the SM1 SCRF trajectories from Figure 4, with the dielectric constant calculated using either eq. (9) or eq. (S3), with the CL trajectories included for comparison.

Analyzing the trajectories with Equation A-10 instead of Equation 2-4 made little difference for $y \leq 3$, since $\langle \mathbf{M} \rangle^2 \approx 0$ at those dipole densities (see Table 2.4). However, at

higher dipole density, Equation 2-4 generated numbers substantially higher than Equation 2-10 after the ferroelectric transition. Results analyzed using Equation A-10 remained much closer to the CL result than those analyzed using Equation 2-4. The dielectric constant from Equation A-10 also converged to $2/3$ of the Equation 2-4 dielectric constant due to different limiting behavior in the two functions as $\varepsilon_s$ approaches infinity, which can most easily be seen if Equation A-10 is rearranged to a form similar to Equation 2-4.

Results using the SCRF boundary condition and Equation 2-10 compared well with those using a static reaction field, where $\varepsilon_s$ remained constant for the entire simulation. Results are shown in Figure A.3.

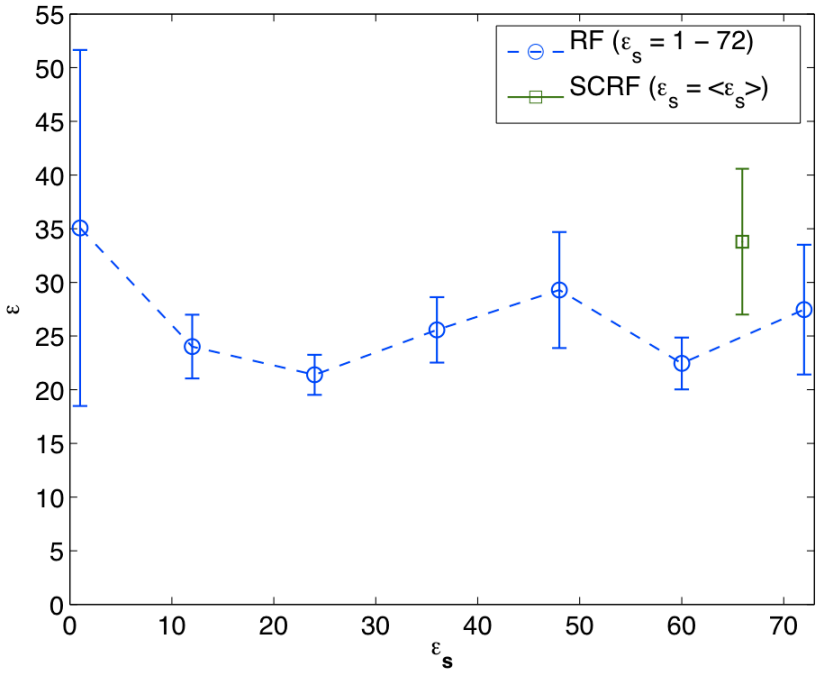


**Figure A.3.** Comparison of SCRF and static RF results for the EM1 fluid, with $N = 1728$ and $T = 293$K. Results were averaged from the last 15000 cycles of five 45000-cycle runs.

While $\varepsilon_s > \varepsilon$ even for the isotropic EM1 fluid, the static RF and SCRF results were consistent when analyzed using eq. (S10). The small variation in the dielectric constant over the range of reaction field strengths examined also underscores the low sensitivity of the EM1 fluid to reaction field strength.

## A.4. CRC data for liquids

The following is a list of all 33 liquids used for the experimental data in Figure 2-3. All data are from the current online version of the CRC Handbook of Chemistry and Physics.[16]

**Table A.1.** List of small organic liquids shown in Figure 2.4 and A.4

| Species | $\varepsilon$ | $y$ | $T$ (K) | $\mu$ (D) | $\rho_N$ (Å$^{-3}$) | $n$ |
|---|---|---|---|---|---|---|
| 1,4-Dioxane | 2.22 | 0.00 | 293.2 | 0.00 | 0.007 | 1.42 |
| Toluene | 2.38 | 0.03 | 296.4 | 0.38 | 0.006 | 1.49 |
| Thiophene | 2.74 | 0.08 | 293.2 | 0.55 | 0.008 | 1.53 |
| Furan | 2.88 | 0.12 | 298.2 | 0.66 | 0.008 | 1.42 |
| Diethyl ether | 4.27 | 0.24 | 293.2 | 1.10 | 0.006 | 1.35 |
| Chloroform | 4.81 | 0.27 | 298.0 | 1.04 | 0.007 | 1.48 |
| Diethyl sulfide | 5.72 | 0.48 | 298.2 | 1.59 | 0.006 | 1.44 |
| Ethyl acetate | 6.02 | 0.67 | 293.2 | 1.78 | 0.006 | 1.37 |
| Dimethyl sulfide | 6.70 | 0.68 | 294.2 | 1.55 | 0.008 | 1.44 |
| Tetrahydrofuran | 7.52 | 0.77 | 295.2 | 1.75 | 0.007 | 1.41 |
| Methyl acetate | 7.07 | 0.79 | 288.2 | 1.72 | 0.008 | 1.36 |
| Methylene chloride | 8.93 | 0.82 | 298.0 | 1.60 | 0.009 | 1.42 |
| Pyrrole | 8.00 | 0.94 | 293.0 | 1.77 | 0.009 | 1.51 |
| Pyridine | 13.26 | 1.27 | 293.2 | 2.22 | 0.007 | 1.51 |
| Trifluorotoluene | 9.22 | 1.36 | 298.2 | 2.86 | 0.005 | 1.41 |
| Acetic anhydride | 22.45 | 1.73 | 293.2 | 2.80 | 0.006 | 1.39 |
| Methyl ethyl ketone | 18.56 | 1.81 | 293.2 | 2.78 | 0.007 | 1.38 |
| Cyclohexanone | 16.10 | 2.12 | 293.0 | 3.25 | 0.006 | 1.45 |
| Propionaldehyde | 18.50 | 2.32 | 290.2 | 2.72 | 0.009 | 1.36 |
| Acetone | 21.01 | 2.33 | 293.2 | 2.88 | 0.008 | 1.36 |
| Methyl isocyanate | 21.75 | 2.78 | 288.7 | 2.80 | 0.010 | 1.37 |
| Acetaldehyde | 21.01 | 2.82 | 291.1 | 2.75 | 0.011 | 1.33 |
| tert-Butanenitrile | 21.10 | 2.96 | 293.2 | 3.95 | 0.005 | 1.38 |
| n-Butanenitrile | 24.83 | 3.32 | 293.2 | 3.73 | 0.007 | 1.38 |
| Benzonitrile | 25.90 | 3.55 | 293.2 | 4.18 | 0.006 | 1.45 |
| Nitrobenzene | 35.60 | 3.62 | 293.0 | 4.22 | 0.006 | 1.56 |
| Dimethylformamide | 38.25 | 3.92 | 293.2 | 3.82 | 0.008 | 1.43 |
| Dimethyl sulfoxide | 47.24 | 4.57 | 293.2 | 3.96 | 0.008 | 1.44 |
| Nitromethane | 37.27 | 4.64 | 293.2 | 3.46 | 0.011 | 1.38 |
| Acrylonitrile | 33.00 | 4.82 | 293.2 | 3.92 | 0.009 | 1.39 |
| Propionitrile | 29.70 | 4.84 | 293.2 | 4.05 | 0.009 | 1.37 |
| γ-Butyrolactone | 39.00 | 4.97 | 293.2 | 4.27 | 0.008 | 1.43 |
| Acetonitrile | 36.64 | 6.11 | 293.2 | 3.93 | 0.012 | 1.34 |

We also calculated polarizable Onsager[10] dielectric constants for all liquids in the table above, using the relation

$$\frac{\left(\varepsilon - n^2\right)\left(2\varepsilon + n^2\right)}{\varepsilon\left(n^2 + 2\right)^2} = \frac{4\pi\rho_N\mu^2}{9kT} \quad \text{(A-11)}$$

where $n$ is the refractive index of the liquid and $\mu$ is the gas-phase dipole moment.

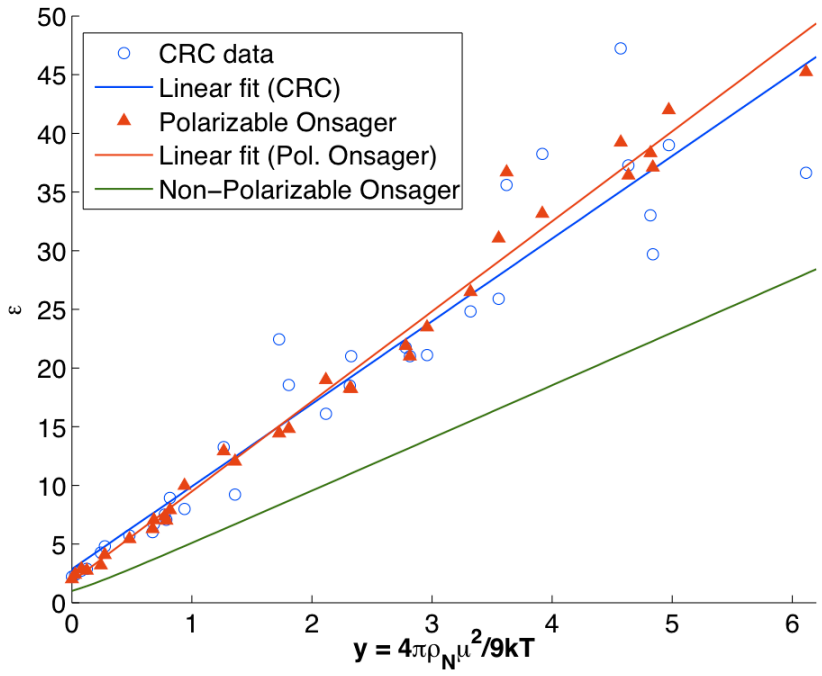


**Figure A.4.** Comparison of the polarizable and non-polarizable Onsager models for the 33 liquids in Table A.1.

These results are compared with experimental values in Figure S4, and showed reasonably strong agreement with the CRC values and indicated that $g_K$ is near unity for most of these liquid. The polarizable Onsager results are also fit more closely by the linear model ($r^2 = 0.98$) than the CRC data ($r^2 = 0.90$), likely due to a combination of small variance in refractive indices and larger variance in the degree of intermolecular correlation. However, in nearly all cases, the polarizable Onsager model produces a better fit to the CRC data than the non-polarizable model. The difference is particularly

striking at high dipole density, and underscores the importance of incorporating polarizability in future simulations.

## A.3. Simulation Convergence

Total energy for the simulations was recorded every cycle ($N$ trial moves), and the $\Delta U$ for the averaged region of the simulation was compared with Var($U$) over the same region to ensure that $\Delta U <$ Var($U$), and the total energy traces for a number of simulations were audited to see if the energy appeared stable. A complete trace and a magnified trace of the averaging region is given for a 4096-particle SM1 (Figures A.5 and A.6) simulation and a 1728-particle EM1 simulation (Figures A.7 and A.8). The expectation value of the energy is shown as a black, dashed line.

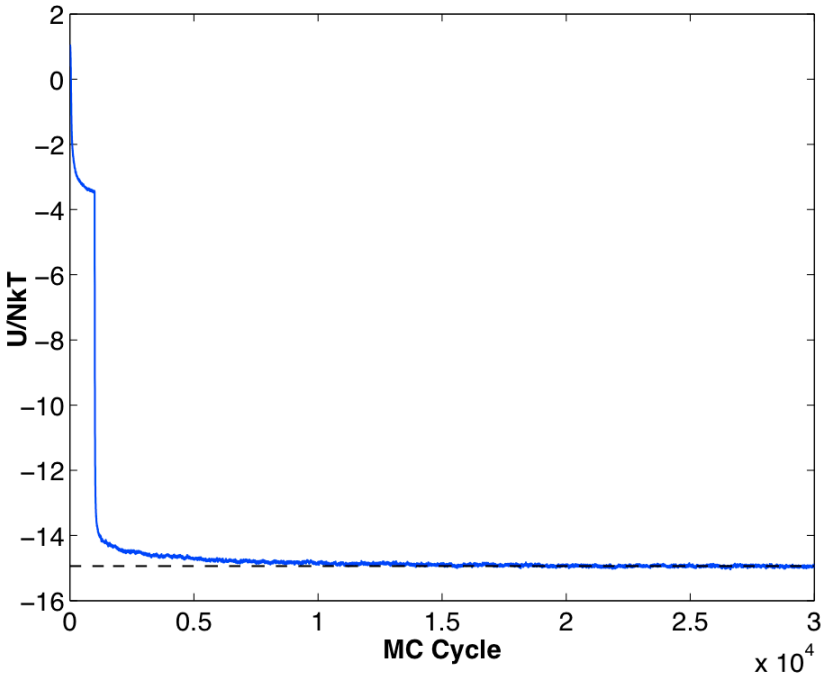


**Figure A.5.** Energy convergence for a representative $N$ = 4096 SM1 simulation using the SCRF boundary condition at $T$ = 293K, showing all MC cycles.

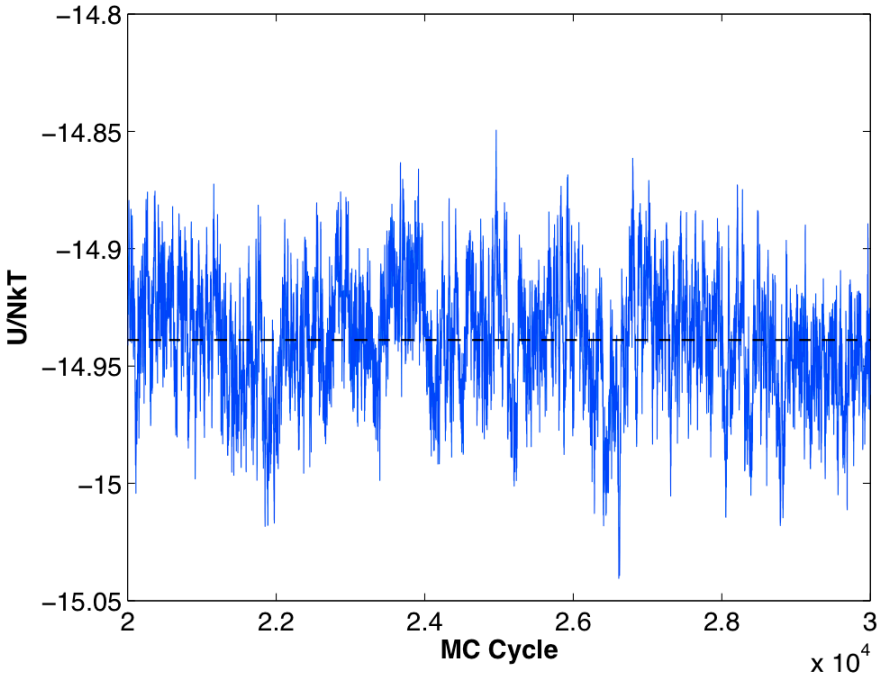


**Figure A.6.** Energy convergence for a representative $N = 4096$ SM1 simulation using the SCRF boundary condition at $T = 293$K, showing only the cycles averaged over to obtain expectation values for properties.

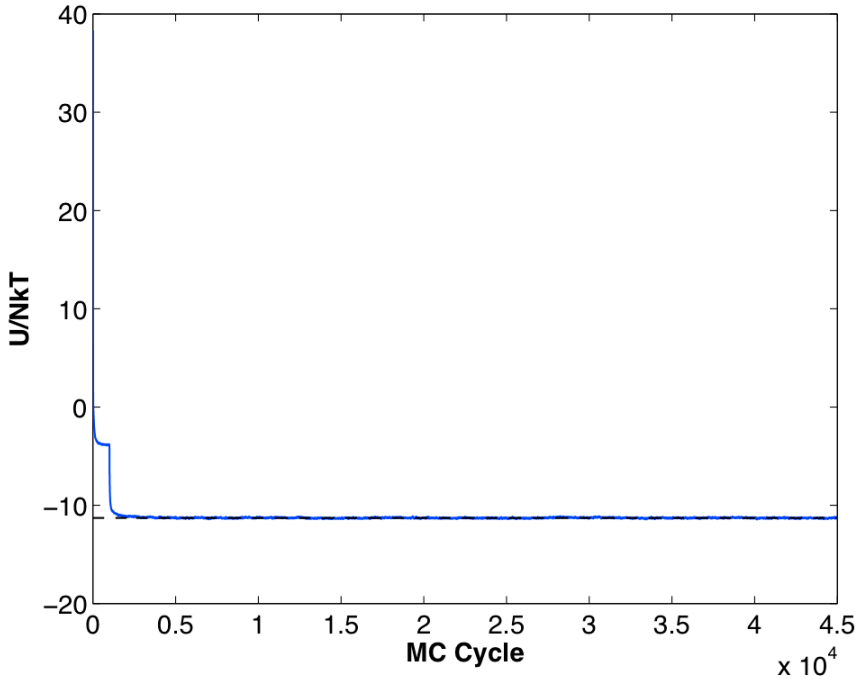


**Figure A.7.** Energy convergence for a representative $N = 1728$ EM1 simulation using the SCRF boundary condition at $T = 293$K, showing all MC cycles.

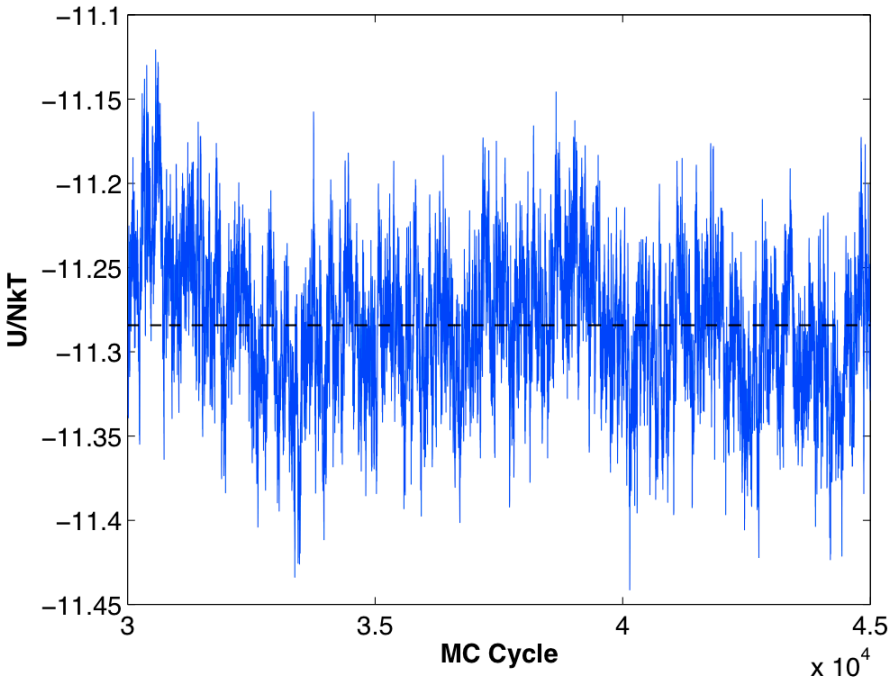


**Figure A.8.** Energy convergence for a representative $N = 1728$ EM1 simulation using the SCRF boundary condition at $T = 293$K, showing only the cycles averaged over to obtain expectation values for properties.

## A.4. Radial Distribution Function

We calculated the radial distribution function

$$g(r) = \frac{V \sum_{i}^{N} \sum_{j>i}^{N} n_{ij}(r, r+dr)}{2\pi N(N-1) r^2 dr} \quad \text{(A-12)}$$

in order to verify that the models used for the simulations were indeed in the liquid phase, with short-range radial correlation but no long-range order in positions. Both the SM1 and EM1 models showed significant correlation at short distances (first few neighbor shells), but correlation rapidly decayed with distance. The lack of long-range correlation indicates that SM1 and EM1 fluids are indeed liquids. Unlike orientational correlation, radial correlation was independent of electrostatic boundary conditions. SM1 results are shown in Figure A.8, EM1 results are shown in Figure A.9.

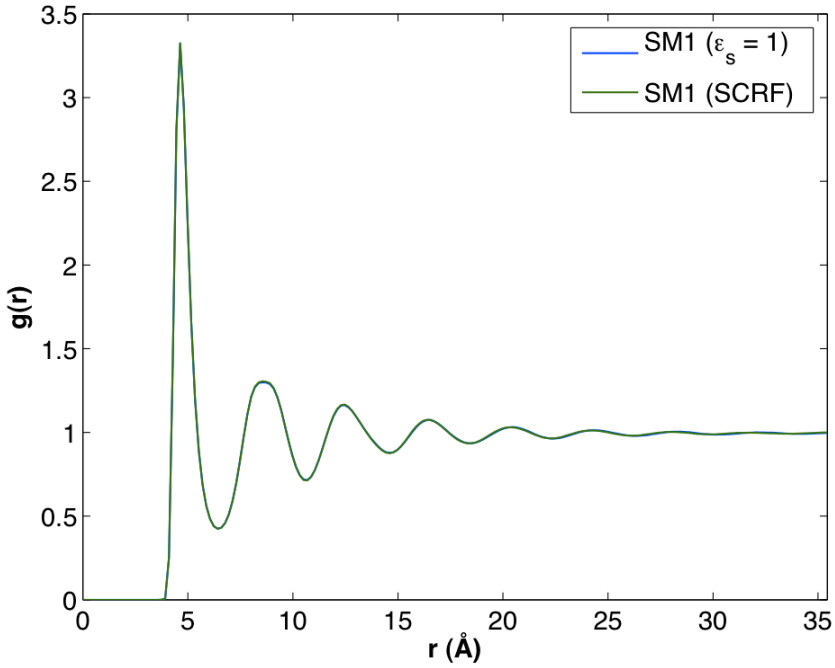


**Figure A.9.** Radial distribution function (Equation A-12) for representative $N$ = 4096 SM1 simulations at $T$ = 293K, calculated every 100 cycles during the averaging portion of the simulations. The average of a set of five simulations is shown.

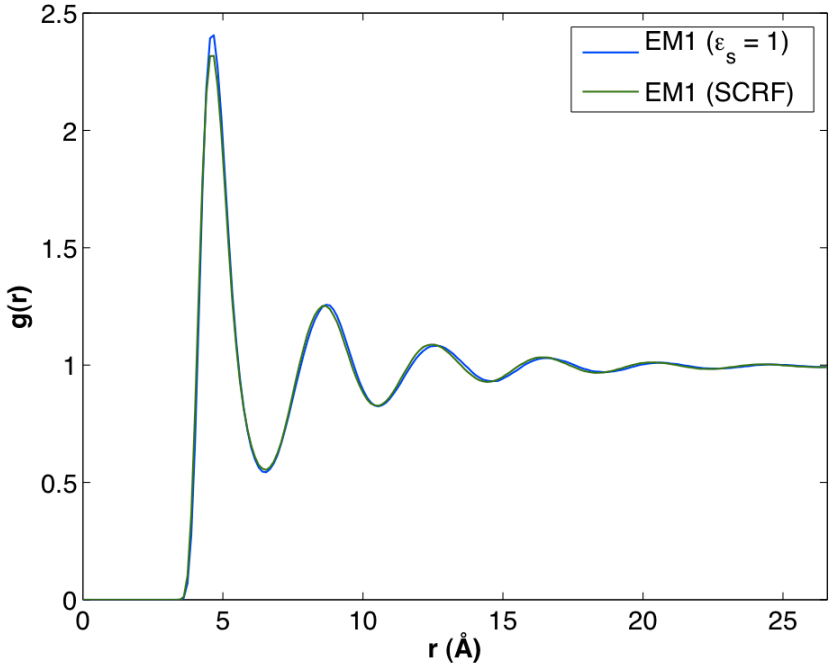


**Figure S10.** Radial distribution function (Equation A-12) for representative $N$ = 1728 EM1 simulations at $T$ = 293K, calculated every 100 cycles during the averaging portion of the simulations. The average of a set of five simulations is shown.

## A.5. Confirmation of Ferroelectric Phase Transition

In order to verify the location and magnitude of the ferroelectric phase transition, we used Equation 2-13 to calculate the spontaneous polarization for the Stockmayer simulations shown in Figure 2. Substantial spontaneous order begins developing around $y = 3.25$ ($\mu^{*2} = 2$, $\rho^* = 1.16$), a similar dipole density to the phase transition observed in the hard-sphere fluid at $\rho^* = 0.95$ by Weis and Levesque.[17] No spontaneous order developed at any dipole density for the SC boundary condition, indicating that the polarization of the domains within the simulation cell cancelled each other out. Results are shown in Figure A.11.

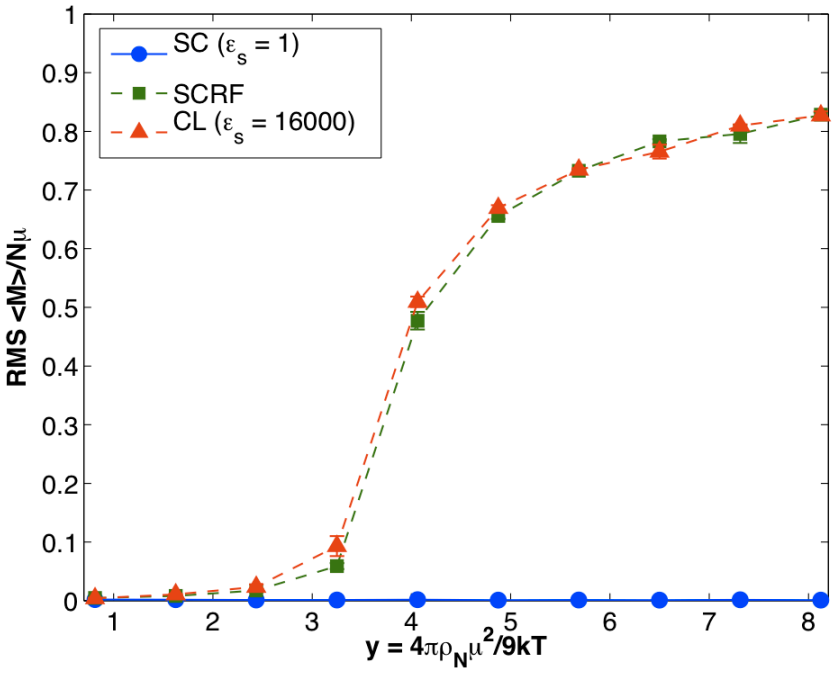


**Figure A.11.** Normalized RMS magnitude of **M** (Equation 2-13) as a function of dipole density, calculated from the same data as Figure 2. Simulations run using the SC boundary condition did not develop net acentric order at any of the dipole densities examined.

## A.6. Kirkwood g-factors

Kirkwood g-factors[15, 18] used for calculating dielectric constants in the manuscript were calculated using the two-term version of Equation 2-9. These correlation factors are tabulated in Table A.2, including both the full (Var(**M**)) and truncated ($\langle \mathbf{M}^2 \rangle_0$) g-factors for the SM1 and EM1 fluids (data from Figure 2.1 and Figure 2.6). All three boundary conditions are included, and data is formatted in a manner similar to Table 4. Data from Table 2.4 is not repeated. Simulations in which pervasive ferroelectric behavior was observed (i.e. SM1 fluid under SCRF or CL boundary conditions) tend to have large differences between the short and long forms due to large values of $\langle \mathbf{M} \rangle_0^2$.

**Table A.2.** Kirkwood correlation factors used to calculate ε for SM1 and EM1 fluids

| System | Boundary Cond. | $g_K$ (Var(M)) | $g_K$ ($\langle \mathbf{M}^2 \rangle_0$) | Var(M)/ $\langle \mathbf{M}^2 \rangle_0$ |
|---|---|---|---|---|
| SM1 - 512 | SC | 0.133 ± 0.002 | 0.138 ± 0.003 | 0.97 |
| | SCRF | 3.86 ± 0.76 | 342.6 ± 1.3 | 0.011 |
| | CL | 4.99 ± 0.89 | 343.4 ± 1.3 | 0.015 |
| | | | | |
| SM1 - 1728 | SC | 0.140 ± 0.003 | 0.143 ± 0.003 | 0.98 |
| | SCRF | 6.25 ± 0.62 | 1069 ± 5 | 0.0058 |
| | CL | 5.41 ± 1.06 | 1062 ± 10 | 0.0051 |
| | | | | |
| SM1 - 4096 | SC | 0.134 ± 0.003 | 0.137 ± 0.002 | 0.97 |
| | SCRF | 6.15 ± 2.98 | 2114 ± 386 | 0.0029 |
| | CL | 10.49 ± 3.728 | 2116 ± 223 | 0.0047 |
| | | | | |
| EM1 - 512 | SC | 0.139 ± 0.005 | 0.144 ± 0.005 | 0.97 |
| | SCRF | 0.778 ± 0.115 | 0.891 ± 0.125 | 0.873 |
| | CL | 1.36 ± 0.16 | 2.19 ± 0.35 | 0.62 |
| | | | | |
| EM1 - 1728 | SC | 0.138 ± 0.005 | 0.142 ± 0.006 | 0.98 |
| | SCRF | 1.32 ± 0.22 | 2.19 ± 0.64 | 0.60 |
| | CL | 1.74 ± 0.23 | 2.45 ± 0.40 | 0.70 |
| | | | | |
| EM1 - 4096 | SC | 0.138 ± 0.002 | 0.139 ± 0.003 | 0.99 |
| | SCRF | 1.49 ± 0.11 | 1.73 ± 0.16 | 0.86 |
| | CL | 2.50 ± 0.20 | 3.03 ± 0.31 | 0.83 |

## A.7. Applied-field calculations

A set of simulations at different external field strengths was used to examine whether the polarization of the SM1 and EM1 fluids was linear with respect to field under different boundary conditions. Simulations were run at $\mathbf{E}_0 = 0$, 100, 200, and 300 V/μm, with the field oriented along the +*z* axis of the simulation cell. The external field was included by adding the following term to the Hamiltonian (Equation 2-11):

$$U_{ext} = \sum_{i=1}^{N} \boldsymbol{\mu}_i \cdot \mathbf{E}_0 \qquad \text{(A-13)}$$

The dielectric constant can then be calculated directly from the ordering of the molecules in response to the field[14, 19] by combining Equatons 2-2 and 2-12.

$$\frac{(\varepsilon - 1)(2\varepsilon_s + 1)}{2\varepsilon_s + \varepsilon} E_{0,z} = 4\pi\rho_N |\mu| \langle \cos\theta \rangle \qquad \text{(A-14)}$$

We then compared the calculated acentric order with respect to field, $\langle \cos\theta \rangle_{E_0}$ with the degree of acentric order that would be predicted based on the fluctuation calculations at $\mathbf{E}_0 = 0$. This prediction can be made by substituting Equation 2-9 into Equation 2-7 to obtain

$$\langle \cos\theta \rangle_{g_K} = \frac{\langle \mathbf{M}_z \rangle_{g_K}}{N\mu} = \frac{\mu E_0}{3kT} g_K \qquad \text{(A-15)}$$

assuming an intercept of $\langle \cos\theta \rangle_{g_K} = 0$ at $\mathbf{E}_0 = 0$. Values subscripted with $g_K$ are predicted based on zero-field calculations.

Under the SC boundary condition, the response to the field was linear over the entire range of external fields we examined, and very close to the response predicted based on fluctuations at zero field. Results appear in Figure A.12.

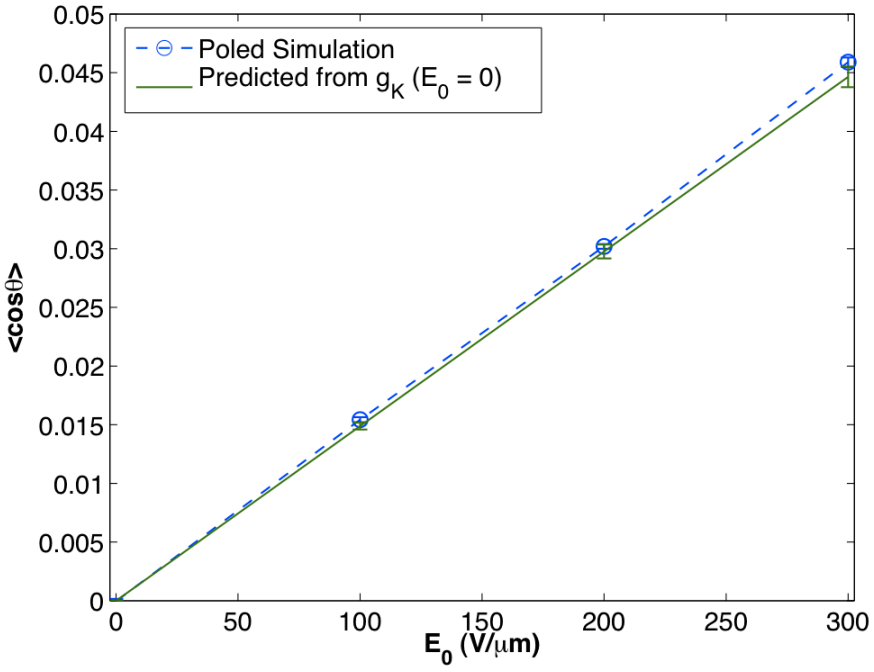


**Figure A.12.** Polarization of SM1 fluid under the SC boundary condition with $N = 4096$ and $T = 293$K. Results were averaged over the last 8000 cycles from ten 24000-cycle MC runs. Fluctuation-based simulations used the full version of eq. (9) for $g_K$. Lennard-Jones interactions were truncated after 35.44 Å (eight neighbor shells), where the length of a side of the box is 70.88 Å (16 x 16 x 16 initial lattice of particles).

A linear relationship did not hold for SM1 under the SCRF or CL boundary conditions; both a nonzero intercept and saturated polarization were observed. Under both of these boundary conditions, the system was pervasively ferroelectric, with strong net acentric ordering of the entire box. Systems that spontaneously polarized tended to saturate ( $\langle \cos\theta \rangle \approx 1$) once an external field was applied, making a linear response approach with the same field strengths used in Figure A-12 ineffective. An example of linear response breakdown is shown in Figure A-13.

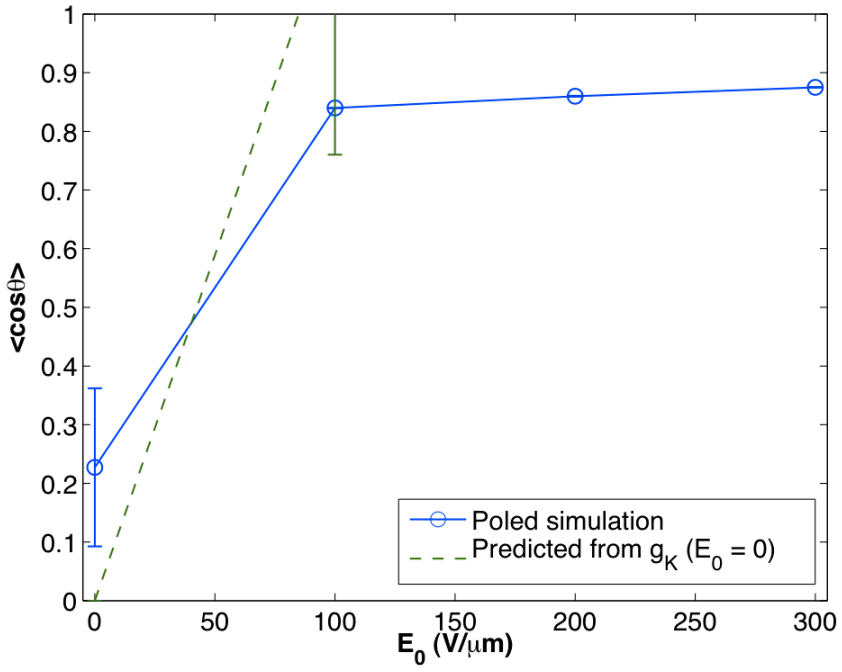


**Figure A.13.** Breakdown of linear response in the SM1 fluid under the CL boundary condition, with $N = 4096$ and $T = 293$K. Averages were taken from sets of five simulations. As $\langle \cos\theta \rangle$ cannot exceed unity, unphysical predicted values are truncated.

Obtaining a dielectric constant from the applied-field simulations in Figure A.13 is complicated not only by the rapid saturation behavior in response to $E_0$, but also by the instability of $\langle \cos\theta \rangle$ at zero field. Due to the unphysical predictions of a linear model at high field, examining the behavior of a ferroelectric system such as the SM1 fluid under an applied field would require inclusion of higher-order terms in E in the fluctuation expansion. Such a non-linear model has recently been examined for the dipolar Yukawa potential by Szalai et al.[20]

Unlike the SM1 fluid, the EM1 fluid showed nearly linear response under both the SC and the CL boundary conditions. The results for the SC boundary condition were nearly identical to the corresponding SM1 results, and are shown in Figure A.14.

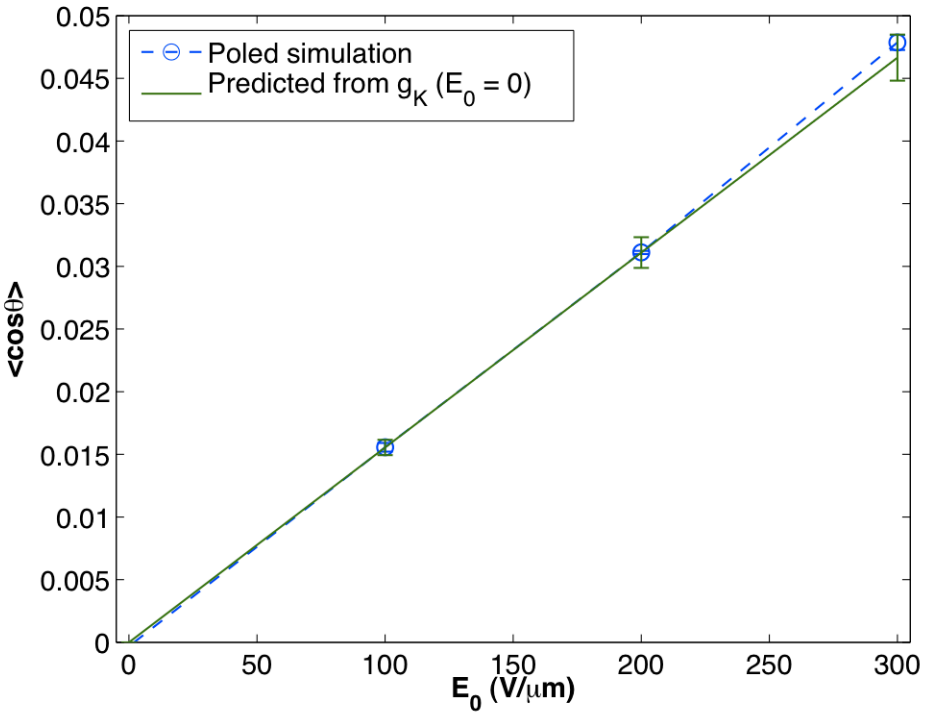


**Figure A.14.** Polarization of EM1 fluid under the SC boundary condition with $N = 1728$ and $T = 293$K. Results were averaged over the last 1500 cycles from five 45000-cycle MC runs. Fluctuation-based simulations used the full version of eq. (9) for $g_K$. Lennard-Jones interactions were truncated after 17.72 Å (four neighbor shells), where the length of a side of the box is 53.16 Å (12 x 12 x 12 initial lattice of particles).

Under the CL boundary condition, the EM1 fluid showed slight deviation from linear response at high field strength, with a shape similar to the Langevin function, but did not fully saturate. The fluctuation-based simulations also underestimated the polarization slightly when compared with the direct method. Results appear in Figure A.15.

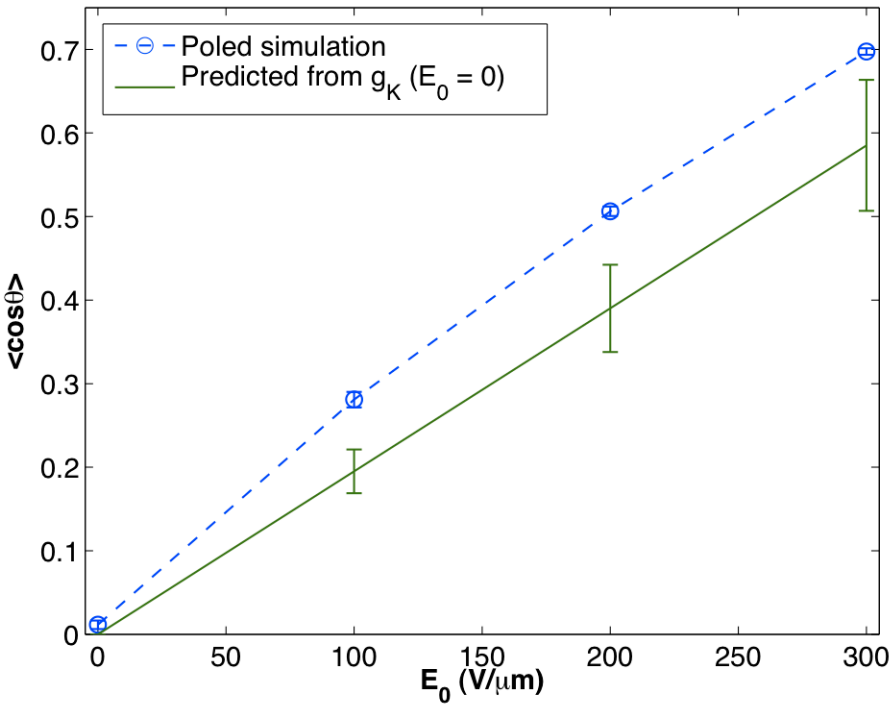


**Figure A.15.** Polarization of the EM1 fluid under the CL boundary condition, with $N$ = 1728 and $T$ = 293K. Averages were taken from sets of five simulations.

In the set of data shown above, the order calculated in response to field is not linear over the range $\mathbf{E}_0$ = 100 to 300, indicating that simulations of the EM1 fluid in response to a field should be done for $\mathbf{E}_0$ < 100 V/μm to avoid nonlinear effects. Furthermore, longer or larger simulations may be needed to ensure that the fluctuation magnitude is not being too heavily affected by cutoffs or by the slower convergence of fluctuation calculations compared to applied-field calculations.[19]

## A.8. References for Appendix A

1. Rommel, H. L.; Robinson, B. H., Orientation of Electro-optic Chromophores under Poling Conditions: A Spheroidal Model. *Journal of Physical Chemistry C* **2007,** *111* (50), 18765-18777.
2. Press, W. H., Teukolsky, S.A., Vetterling, W.T., Flannery, B.P., *Numerical Recipes in C*. 2nd ed.; Cambridge University Press: Cambridge (UK), 1992.
3. C++ Reference. http://www.cplusplus.com/reference/ (accessed 03/09/2009).
4. *GNU Compiler Collection*, 4.2.1; Free Software Foundation: 2007.

5. Rocks Clusters. http://www.rocksclusters.org/ (accessed 03/09/2009).
6. *Matlab*, r2009b; The Mathworks: Natick, MA, 2009.
7. Sibelman, B. H. *Dipole X3D Translator*, 2.0; 2009.
8. Behr, J. *Instant Player*, 2.00b5; Fraunhofer GmbH: 2008.
9. Debye, P., *Polar Molecules*. Dover Publications: New York, 1929.
10. Onsager, L., Electric moments of molecules in liquids. *Journal of the American Chemical Society* **1936,** *58*, 1486-93.
11. Hansen, J.-P., McDonald, I.R., *Theory of Simple Liquids*. 3rd ed.; Elsevier: Amsterdam, Netherlands, 2006.
12. Fröhlich, H., *Theory of Dielectrics*. 2nd ed.; Clarendon Press: Oxford, 1958.
13. (a) Bartke, J.; Hentschke, R., Phase behavior of the Stockmayer fluid via molecular dynamics simulation. *Physical Review E: Statistical, Nonlinear, and Soft Matter Physics* **2007,** *75* (6-1), 061503/1-061503/11; (b) Bartke, J.; Hentschke, R., Dielectric properties and the ferroelectric transition of the Stockmayer-fluid via computer simulation. *Molecular Physics* **2006,** *104* (19), 3057-3068.
14. Leach, A. R., *Molecular Modeling: Principles and Applications*. 2nd ed.; Pearson Education: Harlow (UK), 2001.
15. Allen, M. P., Tildesley, D.J., *Computer Simulations of Liquids*. Clarendon: Oxford (UK), 1987.
16. Lide, D. R., *CRC Handbook of Chemistry and Physics*. 90th ed.; CRC Press: Baton Rouge, LA, 2009.
17. Weis, J. J.; Levesque, D., Orientational order in high density dipolar hard sphere fluids. *The Journal of Chemical Physics* **2006,** *125* (3), 034504-5.
18. Kirkwood, J. G., The dielectric polarization of polar liquids. *Journal of Chemical Physics* **1939,** *7*, 911-19.
19. Alper, H. E.; Levy, R. M., Computer simulations of the dielectric properties of water: studies of the simple point charge and transferrable intermolecular potential models. *Journal of Chemical Physics* **1989,** *91* (2), 1242-51.
20. Szalai, I.; Nagy, S.; Dietrich, S., Nonlinear dielectric effect of dipolar fluids. *The Journal of Chemical Physics* **2009,** *131* (15), 154905-9.

# Appendix B: Additional Calculations on the Static Dielectric Constant of Acetonitrile

## B.1. Introduction

In order to follow up on the success of the acetonitrile-like EM1 model[1] used in Chapter 2, further refinements were made in an attempt to more closely model the experimental dielectric constant of acetonitrile using the rigid-body Monte Carlo (RBMC) technique. These calculations were also compared with MD calculations run using Tinker 5.1[2] and three published force fields (OPLS,[3] MMFF,[4] and AMOEBA[5]). Calculations with the OPLS force field were run using both three-site (united-atom, with the methyl group replaced by a single sphere) and six-site (atomistic) potentials. AMOEBA calculations included a (computationally expensive) self-consistent treatment of linear polarizability. Neither MMFF nor OPLS include treatment of polarizability.

## B.2. Computational Methods

### *B.2.1. RBMC methods*

RBMC calculations on the improved spheroidal model of acetonitrile (EM2) were run using a Hamiltonian similar to that from Chapter 4, but also including the dispersive (attractive) component of the Lennard-Jones potential;

$$U = \sum_i \left\{ \sum_{j>i} \left[ 4\varepsilon_{LJ} \left( \left( \frac{\sigma_{eff}(i,j)}{r_{ij}} \right)^{12} - \left( \frac{\sigma_{eff}(i,j)}{r_{ij}} \right)^{6} \right) + \frac{1}{\varepsilon_\infty r_{ij}^3} \left( \boldsymbol{\mu}_i \cdot \boldsymbol{\mu}_j - 3(\boldsymbol{\mu}_i \cdot \hat{\mathbf{r}})(\hat{\mathbf{r}} \cdot \boldsymbol{\mu}_j) \right) - \frac{1}{\varepsilon_\infty R_C^3} \frac{2(\varepsilon - \varepsilon_\infty)}{(2\varepsilon + \varepsilon_\infty)} \boldsymbol{\mu}_i \cdot \boldsymbol{\mu}_j \right] - \left( \frac{3\varepsilon}{2\varepsilon + \varepsilon_\infty} \right) \boldsymbol{\mu}_i \cdot \mathbf{E}_p \right\} \quad \text{(B-1)}$$

the definitions of the variables are the same as in Chapter 4. The main difference from the potential used in Chapter 2 is the presence of the high-frequency/background dielectric constant $\varepsilon_\infty = n^2$ (as used in Chapter 4), which attenuates dipole-dipole interactions and applied field strength; this was set to

1.8 (the square of the experimental refractive index of acetonitrile) for the EM2 model. The EM1 model does not contain implicit treatment of polarizability. All EM2 calculations were run in the NVT ensemble under SCRF boundary conditions, and simulations contained 1728 particle, resulting in a cubic cell 53.16 A to a side. Run length was set to 120000 cycles, using the last 60000 cycles for calculating average properties. The first 4000 cycles were run without electrostatics and used simulated annealing to disrupt the starting lattice. Data was obtained by averaging over five trajectories.

### *B.2.2. MD methods*

Molecular dynamics calculations were run at 293K in Tinker 5.1 in the NVT ensemble using particle-mesh Ewald[6] for long-range electrostatics, with conductive outer boundary conditions.[7] Calculations used a 1.0 fs time step and a Berendsen[8] thermostat to control temperature. Simulations contained either 512 molecules (35.44 A per side) or 1000 molecules (44.3 A per side). Simulations used the following procedure; velocities were reset for each stage:

1. Construct lattice using TINKER's XYZedit utility
2. Minimize to a RMS gradient of < 10 kcal/mol-A using TINKER's MINIMIZE utility
3. 10 ps of NVT MD at 500K without electrostatics
4. 40 ps of NVT MD at 293K (except for AMOEBA runs)
5. 250 ps of NVT MD at 293K
6. 250 ps of NVT MD at 293K, sampling every 0.1 ps
7. Process trajectory with TINKER's analyze utility to obtain energies (U) and total dipole moments (**M**) for each frame

### *B.2.3. Data analysis*

Dielectric data from the RBMC runs were analyzed[1] using the following modified form of Equation 2-2

$$(\varepsilon - \varepsilon_\infty)\mathbf{E} = \frac{4\pi\mathbf{M}}{V} \qquad \text{(B-2)}$$

For simulations at zero external field, the Kirkwood fluctuation expansion from Equation 2-7 was used to estimate $\langle \mathbf{M} \rangle$, such that

$$\frac{(\varepsilon - n^2)(2\varepsilon + n^2)}{9\varepsilon} = y g_K \qquad \text{(B-3)}$$

where $y$ is the reduced dipole density (Equation 2-8) and $g_K$ is the Kirkwood[7, 9] correlation factor (Equation 2-9).

Dielectric data from the MD calculations under conductive boundary conditions were analyzed using Equation 2-10 with $\varepsilon_s \to \infty$, such that

$$\varepsilon = 3 y g_K + 1 \quad \text{(B-4)}$$

Finally, enthalpies of vaporization[10] were calculated from the total energies of the systems as

$$\Delta H_{vap} = N u_{gas} - U_{total} + RT \qquad \text{(B-5)}$$

where $u_{gas}$ is the energy of an isolated molecule in J/mol. In the case of the RBMC simulations, the energy of an isolated molecule is zero.

## B.3. Results

RBMC results are shown in Table B.1; EM1 results from Chapter 2 are included for comparison, along with experimental values from the CRC Handbook of Chemistry and Physics. Corresponding MD data with the OPLS, MMFF, and AMOEBA force fields is shown in Table B.2. Errors are reported as standard error of the mean

**Table B.1.** RBMC results for acetonitrile

| Model | N | μ (D) | $n^2$ | T (K) | $\Delta H_{vap}$ (kJ/mol) | ε |
|---|---|---|---|---|---|---|
| EM1 | 1728 | 4.09 | 1 | 293 | 29.91 ± 0.01 | 33.8 ± 6.8 |
| EM1 | 4096 | 4.09 | 1 | 293 | 29.89 ± 0.001 | 42.5 ± 3.6 |
| EM2 | 1728 | 3.92 | 1.8 | 293 | 29.11 ± 0.004 | 33.8 ± 3.9 |
| EM2 | 1728 | 3.92 | 1.8 | 293 | 29.21 ± 0.01 | 35.1 ± 0.7 |
| Ref. | - | 3.92 (gas) | 1.8 | 287~303 | 32.94 | 36.64 |

**Table B.2.** Molecular dynamics results are shown in Table B.2

| Force Field | N | μ (D) | T (K) | $\Delta H_{vap}$ (kJ/mol) | ε |
|---|---|---|---|---|---|
| AMOEBA09 | 512 | 3.92 | 293 | 42.25 ± 0.01 | 31.7 ± 1.1 |
| MMFF94 | 1000 | 4.51 | 293 | 15.71 ± 0.01 | 28.0 ± 1.2 |
| OPLS08 (UA) | 512 | 3.45 | 293 | 25.49 ± 0.01 | 19.4 ± 0.8 |
| OPLS08 (UA) | 1000 | 3.45 | 293 | 25.51 ± 0.01 | 20.5 ± 0.4 |
| OPLS08 (AA) | 512 | 4.13 | 293 | 16.37 ± 0.01 | 20.3 ± 0.7 |
| Ref. | - | 3.92 (gas) | 287~303 | 32.94 | 36.64 |

## B.4. Conclusion

The changes made to the EM1 model to form the EM2 model (using the experimental dipole moment and refractive index, as well as an augment $\varepsilon_{LJ}$ of 300K instead of 217K) resulted in a slight reduction in the calculated dielectric constant compared to the EM1 model. The EM2 value was within error of the experimental value, and outperformed even the sophisticated AMOEBA force field. While less impressive in an absolute sense than the self-consistent mean-field hypernetted chain calculations by Fries et al.,[11] which used a similar level of electrostatic rigor to the AMOEBA force field (polarizable multipoles) to obtain a

value of 35.18, it is still surprisingly close for a coarse-grained calculation. Additionally, despite being parameterized for liquids,[12] the OPLS force field performed poorly on this metric, and was outperformed by the MMFF94 force field on the dielectric constant. The EM1 model obtained the most accurate heat of vaporization, followed by the EM2 and three-site OPLS models.

## B.5. Acknowledgements for Appendix B

Thanks to Bruce E. Eichinger and Andreas F. Tillack for useful discussion, Jay Ponder for technical support regarding Tinker, as well as the National Science Foundation (STC-MDITR DMR-0120967 and DMR-0905686), the Air Force Office of Scientific Research (FA9550-09-1-0589), and the University of Washington Student Technology Fund for financial support.

## B.6. References for Appendix B

1. Johnson, L. E.; Barnes, R.; Draxler, T. W.; Eichinger, B. E.; Robinson, B. H., Dielectric Constants of Simple Liquids: Stockmayer and Ellipsoidal Fluids. *Journal of Physical Chemistry B* **2010,** *114* (25), 8431-8440.
2. Ponder, J. *TINKER*, 5.1; Washington University: St. Louis MO, 2010.
3. Jorgensen, W. L.; Tirado-Rives, J., The OPLS Potential Functions for Proteins. Energy Minimizations for Crystals of Cyclic Peptides and Crambin. *Journal of the American Chemical Society* **1988,** *110* (6), 1657-1666.
4. Halgren, T. A., Merck Molecular Force Field. I. Basis, Form, Scope, Parameterization, and Performance of MMFF94. *J Comput Chem* **1996,** *17* (5), 490-519.
5. Ponder, J. W.; Wu, C.; Ren, P.; Pande, V. S.; Chodera, J. D.; Schnieders, M. J.; Haque, I.; Mobley, D. L.; Lambrecht, D. S.; DiStasio Jr., R. A.; Head-Gordon, M.; Clark, G. N. I.; Johnson, M. E.; Head-Gordon, T., Current Status of the AMOEBA Polarizable Force Field. *Journal of Physical Chemistry B* **2010,** *114* (8), 2549-2564.
6. Darden, T.; York, D.; Pedersen, L., Particle mesh Ewald: An N•log(N) method for Ewald sums in large systems. *The Journal of Chemical Physics* **1993,** *98* (12), 10089-10092.
7. Allen, M. P., Tildesley, D.J., *Computer Simulations of Liquids*. Clarendon: Oxford (UK), 1987.

8. Berendsen, H. J. C.; Postma, J. P. M.; van Gunsteren, W. F.; DiNola, A.; Haak, J. R., Molecular dynamics with coupling to an external bath. *The Journal of Chemical Physics* **1984,** *81* (8), 3684.
9. Kirkwood, J. G., The dielectric polarization of polar liquids. *Journal of Chemical Physics* **1939,** *7*, 911-19.
10. McQuarrie, D. A.; Simon, J. D., *Physical Chemistry: A Molecular Approach*. University Science Books: Sausalito, CA, 1997.
11. Fries, P. H.; Richardi, J.; Krienke, H., Dielectric and structural results for liquid acetonitrile, acetone and chloroform from the hypernetted chain molecular integral equation. *Molecular Physics* **1997,** *90* (5), 841-853.
12. Kaminski, G.; Jorgensen, W. L., Performance of the AMBER94, MMFF94, and OPLS-AA Force Fields for Modeling
Organic Liquids. *Journal of Physical Chemistry* **1996,** *100* (46), 18010-18013.

# Appendix C. Additional Data Tables for Comparison of DFT Methods

The following tables contain the calculated hyperpolarizabilities used for the comparisons in Chapter 5. Data are reported in the perturbation series convention; experimental values[1] were extrapolated to the static limit using Equation 5-4, experimental $\beta_{zzz}$ values for EZ-FTC were obtained by applying Equation 5-3. CLD-1 HRS measurements were referenced against EZ-FTC and are reported as ratios only.

## C.1. Data Tables

**Table C.1.** $\beta_{HRS}(0)$ (in units of $10^{-30}$ esu)

| Method | EZ-FTC | CLD-1 | CLD-1/EZ-FTC |
|---|---|---|---|
| B3LYP | 630 | 574 | 0.91 |
| PBE0 | 569 | 582 | 1.02 |
| BHandHLYP | 362 | 444 | 1.23 |
| M062X | 389 | 519 | 1.33 |
| CAM-B3LYP | 357 | 471 | 1.32 |
| LC-BLYP | 135 | 175 | 1.30 |
| ωB97X | 181 | 255 | 1.41 |
| HF | 79 | 96 | 1.22 |
| PM6 | 143 | 150 | 1.05 |
| MP2 (B3LYP) | 751 | 1137 | 1.51 |
| MP2 (M062X) | 428 | 596 | 1.39 |
| HRS (extrap.) | 680 ± 350 | - | 1.71 ± 0.076 |

**Table C.2.** $\beta_{HRS}(-2\omega,\omega,\omega)$ at 1906nm (in units of $10^{-30}$ esu)

| Method | EZ-FTC | CLD-1 | CLD-1/EZ-FTC |
|---|---|---|---|
| B3LYP | 1218 | 1069 | 0.88 |
| PBE0 | 985 | 1011 | 1.03 |
| BHandHLYP | 486 | 615 | 1.27 |
| M062X | 539 | 750 | 1.39 |
| CAM-B3LYP | 483 | 663 | 1.37 |
| LC-BLYP | 166 | 203 | 1.22 |
| ωB97X | 217 | 314 | 1.45 |
| HF | 88 | 111 | 1.26 |
| PM6 | 132 | 139 | 1.05 |
| HRS | 1360 ± 700 | - | 1.8 ± 0.08 |

**Table C.3.** βzzz(0) (in units of $10^{-30}$ esu)

| Method | EZ-FTC | CLD-1 | CLD-1/EZ-FTC |
|---|---|---|---|
| B3LYP | 1396 | 1034 | 0.74 |
| PBE0 | 1260 | 1070 | 0.85 |
| BHandHLYP | 783 | 827 | 1.06 |
| M062X | 833 | 1023 | 1.23 |
| CAM-B3LYP | 765 | 904 | 1.18 |
| LC-BLYP | 277 | 339 | 1.22 |
| ωB97X | 374 | 496 | 1.33 |
| HF | 159 | 170 | 1.07 |
| PM6 | 287 | 211 | 0.74 |
| MP2-B | 1621 | 2387 | 1.47 |
| MP2-M | 910 | 1271 | 1.40 |
| HRS (extrap) | 1640 ± 845 | - | 1.71 ± 0.076 |

**Table C.4.** $\beta_{zzz}(0)$ calculated from BHRS(0) using Equation 5-3 (in units of $10^{-30}$ esu)

| Method | EZ-FTC | CLD-1 | CLD-1/EZ-FTC |
|---|---|---|---|
| B3LYP | 1522 | 1386 | 0.91 |
| PBE0 | 1374 | 1406 | 1.02 |
| BHandHLYP | 874 | 1072 | 1.23 |
| M062X | 940 | 1254 | 1.33 |
| CAM-B3LYP | 862 | 1138 | 1.32 |
| LC-BLYP | 326 | 423 | 1.30 |
| ωB97X | 437 | 616 | 1.41 |
| HF | 191 | 232 | 1.22 |
| PM6 | 345 | 362 | 1.05 |
| MP2-B | 1814 | 2746 | 1.47 |
| MP2-M | 1034 | 1439 | 1.40 |

**Table C.5.** $\beta_{zzz}(-\omega,0,\omega)$ at 1310nm (in units of $10^{-30}$ esu)

| Method | EZ-FTC | CLD-1 | CLD-1/EZ-FTC |
|---|---|---|---|
| B3LYP | 2085 | 1547 | 0.74 |
| PBE0 | 1773 | 1538 | 0.87 |
| BHandHLYP | 957 | 1042 | 1.09 |
| M062X | 1039 | 1310 | 1.26 |
| CAM-B3LYP | 941 | 1145 | 1.22 |
| LC-BLYP | 308 | 380 | 1.23 |
| ωB97X | 428 | 575 | 1.34 |
| HF | 173 | 188 | 1.09 |
| PM6 | 275 | 212 | 0.77 |
| HRS (extrap.) | 2708 ± 1430 | - | 1.76 ± 0.078 |

## C.2. References for Appendix C

1. (a) Bale, D. H. Nonlinear optical materials characterization studies employing photostability, hyper-Rayleigh scattering, and electric field induced second harmonic generation techniques. University of Washington, Seattle, WA, 2008; (b) Bale, D. H.; Eichinger, B. E.; Liang, W.; Li, X.; Dalton, L. R.; Robinson, B. H.; Reid, P. J., Dielectric dependence of the first molecular hyperpolarizability for electro-optic chromophores. *J Phys Chem B* **2011,** *115* (13), 3505-13.

# Appendix D: Coumarin-Based Photocrosslinking Agent for Surfactant-Coated DNA Films

## D.1. Introduction

Cou-$C_6$ is a cationic surfactant intended to supplement aliphatic, quaternary ammonium surfactants such as CTMA (cetyltrimethylammonium bromide) or CTAB (cetyltriethylammonium bromide) in coating DNA for biophotonics applications[1] and introduce a photocrosslinkable moiety into the DNA/surfactant composite. Crosslinkable compounds such as PPIF (poly-(phenylisocyanate-co-formaldehyde) have previously been used to harden DNA-based films[1d]; however, integration of the crosslinkable moiety into the surfactant may assist in improving film homogeneity and reducing optical loss. The structure of Cou-$C_6$ is shown in Figure D.1.

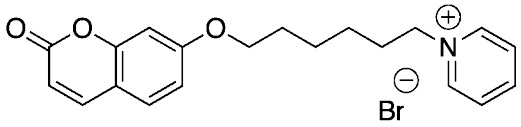


Chemical Formula: $C_{20}H_{22}BrNO_3$
Molecular Weight: 404.30
Elemental Analysis: C, 59.42; H, 5.48; Br, 19.76; N, 3.46; O, 11.87

**Figure D.1.** Structure of Cou-$C_6$ (internally DLE-4-40)

While initially synthesized at multi-gram scale with a six-carbon chain between the coumarin and the pyridinium, the length of the linker can be adjusted as needed to control thermal properties and improve coumarin-coumarin contact, as can the quaternary amine. A ten-carbon analog was previously synthesized at small scale (tens of milligrams), and is shown in Figure 2a. The first of the coumarin-based crosslinkers[2] synthesized at any scale, shown in Figure 2b, used a twelve-carbon chain and triethylamine (TEA) for quaternization. The TEA was

replaced with pyridine to both improve yields and minimize damage to chromophores if similar chains are attached to a dye.

**D.2a.** (Cou-$C_{10}$)

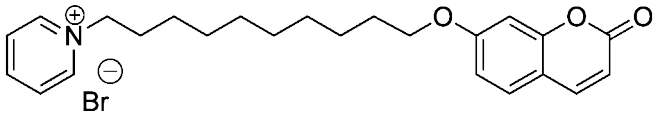


Chemical Formula: $C_{24}H_{30}BrNO_3$
Molecular Weight: 460.40
Elemental Analysis: C, 62.61; H, 6.57; Br, 17.36; N, 3.04; O, 10.43

**D.2b.** (Initial design)

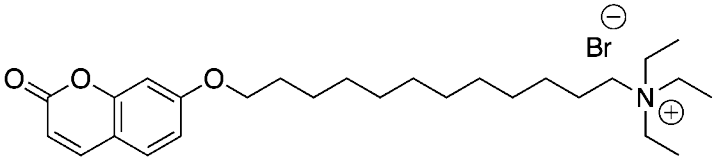


Chemical Formula: $C_{27}H_{44}BrNO_3$
Molecular Weight: 510.55
Elemental Analysis: C, 63.52; H, 8.69; Br, 15.65; N, 2.74; O, 9.40

**Figure D.2.** Structure of Cou-$C_{10}$ (internally LEJ-2-20) (D.2a) and initial twelve-carbon crosslinkable surfactant synthesized by Stephanie Benight in 2010 (D.2b)

The coumarin moiety in these surfactants undergoes a [2+2] cycloaddition upon exposure to ultraviolet light, forming a dimer connected by a four-membered ring[3]. If the surfactants are tightly bound to the DNA, this process could anchor adjacent chains together and strengthen the material against both solvents and increases in temperature.

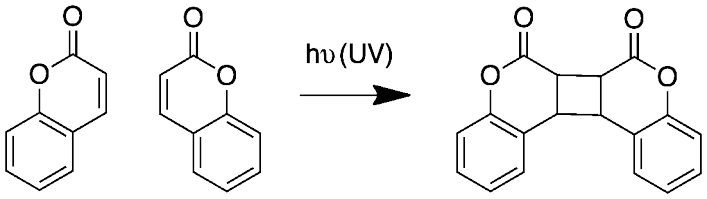


**Figure D.3.** Schematic of coumarin crosslinking

High intensity UV in the ~350nm range is required for rapid crosslinking; broadband light from a 500W mercury arc lamp or similar source is sufficient to affect nearly all of the coumarin in a film or solution within 30 minutes.

## D.2. Incorporation of Coumarin into Surfactant-Coated DNA:

The crosslinker can be added to CTMA-DNA during either the DNA preparation process or before spin-coating films. Both processes are detailed below, but the former method is preferred for optimal stoichiometry.

### *Method D.1. Preparation of CTMA-Cou-DNA (preferred method)*

The process of preparing crosslinkable CTMA-DNA is nearly identical to that of preparing CTAB-DNA or CTMA-DNA[1d], except that a fraction of the ordinary surfactant (e.g. CTMA) is replaced with the coumarin surfactant when preparing the initial aqueous solutions. For example, instead of a 4 mg/ml solution of CTMA, a solution of 2.8 mg/mL CTMA and 1.2 mg/mL Cou-$C_6$ could be used to produce a mixture that is 30% coumarin surfactant by mass. This solution is then titrated into an aqueous solution of DNA, forming a white precipitate. This precipitate can be filtered off and can be re-suspended in short-chain alcohols such as methanol, ethanol, or butanol. Filtering proved to be problematic using filter paper (either hardened or non-hardened), but a nylon filter similar to those used for preparing CTMA-DNA may work. The water can also be removed by centrifuging at ≥ 4500 RPM. If further purification is needed, the resulting solids can then be dissolved in ethanol, decanted or filtered using a coarse filter, and dried using rotary evaporation. The material will form a hard, transparent film on the inside of the flask used for evaporation.

### *Method D.2. Addition to existing CTMA-DNA or CTAB-DNA (alternate method)*

Alternately, CTMA-DNA (or similar, such as CTAB-DNA), the coumarin surfactant, and any dyes used to prepare a film can be massed dry and dissolved in butanol directly before spin-coating, with the coumarin surfactant replacing a portion of the CTAB-DNA. The amount of coumarin surfactant should be kept smaller when using this procedure, or some of the solids may not dissolve. After mixing and heating the solutions, they can be spin-coated like ordinary CTMA-DNA solutions. Unlike with Method 1, the DNA will not be stoichiometrically coated with surfactant, and free surfactant will remain in solution. Therefore, method 1 is preferred.

## D.3. Characterization

### *D.3.1. Optical characterization of thin films*

Six films of material prepared using Method 2 were spin-coated from butanol and characterized by UV/Vis before and after crosslinking with broadband UV light. No films were made using material made by Method 1. Three films (SJB-6-167-1A,B,C) were prepared using a mixture of 15% DLE-4-40 AND 85% CTAB-DNA in butanol (10% solids by mass), while the other three (SJB-6-167-2A,B,C) used 30% Cou-$C_6$ and 70% CTAB-DNA in butanol at the same concentration. Higher concentrations were unable to be tested due to solubility issues, possibly due to the age of the CTAB-DNA. Films were exposed to broadband UV from a 500W mercury arc lamp for three different time intervals (5min, 15min, and 30min). All films showed a reduction in the intensity of the

coumarin peak at 323nm upon exposure to the intense UV light. Crosslinking was nearly complete for the 15% samples (batch 1) after five minutes, but took longer for the 30% samples (batch 2), nearing completion after 30min. Results for batches 1 and 2 are shown in Figures D.4 and D.5, respectively. Spectra were recorded on a Varian Cary 5000 spectrophotometer. Absorbances were normalized due to a shift in the instrument baseline and spectra were referenced against a clean glass slide.

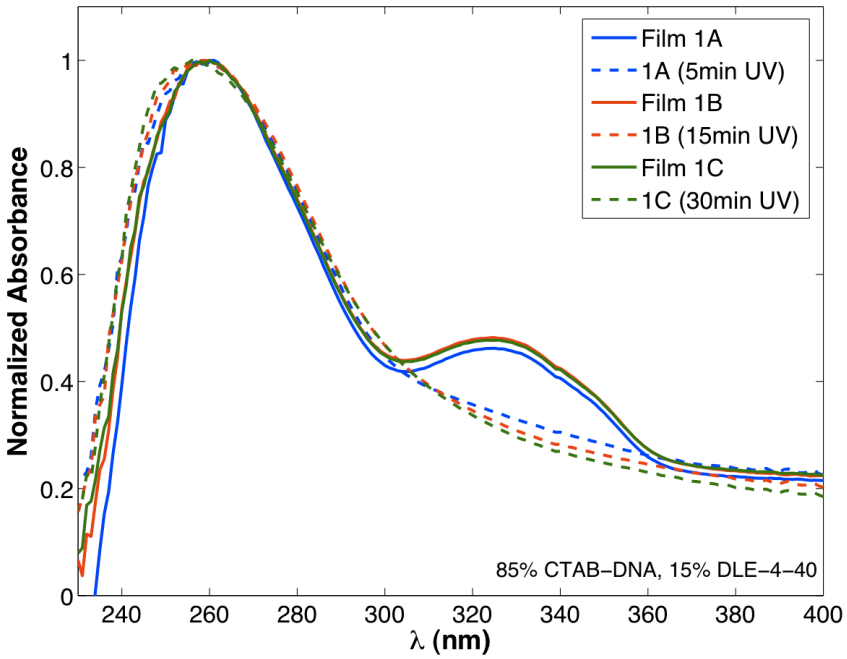


**Figure D.4**. Crosslinking of 15% Cou-$C_6$ CTAB-DNA films monitored by UV/Vis

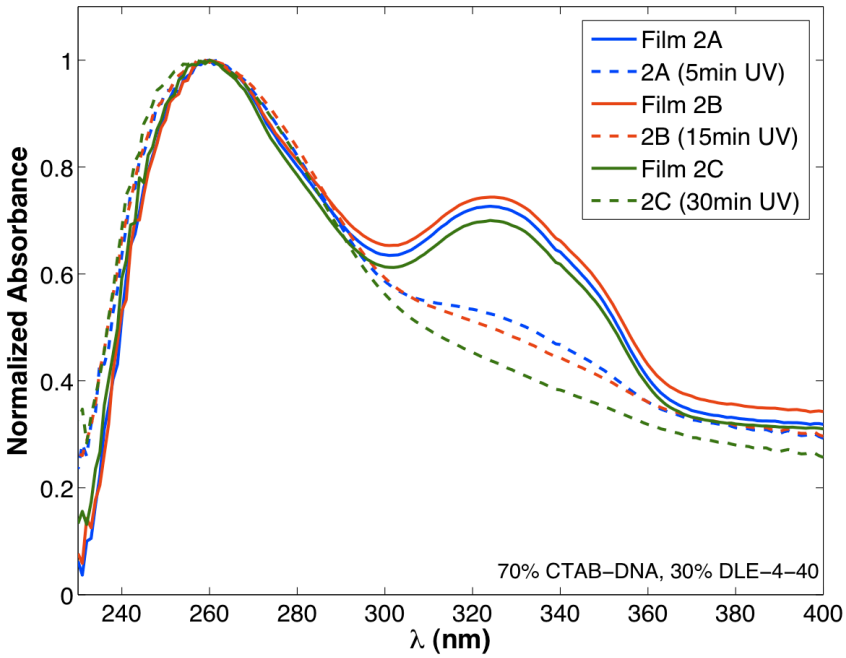


**Figure D.5.** Crosslinking of 30% Cou-$C_6$ CTAB-DNA films monitored by UV/Vis

Crosslinked films retained high transparency at telecommunications wavelengths, with transmissivities of 95% or greater. Near-infrared spectra are shown in Figure D.6.

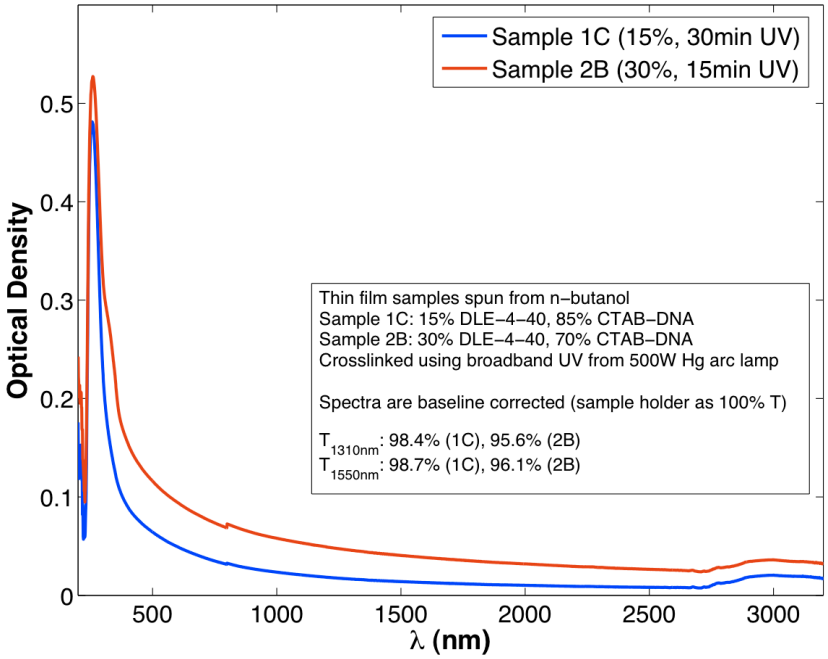


**Figure D.6.** UV/Vis/NIR spectra of two crosslinked films

### *D.5.2. Optical characterization in solution*

The materials produced by both methods show a distinct coumarin peak at about 324nm when re-dissolved in methanol; this peak disappears upon exposure of the solution to strong UV light. Two example sets of solution-phase spectra (before and after 30min of crosslinking) are shown below. The first (Figure D.7) is from a mixture of pre-prepared CTAB-DNA and Cou-$C_6$ (Method 2); the second (Figure D.8) is from DNA coated with CTMA and Cou-$C_6$ (Method 1). Spectra were recorded on a Varian Cary 5000 spectrophotometer in fused silica cuvettes with a butanol reference and temperature controlled at 25°C by

means of an in-instrument Peltier heating/cooling plate. Concentrations of each component are given on the graphs, which are not normalized. A slight reduction in DNA peak (260nm) intensity is observed, though it is unclear if this is due to degradation or material precipitating out of solution during the crosslinking (solids were observed to appear in both cases).

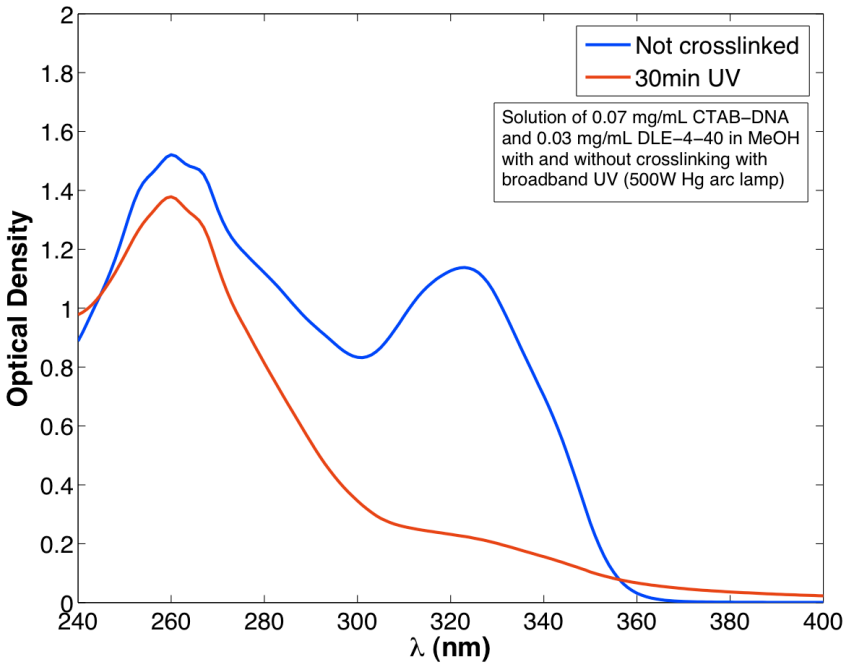


**Figure D.7.** UV/Vis spectra of CTAB-DNA + Cou-$C_6$ before and after exposure to UV

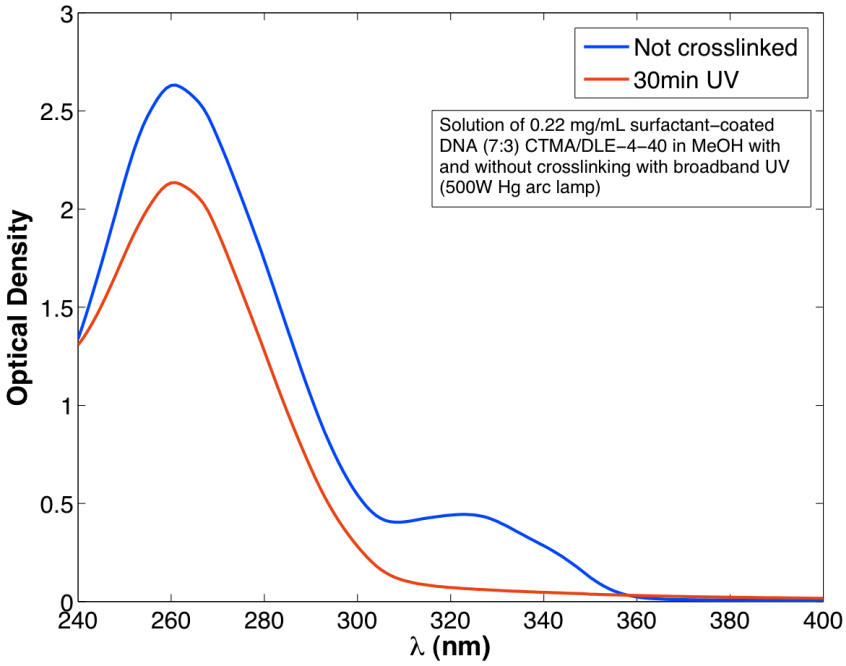


**Figure D.8.** UV/Vis spectra of CTMA-Cou-DNA before and after exposure to UV

The principal difference between the spectra above is the ratio of the DNA peak intensity to the coumarin peak intensity; while some of this is accounted for by the larger amount of coumarin relative to DNA from the runs using Method 2, it is also possible that Cou-$C_6$ has somewhat lower affinity for DNA than CTMA. Additionally, and likely due to the higher concentration of coumarin, the solution prepared using Method 2 turned yellow upon UV exposure, while the solution prepared using Method 1 did not.

### *D.3.3 Thermal Characterization*

The glass transition temperature ($T_g$) of unmodified CTMA-DNA is 148°C[4], similar to common polymers used as hosts for organic nonlinear optical chromophores, such as amorphous polycarbonate[5] (149 °C) and poly(methylmethacrylate)[6] (105°C). However, adding guest molecules to a

polymer mixture tends to lower $T_g$. Composites containing surfactant-coated DNA and Cou-$C_6$, as well as samples of pure Cou-$C_6$ were evaluated by differential scanning calorimetry (DSC) using a TA Instruments DSC-Q20. Two cycles from $T_{min}$ to $T_{max}$ and back at a heating/cooling rate of 10° C/min were run for each sample, preceded by an initial, lower-temperature pass if substantial trapped solvent was observed, and transitions temperatures were recorded from the final pass.

Adding the Cou-$C_6$ reduces the $T_g$ and melting point ($T_m$) of the non-crosslinked material compared to CTMA-DNA; the $T_g$ is 99.1°C and the Tm is 150.27°C; a second $T_m$-like transition is also observed at 170.1°C. A DSC thermogram of the material produced using Method 1 is shown in Figure D.9. The material produced with CTAB using Method 2 showed less favorable thermal properties, with a $T_m$-like transition at 100.7°C. These results are shown in Fig. D.10. Results for crosslinked materials were inconclusive due to small sample sizes and difficulty scraping films off of the glass and into the DSC cup.

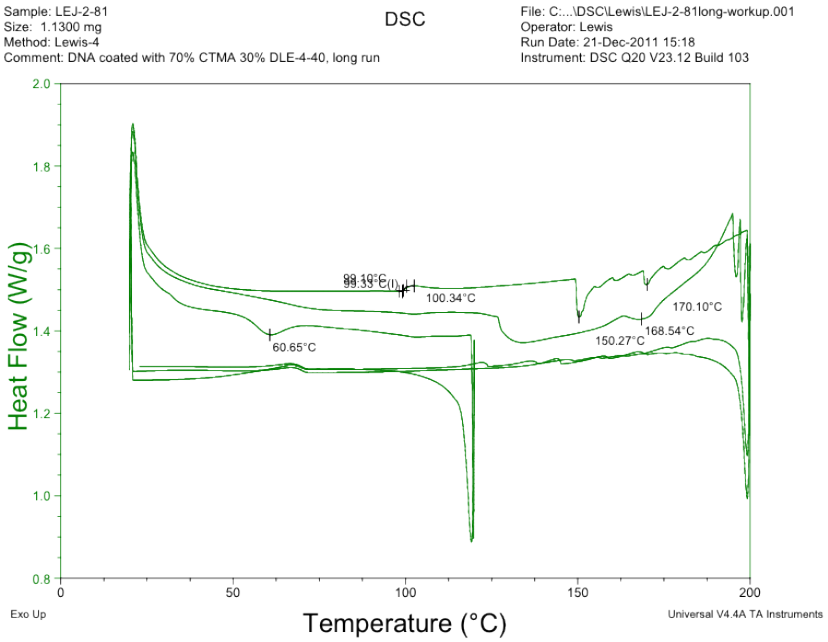


**Figure D.9a.** DSC thermogram of CTMA-Cou-DNA (Method 1). 70% CTMA/30% Cou-$C_6$ was used for coating the DNA. The uppermost trace is the third heating cycle, and exotherms point upwards. The first cycle was only run to 120°C with a 10min isotherm at maximum temperature to remove residual solvent. The region of interest is detailed in Figure D.9b.

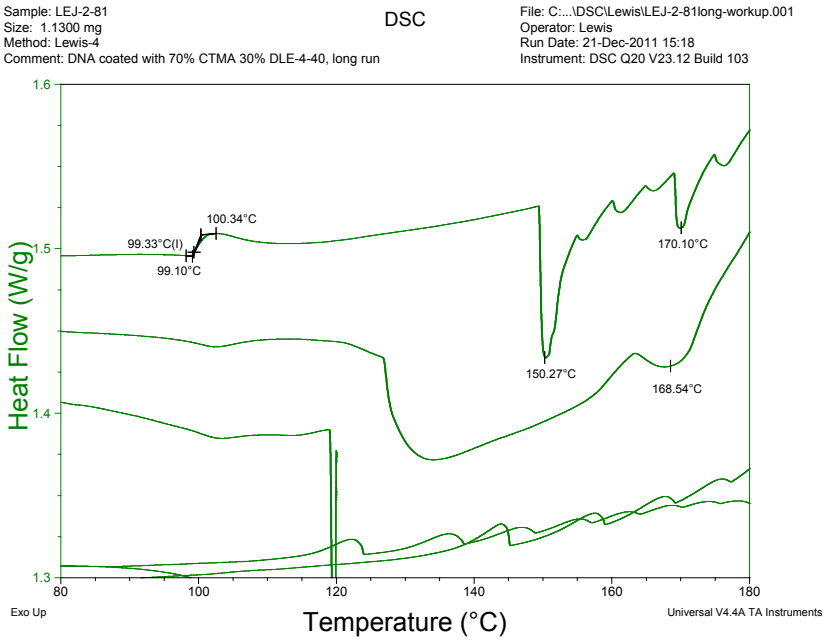


**Figure D.9b.** Magnification of key transitions from Figure 8a. The third heating cycle is the top trace, and the second heating cycle is immediately below it. The glass transition at 99.1 °C and both endotherms (150.3 °C and 170.1 °C) sharpen upon annealing

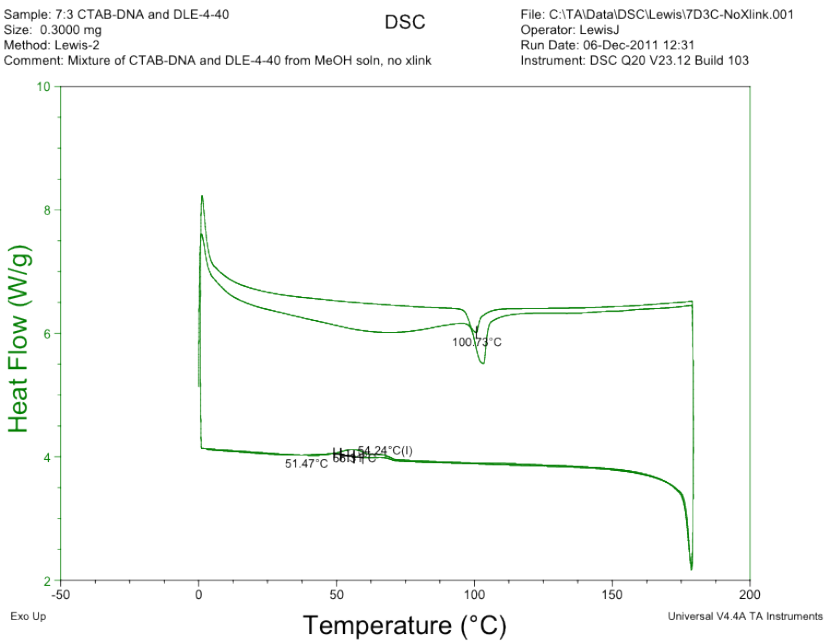


**Figure D.10.** DSC thermogram of mixed 30% Cou-$C_6$ + 70% CTAB-DNA (Method 2) after re-precipitation from methanol. Only two cycles were run; exotherms point upwards and heating cycles are on top.

Pure Cou-$C_6$ proved difficult to characterize thermally due to strong transitions that appeared on the first pass of the DSC but did not reappear, and the lack of an apparent melting point on subsequent passes. The material in the DSC pan also appeared not to melt or decompose (visually the same, negligible mass change) if heated to less than 200°C, and the sharp transition at 86.3 °C appeared whether or not the material was dried under vacuum for 70 hrs before the measurement; it may involve a rearrangement of the coumarins in the material. A DSC thermogram over the 20-200°C range is shown in Figure D.11.

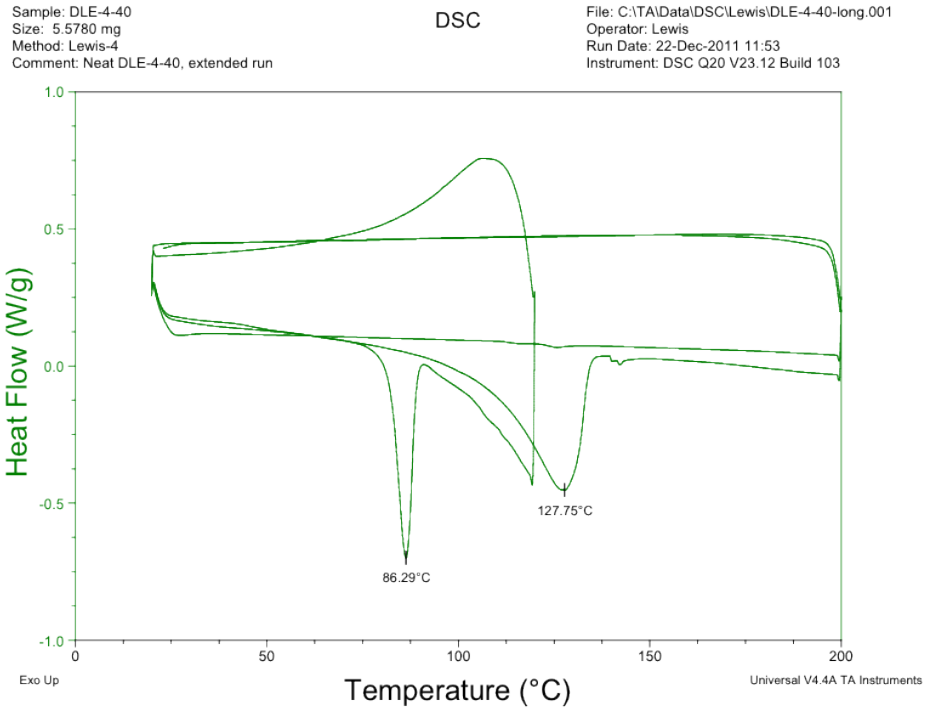


**Figure D.11.** DSC thermogram of pure Cou-$C_6$ (DLE-4-40). Here, the upper traces are cooling and the lower traces are heating

To further investigate the thermal behavior, the same sample from Figure 10 was heated to decomposition immediately following the end of the lower-temperature run. An apparent $T_g$ was found at 206.1 °C, and the material decomposed at 249 °C without an obvious melting point before decomposition. Results are shown in Figure D.12.

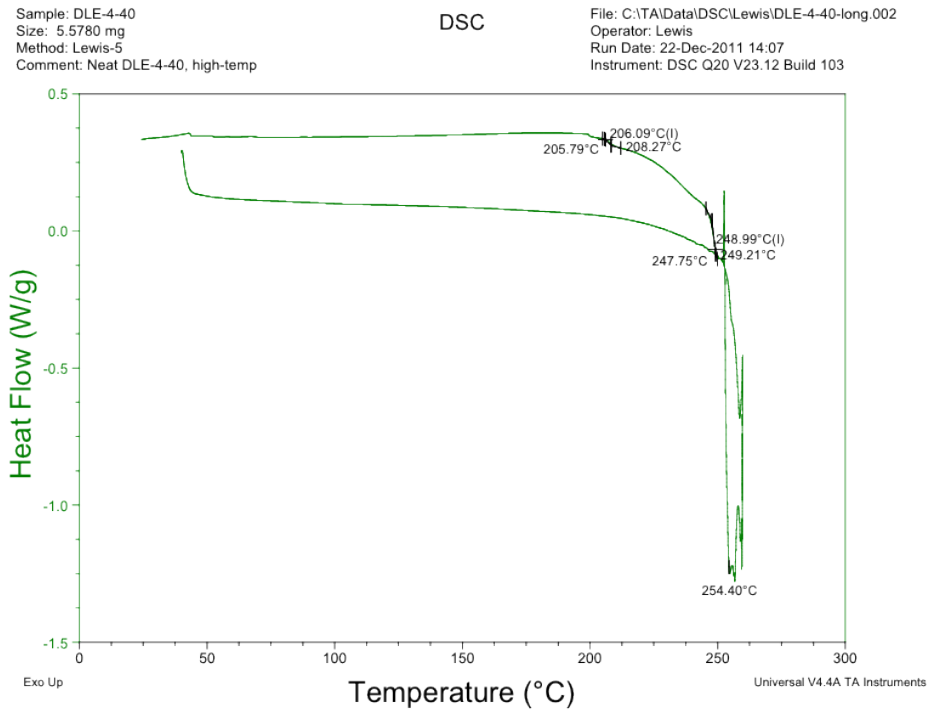


**Figure D.11.** Thermal decomposition of Cou-$C_{6.}$ Here, the upper trace is heating and the lower trace is cooling

### *D.3.4. Electrical Characterization*

Films of Cou-$C_6$ (Samples 1C and 2B) on glass slides were tested for two-point resistivity using an off-the-shelf Radio Shack multimeter at a probe distance of 1cm. Resistance at this distance was beyond the dynamic range of the instrument, furthermore, moving the probes closer had no effect. While more extensive characterization is needed, the electrical resistivity of the film is very high (>>1 MΩ-cm).

## D.4. Synthesis

Cou-$C_6$ was synthesized by Delwin Elder, who developed an improved procedure based on earlier, small-scale syntheses by Stephanie Benight and by Lewis Johnson. The synthesis is detailed in Scheme D.1.

**Scheme D.1.** Synthesis of Cou-$C_6$ (DLE-4-40)

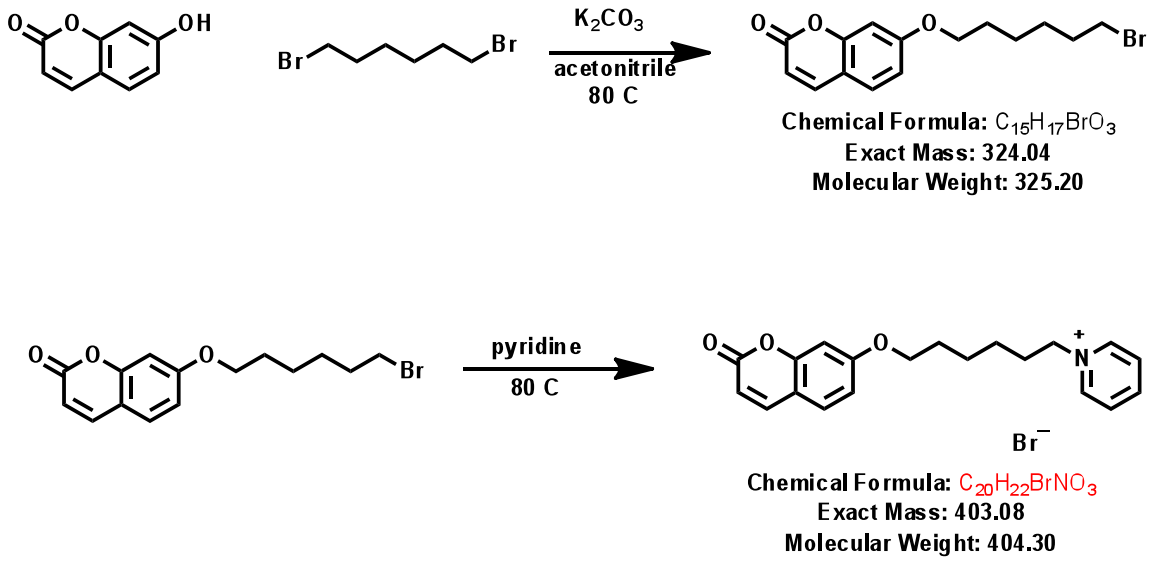


*Step 1:* A round bottom flask was purged with nitrogen and charged with 12.79 g (0.0925 mol, 1 equ) $K_2CO_3$, followed by 15.00 g (0.0925 mol, 1 equ) 7-hydroxycoumarin, 150 mL of HPLC grade acetonitrile, and 42.0 mL (0.273 mol, 3 equ) 1,6-dibromohexane. The reaction was heated to reflux for 40 hr. The precipitated potassium salts were filtered off and the precipitate was washed with 50 mL acetonitrile. The solvent was stripped off by rotary evaporation, leaving desired product as a white solid and excess dibromohexane. The precipitate was collected by filtration and washed with 2.5 L hexane, then dried *in vacuo*. **Yield:** 18.41 g (61.2%) (DLE-4-38-4).

*Step 2:* A round bottom flask was charged with 10.02 g (0.0308 mol) product from step 1 (coumarin alkylbromide), fitted with condenser and purged with nitrogen. To this was added 150 mL (1.85 mol, 60 equ) pyridine. The reactant was insoluble at room temperature, but dissolved upon heating to 80° C. Heating to 80° C was continued for 2.5 days. Most of the pyridine was removed by distillation under reduced pressure. Upon cooling, a precipitate formed. The precipitate was collected by filtration and washed with 5 x 100 mL toluene to remove pyridine then 3 x 100 mL hexane to remove toluene. The product was purified by passing through a plug of silica gel using gradient elution with 9:1 dichloromethane:methanol to 7:3 dichloromethane:methanol. Removal of solvent by rotary evaporation at 45°C yielded a viscous, yellow liquid, which solidified promptly after removal from heat and was dried *in vacuo* overnight at ambient temperature. **Yield:** 9.29 g (74.6% yield) (DLE-4-40-3).

## D.5. Summary and Outlook

A novel, crosslinkable surfactant for coating DNA was synthesized and incorporated into DNA/surfactant composites using two different methods, (1) direct coating of DNA with crosslinker and CTMA, and (2) mixing of existing CTAB-DNA with the crosslinker. The first method produces a more homogeneous material and is preferred over mixing with existing CTMA-DNA. Crosslinking behavior was characterized by UV/Vis spectroscopy in thin films and in solution. The coated DNA retains a strong coumarin absorbance peak at 323nm that disappears upon exposure to broad-band UV, indicative of crosslinking of the coumarin. The transmissivity of the material in the near-infrared is not substantially affected by the addition of the crosslinker. Both the

coated DNA and pure crosslinker were also characterized by DSC, with the glass transition temperature of non-crosslinked material reduced to 99.1°C. The glass transition temperature of crosslinked material has yet to be characterized as film scrapings yielded an inadequate quantity of material.

Further characterization of the coumarin-based crosslinker would require synthesis of materials of different chain lengths, preparation of DNA coated with different ratios of CTMA and Cou-$C_6$ (or other chain lengths), thermal characterization of crosslinked films, and characterization of the complex refractive index of the material. Furthermore, dyes would need to be incorporated and tested for photostability under crosslinking conditions, and if photostability was poor under broadband UV (as found by Stephanie Benight in unpublished work on C1, a coumarin-functionalized chromophore[7], a filter system would need to be designed to maximize usable light for crosslinking while minimizing damage to the NLO dye.

## D.6. Acknowledgements for Appendix D

Thanks to Stephanie Benight for starting this project, including developing the first version of the surfactant and making the Cou-$C_6$ films, Delwin L. Elder for optimizing and scaling up the synthesis of Cou-$C_6$, Emily Heckman for useful discussion, and providing both CTMA-DNA and the crosslinking lamp, and Andreas Tillack and Wes Winn for assistance with installing and testing the crosslinking lamp, and the Jen group (esp. Josh Davies) for use of their crosslinking lamp. Funding from AFRL and the NSF STC-MDITR (DMR-0120967) is also gratefully acknowledged.

## D.7. References for Appendix D


1. (a) Grote, J. G.; Diggs, D. E.; Nelson, R. L.; Zetts, J. S.; Hopkins, F. K.; Ogata, N.; Hagen, J. A.; Heckman, E.; Yaney, P. P.; Stone, M. O.; Dalton, L. R., DNA Photonics [Deoxyribonucleic Acid]. *Molecular Crystals and Liquid Crystals* **2005,** *426* (1), 3-17; (b) Grote, J. G.; Ogata, N.; Hagen, J. A.; Heckman, E.; Curley, M. J.; Yaney, P. P.; Stone, M. O.; Diggs, D. E.; Nelson, R. L.; Zetts, J. S.; Hopkins, F. K.; Dalton, L. R., Deoxyribonucleic Acid (DNA) based nonlinear optics. *Proceedings of SPIE* **2003,** *5211*, 53-62; (c) Heckman, E. M., Poling and optical studies of DNA NLO waveguides. *Proceedings of SPIE* **2005,** *5934*, 593408-593408-7; (d) Heckman, E. M.; Hagen, J. A.; Yaney, P. P.; Grote, J. G.; Hopkins, F. K., Processing techniques for deoxyribonucleic acid: Biopolymer for photonics applications. *Applied Physics Letters* **2005,** *87* (21), 211115.
2. Johnson, L. E.; Benight, S. J.; Rawal, M.; Robinson, B. H. *NLO Chromophore/Surfactant Systems for Biophotonics Applications (Report to AFRL)*; University of Washington: 2010.
3. (a) Tian, Y.; Kong, X.; Nagase, Y.; Iyoda, T., Photocrosslinkable Liquid-Crystalline Block Copolymers with Coumarin Units Synthesized with Atom Transfer Radical Polymerization. *Journal of Polymer Science: Part A: Polymer Chemistry* **2003,** *41* (2197-2206); (b) Wolff, T.; Görner, H., Photodimerization of coumarin revisited: Effects of solvent polarity on the triplet reactivity and product pattern. **2004**; (c) Anet, R., The Photodimers of Coumarin and Related Compounds. *Canadian Journal of Chemistry* **1962,** *40*, 1249-1256.
4. Heckman, E. The Development of an All-DNA-BAsed Electro-Optic Waveguide Modulator. University of Dayton, Dayton, OH
, 2006.
5. Brunelle, D. J., Polycarbonates. In *Kirk-Othmer Encyclopedia of Chemical Technology*, John Wiley and Sons: 2001.
6. Slone, R. V., Methacrylic Polymers. In *Kirk-Othmer Encyclopedia of Chemical Technology*, John Wiley and Sons: 2003.
7. Benight, S. J.; Johnson, L. E.; Barnes, R.; Olbricht, B. C.; Bale, D. H.; Reid, P. J.; Eichinger, B. E.; Dalton, L. R.; Sullivan, P. A.; Robinson, B. H., Reduced Dimensionality in Organic Electro-Optic Materials: Theory and Defined Order. *Journal of Physical Chemistry B* **2010,** *114* (37), 11949-11956.

# VITA

Lewis E. v.d.L. Johnson was born and raised in Seattle, Washington. He has had a lifelong interest in science, and while in 10$^{th}$ grade at the Northwest School, his NSIP team developed an experiment that was flown on a sounding rocket from NASA's Wallops Flight Facility. He attended Pomona College in Claremont, California, where he received his Bachelor of Arts in Chemistry in May 2007. As an undergraduate, he conducted research at NOAA on reactive chemical hazards with Dr. James Farr, contributing towards the development of a new version of the Chemical Reactivity Worksheet, as well as research on electrostatically self-assembled thin films with Prof. Malkiat Johal at Pomona College. Lewis returned to Seattle for graduate school at the University of Washington, conducting his doctoral research under the supervision of Prof. Bruce H. Robinson. He conducted both computational and experimental research related to organic nonlinear optical materials, including using several computational modeling techniques to study ordering, dielectric behavior, and optical properties of soft-matter materials for electro-optic and biophotonic applications. His research also included collaborations with research groups in biology, physics, and materials science. During graduate school, he presented at the 2011 ACS National Meeting and co-authored numerous publications. He graduated with a Doctor of Philosophy in Chemistry and Nanotechnology in June 2012. Outside of the lab, Lewis enjoys photography, writing, running, curling, and softball, among other interests.